J. D. Verhagen

Delft University of Technology

Spatially explicit WEF modelling in transboundary river basins

A new methodology to study the value of cooperation in regional water management

J. D. Verhagen

TUDelft

TUDelft

Spatially explicit WEF modelling in transboundary river basins

A new methodology to study the value of cooperation in regional water management

by

J.D. (Jeroen) Verhagen

to obtain the degree of Master of Science
at the Delft University of Technology,
to be defended publicly on Thursday August 27, 2020 at 14:00.

Student number:	4302214	
Thesis committee:	Prod. dr. ir. P. van der Zaag,	TU Delft, IHE Delft
	Dr. ir. E. Abraham,	TU Delft
	Dr. S. Pande,	TU Delft

An electronic version of this thesis is available at http://repository.tudelft.nl/.

Cover page: McKinsey & Company

TU Delft

Executive Summary

Water, energy and food resources are fundamental for human survival and are critical for supporting economic development. However, ensuring adequate supply is a major concern for the entire world, specifically in some countries and regions. Under the pressure of population growth, economic development, international trade, urbanization, diversifying diets, cultural and technological changes, global projections indicate a significant further increase in demand for water, energy and food over the next decades. Moreover, the development of these water, energy and food resources are intertwined. As a result, when demand grows, but resources are no longer abundant, competition between sectors increases. Especially in regions with upstream-downstream water connectivity, a national sectoral approach may result in friction, a decrease in mutual trust and international conflicts. On the other hand, the synergistic effects associated with regional resource coordination can contribute to improved resource availability and downstream livelihoods.

To overcome the shortcomings of the current generation of hydro-economic and WEF-nexus models in describing resource cooperation at regional level, in this study a new WEF-framework has been developed in which the heterogeneity in agro-climatic, socio-economic and resource availability, as well as the description of water and electric conveyance infrastructure is included spatially and temporally explicitly. The aim of this research is to create an integrated WEF-framework and to investigate the possibilities for, the relevance of and the challenges and difficulties associated with the implementation of such an integrated model.

The proposed framework includes the river conveyance infrastructure in a multi state river basin by means of a dynamic network model. In addition, a novel approach is used to describe both irrigated and rainfed agriculture in great detail on a regional scale, enabling a good representation of crops with multiple growing cycles per season, a distinction between annual and perennial crop management and the inclusion of agricultural losses. The framework is implemented as a model predictive control (MPC) problem. In this control problem, the reservoir operations and agricultural planning resulting in maximum economic value creation with the available resources are determined with the help of a non-linear problem solver. Receding horizon control accomplishes as part of the MPC framework feedback against uncertain disturbances (e.g. deviations in climate forcing) by applying only the optimal outputs in the first instance of the horizon in simulation and then updating the system states using new information. In addition, this control technique enables information exchange between riparian states within each MPC iteration. This allows us to add two new cooperation scenarios between the often studied scenarios of unilateralism and full coordination, with which the value of information exchange of river flows and trade flows can be studied.

Once developed, the framework is applied in the Eastern Nile basin. The Eastern Nile Basin is home to a large and rapidly growing population. Along with future population growth, changes in socio-economic conditions are expected, which will improve the coverage of the electricity grid and alter diets and water consumption. To meet the growing demand for food and energy, the Nile riparian countries have developed, and intend to further develop, their water resources. However, currently this development takes place unilaterally and can thereby threaten the livelihood in the downstream countries that are highly dependent on these water resources. The application of the proposed model framework aims to describe the qualitative and quantitative benefits and impacts of further collaboration in resource management within a predefined structural environment.

Simulation experiments with a monthly time step are conducted over a historical period between 1990-2010 and a future period between 2020-2040, by screening and incorporation of data on structural, socio-economic and climate constraints and demands. In addition to the four named cooperation scenarios, experiments are compiled to determine trade-offs between hydropower and agricultural water demand, the robustness of the solutions to imperfect climate foresights and the economic trade-offs related to different levels of agricultural self-sufficiency.

Comparative research with trade data from the FAO database indicates that historically every riparian state in the Eastern Nile basin could have benefited from the proposed integrated resource management, even in the unilateral national cases. Despite the variability in extent, all proposed and included forms of cooperation would have been beneficial for all individual states. Regionally, the flow-information, trade-information and regional coordination scenarios could have provided additional benefits of $32, $37 and $50 billion respectively throughout the period. Sharing information about the expected border flows would have generated, relatively in Sudan and absolutely in Egypt, by far the largest additional benefits. However, these benefits appear to correlate strongly with perfect climate foresight information. Because of its upstream location, Ethiopia could not have benefited economically from this flow information sharing. Overall, the benefits of resource optimization would have been relatively small in Ethiopia due to the limited infrastructure present during this period. In addition to the quantitative benefits mentioned, regional coordination also would have enabled the states to increase their resilience against long-lasting droughts and price fluctuations in the external market.

Results of the future model experiments suggest that every state will be disadvantaged in a regional coordinative scenario. To correct these physically and mathematically incorrect results, the current soft constrained implementation of the non-smooth complementarity relations for the reservoir filling process will have to be reconsidered. These non-smooth functions are the first out of three major difficulties encountered when implementing the proposed framework. Other difficulties arise when describing processes on different time scales (e.g. annual crop seasons) and when keeping the problem robust (in case predictions deviate from real events).

Overall, the case study illustrates that the proposed framework can account for spatial and temporal multisectoral trade-offs while finding non-trivial solutions for varying forms of national and regional cooperative resource management. Moreover, the operational resource reallocation choices proposed by this new framework and the spatial diversity in productivity that were discovered indicate that inadequate inclusion of these heterogeneities in WEF-nexus studies results in incomplete and potentially incorrect conclusions.

Acknowledgements

Before you lies the product of my master thesis in civil engineering - water management. At the beginning of my studies I did not expect to finish my student days at this faculty and department. However, after successfully completing my bachelor in mechanical engineering, I was ready for new adventures and challenges. The unequal access to available fresh water and the resulting impeding and existing national and international conflicts, as well as the combination of technical and humanitarian, diplomatic and political disciplines involved, made water management the choice for my further development.

One of the headlines published during my educational transition that has stayed with me and is prominently featured on my bulletin board ever since, describes the conflict surrounding the construction of the Grand Ethiopian Renaissance dam. Therefore I felt immediately attracted to the offered opportunity to further investigate the problems and possible solutions in this river basin during my thesis.

The realization of this thesis is the result of more than a year of hard work, first at the faculty, later because of the ongoing epidemic from home. The free nature of the thesis subject caused the scope of the project to shift an broaden over time. The many formative periods that this entailed, made writing this thesis a truly amazing adventure, which resulted in the necessary portion of self-knowledge and a leap forward in my skills set.

I could not have achieved the result published in this report without the help of a group of people surrounding me. First of all I would like to thank my thesis committee for their contribution. Thank you, Edo, for believing in this project and in my capacities to bring it to a successful conclusion. Without your enthusiasm, knowledge and support I would not have gotten this far. Thank you to Pieter van der Zaag and Saket Pande for your time and fruitful comments and feedback that took this thesis to the next level. In addition, I would like to thank my friends from the bachelor's, master's and beyond who have believed in me throughout my studies, and have given special support during my thesis. A special thanks also goes to my fellow graduates. The joint lunches, coffee breaks, fried fish and Friday afternoon drinks, as well as your goodwill to listen and help, have been a support during this period. Finally I am grateful to my parents and brothers who have supported my personal development throughout my student years, even when it turned out to take a little bit longer than planned.

J.D. (Jeroen) Verhagen
Delft, Augustus 2020

Readers guide

This report consists of two parts. The first part (part A) introduces a new methodology to study the value of cooperation in transboundary river basins. In the second part (part B), this method is applied in the Eastern Nile basin. The discussion, conclusion and future research focused on the method presented in part A follow in part B together with the discussion, conclusion and future research focused on the case study.

Contents

A case study in the Eastern Nile river basin.

List of Figures

List of Tables

Symbols, Abbreviations and Formulations

List of abbreviations

AHD	Aswan High Dam
AIM	Asia pacific Integrated Model
CRGE	Climate Resilient Green Initiative
CRU	Climate Research Unit
EAPP	Eastern Africa Power Pool
ENTRO	Eastern Nile Technical Regional Office
FAO	Food and Agricultural Organization
FIFO	First In First Out
FSC	Food Supply Chain
GAEZ	Global Agro Ecological Zones
GERD	Grand Ethiopian Renaissance Dam
GO	Global Optimization
ICS	Inter connected Supply
IWRM	Integrated Water Resource Management
LRC	Lower Rule Curve
MIRCA	Monthly Irrigated and Rainfed Crop Areas
MPC	Model Predictive control
NBI	Nile Basin Initiative
NLP	Non Linear Programming
RAW	Readily Available Water
RCP	Representive Concentration Pathways
SDG	Sustainable Development Goals
SMHI	Swedisch Meteorological and Hydrological Institute
SRES	Special Report on Emission Scenarios
SSEC	South Sudan Electricity Cooperation
SSP	Shared Socioeconomic Pathway
TAW	Total Available Water
URC	Upper Rule Curve
WEF	Water,Energy and Food

List of symbols

Variable	Description	Quantity
A_{agri}	agricultural surface area	$[l^2]$
A_{harv}	crop harvest area	$[l^2]$
A_{occ}	crop occupation area	$[l^2]$
A_{res}	reservoir surface area	$[l^2]$
$c_{\text{agri-ch}}$	maximum change in agricultural cropping pattern between seasons	[ ]
c_{cap}	electric capacity factor	[ ]
c_{dry}	product dry weight fraction	[ ]
$c_{\text{e-loss}}$	national network distribution losses	[ ]
$c_{\text{e-loss-int}}$	network loss on internation high voltage transmission lines	[ ]
c_{flow}	river flow los fraction due to seepage and evaporation	$[l^{-1}]$
c_{int}	compound rate	[ ]
c_{mf}	crop management factor	[ ]
$c_{\text{min-ET}}$	minimum required evapotranspiration ratio	[ ]
c_{p}	specific heat	$[l^2 \cdot t^{-2} \cdot T^{-1}]$
c_{suff}	self-sufficiency ratio	[ ]
$c_{\text{st-loss}}$	product distribution and storage loss	[ ]
$c_{\text{trade-loss}}$	international product trade loss	[ ]
e_{a}	actual vapour pressure	$[m \cdot l^{-1} \cdot t^{-2}]$
e_{s}	saturated vapour pressure	$[m \cdot l^{-1} \cdot t^{-2}]$
E	open water evapocration	$[l]$
E_{diet}	per capita caloric energy intake	$[m \cdot l^2 \cdot t^{-2}]$
E_{e}	energy generation by single plant	$[m \cdot l^2 \cdot t^{-2}]$
$E_{\text{e-avail}}$	available electric energy	$[m \cdot l^2 \cdot t^{-2}]$
$E_{\text{e-con}}$	electric energy consumed	$[m \cdot l^2 \cdot t^{-2}]$
$E_{\text{e-dump}}$	electric energy dumped (in case of excess production)	$[m \cdot l^2 \cdot t^{-2}]$
$E_{\text{e-exp-fxd}}$	energy export according to long term (year) contracts	$[m \cdot l^2 \cdot t^{-2}]$
$E_{\text{e-exp-var}}$	energy export according to short term (timestep) contracts	$[m \cdot l^2 \cdot t^{-2}]$
$E_{\text{e-gen}}$	national electric energy generation	$[m \cdot l^2 \cdot t^{-2}]$
$E_{\text{e-imp-fxd}}$	energy import according to long term (year) contracts	$[m \cdot l^2 \cdot t^{-2}]$

Variable	Description	Quantity
$E_{\text{e-imp-var}}$	energy import according to short term (timestep) contracts	$[m \cdot l^2 \cdot t^{-2}]$
$E_{\text{e-non-renew}}$	energy generation by all non renewable plants	$[m \cdot l^2 \cdot t^{-2}]$
$E_{\text{e-renew}}$	energy generation by all renewable plants	$[m \cdot l^2 \cdot t^{-2}]$
$E_{\text{e-trade}}$	net electric energy trade	$[m \cdot l^2 \cdot t^{-2}]$
ET_{a}	actual evapotranspiration	$[l]$
ET_{o}	reference evapotranspiration	$[l]$
ET_{p}	potential evapotranspiration	$[l]$
f_{animal}	fraction of animal energy intake by specifc animal product	[ ]
f_{basket}	specific product consumption as fraction of animal feed	[ ]
$f_{\text{b-group}}$	feed basket group fraction	[ ]
f_{cut}	relative duration of a growth cycle with respect to Ngrw	[ ]
f_{hedge}	fraction of active reservoir storage used for hedging	[ ]
f_{loss}	reduction factor for river outflow due to seepage and evaporation	[ ]
f_{routing}	delayed fraction of past inflows leaving a river stretch	[ ]
$f_{\text{routing-loss}}$	fraction combining the effects of delay and loss in river outflow	[ ]
f_{stg}	relative duration of a growth stage within a growth cycle	[ ]
f_{store}	fraction of past inflow stored in river stretch	[ ]
$f_{\text{vegetative}}$	fraction of energy intake by specific vegetative product	[ ]
$f_{\text{v-group}}$	food group energy intake fraction	[ ]
F_{con}	product consumption for food, feed or raw material for processing	$[m]$
$F_{\text{con-process}}$	product consumption for use as raw material for processing	$[m]$
$F_{\text{con-suff}}$	minimum of production and self sufficiency target	$[m]$
F_{exp}	product export quantity	$[m]$
F_{feed}	product consumption for animal feed	$[m]$
F_{food}	product consumption for human food consumption	$[m]$
F_{imp}	product import quantity	$[m]$
F_{process}	quantity of a product used for conversion into another product	$[m]$
F_{prod}	food production by agriculture and conversion	$[m]$
$F_{\text{prod-agri}}$	agricultural product harvest	$[m]$
$F_{\text{prod-basin}}$	irrigated agricultural harvest within the main basin	$[m]$
$F_{\text{prod-outside}}$	irrigated agricultural harvest outside the main basin	$[m]$
$F_{\text{prod-process}}$	product processing output quantity	$[m]$
$F_{\text{prod-rain}}$	rainfed agricultural harvest	$[m]$
F_{trade}	net product import	$[m]$

Variable	Description	Quantity
g	gravitational acceleration	$[l \cdot t^{-2}]$
g_{n}	index for the completed timesteps within current growing season	[ ]
g_{y}	soil heat flux	$[m \cdot t^{-3}]$
G_{y}	index for the startyear of current growing season	[ ]
h_{net}	net water head over turbine	$[l]$
h_{res}	surface water level of reservoir	$[l]$
h_{ror}	run-of-the-river design elevation	$[l]$
h_{tail}	turbine outlet elevation	$[l]$
H_{drain}	drainage per surface area unit	$[l]$
H_{evap}	net evaporation flux	$[l]$
H_{fuel}	fuel combustion heat	$[l^2 \cdot t^{-3}]$
H_{irr}	irrigation supply per surface area unit	$[l]$
$H_{\mathrm{vegatative}}$	product caloric value	$[l^2 \cdot t^{-2}]$
$I_{\mathrm{constraint}}$	overall soft constraint penalty	[ ]
$I_{\mathrm{cs\text{-}cyc}}$	soft constraint costs for deviation from rule curve	[ ]
$I_{\mathrm{cs\text{-}fill}}$	soft constraint costs for premature turbine flow during reservoir filling	[ ]
$I_{\mathrm{cs\text{-}flow\text{-}agree}}$	soft constraint costs for penalizing international flow agreements	[ ]
$I_{\mathrm{cs\text{-}hedge}}$	soft constraint costs for water consumption from hedge storage	[ ]
$I_{\mathrm{cs\text{-}spill}}$	soft constraint costs for spill flow	[ ]
$I_{\mathrm{e\text{-}fuel}}$	fuel costs for power generation	[ ]
$I_{\mathrm{e\text{-}fxd}}$	fixed electricity costs	[ ]
$I_{\mathrm{e\text{-}net}}$	net income from energy sector	[ ]
$I_{\mathrm{e\text{-}o\&m}}$	operational expenditures electricty generation	[ ]
$I_{\mathrm{e\text{-}shortage}}$	electricity shortage costs	[ ]
$I_{\mathrm{e\text{-}trade}}$	national income electricity trade	[ ]
$I_{\mathrm{e\text{-}var}}$	variable expenditures electricty generation	[ ]
$I_{\mathrm{f\text{-}fxd}}$	fixed cost product production	[ ]
$I_{\mathrm{f\text{-}net}}$	net income from agricultural sector	[ ]
$I_{\mathrm{f\text{-}seed}}$	seed expenditures	[ ]
$I_{\mathrm{f\text{-}trade}}$	nationale income from product trade	[ ]
$I_{\mathrm{f\text{-}var}}$	variable costs product production	[ ]
I_{min}	minimum required income	[ ]
K_{cc}	resulting crop coefficient per timestep	[ ]
$K_{\mathrm{cc\text{-}stg}}$	average crop coefficient value for a single stage duration a timestep	[ ]

Variable	Description	Quantity
K_{s}	water stress coefficient	[ ]
K_{stg}	crop coefficient at the beginning of a growth stage	[ ]
$l_{\text{e-trade}}$	length of transmission lines between two states	$[l\ ]$
l_{river}	length of a river stretch	$[l\ ]$
$l_{\mathrm{tranmission}}$	length of a single transmission line	$[l\ ]$
n_{cycle}	number of the timestep within a year at which a growing cycle starts	[ ]
n_{seed}	number of the timestep within a year at which the growing season starts	[ ]
N_{cut}	number of growing cycli (cuts) per growing seasons	[ ]
N_{grw}	numbers of timesteps between sowing and harvest	[ ]
$N_{\text{grw-cut}}$	duration of a single growing cycle in timesteps	[ ]
N_{hist}	number of past timestep from which water could be stored in a stretch	[ ]
N_{iter}	number of MPC iterations completed	[ ]
$N_{\text{opt-end}}$	number of last time step in horizon since start of experiment	[ ]
N_{pop}	population size	[ ]
N_{step}	number of timesteps within a year	[ ]
p_{a}	slope of linearized reservoir storage-area relation	$[l^{-1}\ ]$
p_{agree}	price for penalizing international flow agreements	[ ]
p_{b}	offset of linearized reservoir storage-area relation	$[l^{2}\ ]$
p_{cyc}	price for deviation from rule curve	[ ]
$p_{\text{e-amort}}$	amortization price electric plant	$[m^{-1} \cdot l^{-2} \cdot t^{3}\ ]$
$p_{\text{e-fuel}}$	power plant fuel price	$[m^{-1}\ ]$
$p_{\text{e-int}}$	international electricity trade price	$[m^{-1} l^{-2} t^{2}\ ]$
$p_{\text{e-o\&m}}$	operational and management price electric plant	$[m^{-1} l^{-2} t^{2}\ ]$
$p_{\text{e-shortage}}$	energy shortage price (energy production value)	$[m^{-1} l^{-2} t^{2}\ ]$
$p_{\text{f-amort}}$	irrigated agriculture amortization price	$[l^{-2}\ ]$
$p_{\text{f-fert}}$	fertilizer price	$[l^{-2}\ ]$
p_{fill}	price for premature turbine activity	[ ]
$p_{\text{f-int}}$	international product trade price	$[m^{-1}\ ]$
$p_{\text{f-labour}}$	labour price	$[l^{-2}\ ]$
$p_{\text{f-process}}$	fixed processing price	$[m^{-1}\ ]$
$p_{\text{f-process-var}}$	variable processing price	$[m^{-1}\ ]$
$p_{\text{f-seed}}$	seed price	$[l^{-2}\ ]$
$p_{\text{f-trans}}$	international transport costs	$[m^{-1} \cdot l^{-1}\ ]$
p_{hedge}	price for water consumption from hedge storage	[ ]

Variable	Description	Quantity
p_{spill}	price of spillway activity	$[l^{-3}]$
P	precipitation	$[l]$
P_{e}	installed electric capacity of plant	$[m \cdot l^2 \cdot t^{-3}]$
P_{eff}	effective precipitation	$[l]$
q_{a}	slope of linearized reservoir storage-elevation relation	$[l^{-2}]$
q_{b}	offset of linearized reservoir storage-elevation relation	$[l^1]$
Q_{gate}	gate discharge	$[l^3 \cdot t^{-1}]$
Q_{off}	offtake discharge	$[l^3 \cdot t^{-1}]$
Q_{turb}	turbine discharge	$[l^3 \cdot t^{-1}]$
r_{a}	aerodynamic resistance	$[t \cdot l^{-1}]$
r_{s}	surface resistance	$[t \cdot l^{-1}]$
R_{n}	net radiation	$[m \cdot t^{-3}]$
S_{active}	active reservoir storage	$[l^3]$
S_{cyc}	rule curve storage	$[l^3]$
S_{fill}	storage during reservoir filling	$[l^3]$
S_{food}	product storage	$[m]$
S_{hedge}	storage in hedge buffer of reservoir	$[l^3]$
S_{res}	reservoir storage	$[l^3]$
t	duration of a timestep	$[t]$
t_{river}	concentration time of a river stretch	$[t]$
t_{stg}	duration of a stage during a crop cycle	$[t]$
$t_{\text{stg-end}}$	end time of a growth stage since the start of a growing cycle	$[t]$
$t_{\text{stg-start}}$	start time of a growth stage since start of the growth cycle	$[t]$
v_{river}	average flow velocity in a river stretch	$[l \cdot t^{-1}]$
V_{agree}	yearly flow between countries	$[l^3]$
V_{back}	reservoir backwater gate	$[l^3]$
V_{drain}	volume drained from agricultural field back into the river system	$[l^3]$
V_{evap}	net evaporation volume	$[l^3]$
$V_{\text{fill-step}}$	minimum required outflow per timestep during reservoir filling	$[l^3]$
$V_{\text{fill-year}}$	minimum required outflow per year during reservoir filling	$[l^3]$
V_{gate}	gate outflow volume	$[l^3]$
V_{hedge}	part of outflow reduced in hedging protocol	$[l^3]$
V_{in}	inflow volume	$[l^3]$
V_{irr}	irrigated volume	$[l^3]$

Variable	Description	Quantity
V_{off}	diverted volume at an offtake node	$[l^3]$
V_{out}	outflow volume	$[l^3]$
V_{spill}	spill volume	$[l^3]$
V_{src}	runoff flowing into the river system at a source node	$[l^3]$
V_{turb}	turbine outflow volume	$[l^3]$
W_{fuel}	fuel consumption	$[m]$
y_{n}	index of a timestep within a year	[ ]
y_{y}	index for the year in which a timestep falls	[ ]
Y_{a}	harvested fresh crop mass	$[m\ ]$
Y_{m}	maximum attainable crop yield	$[m\ ]$
Y_{p}	agro-climatic potential yield	$[m\ ]$
Z	all optimization variables	[ ]
Z_{agri}	optimization variables related to the agricultural production	[ ]
Z_{cyc}	optimization variables related to reservoir cyclicity	[ ]
Z_{electric}	optimization variables related to the energy balance	[ ]
Z_{flow}	optimization variables related to the water balance	[ ]
Z_{prod}	optimization variables related to the food balance	[ ]
δ_{A}	new planted area at start of growing season	$[l^2\ ]$
Δ	saturation vapour pressure slope	$[m \cdot l^{-1} \cdot t^{-2} \cdot T^{-1}\ ]$
ΔK_{stg}	crop coefficient change during timestep	[ ]
$\Delta S2\text{-cyc}$	normalised auxiliary variable for deviation from rule curve	[ ]
$\Delta S2\text{-fill}$	normalised auxiliary variable for reservoir filling	[ ]
$\Delta t\text{stg}$	duration of a particulair growth stage within a single timestep	$[t\ ]$
η_{eff}	effective fraction of precipitation	[ ]
$\eta_{\text{F-conv}}$	product conversion efficiency	[ ]
$\eta_{\text{feed-conv}}$	feed conversion efficiency	[ ]
η_{fuel}	fuel plant conversion efficiency	[ ]
η_{hydro}	hydro energy conversion efficiency	[ ]
η_{irr}	irrigation efficiency	[ ]
ρ	fresh water density	$[m \cdot l^{-3}\ ]$
ρ_{a}	air density	$[m \cdot l^{-3}\ ]$

List of mathematical sets

Variable	Description
A	set of all agricultural sites
B	set of outside river basins
C	set of all crops
D	set of all inactive nodes
F	set of all source nodes
G	set of all product groups
H	set of all run-of-the-river nodes
I	set of all irrigated agriculture nodes
J	set of all surface water reservoir nodes
L	set of all transmission lines
M	set of river stretches (linkages)
N	set of all nodes
O	set of all offtake nodes
P	set of all products
Q	set of all animal products
R	set of all rainfed pixels
S	set of countries bordering to the transboundary river
U	set of all confluence nodes
V	set of all non-renewable generation sources
W	set of all renewable generation sources

List of mathematical formulations

Formulation	Description
$\lceil x \rceil$	ceil of variable
$\lfloor x \rfloor$	floor of variable
$\lvert x \rvert$	absolute value of variable
$x \cdot y$	multiplication
x/y	division
$\mathbf{1}_{a<b}$	logical operator
$\bar{x}$	variable upper bound
$\underline{x}$	variable lower bound

Part A:

Optimization of operational river management and regional water planning

1 Introduction

"Managing water as an economic good is an important way of achieving efficient and equitable use, and of encouraging conservation and protection of water resources." - United Nations, 1992

1.1. Resources in transboundary river basins

Water, food and energy resources are fundamental for human survival and are critical for supporting economic development. However, ensuring adequate supply is a major concern for the entire world and some countries and regions specifically. Over the last 50 years, population growth and economic prosperity have led to a sharp increase in food demands. Due to an intensification of land and water resources, the world's agricultural production has grown between 2.5 and 3 times [Earthscan and FAO, 2011]. With this increase in food production, withdrawals for agriculture have been rising. Globally, agriculture accounts for 70 percent of all water withdrawn from aquifers, streams and lakes and 30 percent of total energy consumed [FAO, 2011a]. Although this water consumption represents a small fraction (6 percent) of the internal renewable water resources at a global level, the regional discrepancies are large. Especially in the Middle East, Northern Africa and Central Asia, intensification of agriculture has led to most of the exploitable water being already withdrawn, with 80–90 percent of that going to agriculture [Earthscan and FAO, 2011]. At the same time, demand from other sectors, particularly municipal and industrial demand, has been growing faster than agricultural demand.

Under the pressure of population growth, economic development, international trade, urbanization, diversifying diets, cultural and technological changes, global projections indicate a significant further increase in demand for freshwater, energy and food over the next decades [Hoff, 2011]. Assuming a Shared Socioeconomic Pathway (SSP2) in which social, economic, and technological trends do not shift markedly from historical patterns, population growth of up to 9 billion people in 2050 will be accompanied by an increase in food demand of more than 60 percent compared to 2005 [Valin et al., 2014], an increase in energy demand of more than 80 percent [Bauer et al., 2017] and an increase in global water demand of 50 percent [Flammini et al., 2014; Wada et al., 2016]. Growth in demand will be particularly strong in developing countries [Flammini et al., 2014], causing a further aggravation of the water stress in the Middle East, Northern Africa and Central Asia. On the other side of the balance, climate change, increasing pollution, degradation, urbanization and other trends can pose local challenges for the resource supply.

However, the development of these resources is not unrelated. Water, energy and food resources have many shared attributes in terms of existing access, change in demand, supply constraints, spatial and temporal availability, tradability and market structure [Bazilian et al., 2011]. The three resources are highly interrelated where one is input for the other in several cases. Water is used for agricultural production, forestry and fishery, along the entire agri-food supply chain, and it is required to generate energy in different forms. At the same time, the food production and supply chain are major electricity consumers. Furthermore, energy is used to produce, transport and distribute food as well as to extract, pump, transport and treat water resources [FAO, 2014]. Sectoral policies can therefore impose unintended consequences on other sectors. As demand grows, but resources are no longer abundant, there is increasing competition within a country over resources between sectors. This may increase the risk of conflict and ultimately undermine the water, energy, food and environmental security.

In transboundary river basins, resource management becomes even more complex. The upstream-downstream connectivity of water makes downstream communities deeply dependent on upstream management and ecosystem services for irrigation, hydropower, drinking water, soil fertility and nutrients, calling for policy not only between sectors, but also across boundaries [Rasul, 2014]. Especially

when the resources become scarcer, cooperation becomes crucial to secure resource availability and protect downstream livelihoods. However, when the riparian states fail to recognize the trade-offs and externalities, this not only constraints the use of the natural resources, but may result in friction between countries and reduced trust. At best this hinders regional development, but at worst it results in regional conflicts. Given that transboundary basins cover almost half of the Earth's surface, and that more than 40 percent of the population finds housing here [UN Water, 2008], a unilateral approach is not the solution to the increasing global resource demand. On the other hand, an international cross-sectoral approach to manage the synergies and trade-offs between common resources can help to improve water, energy and food security [Rasul, 2014].

1.2. Hydro-economic framework

Hydro-economic models are a widely used method to study resource cooperation in transboundary river basins. Numerous examples where hydro-economic models have been applied in the major transboundary river basins are found in the scientific literature [Ringler et al., 2004; Arjoon et al., 2016a; Hoff et al., 2011; de Condappa et al., 2009; Spalding-Fecher et al., 2017]. Although the concept dates back several decades, development has been boosted by the presentation of the Integrated Water Resource Management (IWRM) approach during the 1992 World Summit on Sustainable Development [Harou et al., 2009], in which sustainable co-development of water, land and related resources should maximize the economic and social welfare. Hydro-economic models make use of this philosophy by not studying river water as a standalone system, but in a holistic approach along with agricultural production, hydropower generation and environmental services. The water demands are not fixed requirements but rather functions where quantities of water have different economic values at different times and locations [Harou et al., 2009]. Central to this integrated approach is that water systems can be used as a source of economic consumption and a sink for the negative by-products of economic production, and hence have economic value [Brouwer and Hofkes, 2008]. So the interaction between water and economic development works both ways. Water can be used for economic benefits, but these benefits have implications that complicate economic development later or elsewhere.

All major hydrologic processes, structural parts and economic relationships are represented spatially and temporally distributed in hydro-economic models [Harou et al., 2009]. Such a detailed description of water, infrastructure, land use, and economic relationships is important to account for the trade-offs, demands and constraints that apply at a location as a result of environmental, hydrologic, and socio-economic characteristics. These spatial hydrologic relationships in the river system and the water demand and production relationships of water using sectors are represented in the core of the models by sets of non(linear) mathematical equations [Bekchanov et al., 2015]. Node-link networks are most commonly used as a graphical representation of these mathematical representations [Brouwer and Hofkes, 2008]. The water flows naturally through the hydrological network in the river basin, but can be modified by structures present in the nodes. Depending on the node's characteristics, the flow can be stored or allocated for economic value production by means of agricultural, energy, industrial, municipal or environmental consumption.

When implementing hydro-economic models, a distinction is made between optimization approaches and simulation approaches. In the former are water allocations and management decision driven by the economic value of water whilst in the latter these decisions are economically evaluated [Harou et al., 2009]. Although the models are easily interchangeable by adding or removing objective functions and equations for rule based water distribution, they can be used to answer various issues. Simulation models, after being calibrated to reproduce the behaviour of real water systems, can be used to assess different scenarios of physical, environmental (e.g. drought and flooding) or management-induced change. In this way, the benefits, inefficiencies and consequences of a variety of management practices can be quantified. Optimization models, on the other hand, can be used to determine a hypothetical best case and capture trade-offs in resource allocation. Both approaches can also be combined to allow for more thorough testing of the sensitivity of optimal solutions than would be possible with optimization approaches alone [Harou et al., 2009; Bekchanov et al., 2015].

Hydro-economic models have a strong potential in representing the spatial and temporal relations between water and energy, water and food and water and ecosystem services. The flexible implementation can provide insight into current, future and optimal river water allocation strategies. However, the hydro-economic framework has a number of strong disadvantages. Such models use basins, watersheds or water bodies as a geographical unit, while economics, trade and policies often refer to administrative boundaries of a country or a region [McKinney, 1999]. Moreover, such models are evaluated economically without describing the demand side of the resource balances and the contribution of other forms of production, which cannot be linked directly to a river system, to these balances, i.e. the models work with open resource balances and assume infinite demand for food and electricity. To truly study the maximum benefits and trade-offs between the available resources, the system should be evaluated at a national level and include the demand side and other forms of production.

1.3. WEF-nexus framework

The nexus approach is a framework that makes it possible to study these closed balances within administrative boundaries. It is a multi-centric approach compared to IWRM and other integrated approaches that mostly originate from one particular sector [Liu et al., 2017]. By explicitly focusing on one sector, there is the risk of prioritizing the development goals related to this resource over others, thereby reinforcing traditional sectoral approaches [Altamirano et al., 2018]. The nexus presents a conceptual approach to better understand and systematically analyse the resource interdependencies, and to work towards a more coordinated management and use of natural resources across sectors and scales [Daher and Mohtar, 2015; Bazilian et al., 2011; FAO, 2014]. The resource nexus therefore presents a set of context-specific interlinkages between two or more natural resources. What resource balances to include depends on the objective of the study. In this study the focus is on the interdependencies between Water, Energy and Food (WEF).

Since the introduction at the World Economic Forum in 2011, the WEF-nexus philosophy has been applied at different scales with various research methods. Qualitative methods are generally used to describe the current state of the nexus balances, the important interlinkages and the involvement of stakeholders in the region of interest by use of social methods like questionnaire surveys or ontology engineering. The methods are suitable for mapping the system, but cannot be used to quantify the impact of changes in management, socio-economics or environment. Quantitative research methods therefore processes the found relations in management models and cost-benefit analyses [Endo et al., 2015]. Conversely, quantitative methods can be used to confirm and/or invalidate the qualitative relationships found. The interconnection between the found relationships in these quantitative methods can be realized in two ways. In soft- or loose-coupled systems, existing modules for different balances are linked together through the outputs, so that the factors in one system are exogenous to the other systems. Despite the advantage of simplicity this approach has a limitation in considering feedbacks among the individual systems of the WEF-nexus. Therefore, hard- or tight coupling of processes between different sectors, in which the factors from one system are endogenous to other systems, are preferable to study the feedback effects [Liu et al., 2017]. The scale on which WEF nexus methodologies are applied is quite diverse. Literature illustrates examples of applications on city, basin, national, regional and global scale [Zhang et al., 2018]. As the system scale moves up, a higher degree of data aggregation is likely to be required. Conversely, as the system scales down, more detail of the inner mechanisms is likely to be represented.

Despite the number of publications regarding the WEF-nexus and the advantages it has over hydro-economic models, there are some major challenges that need to be overcome before the models can contribute to policy and management decisions regarding the achievement of the Sustainable Development Goals (SDG). Three major challenges for regional nexus studies are related to 1) the delineation of the system boundaries and scales, 2) the spatial and temporal resolution and 3) the resource connectivity. The difficulty in setting the scale of a regional nexus study is that the scales of processes within the nexus analysis tend to differ. Certain processes take place on smaller scales (e.g. hydropower generation), while other processes take place on larger scales (e.g. international product trade) [Zhang et al., 2018; Bleischwitz et al., 2018]. Proper implementation therefore requires a multi-scale nexus approach. Moreover, such an approach could enable the implementation of a fine spatial and temporal resolution, required to describe the heterogeneity in land, energy, and water

resources that are missing in the current generation of regional nexus models [Johnson et al., 2019]. In this way, local constraints with regard to water, energy, and food can be incorporated in the resource balances, and the impacts of spatial resource reallocation strategies can be studied. In addition to a fine resolution, the latter requires improved resource connectivity via trade, electricity and water conveyance infrastructure [Johnson et al., 2019].

1.4. General equilibrium models

Since both aforementioned models contain only a limited number of economic sectors, they are unable to describe the economic propagation of changes in the water, energy and food sectors into other sectors. These model types which contain only a limited number of economic sectors are referred to as Partial Equilibrium (PE) models [Johnson et al., 2019]. However, often a change in an economic system will have consequences far beyond the sector in which the change is taking place. Computable General Equilibrium (CGE) models can provide an economy-wide perspective for understanding those consequences. By describing the price endogeneity and market-based interactions between economic actors [Kahsay et al., 2019], these models provide insight into macroeconomic consequences of policy and environmental changes [Gilbert, 2017]. While GCE models provide a very detailed and theoretically consistent description of the economic relationships between sectors [Johnson et al., 2019], they are highly spatially aggregated. Therefore, these models fail to account for the spatially relevant details in resource availability, production and consumption. Moreover, these models have been criticized for their dependence on non-econometrically estimated parameters [Kahsay et al., 2019], the uncertainty in experimental design and the very high investment in human capital required for production and operation [Gilbert, 2017].

1.5. Research objective

Considering the shortcoming of hydro-economic models and the current generation of WEF-nexus models, a new approach for studying transboundary resource cooperation is proposed. Because the strengths of one model type seem interchangeable with the shortcomings of the other model type, in this approach both model types are integrated in a new regional WEF-nexus framework. This yields a holistic hard-linked quantitative WEF-framework with closed resource balances within national administrative boundaries in which the river conveyance infrastructure is spatially and temporal explicitly included by means of a node-link network. In addition to the integration of river infrastructure, other forms of heterogeneity are described as much as possible on the scale at which the processes take place. The economic propagation into other sectors is not considered in this study.

The aim of this research is therefore to investigate the possibilities for, the relevance of and the challenges and difficulties associated with the explicit integration of both the spatial and temporal heterogeneity in resource availability, agro-climatic constraints, and socio-economic characteristics and the river and electric conveyance infrastructure in regional WEF-nexus models.

The framework is developed as a combined optimization-simulation framework to allow for more thorough testing of optimal solutions by means of scenarios and sensitivity analyses. The used Model Predictive Control (MPC) strategy makes it possible to aim for optimal solutions while being able to explicitly integrate resource and infrastructure constraints and to account for changes and uncertainties in the predicted environment. In this control strategy, a nonlinear problem solver is used to ensure a realistic representation of hydropower generation and food production. The easy accessible and adaptable input data and the predefined variations in constraint and objective settings make the proposed framework flexible and suitable to study the impact of changes in socio-economic, hydrologic and climate characteristics in addition to different cooperation scenarios, ranging in four steps from unilateral to regional coordination.

2
Theoretical framework

This chapter aims to provide the theoretical background of the study. It starts with a section on the current operational practices of surface water reservoirs. Subsequent sections discuss agricultural yield functions, introduce a systematic approach to food losses and give an introduction in the model predictive control approach.

2.1. Surface water reservoir operational rules

Surface water reservoirs are structures that enable the storage of river flow. By regulating the release over time, the available storage capacity makes it possible to manipulate the natural river flow in such a way that it can be used in the most efficient way for (downstream) purposes such as hydropower generation, irrigation, municipal and industrial use or flood control. In areas with seasonal water availability, surface water reservoirs are essential for solving current and future water issues. The predicted climate change and the growing water needs due to economic progress are therefore reasons for a global boom in dam construction [Zarfl et al., 2015]. The control of surface water reservoirs is central in the methodology proposed in this study. To understand how a coordinated planning for surface water reservoirs can result in a greater value creation, the current operational practices are explained.

Reservoir operations are most commonly guided and managed by operating rule curves. The operating rules define the reservoir release as a function of the existing storage level, the expected inflow and the overall release target during different times of the year [Chang et al., 2005]. The implicit assumption here is that a reservoir can best satisfy its purposes if the storage levels in the reservoir are maintained at the levels specified by the rule curve. Therefore they can be defined as the whole of operating criteria and guidelines that coordinate the storage and outflows from reservoirs [Haugh et al., 2014].

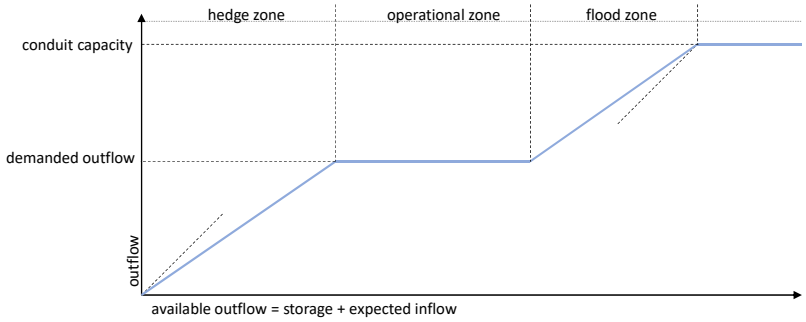

Figure 2.1: A piecewise linear rule for reservoir operation at a single time instance. Hedging (an where the outflow is reduced) occurs when the available outflow is smaller than a predefined hedge level. For flood mitigation, more water is released than the demanded outflow when the available outflow exceeds a predefined flood level. The dotted lines in the hedge and flood operating zones indicate respectively that hedging take place even when the available outflow is greater than the demand, and that the risk of flooding is traded-off with future water availability.

The rule curves divide the active reservoir storage into several zones. The number of zones may differ depending on the number of reservoir purposes and the prevailing cultural practices. Generally speaking, however, it can be said that there are three main zones [Liu et al., 2011; Adeloye and Dau, 2019; Men et al., 2019; Krogt, 2008]: the hedge zone, the operational zone and the flood control zone. By use of Figure 2.1, the different zones are explained for a single time instance. The available outflow is hereby the sum of the storage (above the dead storage) at the considered time instance and the anticipated inflow during the month. The demanded outflow is the quantity required to facilitate all reservoir

purposes (e.g. irrigation water and turbine flow). Starting upwards from the dead storage level, first lies the hedge zone. This zone is situated between the dead storage level and LRC (Lower Rule Curve). When the available outflow is lower than LRC, a hedge protocol comes into action and less than the demanded outflow is released. Hedging not only takes place when the available outflow is less than the demanded outflow, but also during normal operational periods where there is sufficient water to meet the full demand [Adeloye and Dau, 2019]. The essence of these hedging rules is to save water by frequent small water shortages so as to reduce the risk of severe water shortages in a later period [Men et al., 2019]. The outflow during hedging depends on the priority of the demands. With an increasing amount of available water, the highest-prioritized demand is met first, followed by the lower prioritized outflows [Sharad, 2020]. The operational zone is situated between the LRC and the URC (Upper Rule Curve). In this zone, all demands can be met, and exactly the demanded outflow is released. If the available outflow increases further, we end up in the flood control zone. The storage in this zone is meant to retain a design flood event and is empty during normal reservoir operations. Proper use of this flood control storage will reduce the need for spilling and thereby downstream flooding. When the storage in this pool does become active, additional spill capacity (via turbines, gates or weirs) is used to lower the reservoir level. With a growing available outflow, the outflow will increase until maximum capacity is reached. From that moment on, further inflow will increase the reservoir storage till the maximum capacity is reached and overflow occurs.

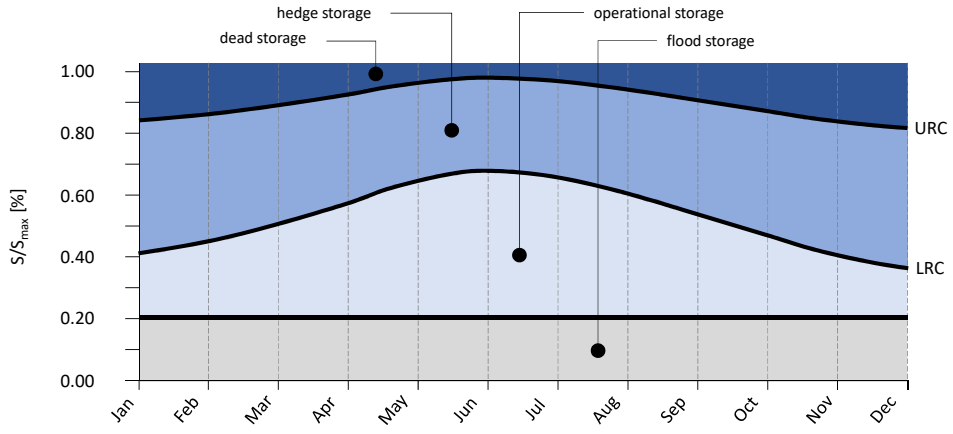

Figure 2.2: An example of a rule curve where for all months the storage fractions related to the before mentioned zones are indicated.

Because the influx and the demand can vary significantly per time instance, the rules vary with the time of the year. Using historical discharge data and future predications, a unique piecewise linear rule can be created for any time instance during a year. When the assumption is made that the forecasted monthly inflow is equal to the historic monthly runoff, the operational zones mentioned in Figure 2.1 become solely a function of the storage at the beginning of the time instance. By connecting the piecewise linear rules for each time period during a year, operating rule curves are created as illustrated in Figure 2.2.

Because rule curves can be used to express operational decisions in a visual way, they are continuous between consecutive time periods, and their monotonically increasing relationship between reservoir release and storage seems intuitive, they are widely applied in practice [Liu et al., 2011]. Unfortunately, conventional operating rule curves describe individual reservoir releases based on the storage within it. Because rule curves are not able to describe the spatiotemporal dependencies among multi-reservoir systems, they are typically limited to single reservoirs [Liu et al., 2011]. Clearly, these rule curves do not acknowledge the full potential for coordinated operation between the reservoirs. By coordinating the operation of cascaded reservoirs, i.e. reservoirs in series, synergistic effects occur.

2.2. Agro-hyrological modelling

This section explains how the yield is related to the water resources uptaken by a crop. This relationship, which is described in a crop-water production function, is used in the proposed method to compute spatially the agricultural yields. The description of these functions in the next subsection will show that the yield depends on the ratio between potential and actual evapotranspiration and some crop specific characteristics. The methods used in literature to compute and describe these variables and characteristics are elaborated in the following paragraphs. This review makes clear that some of these methods, while usefull at field scale, are not applicable for planning models with longer time steps.

2.2.1. Crop-water production functions

Incorporating the responses of yields to varying levels of inputs is necessary to obtain a realistic representation of the economic benefits and the availability of resources [Lanzer and Paris, 1981]. At farm scale, a variety of models exist that describe the relationship between yield and the input supply. Some of these advanced models describe the yield as a function of added nutrients, water supply, soil conditions an environmental factors. Such models that include field conditions can be used to improve on-farm water management. However, when considering the use of water resources at regional scales, these are not applicable and simpler agricultural production models are needed.

Water production functions are a simpler and more convenient means to quantify crop responses with respect to the available water. These functions assume that inputs other than water, such as fertilizers and pesticides do no limit crop yields. Only water stress is assumed to affect the plant yield due to a reduction of leaf area and photosynthesis, and a slow down of root elongation [Verstraeten et al., 2008]. These functions may be formulated as a relation between the yield and (a) the depth of irrigation, (b) the total field water supply (sum of effective rainfall, irrigation water and soil storage) or (c) the actual evapotranspiration. The relation between the actual evapotranspiration and the crop yield appears to be linear [Stewart and Hagan, 1973; Hanks et al., 1980], and hence is most widely applied.

If a relation includes, besides the quantity of water deficits, also the timing of deficits, it is referred to as a dated water production function. These functions are more complex because they need to include the interaction of water stress in different periods. Therefore it is often assumed that water stresses act independent during the different growth stages, and that the combined effect is found by adding or multiplying the effects of 'independent' stresses [Rao et al., 1988]. Although these post evaluated dated relations have proven to predict crop yields quite well, the parameters of these functions need to be determined locally [Hill et al., 1987]. Because data to determine these parameters often lacks in developing countries, Doorenbos and Kassam presented a generalized water-yield relation in FAO paper No. 33 [Doorenbos and Kassam, 1979]. This relation has proven to be useful for general planning, design and operation of irrigation projects and for the rapid assessment of yield reductions under limited water supply [Steduto et al., 2012]. The relation uses a single empirical yield response factor (K_y) to integrate the complex linkages between water use and crop production. The yield response factor captures many biological, physical and chemical processes that influence the relation between production and water use by a crop. The response factor is crop specific and varies over the growing season [Steduto et al., 2012]. With Y_m and Y_a respectively the maximum and actual yield, ET_p and ET_a respectively the potential and actual evapotranspiration, the relation is given by:

$$\left(1-\frac{Y_a}{Y_m}\right)=K_y\left(1-\frac{ET_a}{ET_p}\right) \tag{2.1}$$

For application in irrigation scheduling, the effects of water stresses in N different growing stages need to be combined. According to Hill et al. [1987], a simple multiplicative model (Equation 2.2) is valid for most crops grown under irrigated conditions.

$$\frac{Y_a}{Y_m}=\prod_{i=1}^{N}\left(1-K_{y,i}\left(1-\frac{ET_a}{ET_p}\right)_i\right) \tag{2.2}$$

2.2.2. Maximum yield

In the description of the crop yields, a distinction is made between between the potential yield (Y_p), the maximum yield (Y_m) and the actual yield (Y_a). The potential yield is the yield of a cultivar grown in water and nutrient rich conditions and in absence of biotic stress. Potential yield is location and crop specific and determined solely by the prevailing climate conditions (temperature, radiation, CO2 and moisture regimes), the genetic traits and the extent to which these genetics are adapted to the prevailing climate. The potential yield does not depend on the soil properties assuming that these can be improved by proper management. The decrease from the potential yield to the maximum yield is, under non water and nutrient limited conditions, caused by biotic reduction factors (weeds, pests, diseases and pollutant) and management factors (sowing date, cultivar maturity, plant density, nutrient management and crop protection). Stated otherwise, the maximum crop yield is defined as the harvested yield of a crop fully adapted to its environment, where water, nutrients and diseases are not limiting [Doorenbos and Kassam, 1979]. The actual yield is defined as the yield of a cultivar grown in an average field. Therefore, it is exposed to limitations in water and nutrient supply in addition to biotic and management practices [Van Ittersum et al., 2013].

2.2.3. Potential evapotranspiration

Evapotranspiration is a combination process of evaporation from soil surfaces and transpiration by crops. The potential evapotranspiration Y_p is the evapotranspiration that would occur when crop-water requirements are fully met and depends solely on climatological parameters and crop characteristics. The main climatological parameters affecting evapotranspiration are radiation, air temperature, humidity and wind speed. Under identical climatological circumstances, the evapotranspiration differs between species and over the growth season because of differences in resistance to transpiration, crop height, crop roughness, reflection and ground cover.

A large number of (semi-) empirical locally calibrated methods are developed to compute the potential evapotranspiration for a variety of crops. These methods can be divided over five groups: empirical, mass transfer, combination, radiation and temperature based. The best applicable method depends on the application. The Penman-Monteith combination method is, despite its significant data requirements, generally considered to be most satisfying because it has a strong physical basis, as it results from a combination of mass and energy conservation, and the highest accuracy in lysimeter measurements [Luxemburg and Coenders, 2017; Oudin et al., 2005]. Therefore, and to overcome the limited global validity of other methods, the Penman-Monteith method is recommended by the FAO for computation of the potential evapotranspiration [Allen et al., 1998]. To enable the application of this method at locations with limited climate data, the FAO provides guidelines to estimate missing climate data. Alternatively they propose the Hargreaves equation to estimate the potential evapotranspiration in data scarce environments.

To seperate climatological effects from crop effects in the computation of the potential evaporation, and thereby obviate the need to compute unique resistance parameters for all crops and growth stages, a reference crop evapotranspiration ET_o is introduced. The reference crop is defined as a hypothetical grass surface with a height of 0.12 metre, a fixed surface resistance of 70 s/m and an albedo (reflectance) of 0.23 [Allen et al., 1998]. The potential evapotranspiration of all crops at all growth stages is related to the evapotranspiration from this reference crop by means of crop coefficient K_c:

$$ET_p = K_c \cdot ET_o \tag{2.3}$$

The crop coefficient combines specific effects of crop height, reflectance, resistance and soil evaporation. To incorporate the time dependency of crop characteristics, crop coefficients - under typical growing conditions - for four growth stages are specified in FAO paper No. 24 [Doorenbos, 1975]. A distinction is made between the initial, crop development, mid-season and late season stage (see Figure 2.3).

Although the crop coefficients vary predominantly with crop characteristics, they depend to a limited extent on management practices and climate conditions. Management practices are effecting the crop coefficient especially during the initial and crop development stages. As the ground cover is low during these periods, the effect of soil evaporation is -especially for frequent wetted soils- significant. Climate conditions are mainly effecting the mid and late season stage. The crop coefficient will be higher in more arid climates with high wind speed conditions, and lower in more humid climates with lower wind speeds. Although these climate and management effects may be neglected in general planning studies, it is recommended to refine the K_c values for in depth irrigation studies [Allen et al., 1998].

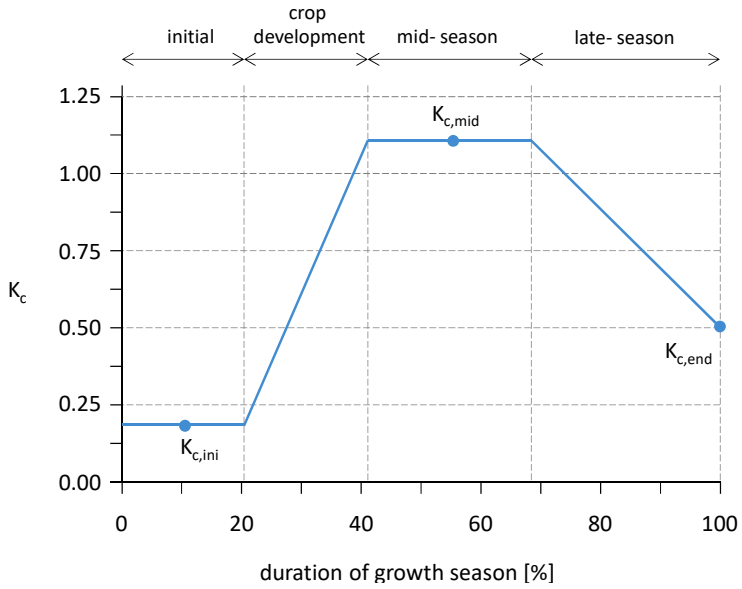

Figure 2.3: Crop coefficients for an imagenary crop over a single cycle cycle. Four stages are distinguished within a growing cycle. The crop coefficient is piecewise lineair function characterised by the values in the initial stage, the mid season stage and during harvest.

FAO Penmann-Monteith The Penman-Monteith method is, with the inclusion of crop resistance factors, derived from the Penman equation for open water evaporation and given by:

$$\lambda \cdot ET_\mathrm{p} = \frac{\Delta(R_\mathrm{n} - G) + \rho_\mathrm{a} \cdot c_\mathrm{p} \frac{e_\mathrm{s} - e_\mathrm{a}}{r_\mathrm{a}}}{\Delta + \gamma \left(1 + \frac{r_\mathrm{s}}{r_\mathrm{a}}\right)} \tag{2.4}$$

with R_n the net radiation, G the soil heat flux, ρ_a the air density, c_p the specific heat of air, Δ the slope of the saturation vapour pressure, $e_\mathrm{s} - e_\mathrm{a}$ the vapour pressure deficit, γ the psychometric constant, and r_s and r_a the surface and aerodynamic resistance.

The surface and aerodynamic resistance are functions of crop characteristics, and therefore differ over the growing season. Inserting the resistance parameter values of the reference crop in Equation 2.4 yields an expression for the reference evapotranspiration which only depends on climatological parameters. Given the geographical location, and daily-, weekly- or monthly data about air temperature, humidity, radiation and wind speed, the FAO reference evapotranspiration is given as:

$$ET_\mathrm{o} = \frac{0.408 \cdot \Delta(R_\mathrm{n} - G) + \gamma \frac{900}{T+273} u_2 \cdot (e_\mathrm{s} - e_\mathrm{a})}{\Delta + \gamma \cdot (1 + 0.34 \cdot u_2)} \tag{2.5}$$

with T the temperature in degree Celsius and u_2 the wind speed at an elevation of two metres.

2.2.4. Actual evapotranspiration

The actual evapotranspiration in agricultural fields differs from the potential evapotranspiration, as it accounts for soil water deficits. As long as soil water is available for the crop, the actual evapotranspiration equals the maximum evapotranspiration. However, a reduction of the soil water content will gradually reduce the actual evapotranspiration [Steduto et al., 2012].

Several functional relationships, which express the actual evapotranspiration as a function of potential evapotranspiration and soil moisture, exist. The most widely adopted and preferred relation is given in FAO paper No. 56 by Allen et al. [1998]. The effects of soil water stress are described by multiplying the potential evaporation by the water stress coefficient K_s:

$$ET_a = K_s \cdot ET_p \tag{2.6}$$

The water stress coefficient K_s is a piecewise linear function of the moisture content (see Figure 2.4 line A). The coefficient value equals unity over the Readily Available Water (RAW) domain, and decreases to zero over the remainder of the Rotal Available Water (TAW) domain.

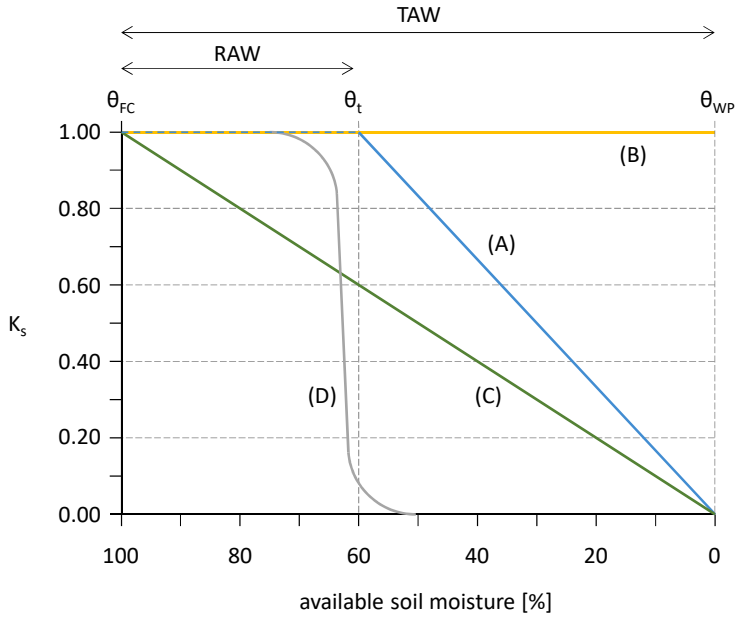

Figure 2.4: Different relationships between the actual evaporation and the soil moisture. The figure shows the relation proposed by Allen (A), Veihmeyer and Hendrickson (B), Thornthwaite (C), and Penman (D) (Figure based on Allen et al. [1998]; Ward and Robinson [1967])

The total water available for plant uptake is defined as the storage in the root zone between the field capacity and permanent wilting point. The field capacity (θ_{FC}) indicates the moisture content which can be retained against gravity by the top layer of the ground. After a precipitation event, all moisture retained above the field capacity is lost by deep percolation. The remaining water is in the course of time taken up by the plant roots or evaporated, gradually drying the ground. The dryer the soil becomes, the more tightly the remaining water is retained to the soil matrix, and the more difficult for a plant to extract it. The wilting point (θ_{WP}) is the soil moisture content at which it is no longer possible for plants to absorb water from the soil matrix. The storage in the soil matrix between field capacity and wilting point differs between soils and is given by a soil moisture characteristic. This characteristic gives the relation between the moisture content ($\theta = V_{water}/V_{soil}$) and the suction pressure (pF $= \log_{10}$(h) with h in [cm]). The suction pressure at field capacity differs between soils and ranges between 1.8-2.2. The permanent wilting point is for almost all soils characterised by a pF of 4.2 [Brouwer et al., 1985; Savenije, 2014].

Although water is theoretically available for uptake over the whole TAW domain, stronger bonds with the soil matrix reduce water uptake well before the wilting point is reached. The moisture content at which the crop begins to experience water stress is defined as the threshold moisture content (θ_t). The available storage between the field capacity and this threshold is referred to as the readily available water, and given as a fraction of the total available water: $\text{RAW} = p \cdot \text{TAW}$.

The value of the factor p differs between crops, and is to a small extent dependent on the climate conditions and the soil characteristics. For hot dry weather conditions, with high evaporative power, p is 10-25% less than under standard conditions, causing water stress to occur even when the soil is relatively wet. When the crop evapotranspiration is low, p will be up to 20% more than under standard conditions. For fine textured soils (clay) the standard p values should be reduced by 5-10%, while for more coarse textured soils (sand), they should be increased by 5-10% [Allen et al., 1998]. Besides the relation given in FAO paper No. 56, several other relations between soil moisture content and actual evaporation have been proposed. Figure 2.4 depicts, besides the FAO relation, also the relation according to: Veihmeyer and Hendrickson (line B), Thornthwaite (line C), and Penman (curve D) [Ward and Robinson, 1967].

Independently of the relation used to compute the actual evaporation from the potential evaporation, a daily computation of the soil moisture content is required. For agricultural fields, a simple bucket model without lateral flow is suggested in FAO paper NO. 56. Effective precipitation, irrigation and capillary rise add water to the root zone, while actual evapotranspiration, runoff, infiltration and deep percolation remove water from the root zone. Runoff, infiltration and effective precipitation are site specific. The deep percolation flow is assumed to be zero unless the moisture content exceeds the field capacity. If the moisture content is larger than the field capacity, the deep percolation flow assures the moisture content to be at field capacity at the beginning of the next day. Capillary rise may, if the water table is more than one metre below the bottom of the root zone, be assumed to be nonexistent.

2.3. Food loss

Approximately 32% of all food mass produced globally is wasted. Expressed in calories, the numbers are even more shocking as approximately one out of every four calories grown to feed people is not consumed [Gustavsson et al., 2011; Lipinski et al., 2013]. The causes for and the extent of food loss vary throughout the world and are strongly dependent on the specific socio-economic conditions prevailing in a given country. Where food loss is in itself a challenge for global food security, it is even more challenging from a WEF-nexus point of view. With the latter point of view, food losses do not only represent a loss of caloric value, but as well a loss of the required land, water and energy resources.

Food loss refers to the parts of vegetative and animal products that are harvested or produced for human consumption, but due to losses in the Food Supply Chain (FSC) never reach the customer. In this study is the term food loss used for all losses occurring in the FSC. However, often a distinction is made between food loss and food waste. Food loss is the loss of edible food products due to spills or quality reduction during the production, postharvest and processing stages in the food supply chain, i.e. the losses in the supply chain before the products reach the customer. This loss is the unintended result of an agricultural process or technical limitation in storage, infrastructure, packaging, or marketing. Food losses occurring in the latest links of the FSC are referred to as food waste. It concerns food that, although qualitative fit for human consumption, does not get consumed and is discarded. These losses are related to retailers' and consumers' behaviour [Gustavsson et al., 2011; Lipinski et al., 2013].

In a further division, all losses in the FSC can be divided into five groups, being losses during: agricultural production, transportation and storage, processing, distribution and consumption [Gustavsson et al., 2011]. Agricultural losses occur due to damage or spillage during harvest operation. Transporation and storage losses are the result of spillage and degradation during storage and transportation between farms, storage and processing facilities. Processing losses are related to industrials and domestic food processing like canning, slicing and pressing. The last two represent the losses caused by distribution in the market system and waste at household level. This subdivision is important to propose a tailor-made solution for the food losses. In general, for more developed countries, the food losses in the first links of the FSC decrease. However, this is due to the increased prosperity at

the expense of an increase in losses during distribution and consumption. This division of food losses will be used in the proposed methodology to compensate for the losses in the food balance. All five groups have their own unique implemenatation in the framework, of which solely the transportation and storage losses will be incorporated explicitly.

2.4. Model predictive control strategies

Model Predictive Control (MPC) is a model based control strategy, which finds its origin in the chemical and process industry, where products are fabricated within small well-defined operating limits. Because ordinary feedback controllers fail when working close to constraints, model based control strategies were introduced. By adding information on the internal system into the control process, constraints can be explicitly accounted for [Camacho and Alba, 2013], enabling the system to operate stably close to the limits [Van Overloop, 2006]. Because the control structure is not defined in advance, automatic adjustments of the control structures can be made on the basis of given controller objectives, constraints and actual operating conditions, giving MPC techniques a high degree of flexibility [van den Boom and Backx, 2010]. The model predictive control strategies operate a process such that unwanted dynamic properties are acted on and compensated before they occur [van den Boom and Backx, 2010; Van Overloop, 2006]. In addition can MPC techniques easily be adapted to changes in systems dynamics, because changing model specifications do not require a complete redesign of the controller [Gorinevsky, 2005]. The latter properties of the MPC technique are favourable features in the control of water systems.

Although often referred to as a single technique, model predictive control is better referred to as a collection of control strategies following a similar methodology. According to van den Boom and Backx [2010], five features present in every MPC controller are: (1) a model of the internal system and external disturbances; (2) a performance measure or objective function; (3) constraints; (4) an optimizer; and (5) a receding optimization horizon.

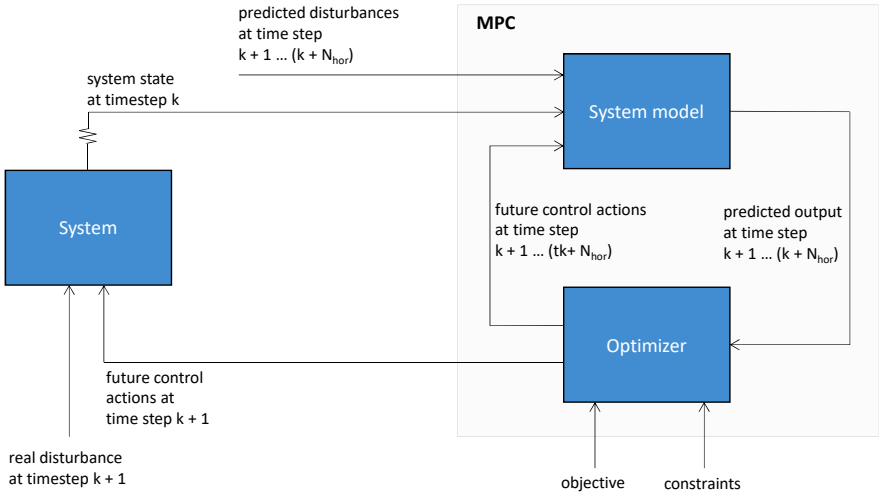

Figure 2.5: The working principle of a discrete time implementation of the MPC technique. The system's state is used to compute the optimal set of control actions while being subjected to predicted distrubances and constraints. The first actions of this sequence are used to control the system.

The internal system is the part of the control system which can be affected by control actions. It will be used to estimate future system behaviour and predict state and output signals [van den Boom and Backx, 2010]. Different MPC strategies can use different model representations for the relations between model outputs and measurable inputs in the internal systems. Most used model formulations are impulse response functions, steps functions, transfer functions, state space representations and non-linear models [Camacho and Alba, 2013]. The presence of a model is essential for the operation of a MPC system, but at the same time its major drawback. After all, the reliability of the model results depend on the accuracy and truthfulness of the model design. Therefore, MPC is only applicable when

one has a clear insight in the system dynamics [Rawlings, 2000]. External disturbances are factors that affect the internal system dynamics, but cannot be controlled. A disturbance model is required to describe the behaviour to non-measurable inputs.

The objective function, constraint and optimizer are all part of an optimization algorithm. This algorithm computes, over an optimization horizon, a sequence of future control signals -subject to the stated constraints- that minimizes or maximizes the objective function. From the optimal control sequence, only the first (few) control actions are applied to the process. Afterwards, the horizon is shifted one timestep and the optimization is restarted with the most recent states as initial conditions of the optimal control problem [van den Boom and Backx, 2010; Alessio and Bemporad, 2009]. This principle is referred to as the receding horizon principle. To prevent a system from becoming unfeasible due to uncertain disturbances or internal dynamics, robust model approaches can be applied. These methods aim to guarantee a minimal model performance and stability in the presence of bounded modelling errors [Herzog and Keller, 2011]. The latter can be achieved by relaxing some outputs constraints and treating them as soft constraints [Rawlings, 2000].

The working principle of a MPC technique is explained in Figure 2.5. At discrete timestep k are the systems states used as input for the MPC controller. A set of future control actions over the optimization horizon $k+1 : k+N_{\text{opt}}$ is together with the predicted disturbances over this timeframe used to predict the system's response and future outputs. By defining a new set of control actions based on the predicted outputs in an iterative process, the optimization function can determine the optimal control sequence that satisfies the constraints. From the optimal control sequence, the first actions are used to operate the system at time instance $k+1$. Because the real disturbances deviate from the predicted disturbances, will the actual system state at time instance $k+1$ not correspond with the predicted system states. Therefore, a new optimization round takes place in which the system states are updated. By using the predicted control actions from the previous time instance as the starting point for the optimization (warm starting), the required computational time for the optimization can be reduced significantly [John and Yıldırım, 2008].

2.4.1. Optimization techniques

An optimization problem is generallly stated by the standard form in Equation 2.7. The goal of the optimization is to find the set of optimization variables x that minimize the objective function $f(x)$ while being constrained by inequality constraints $g(x)$ and equality constraints $h(x)$.

$$\begin{aligned} \min_{x\in\mathbb{R}} \quad & f(x) \\ \text{s.t.} \quad & g(x) \leq 0 \\ & h(x) = 0 \end{aligned} \tag{2.7}$$

A wide variety of optimization techniques can be used to perform the optimisation required within the MPC. However, not all techniques are equally useful in complex multi-reservoir systems. Linear programming techniques are efficient for large scale problems but require all constraints and the objective to be linear. Although the world is not linear, many problems can be approximated by a linear system in an appropriate mathematical way by means of a linearization. Unfortunately, due to the nonlinear relationship for hydropower generation, reservoir systems are by definition a nonlinear problem. A proper mathematical formulation of this system therefore requires either nonlinear objective functions or nonlinear constraints.

Nonlinear models are inherently much more difficult to optimize compared to linear programming. Figure 2.6 illustrates the search space of a two variable linear and nonlinear problem. For a linear system are the optima restricted to the corners of the feasible region, while a minimum could appear anywhere in the search space in case of nonlinear systems. In addition, a linear system is characterised by the presence of a single optima in the feasible search space, while for nonlinear problems multiple (local) optima may be present. Moreover, due to the non-linear objectives and constraints, these optima can be found in various disconnected (discontinguous) feasible regions [Chinneck, 2015].

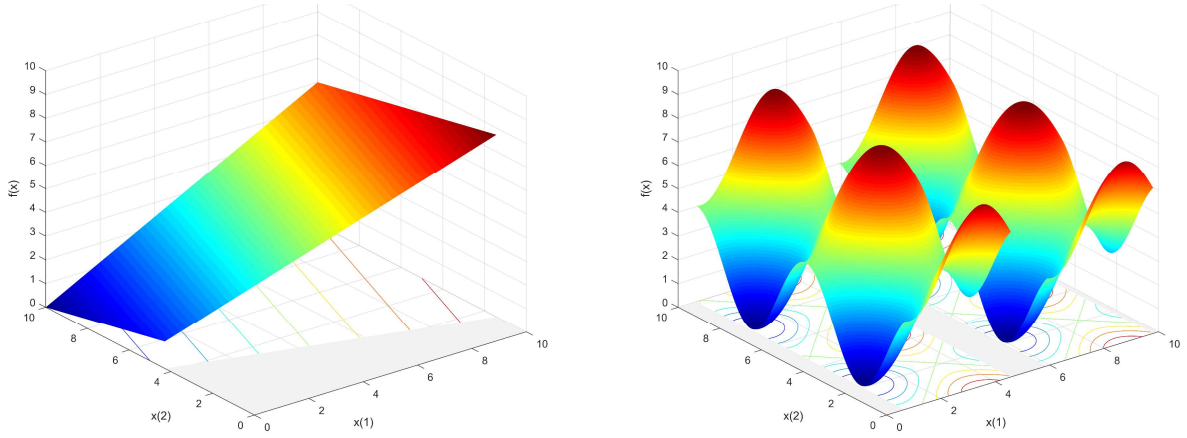

Figure 2.6: An example of the search space for a linear and nonlinear problem. The contour on the bottom of the surface graph shows the location of the maxima en minima. The grey area illustrates the infeasible part of the search space. The left figure shows the search space for the linear function with $f(x) = 0.6 * x_1 + 0.2 * (10 - x_2)$ subjected to the constraint $0.2 * x_1 + 0.7 * x_2 > 3$. The right figure illustrates the non linear search space for $f(x) = 4 + 2 * \cos(1.2 * (10 - x_2)) + 2 * \sin(1.2 * (10 - x_1))$ subjected to $\cos(1.2 * x_1) < 0.7$. This function shows multiple local minima within multiple feasible regions.

As long as the system only consists of smooth functions, one or more of which are non-linear, roughly two methods can be applied: Non Linear Programming (NLP) and Global Optimization techniques (GO). NLP solvers exploit the problem's smoothness by computing the gradient, and move based on this information in the direction of the negative gradient. Using first and second partial derivatives the solvers accounts for the feasibility, duration and curvature of the constraints and objectives [Solvers, 2016]. The disadvantage of these gradient based methods is that the algorithms are very short-sighted. They will always move in the direction of a minima in the direct vicinity of the starting point. As a results, they can only converge to local minima. In addition, the minimum found depends on the user specified start position. Only when the search space is convex are NLP solvers guaranteed to converge to the global minimum. For these problems are NLP solvers, up to very large size, most efficient. In case of non-convexity (local convexity), the computational time increases due to the multiple feasible regions and points within these regions. There is a variety of available NLP solvers, but the performance of each algorithm is problem specific. However, in general it can be stated that interior point methods are very effective on the largest problems [Solvers, 2016; Bradley et al., 1977]. For small non convex nonlinear problems, GO techniques offer a suitable alternative. This method includes multistart techniques and nature based algorithms (e.g. genetic algorithms). These methods provide a limited guarantee that the global solution will be found, but at the price of high computational demands [Solvers, 2016].

In the following chapters it will become clear that besides hydropower, agriculture and some other functions require a nonlinear implmentation as well. Moreover, a large number of optimization variables is required to integrate the spatial and temporal variability. Interior point techniques are therefore employed to optimize these large nonlinear problems.

2.4.1.1. Complementarity problem

A complementarity constraint is specific mathematical problem type occurring in optimization. It is a problem between two vectors (X and Y) of positively bounded variables (x_i and y_i) subject to the orthogonality requirement, i.e. the inner product of the vectors should be equal to zero. Hence, for each variable pair x_i and y_i, at least one of the variables must be zero [Erleben, 2013]. This is compactly written in the notation:

$$0 \leq y \perp x \geq 0 \tag{2.8}$$

The search space of such an complementarity problem is therefore formed by the positive x and y axis. If the variable pair x_i and y_i is part of a linear relationship as well, the problem is referred to as a linear complementarity problem [Erleben, 2013]. These linear complementary problems appear in the proposed methodology for, among other things, the definition of reservoir spill flows and the limitation of energy generation. Mathematically, these problems are noted as:

$$y = a \cdot x + b \tag{2.9}$$

$$y \geq 0, \quad x \geq 0, \quad x \cdot y = 0 \tag{2.10}$$

The resulting search space can be visualized by projecting the linear relationship on top of the boundaries of the first quadrant (see Figure 2.7). Depending on the value of the slope a and offset b of the linear relationship, there is a (unique) solution. The search space of a feasible problem is therefore limited to one or two points. This feature makes linear complementarity problems non smooth and hard to solve with nonlinear problem solvers [Betts, 2010]. A typical work around this non-smoothness problem is to include the complementarity constraint as a soft constraint [Celeste and Billib, 2010].

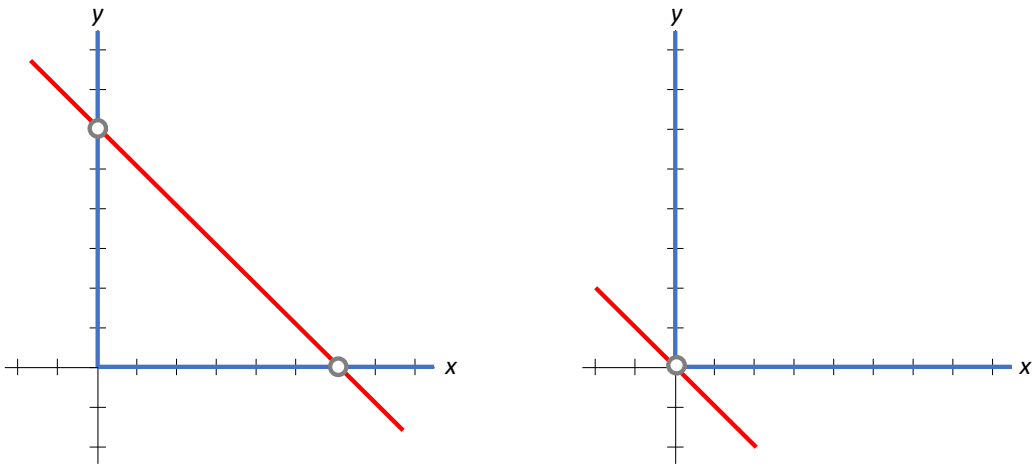

Figure 2.7: An example of the search space for a complementarity constraint. The blue lines bordering the first quadrant indicate the search space for the complementarity of the x and y variables. The red line indicates the linear relation between the variables. Depending on the value of the slope and offset, the search space will consist of two (left) or one (right) fesible point.

3
Methodology

A new framework (referred to as the proposed methodology) for studying the value of cooperation in transboundary river basins is presented. In this method, the strengths of WEF-nexus models and hydro-economic models are combined. The whole has a time-variant implementation whereby social and infrastructure events can be studied not only on their own, but as part of a pathway. A node-link network is used to explicitly integrate the river flow and the existing river infrastructure into the water balance of a spatially explicit WEF-nexus model. Therefore, in contrast to the other national balances, the water balance is described at infrastructure level. Although the proposed method works with national balances for energy and food, agriculture is described spatially explicitly. A novel framework has been developed to describe both irrigated and rain-dependent agriculture in great detail on a regional scale. In this way, a better description for crops with multiple growth cycles per season can be guaranteed and a distinction can be made between the management of annual and perennial crops.

The proposed method uses both simulation and optimization techniques. Optimization is used within simulation experiments to determine the most optimal resource use. Optimality is hereby defined as the allocation that results in the maximum nationwide economic benefits, while being constrained by physical, hydrological, dietary and institutional constraints. Using local variables and indices, the problem is mathematically described as:

$$\begin{aligned} \underset{x_t,u_t}{\text{maximize}} \quad & I = \sum_{t=1}^{T} b_t(x_t,u_t) - s_t(x_t,u_t) \\ \text{subject to} \quad & f_t(u_t) \leq 0 \\ & g_t(x_t) \leq 0 \\ & h_t(x_t,u_t) = x_{t+1} \end{aligned} \tag{3.1}$$

where T is the length of the optimization horizon, b_t the aggregated benefits from food and electricity production and trade, s_t the penalty value of soft constraints, x_t the vector of state variables (e.g. reservoir capacity and food storage capacity), u_t the vector of decision variables (e.g. turbine flow, water withdrawals, cropping patterns, fossil fuel consumption, trade flows, etc.), f_t a set of funtions constraining the decision variables, g_t a set of functions constraining the state variables and h_t a set of functions guarenteeing resource continuum.

Soft constraints are on the one hand used to circumvent complementarity constraints for the reservoir spillway and filling dynamics and on the other hand to increase the robustness of the system (e.g. the inclusion of the hedging dynamics to prevent too low reservoir levels and the description of required cross border flows in dry years).

In the proposed framework, MPC is applied in a receding horizon implementation, where the input sequence that yields an optimal predicted output, while simultaneously satisfying all the constraints, is computed using predicted weather and demand conditions. Receding horizon control accomplishes feedback against uncertain disturbances (e.g. deviations in climate forcing) by applying only the optimal outputs in the first instance of the horizon in simulation and then updating the system states using new information. As the prediction horizon slides along, this process of feedback control using new measurements, prediction and control optimisation is repeated. This process is generally inherently robust to some uncertainty, and good closed loop performance is expected with the simulation model if the water availability and water demand do not change drastically. In addition to the feedback control, this control technique enables information exchange between states within each MPC iteration. This

allows us to add two new cooperation scenarios between the often studied scenarios of unilateralism and full coordination, with which the value of information exchange on river flows and trade flows can be studied. The impacts and benefits of these cooperation scenarios are studied by means of simulation experiments. In addition to these cooperation scenarios, the framework offers a wide range of predefined optimization settings and options to investigate the impacts of, among others, changing diets, population growth and agricultural self-sufficiency.

The method is further elaborated in the following sections and paragraphs. After clarifying the balances used and the system's scales and boundaries, the dynamics of each balance are explained. This is followed by a description of the model predictive building blocks and concluded with the introduction of (new) cooperation scenarios.

3.1. WEF-interactions and system boundaries

A nexus model is a simplification of a complex world with many interactions. The first and most important step in setting up a nexus model is therefore to determine the (scale of the) relevant balances, interactions between these balances and the location of the system boundary. To study the value of regional cooperation in river management, where national interactions are of less importance, national balances are sufficient. The proposed methodology therefore uses a national energy and food balance. The choice for the active stocks and drivers in the balances is further explained in the next section, followed by a description of the system boundaries present.

3.1.1. WEF interactions

Figure 3.1 depicts a relational diagram illustrating the actions and drivers included in the proposed methodology along with the main assumptions/simplifications. Both current and omitted relationships are discussed briefly per balance in the paragraphs below.

3.1.1.1. Water balance

Due to the scarce availability of hydrological models at regional scale, the description of the available water has been disconnected from hydrology. The direct relationship with precipitation, evaporation and land use is therefore lost. For this reason, the description of the groundwater is completely left out of the analysis. After all, without a good model it is impossible to describe which part can and which part cannot be sustainably extracted. The description of the available river water is based on runoff, which is required as input data. While moving in downstream direction, the available flow is further corrected for seepage and evaporation losses. The available water in time and space is changed due to irrigation and hydropower consumpton and usage. Domestic, industrial and environmental flow demands are neglected because they are small compared to irrigation demands, and their value is difficult to describe in economic terms [Ramanan, 2018].

3.1.1.2. Energy balance

The focus of the energy balance is on the electricity generation and consumption. After all, unlike for sustainable generation by means of hydropower plants, other forms of energy generation do not have a direct relationship with the available river flow. Electricity production is directly driven by the electricity demand. The effects of supply and demand on the electricity price and vice versa are therefore left out of the model. Regional electricity demand is, however, influenced by the interaction between the international trade price and the costs of power shortage. National demand, on the other hand, is defined as data and is independent of the GDP, the number of inhabitants and the industry present. Where in reality the electricity production capacity is determined by the expected electricity demand, the capacity of both the sustainable and non-sustainable forms of generation as well as the international transmitters must be predefined. Hence, the dependence on energy demand is lost, causing the available capacity only to have a limiting effect on production.

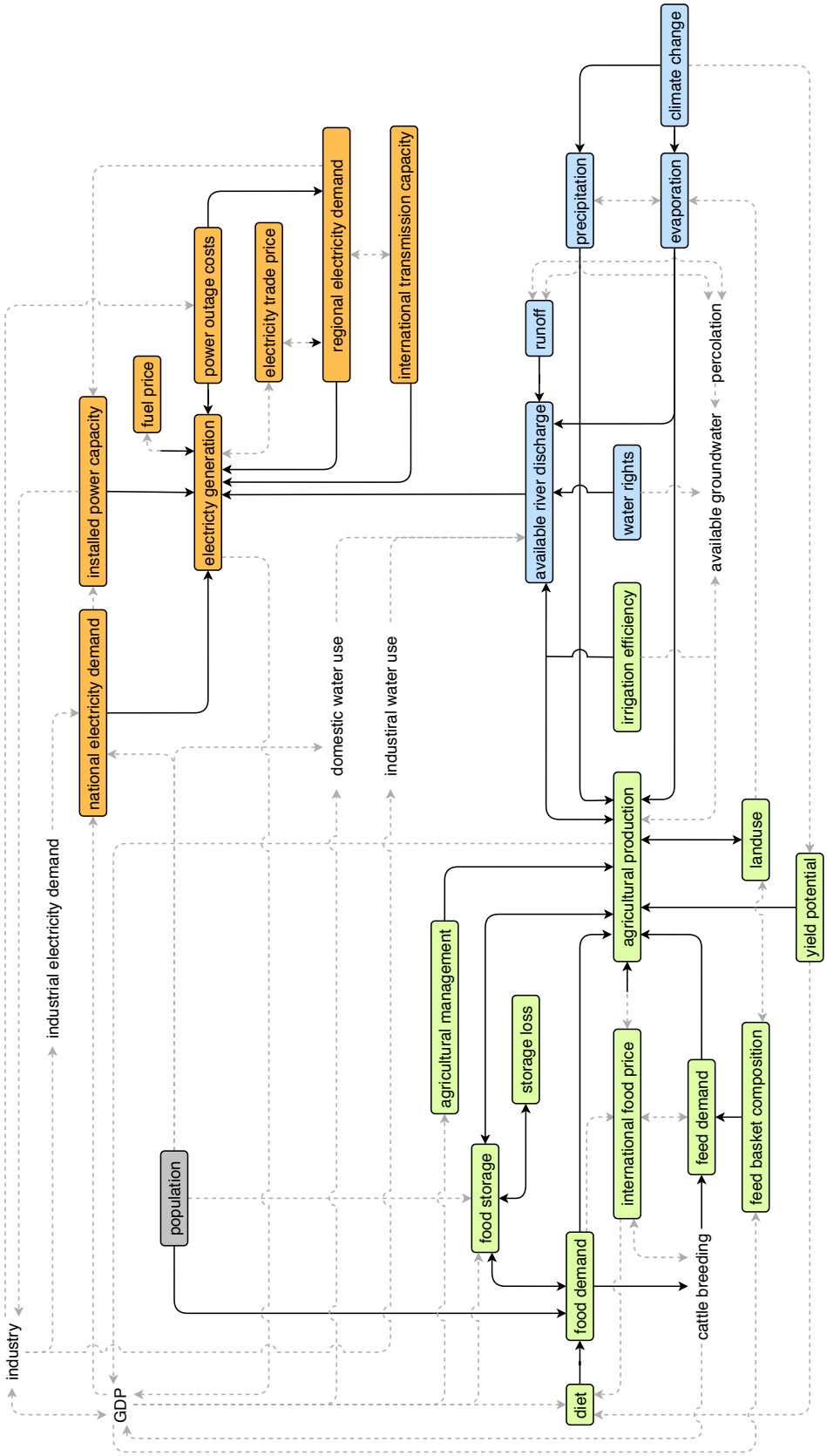

Figure 3.1: A relational diagram showing the implemented relations and major assumptions/simplifications in the proposed methodology. The text boxes represent actions and drivers which are included in the setup, while the strings without a box are not. The full black lines depict the included relations, while the grey lines show the relations not included due to the mentioned simplifications. The orange, green and blue colors represent whether a factor is part of the energy, food or water balance respectively.

3.1.1.3. Food balance

Agricultural production is central to the food balance. Both rain-dependent and irrigated production facilities have been implemented. Production depends on the attainable agro-climatic yield and management practices. However, their relation with changing climate conditions and GDP is neglected. Production is driven by national demand (for both food and feed) and international trade prices. The reverse interaction, in which production influences the price, is disregarded. National production depends on dietary requirements and population size. Although the diet actually relate to GDP, land use and agro-climatic crop feasisibility, it is prescribed as data. Livestock farming, required to meet animal dietary requirements, has been implemented indirectly. The demand for animal products has been converted into vegatative product quantities required for animal feeding. These quantities depend on the composition of the feed basket. Also this composition is described as input data, causing the direct interaction with land use and GDP to be lost.

3.1.2. System boundaries

Because the boundaries of transboundary river basins do not usually correspond with national borders, integrating a transboundary river into a WEF-nexus model results in a wide variety of system boundaries. This section explains the different geographic regions using Figure 3.2.

All countries bordering or providing passage to the considered transboundary river are included in the proposed method, and described by the mathematical set S. The area within the national borders is divided into one or more river basins. One of these river basins concerns the considered transboundary river basin. The others are referred to as *outside basins*, and are described in the mathematical set B. All water infrastructure in the main catchment, like the river flow, is described in a directed node link network. Flow in the links, connecting the nodes, is only possible in the downstream direction. The type of nodes occurring in the network are further explained in Section 3.2.1.

Because the river flows in outside basins are not explicitly included in the method, the contributions of the water infrastructure present in these basins are implemented differently than the infrastructure within the main river basin. Capacities of all hydropower installations outside the main basin are bundled, and the generation is described by use of a capacity factor (see Section 3.2.3.1). Irrigated agriculture is described per outside basin. All available irrigation capacity is bundled in one point per basin. The characteristics (e.g. maximum yield, growth duration, etc.) of this irrigated agricultural field equals the area weighted average of the plantations present in the considered outside basin. Because the water availability in these areas is not fully described in the model, the liberal assumption has been made that these fields never experience water stress.

In addition to the basin boundaries, other system boundaries are located within national borders. These bounderies are used to describe rainfed agriculture. To reduce the number of variables, the rain-dependent agricultural areas have been merged into clusters. A single cluster is referred to as *rainfed pixel r* in the set of all rainfed pixels R. As for the clustered irrigation fields outside the main catchment, the characteristics of a rainfed pixel correspond to the area weighted average of all rain dependent fields within this cluster. Each rainfed pixel is forced with the climate conditions prevailing at the centre point of the rainfed pixel.

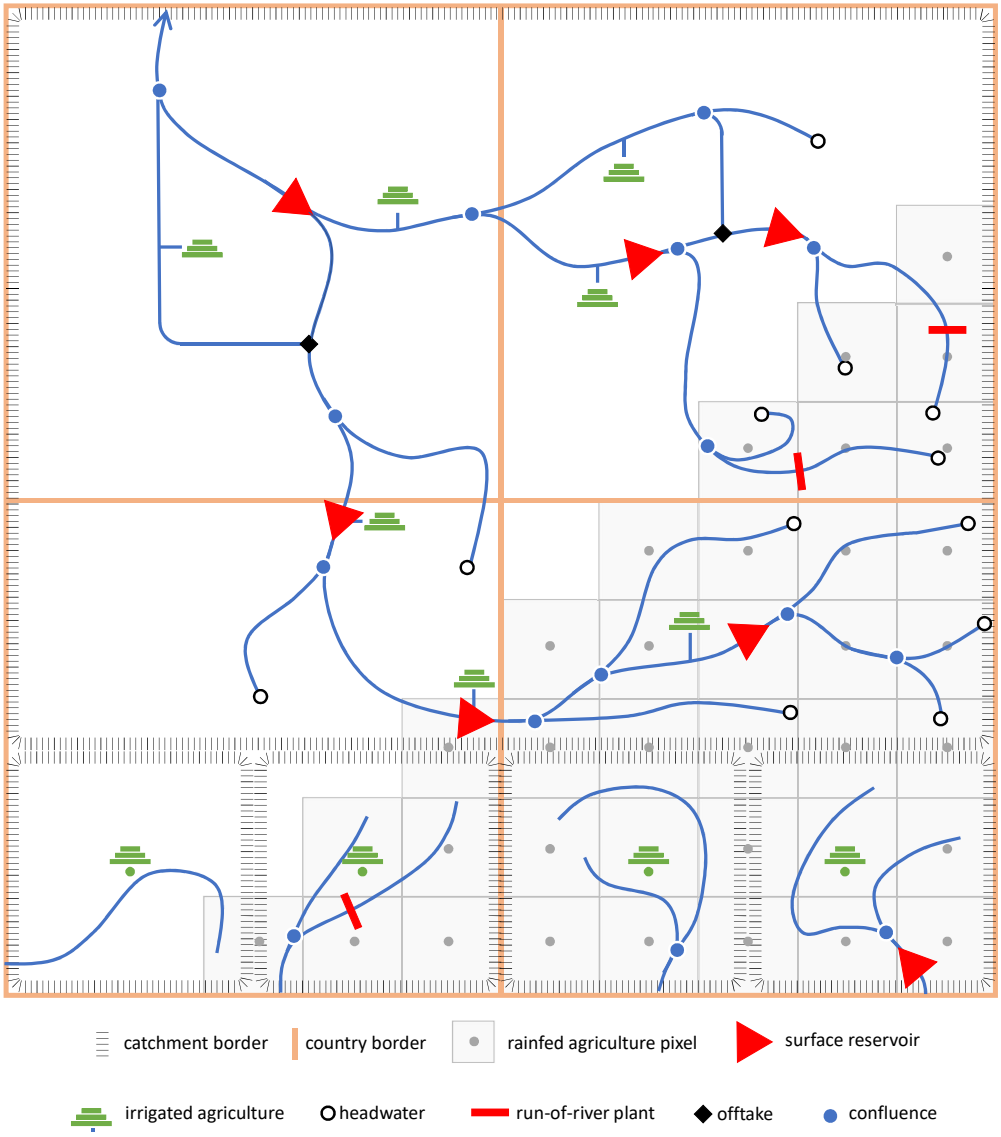

Figure 3.2: A graphical representation of the different geographical regions and their borders and the link-node network with all possible node types.

3.2. System dynamics

This section introduces the dynamics of the water, energy and food balances. These balances are all implemented in a time-variant way, making it possible to study specific infrastructural and social pathways. The water balance describes the dynamics of each node in the node-link network. Unlike most hydro-economic models, river routing is explicitly described. Thereby, the methodology accounts for river flow delays and associated seepage and evaporation losses. The food balance describes the demand, production and trade of food products. A new method has been developed to describe the agricultural production. This method, based on the FAO guidelines, describes agriculture in a spatially explicit manner on a regional scale while accounting for the differences in management between annual and perennial crops. As a result, each rainfed an irrigated site is characterized by a unique set of feasible crops and characteristics for that location. In addition, the new method enables multi-cut crops to grow several cycles within a growing season. Finally, the energy balance describes the interaction between the generation and consumption. Hereby, each generation type has a unique implementation that matches the dynamics of the considered plant.

3.2.1. Water dynamics

The water component of the WEF-nexus is integrated in the proposed framework as a node-link network (see Figure 3.2). The nodes represent all locations where water is stored, demanded or diverted and the linkages represent flows routed between these nodes. The proposed framework distinguishes six node types: surface water reservoirs, run-of-river hydro-electric plants, offtakes, irrigation sites, confluences and source nodes. These nodes can occur separately, but combinations are possible as well. To allow the existing river infrastructure to vary over the model period, the *inactive node* has been defined in addition to the aforementioned node types. In this way, a node is always present at the locations where new infrastructures become active during simulations. However, these nodes show different system behaviour in the periods before and after their commissioning date. In the following paragraphs, the mentioned node types are discussed in further detail. However, before the characteristics of the node types will be clarified, first the flow routing between the nodes is explained.

3.2.1.1. River routing

Because many existing hydro-economic optimization models work with time scales that are equal to or greater than the concentration time of the studied river flow, river routing and the associated delays and losses are not included. The method proposed in this report does account for these delays and losses associated with river flow. However, the framework does not make use of a detailed hydrological model (e.g. Muskingum) [Koussis, 2009]; instead a simple First In First Out (FIFO) delay function is introduced for the river branches. A simple approach is preferred because more detailed models require more (specific) data, which is often not available on regional scales. In addition, a large number of optimization variables are required for such methods [Lugt, 2018].

In the implemented FIFO delay function, each river segment is described by only three characteristics; a length (l_{river}), an average flow velocity (v_{river}) and a loss factor (c_{flow}). The river stretch (link) is modelled as a storage queue, where inflow is enqueued at the tail (upstream) end and outflow is dequeued at the head (downstream) end (see Figure 3.3). The outflow is therefore made up of the summation of fractions of the past inflows. These inflows in the river stretch are equal to the outflow of the node at the upstream end of the directed link. An additional advantage of this method is that it is able describe flood propagation to a certain extent. The summation of delayed inflows over multiple time steps namely causes an increase in discharge (flood wave) to propagate faster through the network than the average flow velocity, and a decrease in discharge to propagate slower than the average flow velocity.

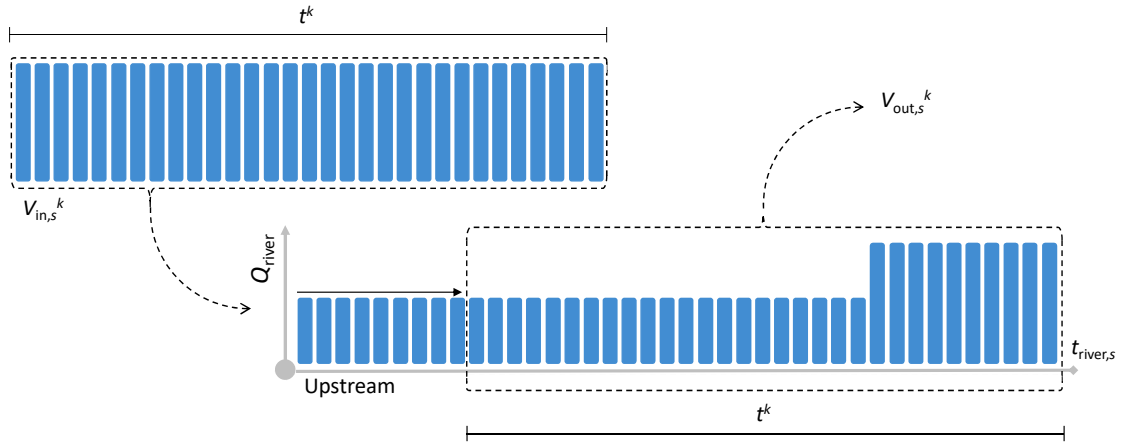

Figure 3.3: Schematic representation of the river delay (queue) function. The new inflow with duration t^k is added at the tail end of the queue (upstream). The last t^k days in the queue are removed and represent the outflow at time step k.

As mentioned, the outflow from river stretch $m \in \text{M}$ during time step k is the sum of past inflows fractions into this river stretch. The magnitude of these fractions depends on the flow duration and evaporation and seepage losses over the stretch. The outflow from is stretch is described by:

$$V^k_{\text{out},m} = \sum_{\tau=0}^{N_{\text{hist},m}} f^k_{\text{routing-loss},m,\tau} \cdot V^{k-\tau}_{\text{in},n} \tag{3.2}$$

with k the index for the time step since the start of a simulation experiment, V_{in} and V_{out} respectively the in- and outflow from the stretch, N_{hist} the number of past time steps from which water could be stored in the stretch, and $f^k_{\text{routing,loss}}$ the fraction accounting for the effects of routing delay and evaporation and seepage losses. The latter two are described by the following equations:

$$N_{\text{hist},m} = \left\lceil \frac{t_{\text{river},m}}{\min\left(t^1, ..., t^{end}\right)} \right\rceil \tag{3.3}$$

$$f^k_{\text{routing-loss},m,\tau} = f^k_{\text{routing},m,\tau} \cdot f_{\text{loss},m} \tag{3.4}$$

with t_{river} the concentration time (duration) of flow in a river stretch ($l_{\text{river}}/v_{\text{river}}$), t the duration of a timetep, and f_{routing} and f_{loss} the fractions accouting for the routing delay and losses respectively.

Because the losses caused by seepage and evaporation (c_{flow}) are constant per river length, the magnitude of the outflow, as a fraction of the inflow, depends solely on the length of the river stretch:

$$f_{\text{loss},m} = (1 - c_{\text{flow},m})^{l_{\text{river},m}} \tag{3.5}$$

The routing delay fraction f_{routing} learns us which part of a historical influx is positioned at the tail end of the queue, and will leave the river storage during the current time step. This depends on the duration of the historical inflow, and the concentration time of the river stretch. The fraction for routing delay is described by:

$$f^k_{\text{routing},m,\tau} = \max\left(0, \min\left(f^k_{\text{store},m,\tau} \cdot t^{k-\tau}, t^k - \sum_{\gamma=\tau+1}^{N_{\text{hist},m}} f^k_{\text{store},m,\gamma} \cdot t^{k-\gamma}\right)\right) \cdot \frac{1}{t^{k-\tau}} \tag{3.6}$$

with f_{store} the fraction of a past inflow being stored in the river segment after inflow but before outflow in the current time step. The fraction of a past inflow being stored in the river stretch is given by:

$$f^k_{\text{store},m,\tau} = \max\left(0, \min\left(t^{k-\tau}, t_{\text{river},m} + t^k - \sum_{\gamma=0}^{\tau-1} t^{k-\gamma}\right)\right) \cdot \frac{1}{t^{k-\tau}} \tag{3.7}$$

Now that the outflow of a river stretch has been defined, the definition of the inflow into a node follows. The inflow at node $n \in \mathrm{N}$ is the summation of the outflow over the set M_n of all river stretches adjacent and upstream of this node:

$$V_{\text{in},n} = \sum_{m \in \mathrm{M}_n} V^k_{\text{out},m} \tag{3.8}$$

3.2.1.2. Surface water reservoir node

A surface water reservoir is defined as an artificial lake behind a man-made structure. A schematic representation of a reservoir node $j \in \mathrm{J}$ is shown in Figure 3.4. A reservoir is characterised by its level - surface area - storage relation, the capacity and elevation of outflows. A reservoir can release flow via: (1) the turbine; (2) the main gate; (3) the spillway; and (4) the backwater gate. Discharge released via one of the first three mentioned outflows ends up in the main river downstream of the reservoir. The outflow from a surface reservoir node is therefore given by:

$$V^k_{\mathrm{out},j} = V^k_{\mathrm{turb},j} + V^k_{\mathrm{gate},j} + V^k_{\mathrm{spill},j} \tag{3.9}$$

with V_{turb} the outflow via the turbine conduit, V_{gate} the flow leaving the reservoir via the gate conduit and V_{spill} the flow spilling over the overflow.

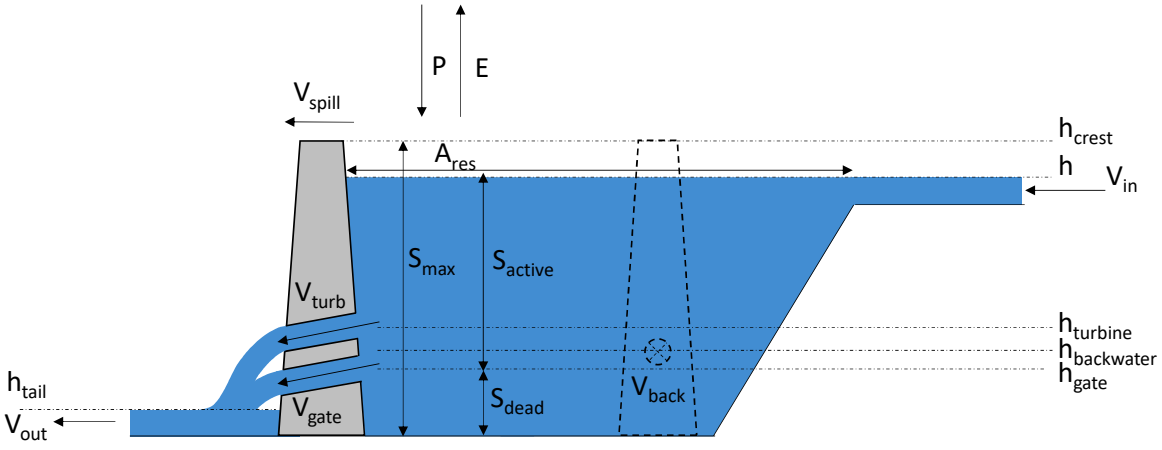

Figure 3.4: Schematic overview of a reservoir node. The figure shows the elevation of the gate (both main and backwater), turbine, crest and tail. In the schematization used in this study, the turbine and gate outflows are assumed to be located at the same elevation. Flow into the surface water reservoir node may leave the storage via the turbine conduit, the gate conduit, via the backwater gate or the overflow. Part of the inflow is lost by evaporation.

Discharge released via the backwater gate may be used for irrigation or flow into a canal. The main gate and the spillway are present at every reservoir, the turbine and the backwater gate are optional. To simplify the constraints and dynamics of the reservoir nodes, for an individual reservoir, all present gates and turbines are modelled to have the same elevation. The storage below this level is referred to as the inactive- or dead storage $\underline{S}_{\mathrm{res}}$, and the storage between this level and the crest level as the active- or live storage S_{active}. The term storage S_{res} is used in this study to refer to the sum of the dead and active storage, having a maximum indicated by $\bar{S}_{\mathrm{res}}$. Because reservoirs can change in height during their existence, the latter variable is a function of time. The outflow through the turbine and gates depends both on the level in the reservoir and the characteristics of the conduit, and can be regulated by changing the outflow surface area. To circumvent the associated non-linear relationship, not the outflow area but the outflow itself is used as a variable in the model. In real world applications, this would require the existence of a local feedback controller to convert the demanded outflow to a conduit setting, which is straighforwad to do using the charateristic equations of the conduit.

Open water evaporation and direct precipitation flows are incorporated in the water balance of reservoir nodes. Seepage flows are neglected as their impact on the water balance is expected to be small compared to the evaporation and outflows. The magnitude of the vertical flow depends on the surface area of the reservoir and the local atmospheric conditions (external disturbance). Because the surface area can vary significantly during a time step (which might be up to months(s) in large scale reservoir optimizations), the net evaporation loss is computed with the average of the reservoir surface area at the beginning and end of the time step. The net evaporation flow V_{evap} is stated as:

$$V^k_{\text{evap},j} = 0.5 \cdot (A^{k-1}_{\text{res},j} + A^k_{\text{res},j}) \cdot H^k_{\text{evap},j} \tag{3.10}$$

with A_{res} the surface area of the reservoir and $H^k_{\text{evap},j}$ the net evaporation flux per unit area in the period between time instances $k-1$ and k. The latter is computed as the difference between the open water evaporation E and precipitation P:

$$H^k_{\text{evap},j} = E^k_j - P^k_j \tag{3.11}$$

Using the reservoir outflows as defined above, the provisional reservoir storage at the end of the time step, neglecting spillway flow for the moment, is described by:

$$\tilde{S}^k_{\text{res},j} = S^{k-1}_{\text{res},j} + V^k_{\text{in},j} - V^k_{\text{turb},j} - V^k_{\text{gate},j} - V^k_{\text{back},j} - V^k_{\text{evap},j} \tag{3.12}$$

with $\tilde{S}^k_{\text{res},j}$ the provisional storage at the end of the timstep before spillflow is included, and V_{in} and V_{back} respectively the reservoir inflow and the outflow via the backwater gate.

The outflow over the spillway depends, as the gate flow, on the characteristics of the spillway and the water level. However, also this non-linear relation is simplified. The spilled volume is said to be equal to the volume that exceeds the provisional storage capacity of the reservoir at the end of the time step. The spilled volume $V^k_{\text{spill},j}$ is therefore described by:

$$V^k_{\text{spill},j} = \begin{cases} 0 & \text{if } \delta^k_{\text{res},j} \leq 0 \\ \delta^k_j & \text{if } \delta^k_{\text{res},j} > 0 \end{cases} \tag{3.13}$$

with:

$$\delta^k_j = \tilde{S}^k_{\text{res},j} - \overline{S}^k_{\text{res},j} \tag{3.14}$$

With the spill flow known, the real reservoir storage S^k_j at the end of the time step is desribed by Equation 3.15.

$$S^k_{\text{res},j} = S^{k-1}_{\text{res},j} + V^k_{\text{in},j} - V^k_{\text{turb},j} - V^k_{\text{gate},j} - V^k_{\text{back},j} - V^k_{\text{vert},j} - V^k_{\text{spill},j} \tag{3.15}$$

3.2.1.3. Irrigation node

An irrigation node represents a location where water is substracted from a river or canal and consumed for the purpose of vegetative production. The total surface area of an irrigation site A_{agri} is divided into fields, with one specific type of crop being grown on each field. The total number of fields is therefore equal to the number of specified crops in set C. A schematic representation of irrigation node $i \in \text{I}$ with four fields is depicted in Figure 3.5.

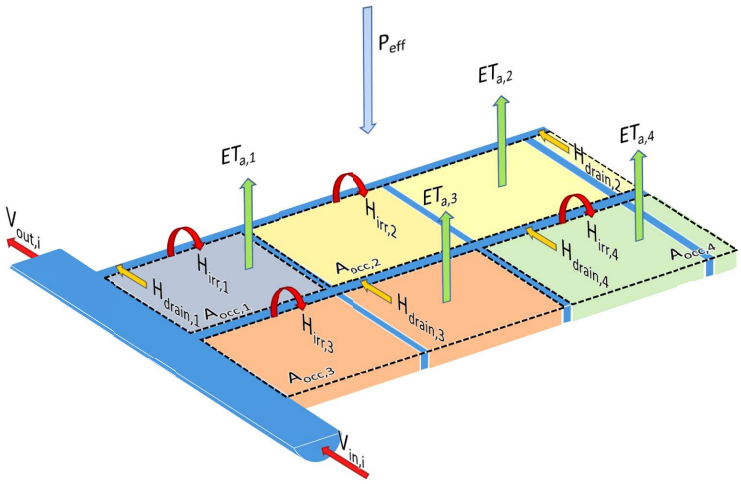

Figure 3.5: Schematic overview of an irrigation node. The incoming flow is divided over the irrigation fields (indicated by the purple, orange, yellow and green areas), each occupating an area indicated by A_{occ}. The effective irrigation supply per unit area H_{irr} and precipitation P_{eff} supply the water available to the crop. The part of the available supply up to the potential evaporation ET_p is actually evaporated ET_a. The remainder is drained back H_{drain} into the river system.

The dynamics of the agricultural production at a site are explained in Section 3.2.2.1. In summary, an irrigation demand H_{irr} (defined per unit area) is extracted for each crop and a drainage amount H_{drain} is returned to the river. Because percolation takes places at a very slow rate, this flux is often negligible compared with surface runoff and subsurface streamflow [Bouwer, 1987; Rahbeh et al., 2013]. With the irrigation and drainage amounts known, the volumes of water extracted for irrigation and drained back into the river system depend on the areas being harvested as described by:

$$V^k_{\text{irr},i,c} = H^k_{\text{irr},i,c} \cdot A^k_{\text{harv},i,c} \tag{3.16}$$

$$V^k_{\text{drain},i,c} = H^k_{\text{drain},i,c} \cdot A^k_{\text{harv},i,c} \tag{3.17}$$

with V_{irr} the volume extracted for irrigational purposes, V_{drain} the volume drained back into the river system, and A_{harv} the area planned to be harvested at the end of the growth cycle (see Section 3.2.2).

The outflow from an irrigation node is now descibed by the node inflow and the difference between the irrigation and drainage volumes for all specified crops:

$$V^k_{\text{out},i} = V^k_{\text{in},i} - \sum_{c \in \text{C}} \left(V^k_{\text{irr},i,c} - V^k_{\text{drain},i,c} \right) \tag{3.18}$$

3.2.1.4. Run-of-the-river hydro-electric plant node

A run-of-the-river hydro-electric plant is a power plant, build within a river, having little or no water storage. A schematic representation of a run-of-the-river node $h \in \mathrm{H}$ is illustrated in Figure 3.6.

Figure 3.6: Schematic overview of a run of river node. The figure indicates the upstream and downstream head and the in and outgoing flows. Because the minimal storage of these plants is neglected, the inflow should be equal to the outflow.

For simplicity is the storage capacity, and hence evaporation and precipitation flow, neglected within the system dynamics. Therefore, at all times, is the ingoing flow equal to the sum of the turbine flow and the amount being spilled. The outflow from a run-of-the-river nodes is stated as:

$$V^k_{\mathrm{in},h} = V^k_{\mathrm{spill},h} + V^k_{\mathrm{turb},h} = V^k_{\mathrm{out},h} \tag{3.19}$$

with V_{turb} the flow through the turbine conduit used to generate electricity and V_{spill} the remainder of the node inflow, being spilled and leaving the node unused.

3.2.1.5. Offtake node

An offtake is a man-made bifurcation regulating the flow, from a river, reservoir or canal, into a canal. To guarantee the conservation of mass in an offtake node $o \in \mathrm{O}$, the sum of the diverted flow $V_{\mathrm{off},o}$ and the outflow in the main river downstream of the offtake $V_{\mathrm{out},o}$ should equal the inflow $V_{\mathrm{in},o}$:

$$V^k_{\mathrm{out},o} = V^k_{\mathrm{in},o} - V^k_{\mathrm{off},o} \tag{3.20}$$

3.2.1.6. Confluence node

A confluence node is a location in the river network where two or more upstream river stretches come together. The outflow from confluence node $u \in \mathrm{U}$ is equal to the inflow in this node.

$$V^k_{\mathrm{out},u} = V^k_{\mathrm{in},u} \tag{3.21}$$

3.2.1.7. Source node

A source node is a location where new flow enters the river system. Source nodes are not limited to upstream locations, but can occur anywhere in a river network. The outflow from a source $f \in \mathrm{F}$ is the sum of the node inflow and the source flow V_{src}:

$$V^k_{\mathrm{out},f} = V^k_{\mathrm{in},f} + V^k_{\mathrm{src},f} \tag{3.22}$$

3.2.1.8. Inactive node

Because a node is already included in the node-link network even before it becomes active, different dynamics apply to these nodes before their commissioning dates. Therefore, during the period from the start of the simulation until a certain node comes online, the node is described as an inactive node $d \in \mathrm{D}$ and the node inflow must be equal to the node outflow:

$$V^k_{\mathrm{out},d} = V^k_{\mathrm{in},d} \tag{3.23}$$

3.2.2. Food dynamics

The proposed framework includes a food balance on national level, based on the structure of the FAOSTAT food balances [FAO, 2017]. However unlike the FAO method, the proposed method includes only vegetative products. These products, all of which are gathered in set P, can be placed under one of the twelve food groups in set G, being: cereals, roots, pulses, vegetables, fuits, fibres, narcotics, sugar, nuts, oil, bevarage and forage.

The variation in product storage is the result of the national production, net international trade and consumption. The storage variations comprise changes at all levels, i.e. it comprise changes in government stocks, stocks with manufacturers, importers, exporters, transport and stocks on farms. With S_{food} the product storage, F_{prod} the production quantity, F_{trade} the international trade flux and F_{con} the product consumption, the storage variation between time instances $k-1$ and k is given by:

$$S^{k}_{\text{food},p,s} - S^{k-1}_{\text{food},p,s} = F^{k}_{\text{prod},p,s} + F^{k}_{\text{trade},p,s} - F^{k}_{\text{con},p,s} \tag{3.24}$$

The production flux includes the agricultural harvest $F_{\text{prod-agri}}$ and the yield of product processing $F_{\text{prod-process}}$. The former describes the production of irrigated agriculture within the considered river basin, irrigated agriculture in other river basins within the country and rainfed agriculture. The latter is the process of converting one product into another product. The production is given by:

$$F^{k}_{\text{prod},p,s} = F^{k}_{\text{prod-agri},p,s} + F^{k}_{\text{prod-process},p,s} \tag{3.25}$$

The total national consumption is the summation of multiple consumption fluxes. This framework includes food, feed, process and loss fluxes. Product use for seed and non food applications, as accounted for in the FAOSTAT food balance, are not included in the food balance. Instead, both fluxes are grouped under the trade flux. The former flux to avoid double counting as all new seedlings come at a cost (Section 3.2.4), and the second flux because this concerns an industrial form not included in the proposed framework. The loss flux only concerns the losses due to storage and transport and is defined as a fraction of the other consumption fluxes. The other loss factors (as discussed in Section 2.3) are included indirectly. Agricultural losses are included in the computation of the harvested yield and processing, distribution and consumption losses are covered by the diet description. The national consumption during time step k is stated as:

$$F^{k}_{\text{con},p,s} = (F^{k}_{\text{food},p,s} + F^{k}_{\text{feed},p,s} + F^{k}_{\text{con-process},p,s})/(1 - c^{k}_{\text{st-loss},p,s}) \tag{3.26}$$

with F_{food} the food consumption, F_{food} the feed consumption, $F_{\text{con-process}}$ the quantities used for food processing and $c_{\text{st-loss}}$ the time dependent fraction for storage and distribution losses. The following paragraphs discuss the above mentioned fluxes in more detail. Subsequently, the agricultural harvest, product processing, trade, food and feed fluxes are clarified.

3.2.2.1. Agricultural production

The agricultural production dynamics are spatially explicitly incorporated in the proposed WEF nexus framework, which means that the starting time of the growing season, the duration of the growing season and the potential yield vary spatially across the study area. The total national agricultural production is the accumulated actual yield Y_{act} over all irrigated sites within the main basin $i \in \text{I}_s$, all other basins $b \in \text{B}_s$ and all rainfed pixels $r \in \text{R}_s$:

$$\begin{aligned} \underset{p=c\in\text{C}}{F^{k}_{\text{prod-agri},p,s}} &= F^{k}_{\text{prod-basin},p,s} + F^{k}_{\text{prod-outside},p,s} + F^{k}_{\text{prod-rain},p,s} \\ &= \sum_{i\in\text{I}_s} Y^{k}_{act,i,c} + \sum_{b\in\text{B}_s} Y^{k}_{act,b,c} + \sum_{r\in\text{R}_s} Y^{k}_{act,r,c} \end{aligned} \tag{3.27}$$

The effect of water deficits on crop yields are modelled in the framework using a formulation based on Equation 2.1. A single yield response factor for the entire growth cycle is applied to overcome non linearities that occur when differentiating between the growth stages as described in Equation 2.2. However, before the product harvest itself can be described, some other characteristics of the agricultural model must be familiarized. Therefore, the agricultural area, the growth stages, evapotranspiration and the maximum yield will be explained consecutively. The definitions used thereby will frequently use the indicator $a \in \mathrm{A}$ where A is the set of all agricultural sites $\mathrm{A} = \{\mathrm{I,B,R}\}$.

Agricultural area - Each agricultural area, both irrigated and rainfed, is characterised by an occupation area A_{occ} and a harvest area A_{harv}. For annual crops, both areas are equal. However, for perennial crops the harvest area might be smaller than the occupation area. The difference between the two surfaces can have two causes. Firstly some perennial crops require one or more growing seasons between seeding and the first flowering and seed production stages. In addition, the choice can be made not to harvest certain areas during a specific growing season, causing the crop to go into hibernation. In principle, the occupation areas could add up to the total irrigation area. However, it is possible that certain fields are not cultivated during specific season or within a dry year, causing the sum of the occupation areas to be smaller than the available irrigation area.

For an annual crop are the occupation and harvest area equal to the area sowed during the current growing season. The occupation area of a perennial crop is not only determined by the surface area that has been added during the current growing season, but also by the areas that have been planted or sowed during historic growing seasons. It is hereby assumed that a perennial crop once planted is not removed before the end of its fruiting life. In general - for both annual and perennual crops - the harvest and occupation areas during a growing season are described by:

$$A^{g^k_{\mathrm{y},a,c}}_{\mathrm{occ},a,c} = \sum_{\tau=1}^{T_{\mathrm{harv},c}} \delta^{g^k_{\mathrm{y},a,c}-\tau+1}_{\mathrm{A},a,c} \tag{3.28}$$

$$A^{g^k_{\mathrm{y},a,c}}_{\mathrm{harv},a,c} \leq \sum_{\tau=T_{\mathrm{ini},c}}^{T_{\mathrm{harv},c}} \delta^{g^k_{\mathrm{y},a,c}-\tau+1}_{\mathrm{A},a,c} \tag{3.29}$$

with T_{harv} the number of seasons a crop could be harvested (i.e. its fruiting life), T_{ini} the index of the season at which a new added area is harvested for the first time (i.e. the crop development years), δ_{A} the area planted at the beginning of a specific growing seasons and g_{y} the calendar year in which the growing season started.

Because of the spatially explicit dynamics, the index g_y is both crop and location specific. In addition to the index g_y, the index g_n is introduced. This index counts the number of completed time steps within a growing season. The relationship of both indexes with the time index k is as follow:

$$g^k_{\mathrm{y},a,c} = \left\lceil \frac{k - n_{\mathrm{seed},a,c} + 1}{N_{\mathrm{step}}} \right\rceil + T_{\mathrm{start}} - 2 \tag{3.30}$$

$$g^k_{\mathrm{n},a,c} = k - n_{\mathrm{seed},a,c} - N_{\mathrm{step}} \cdot (g^k_{\mathrm{y},a,c} - 1) \tag{3.31}$$

with N_{step} the number of time steps per calendar year, $T_{\mathrm{start}} - 1$ the calendar year at which the simulation starts and n_{seed} the index for time step within a year at which the growing seasons starts.

Because the areas are defined per growing season, the translation to the model time step has yet to be made. The size of the occupation and harvest area depends on the point in time of the current time

step k with respect to the annual seed- n_{seed} and harvest moment n_{harvest}, respectively the first and last time step of the growing season. The occupation area in time step k is described by:

$$A^k_{\text{occ},a,c} = \begin{cases} A^{g^k_{\text{y},a,c}}_{\text{occ},a,c} & \text{if } g^k_{\text{n},a,c} < N_{\text{grw},a,c} \\ 0 & \text{otherwise} \end{cases} \tag{3.32}$$

with N_{grw} the crop and location specific duration (expressed in number of time steps) between seeding and harvest. An identical formulation as stated in Equation 3.32 holds for the harvest area.

Growth stages - The growth stages are (as explained in Section 2.2.3) related to the crop coefficient which is used to relate the potential evapotranspiration with the reference evapotranspiration. Following the framework as proposed by Doorenbos [1975], a distinction is made between four stages: (1) the initial; (2) crop development; (3) mid-season; and (4) late season stage. This framework is based on a crop that is harvested once per growing season. However, some crops (i.e. grasses) may have multiple growing cycles within a growing season. Therefore, the framework has been modified. The adjustments made allow, for crops being harvested multiple times each growing season ($N_{\text{cut}} > 1$), every stage to occur in every growing cycle. The relative duration of each stage is thereby the same in all growing cycles.

The growing cyclus vary in duration. In general, the first cycle takes longer than the following cycles. Because spatially explicit information about the number of cuttings per year and the duration of the associated growing cycles is not available, the number of cuttings and the relative duration of the growing cycles are only crop specific. However, because the total duration between seeding and the last harvest has been defined spatially, it is possible, due to the definition of the relative cycle duration, that certain growth cycles do not take an integer number of time steps. Because the discrete implementation does require an integer number of time steps, the durations are rounded. This is done by minimizing the rounding difference while maintaining the same number of time steps between seeding and harvest. Mathematically, this is defined in Equation 3.33 with $N_{\text{grw-cut}}$ the duration (measured in number time steps) of a specific growing cycle, f_{cut} the relative duration of each growing cycle and N_{cut} the number of growing cycles per growing season.

$$\begin{aligned} \underset{N_{\text{grw-cut},a,c}(\alpha)}{\text{minimize}} \quad & \sum_{\alpha=1}^{N_{\text{cut},c}} N_{\text{grw-cut},a,c}(\alpha) - N_{\text{grw},a,c} \cdot f_{\text{cut},c}(\alpha) \\ \text{subject to} \quad & N_{\text{grw-cut},a,c}(\alpha) \in \mathbb{N} \\ & \sum_{\alpha=1}^{N_{\text{cut},c}} N_{\text{grw-cut},a,c}(\alpha) = N_{\text{grw},a,c} \end{aligned} \tag{3.33}$$

In contrast to the growing cyles, the stages within a cycle do not have to take an integer number of time steps. The stages can fall within or over multiple time steps. In other words, several stages can occur during a time step, each with a crop coefficient characteristic for that stage. The resulting crop coefficient for a time step is therefore defined as the time weighted average of the contributions from all four crop stages, as stated by:

$$K^k_{\text{cc},a,c} = \sum_{\alpha=1}^{N_{\text{cut},c}} \sum_{\varepsilon=1}^{4} \left(\Delta t^k_{\text{stg},a,c}(\alpha,\varepsilon) \cdot K^k_{\text{cc-stg},a,c}(\alpha,\varepsilon) \right) \cdot \frac{1}{t^k} \tag{3.34}$$

with α and ε local indices to indicate the number of the growing cycle and stage respectively, Δt_{stg} the duration of stage ε in cycle α within the current time step k, and $K_{\text{cc-stage}}$ the average value of the crop coefficient associated with this duration.

The duration Δt_{stg} is described as the difference between a start- and end time of a stage within a cycle, respectively $t_{\text{stg,start}}$ and $t_{\text{stg,end}}$, both counting from the start of the growing cycle. The value of both the start- and end time depends on the location in time of the crop stage relative to the timing of a model time step (Figure 3.7). The start time of the time step is leading as lower bound if the start of the considered time step takes place before the start of the considered stage, and vice versa. The end time of the stage is leading as upper bound if the end of the considered stage takes place before the end of the considered time step, and vice versa. The duration Δt_{stg} is described by:

$$\Delta t^{k}_{\text{stg},a,c}(\alpha,\varepsilon) \; = t^{k}_{\text{stg,end},a,c}(\alpha,\varepsilon) - t^{k}_{\text{stg,start},a,c}(\alpha,\varepsilon) \qquad \substack{1 \le \varepsilon \le 4 \\ 1 \le \alpha \le N_{\text{cut},c}} \tag{3.35}$$

where:

$$t^{k}_{\substack{\text{stg-start},a,c}}(\alpha,\varepsilon) = \min\left(\max\left(\sum_{\kappa=n_{\text{cycle},a,c}(\alpha)}^{k-1} t^{\kappa}, \sum_{\zeta=1}^{\varepsilon-1} t_{\text{stg},a,c}(\alpha,\zeta)\right), \sum_{\zeta=1}^{\varepsilon} t_{\text{stg},a,c}(\alpha,\zeta)\right) \qquad \substack{1 \le \varepsilon \le 4 \\ 1 \le \alpha \le N_{\text{cut},c}} \tag{3.36}$$

$$t^{k}_{\substack{\text{stg-end},a,c}}(\alpha,\varepsilon) = \max\left(\min\left(\sum_{\kappa=n_{\text{cycle},a,c}(\alpha)}^{k} t^{\kappa}, \sum_{\zeta=1}^{\varepsilon} t_{\text{stg},a,c}(\alpha,\zeta)\right), \sum_{\zeta=1}^{\varepsilon-1} t_{\text{stg},a,c}(\alpha,\zeta)\right) \qquad \substack{1 \le \varepsilon \le 4 \\ 1 \le \alpha \le N_{\text{cut},c}} \tag{3.37}$$

with t_{stg} the total duration of a stage in a studied growth cycle, and n_{cyc} the index for the time step (within a calendar year) at which the considered growing cycle starts.

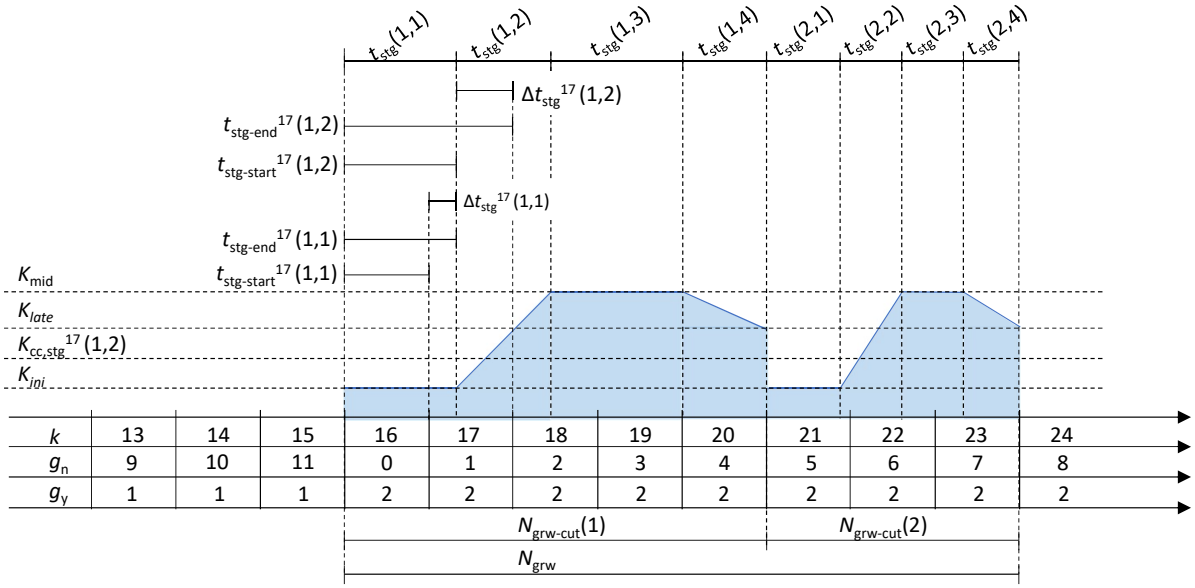

Figure 3.7: An example with a montly timstep ($N_{\text{step}} = 12$) to illustrate some of the defined variables. The blue colored area depicts the growing season with $N_{\text{cut}} = 2$. The horizontal timelines illustrate the length of the stages t_{stg}, and the start time $t_{\text{stg,start}}$, end time $t_{\text{stg,end}}$ and duration Δt_{stg} of the stages in time step 17. The values of the crop coefficient for the stages, and the average of the 2nd stage in time step 17 are indicated on the vertical axis. The lower horizontal table displays the values of the time step index k, the growing season index g_{y} and the season progress index g_{n}.

The total stage duration during a considerd cycle is described by multiplying the relative stage durations f_{stg} with the absolute duration of the considerd growing cycle. As already mentioned, these relative stage lengths are identical between the growth cycles and across the study area. To translate the cycle duration from a number of MPC time steps to a clock time, knowledge of the starting moment n_{cyc} is required. The stage duration t_{stg} and the cycle start index n_{cyc} are descibed by:

$$\underset{\substack{1 \leq \varepsilon \leq 4 \\ 1 \leq \alpha \leq N_{\text{cut},c}}}{t_{\text{stg},a,c}(\alpha,\varepsilon)} = f_{\text{stg},c}(\varepsilon) \cdot \sum_{n_{\text{cyc},a,c}(\alpha)}^{n_{\text{cyc},a,c}(\alpha)+N_{\text{grw-cut},a,c}(\alpha)-1} t^{\kappa} \tag{3.38}$$

$$n_{\text{cyc},a,c}(\alpha) = n_{\text{seed},c} + \sum_{\zeta=1}^{\alpha-1} N_{\text{grw-cut},a,c}(\zeta) \tag{3.39}$$

The average value of the crop coefficient for a given stage during a certain time step depends on the duration of this stage already passed in previous time steps. The resulting value for the first (initial) and third (mid-season) stage is simply the crop coefficient associated with these stages. For the second (development) and fourth (late-season) stage is the duration of the considered stage during the foregoing time steps decisive for the resulting value. The average value is described by:

$$\underset{\substack{1 \leq \varepsilon \leq 4 \\ 1 \leq \alpha \leq N_{\text{cut},c}}}{K^{k}_{\text{cc-stg},a,c}(\alpha,\varepsilon)} = \frac{\Delta K_{\text{stg},c}(\varepsilon)}{t_{\text{stg},a,c}(\alpha,\varepsilon)} \cdot \left(\frac{1}{2} \Delta t^{k}_{\text{stg},a,c}(\alpha,\varepsilon) + \sum_{\kappa=k-g^{k}_{\text{n},a,c}}^{k-1} \Delta t^{\kappa}_{\text{stg},a,c}(\alpha,\varepsilon) \right) + K_{\text{stg},c}(\varepsilon) \tag{3.40}$$

with $K_{\text{stg}} = (K_{\text{ini}}, K_{\text{ini}}, K_{\text{mid}}, K_{\text{mid}})$ the crop coefficient corresponding with the start of the stage and $\Delta K_{\text{stg}} = (0, K_{\text{dev}} - K_{\text{ini}}, 0, K_{\text{late}} - K_{\text{mid}})$ the change in crop coefficient during the stage.

Evapotranspiration - To simplify the system dynamics, soil moisture storage is not included in the water balance of the agricultural fields. Hence, during each time step field inflows should equal field outflows. The available head (field inflow) H_{avail} is the sum of the effective precipitation and irrigation head:

$$H^{k}_{\text{avail},a,c} = \eta_{\text{eff}} \cdot P^{k}_{a} + \eta^{k}_{\text{irr},a} \cdot H^{k}_{\text{irr},a,c} \tag{3.41}$$

with η_{eff} the part of the incoming precipitation P available for crop uptake after percolation and interception losses [Brouwer et al., 1985], and η_{irr} the part of the irrigation head H_{irr} remaining after substraction of evaporation and seepage losses. The applied irrigation technique is decisive for the magnitude of latter mentioned losses [Multsch et al., 2017].

The available head is consumed by crop evapotranspiration ET_{a} or drained back into the river system H_{drain}. In absence of soil storage, the actual evapotranspiration cannot dependent on the moisture content as described in Section 2.2.4. Instead, the actual evapotranspiration equals the available head as long as this is less than the potential evapotranspiration ET_{p} [Multsch et al., 2017]:

$$ET^{k}_{\text{a},a,c} = H^{k}_{\text{avail},a,c} - H^{k}_{\text{drain},a,c} \tag{3.42}$$

with:

$$H^{k}_{\text{drain},i,c} = \begin{cases} 0 & \text{if } ET^{k}_{\text{p},a,c} \geq H^{k}_{\text{avail},a,c} \\ H^{k}_{\text{avail},a,c} - ET^{k}_{\text{p},a,c} & \text{if } ET^{k}_{\text{p},a,c} < H^{k}_{\text{avail},a,c} \end{cases} \tag{3.43}$$

and:

$$ET^{k}_{\text{p},a,c} = K^{k}_{\text{cc},a,c} \cdot ET^{k}_{0,a} \tag{3.44}$$

Maximum yield - To compute the actual yield under water limiting conditions, besides the uniform yield response factors an indication of the local maximum achievable yield is required. Available potential yields Y_{pot} are not a good indicator of the maximum yield as they reflect the constraint free crop yields under the prevailing local temperature, radiation and moisture regimes [Van Ittersum et al., 2013]. Therefore, to describe actual maximum achievable yield a management factor c_{mf} is introduced. This factor combines all management effects (soil quality, nutrition, density, diseases, etc.) and accounts for the deviation between potential and actual achievable maximum yields in absence of water deficits. Because management practice is assumed to be comparable between fields within a country, these factors are country specific. However, since the management practices at rain-dependent sites differ from the management practices in irrigated areas, the following holds within the borders of a country:

$$\underset{i\in \mathrm{I}_s}{c_{\text{mf},i,c}} = \underset{b\in \mathrm{B}_s}{c_{\text{mf},b,c}} \geq \underset{r\in \mathrm{R}_s}{c_{\text{mf},r,c}} \tag{3.45}$$

Harvest - It is assumed that crops are harvested instantaneously at the end of the last time step of the growth cycle. This makes a crop available for consumption or trade in the time step after the last time step of the growing season. All other time steps, the harvest is equal to zero. The harvest at agricultural area a is therefore described by:

$$Y^k_{\text{a},a,c} = \begin{cases} A^k_{\text{harv},a,c} \cdot c_{\text{mf},a,c} \cdot Y_{\text{p},a,c} \left(1 - K_{\text{y},c} \left(1 - \dfrac{\sum^{k-1} ET^{\kappa}_{\text{a},a,c}}{\sum ET^{\kappa}_{\text{p},a,c}} \right) \right) & \text{if } g^{k-1}_{\text{n},a,c} + 1 = \sum_{\zeta=1}^{\alpha} N_{\text{grw-cut},a,c}(\zeta) \\ & \kappa = k - N_{\text{grw-cut},a,c}(\alpha) \\ 0 & \text{otherwise} \end{cases} \tag{3.46}$$

with K_{y} the spatially uniform yield response factor and the potential ET_{p} and actual evapotranspiration ET_{a} described by Equation 3.44 and Equation 3.42 respectively.

Despite the general validity of the above equation, the underlying assumptions for the different agricultural sites differ. For the irrigated areas within the main basin this equation is generally valid without assumptions. Because the river flow in the surrounding basins is not explicitly included in the framework, it is assumed that there is always enough water, and the actual evapotranspiration equals the potential evapotranspiration. Finally, in the rain-dependent areas where irrigation is not possible, the irrigation head is set to zero.

3.2.2.2. Product processing

As mentioned above, product processing is the procedure of converting one product into another within the boundaries of a state. This conversion is included by use of a conversion coefficient $\eta_{\text{F-con}}$. The production of food by processing and the consumption of raw materials required herefore are respectively described by:

$$F^k_{\text{prod-process},p,s} = \sum_{\zeta\in \mathrm{P}} \eta_{\text{F-conv},p,\zeta,s} \cdot F^k_{\text{process},p,\zeta,s} \tag{3.47}$$

$$F^k_{\text{con-process},p,s} = \sum_{\zeta\in \mathrm{P}} F^k_{\text{process},\zeta,p,s} \tag{3.48}$$

with $F_{\text{process},p(1),p(2)}$ the quanity of product 2 consumed for conversion into product 1.

3.2.2.3. Product trade

Product trade is possible between all countries within the study area (regional countries) and with the outside world. The outside world is added as a single country in the proposed framework. Because a trading flux F_{trade} captures all trading activities that actually take place between multiple regions in two considered countries, a trade route is defined between the population centers of gravity of these countries. The length of the trade route l_{trade} (required for the economic description in Section 3.2.4) is characterized as the rectilinear distance between its start and end point.

The net trade flux of state s is the sum of the difference between the import F_{imp} from- and export F_{exp} to all regional countries and the outside world:

$$F^k_{\text{trade},p,s} = \sum_{\zeta \in \{\text{S,extern}\}} \left(F^k_{\text{imp},p,s,\zeta} - F^k_{\text{exp},p,s,\zeta} \right) \tag{3.49}$$

where the import into state s is less than the export to state s due to losses $c_{\text{trade-loss}}$ during transport:

$$F^k_{\text{imp},p,s,\zeta} = (1 - c_{\text{trade-loss}}) \cdot F^k_{\text{exp},p,\zeta,s} \tag{3.50}$$

3.2.2.4. Food demand

The description of the food demand is aimed at meeting the per capita energy intake requirements. More specific dietary constraints have not been included in the proposed methodology. Energy is provided by the consumption of both vegetative and animal products (meat and dairy). The contribution of each vegetative product $f_{\text{vegetative}}$ and each animal product f_{animal} is defined, such that for the summation over all vegetable products $p \in \text{P}$ and animal products $q \in \text{Q}$ holds:

$$\sum_{p \in \text{P}} f^k_{\text{vegetative},p,s} + \sum_{q \in \text{Q}} f^k_{\text{animal},q,s} = 1 \tag{3.51}$$

The description of the animal product consumption follows in Section 3.2.2.5. Food intake of a given vegetative product is determined by the national average diet. This prescribes what the total per capita energy intake is and what part of it originates from a specific product ($f_{\text{vegetative}}$). Using the caloric value of that particular product, the energy demand is translated into a bulk demand. The demand (and supply) for a specific product is described by:

$$F^k_{\text{food},p,s} = N^k_{\text{pop},s} \cdot E^k_{\text{diet},s} \cdot t^k \cdot f^k_{\text{vegetative},p,s} / H_{\text{vegetative},p} \tag{3.52}$$

with E_{diet} the per capita energy intake, N_{pop} the population size, and $H_{\text{vegetative}}$ the calorific value of the considered product.

3.2.2.5. Feed demand

Animal husbandry is indirectly included in the proposed methodology. The animal products are not part of the set of products P which can be directly produced, consumed and traded in the proposed framework. Instead, the consumption of animal products is included by converting them into a quantity of vegetable product required for animal feed. For this, the required amount of animal product is multiplied with a feed conversion efficiency [Mekonnen and Hoekstra, 2010]. This translates the amount of animal product (both meat and dairy) into the required amount of dry weight animal feed. The amount of animal product required is determined in a manner similar as for vegetative products. However, because the food loss factor presented in Equation 3.26 does not account for the losses of animal products, the demand is slightly increased to compensate for these losses as well. The required amount of dry mass is ultimately translated into a feed demand for a specific product by use of the feed basket composition. This prescribes which part of the food comes from a specific product. Because the fluxes are all expressed in fresh weights, the dry feed demand should be converted. Mathematically, the feed demand is stated by:

$$F^k_{\text{feed},p,s} = \sum_{q \in \text{Q}} \left(\frac{N^k_{\text{pop},s} \cdot E^k_{\text{diet},s} \cdot t^k \cdot f^k_{\text{animal},q,s} \cdot \eta_{\text{feed-conv},s}}{H_{\text{animal},q} \cdot (1 - c^k_{\text{st-loss},q})} \right) \cdot \frac{f^k_{\text{basket},p,s}}{c_{\text{dry},p}} \tag{3.53}$$

with H_{animal} the caloric value of an animal product, $c_{\text{st-loss}}$ the loss factor, $\eta_{\text{feed-conv}}$ the feed conversion efficicency, f_{basket} the feed basket composition and c_{dry} to dry weight fraction of a product.

The feed basket composition is generally divided into 4 categories: cereals; forage cops; by-products and pasture [FAO et al., 2014]. Because the latter two categories are not defined as product groups, the sum of the included basket fractions do not have to add up to unity. Sufficient supply for by-products and forages is assumed.

3.2.3. Energy dynamics

The energy balance describes the generation and consumption of electricity. Like the food balance, this energy balance is formulated on a national level. However, the balance composition shows two major differences with respect to the food balance. First of all, the possibility of storing electricity is not included in the proposed method because it is not yet widely used. Secondly, unlike food where the balance must be guaranteed, available electricity $E_{\text{e-avail}}$ can be less than electricity demand $E_{\text{e-dem}}$. The dynamics of the electricity balance are described by:

$$E^k_{\text{e-con},s} + E^k_{\text{e-dump},s} = E^k_{\text{e-avail},s} \tag{3.54}$$

where the loss flux $E_{\text{e-dump}}$ describes the amount of electricity dumped in case of surpluses, i.e. when the total amount of available electricity exceeds the electricity demand:

$$E^k_{\text{e-dump},s} = \begin{cases} E^k_{\text{e-avail},s} - E^k_{\text{e-dem},s} & \text{if } E^k_{\text{e-avail},s} > E^k_{\text{e-dem},s} \\ 0 & \text{otherwise} \end{cases} \tag{3.55}$$

The total available electricity quanitity is the cumulative of the generation $E_{\text{e-gen}}$ and net trade $E_{\text{e-trade}}$, compensated for the national network transmission losses $c_{\text{e-loss}}$:

$$E^k_{\text{e-avail},s} = (E^k_{\text{e-trade},s} + E^k_{\text{e-gen},s}) \cdot (1 - c^k_{\text{e-loss},s}) \tag{3.56}$$

Electricity generation and trading are further described in the following sections.

3.2.3.1. Electricity generation

Generation of electricity can be roughly divided into generation with renewable sources and non-renewable sources. The latter covers generation by fossil power plants, but also nuclear installations. Both methods of generation have a different implementation in the proposed methodology. Also hydropower generated within the main basin has, despite the classification as a renewable source, a unique implementation. This because the renewable resource water, unlike other sources such as heat, sun and wind, has competitive uses in the proposed methodology. The total electricity generation is therefore the cumulative of the non-renewable generation $E_{\text{e-non-renew}}$, the renewable generation $E_{\text{e-renew}}$ and the hydropower generation $E_{\text{e-hydro}}$. The three unique implementations for electricity generation are explained in the following paragraphs.

Non-renewable - Non-renewable generation is the cumulative generation of all members of the set of non-renewable sources V consisting of oil, gas, coal and nuclear. The generation of an individual member is computed by multipying the mass of fuel W_{fuel} with the combustion heat H_{fuel} and the efficiency of the energy conversion η_{fuel}:

$$E^k_{\text{e-non-renew},s} = \sum_{v \in \text{V}} E^k_{\text{e},v,s} = \sum_{v \in \text{V}} W^k_{\text{fuel},v,s} \cdot H_{\text{fuel},v} \cdot \eta_{\text{fuel},v} \tag{3.57}$$

Renewable - Renewable generation is the cumulative generation of all members of the set of renewable sources W consisting of wind, solar, biomass, geothermal and hydropower outside the main basin. The generation by an individual renewable source is described as fraction c_{cap} (referred to as the capacity factor) of the maximum energy production during the timeframe given the maximum electric power capacity $\bar{P}_{\text{e}}$:

$$E^k_{\text{e-renew},s} = \sum_{w \in \text{W}} E^k_{\text{e},w,s} = \sum_{w \in \text{W}} \bar{P}^k_{\text{e},w,s} \cdot c_{\text{cap},w} \cdot t^k \tag{3.58}$$

Hydropower - For the reservoirs and run-of-the-river hydro-electric plants within the main basin, the flow through the turbine and the head between the inlet and outlet of the turbine flow determine the amount of electricity generated per time step:

$$\begin{aligned} E^k_{\text{e-hydro},s} &= \sum_{\zeta \in \{\text{J}_s, \text{H}_s\}} \rho \cdot g \cdot \eta_{\text{hydro},j} \cdot V^k_{\text{turb},j} \cdot h^k_{\text{net},j} \\ &= \sum_{\zeta \in \{\text{J}_s, \text{H}_s\}} E^k_{\text{e},\zeta} \end{aligned} \tag{3.59}$$

with η_j the efficiency of the energy conversion, g the gravitational acceleration, ρ the density of fresh water and h_{net} the elevation of the open water surface. For a run-of-the-river plant, the latter is said to be constant over time and equal to the difference between the design operational elevation and the tail level ($h_{\text{ror}} - h_{\text{tail}}$). For the surface water reservoirs, where the surface elevation is changing over time, the elevation h_{net} is definied as the difference between the average elevation at the start and end of a time step and the tail elevation:

$$h^k_{\text{net},j} = 0.5 \cdot (h^{k-1}_{\text{res},j} + h^k_{\text{res},j}) - h_{\text{tail},j} \tag{3.60}$$

3.2.3.2. Electricity trade

Electricity trade is possible between all states that are connected by an international interconnector. All neighboring countries of the studied riparian states are clustered as the outside world. The maximum capacity of an interconnector between a considered country within the study area and the external world, equals the sum of the capacities between this country and all countries clustered as being the external world. The trading capacity of the various countries within the study area with the external world can therefore vary. As for product trade, an international electricity connector is seen as a connection between the population centers of gravity. However, interconnectors are not present between all states. It is therefore possible that a trade flow between two countries will pass via a third one (see Figure 3.8).

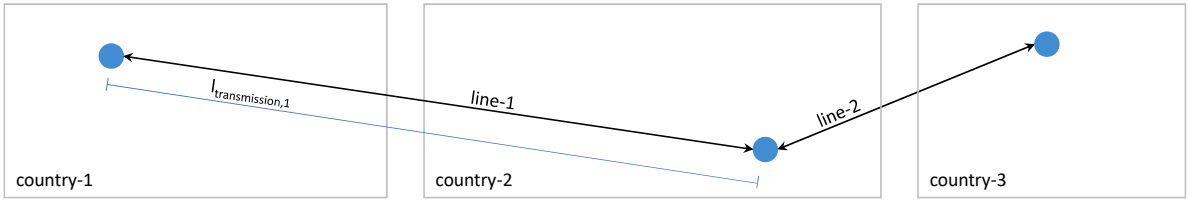

Figure 3.8: An example of electricity trade, where transmission lines are not present between all states. Interconnectors are present between the population centers of country 1 and 2, and country 2 and 3. Hence, electricity trade between country 1 and 3 passes via country 2.

In the implementation of the electricity trading, a distinction is made between long-term contracts, referred to as fixed trade, and short-term contracts, referred to as variable trade. The net trade flux is the summed difference between both fixed and variable import from- and export fluxes to all regional countries and the external world:

$$E^k_{\text{e-trade},s} = \sum_{\zeta \in \{\text{S,extern}\}} \left(E^k_{\text{e-imp-fxd},s,\zeta} + E^k_{\text{e-imp-var},s,\zeta} - E^k_{\text{e-exp-fxd},s,\zeta} - E^k_{\text{e-exp-var},s,\zeta} \right) \tag{3.61}$$

with $E_{\text{e-imp-fxd}}$ and $E_{\text{e-imp-var}}$ the fixed and variable import flux, and $E_{\text{e-exp-fxd}}$ and $E_{\text{e-exp-var}}$ the fixed and variable export quantities.

The import into state s is less than the export to state s due to transportation losses. These transmission losses increase with increasing distance between sender and receiver. The fixed import into a country expressed as a function of the export to that country is described by

$$E^k_{\text{e-imp-fxd},s,\zeta} = E^k_{\text{e-exp-fxd},\zeta,s} \cdot (1 - c_{\text{e-loss-int}})^{l_{\text{e-trade},s,\zeta}} \tag{3.62}$$

with $c_{\text{e-loss-int}}$ the transmission losses per unit length of high voltage interconnection line, and $l_{\text{e-trade}}$ the length of the trade line between sender and receiver. An identical formulation holds for the variable electrcity trade.

The length $l_{\text{e-trade}}$ is measured over the transmission network. Since, as already mentioned, the electricity trade between two countries can take place via a third party, the connection between a sender and receiving country can consist of several segments. The length of the line is therefore the sum of the lengths of these individual segments:

$$l_{\text{e-trade},s_1,s_2} = \sum_{l \in \text{L}_{s_1,s_2}} l_{\text{transmission},l} \tag{3.63}$$

with $\text{L}_{s,s} \subset \text{L}$ the minimum set of interconnectors required to conncect two states, L the set of all interconnectors, and $l_{\text{transmission}}$ the length of a single interconnector.

3.2.4. Economic dynamics

The economics are described on a macro scale. Internal shifts of value are not included in this setup. Only international transaction that shed or shrink the national treasury are included. All incomes and expenditures can be attributed to the agricultural or electrical system. In both systems, the price is predefined and independent of supply and demand. The economic system dynamics of both systems are described in the following sections.

3.2.4.1. Agricultural economics

All incomes and expenditures are divided into three groups, being: the trade costs and incomes, the fixed production costs and the variable production costs. The incomes and expenses related to product trade depend on the quantities and the international unit price of the considered product. The transport costs, which are just as the transport losses borne by the recipient country, depend on the distance over which a product is traded. The net trade income $I_{\text{f-trade}}$ of all products with all trade partners (regional countries and the external world) is given by:

$$I^k_{\text{f-trade},s} = \sum_{p \in \text{P}} \left(\sum_{\zeta \in \{\text{S,extern}\}} \left(p^k_{\text{f-int},p} \cdot F^k_{\text{exp},p,s,\zeta} - \left(p^k_{\text{f-int},p} + p_{\text{f-trans}} \cdot l_{\text{trade},s,\zeta} \right) \cdot F^k_{\text{exp},p,\zeta,s} \right) \right) \tag{3.64}$$

with $p_{\text{f-int}}$ the international commodity prices, and $p_{\text{f-trans}}$ the costs of transportation per unit distance.

The fixed expenditures for food production $I_{\text{f-fxd}}$ comprise of the amortization costs $p_{\text{f-amort}}$ of irrigated agricultural fields and processing facilities $p_{\text{f-process-fxd}}$. The former includes the amortization of pumps, canals and agricultural machinery. The total fixed expenditure is described as a function of the size of the irrigated agricultural sites A_{agri} and the processing capacity $\bar{F}_{\text{prod-process}}$:

$$I^k_{\text{f-fxd},s} = p_{\text{f-amort},\zeta} \sum_{\zeta \in \{\text{I}_s,\text{B}\}} \bar{A}^k_{\text{agri},\zeta} + \sum_{p \in \text{P}} p_{\text{f-process-fxd},p} \cdot \bar{F}^k_{\text{prod-process},p,s} \tag{3.65}$$

The variable costs $I_{\text{f-var}}$ depend on the size of the agricultural area being harvested and the amounts of food being processed. The total costs for the former are made up of costs of fertilizer $p_{\text{f-fert}}$, labor $p_{\text{f-labour}}$ and seeds $p_{\text{f-seed}}$. Because the composition and the amounts of fertilizer, as well as the labor required, can vary greatly per crop type, these costs are crop specific. It is assumed that each time step similair amounts of fertilizer and labor are required. Labor has been added to the framework because it concerns an opportunity cost. After all, if not employed in the agricultural sector, the labor force could be utilized elsewhere. The variable expenses are described by:

$$\begin{aligned} I^k_{\text{f-var},s} = &\sum_{c \in \text{C}} \left(\sum_{a \in \text{A}_s} \left(\left(p_{\text{f-fert},c} + p_{\text{f-labour},c} \right) \cdot A^k_{\text{harv},a,c} + I^k_{\text{f-seed},a,c} \right) \right) + \\ &\sum_{p \in \text{P}} p_{\text{f-process-var},p} \cdot F^k_{\text{prod-process},p,s} \end{aligned} \tag{3.66}$$

with $I_{\text{f-seed}}$ the costs of new plants or seeds. This cost occurs only once per growing season, specific in the first time step of the growing season:

$$I^k_{\text{f-seed},a,c} = \begin{cases} p_{\text{f-seed},c} \cdot \delta^{g^k_{\text{y},a,c}}_{\text{A},a,c} & \text{if } g^k_{\text{n},a,c} = 0 \\ 0 & \text{otherwise} \end{cases} \tag{3.67}$$

With the trade income and the fixed and variable expenditures as described above, the net income from the food sector $I_{\text{f-net}}$ is described by:

$$I^k_{\text{f-net},s} = I^k_{\text{f-trade},s} - I^k_{\text{f-fxd},s} - I^k_{\text{f-var},s} \tag{3.68}$$

3.2.4.2. Electricity economics

Similar to the economic description of the agricultural system, the costs of the electrical system can be divided into trade incomes and expenditures and fixed and variable production costs. The net income of electricity trading is computed using a single electricity trading price $p_{\text{e-int}}$ which is valid for all river states and is therefore independent of the production method. Given that the transmission losses are being paid for by the receiving country, the net income from electricity trading $I_{\text{e-trade}}$ is given by:

$$I^k_{\text{e-trade},s} = p^k_{\text{e-int}} \sum_{\zeta \in \{\text{S,extern}\}} \left(E^k_{\text{e-exp-fxd},s,\zeta} + E^k_{\text{e-imp-var},s,\zeta} - E^k_{\text{e-exp-fxd},\zeta,s} - E^k_{\text{e-exp-var},\zeta,s} \right) \tag{3.69}$$

The fixed costs of energy generation $I_{\text{e-fxd}}$ have been described as amortization costs $p_{\text{e-amort}}$ and depend on the installed capacity of both sustainable and non-sustainable power plants:

$$I^k_{\text{e-fxd},s} = \sum_{\zeta \in \{\text{V,W}\}} p_{\text{e-amort},\zeta} \cdot \bar{P}^k_{\text{e},\zeta,s} + \sum_{\zeta \in \{\text{H}_s,\text{J}_s\}} p_{\text{e-amort},hydro} \cdot \bar{P}^k_{\text{e},\zeta} \tag{3.70}$$

The variable costs $I_{\text{e-var}}$ associated with electricity production are subdivided into operational and management costs $I_{\text{e-o\&m}}$ (Equation 3.71) and fuel costs for the non-renewable power plants $I_{\text{e-fuel}}$ (Equation 3.72). The operational and management costs $p_{\text{e-o\&m}}$ are made up of variable maintanance and personnel costs. Fuel costs $p_{\text{e-fuel}}$ are computed with international fuel prices. Even if a country has certain fossil resources at its disposal, these costs are still charged because they include an opportunity.

$$I^k_{\text{e-o\&m},s} = \sum_{\zeta \in \{\text{V,W}\}} p_{\text{e-o\&m},\zeta} \cdot E^k_{\text{e},\zeta,s} + p_{\text{e-o\&m},hydro} \cdot E^k_{\text{e-hydro},s} \tag{3.71}$$

$$I^k_{\text{e-fuel},s} = \sum_{v \in \text{V}} p_{\text{e-fuel},v} \cdot W^k_{\text{e-fuel},v,s} \tag{3.72}$$

If the available electricity is less than the electricity demand, not all activities can proceed. The costs associated with a shortage of electricity $p_{\text{e-shortage}}$ depend on the production value of a single energy unit. The latter varies between the different energy consuming sectors, and is therefore implemented as a national average. The missed income $I_{\text{e-shortage}}$ is therefore defined by:

$$I^k_{\text{e-shortage},s} = p_{\text{e-shortage}} \cdot \left(E^k_{\text{e-avail},s} - E^k_{\text{e-dem},s} \right) \tag{3.73}$$

With the trade income, the fixed and variable expenditures and the costs of electricity shortage as described above, the net income from the energy sector $I_{\text{e-net}}$ is described by:

$$I^k_{\text{e-net},s} = I^k_{\text{e-trade},s} - I^k_{\text{e-fxd},s} - I^k_{\text{e-var},s} - I^k_{\text{e-shortage},s} \tag{3.74}$$

3.3. Model predictive building blocks

A discrete moving horizon variant of the MPC framework as discussed in Section 2.4 is implemented. Within the MPC framework, a slightly simplified model dynamics is used to compute the optimal water resource planning over a horizon of several years. The optimal planning is herein referred to as the set of actions maximizing the national treasury over the optimization horizon. The optimal agricultural land uses, reservoir operational settings and others, are subsequently used to force the simulation model which follows the full dynamics as introduced before. This section introduces the building blocks of the MPC framework. The optimization problem formulation for the large-scale nonlineair problem is discussed first, followed by the simulation problem formulation.

3.3.1. Optimization problem formulation

The optimization problem is formulated in the software library IPOPT. IPOPT (Interior Point OPTimization) is an open source software package for large-scale nonlinear optimization [Wachter and Biegler, 2006]. Although IPOPT will converge to local minima, it is probably the best open source solver available for large-scale nonlinear problems [Currie and Wilson, 2012]

If a simulation experiment aims to collect data over a timespan ranging from the first time step in year T_{start} to the last time step in year T_{end}, the simulation experiment starts at the beginning of year $T_{\text{start}} - 1$ to reduce the effects of initial data values, and runs for $\bar{N}_{\text{iter}} = (T_{\text{end}} - T_{\text{start}} + 2) \cdot N_{\text{step}}$ iterations. The active time steps, measured from the first time step of the simulation experiment, in a specific optimization horizon are within the range described by:

$$N_{\text{opt-st}} = N_{\text{iter}} + 1 \leq k \leq N_{\text{iter}} + T_{\text{opt}} \cdot N_{\text{step}} = N_{\text{iter}} + N_{\text{opt}} = N_{\text{opt-end}} \tag{3.75}$$

with N_{iter} the number of succesfully finished iterations, T_{opt} the length (measured in calendar years) of the optimization horizon and N_{opt} the duration of the optimization horizon in time steps. The counter N_{iter} is increased by one after each sucessfully finished iteration untill the maximum number of iterations, given by $\bar{N}_{\text{iter}}$, is reached.

To indicate the calendar year and the time step within that year associated with time index k, the indexes y_{y} and y_{n} are introduced. These are given by:

$$y_{\text{y}}^{k} = \left\lfloor \frac{k}{N_{\text{step}}} \right\rfloor + T_{\text{start}} - 2 \tag{3.76}$$

$$y_{\text{n}}^{k} = k - N_{\text{step}} \left\lfloor \frac{k-1}{N_{\text{step}}} \right\rfloor \tag{3.77}$$

The following sections further explain all the features of the optimization problem. However, before discussing the variables, objective and constraints, predefined optimization settings are described.

3.3.1.1. Optimization settings

The infrastructure present and the degree of cooperation between riparian states can both have a significant impact on the value that can be created with the water resources. Besides these model options, there are several optional settings with which the objective and/or constraint can be changed, in order to study the value of certain interventions. Eight optional model settings are explained below:

1) Climate forcing - Standard simulation experiments are performed with perfect climate forcing foresight ($s_{\text{forcing}} = \textit{perfect}$). This assumes that there is complete knowledge about the climate forcing that will come, such that the forcing in the optimization and simulation is identical. This framework allows users to run experiments with imperfect foresight as well ($s_{\text{forcing}} = \textit{imperfect}$). In the latter case are historical time series (forcing of the past X years) used to force the model. This setting allows users to study the value of foresight information and investigate whether some collaboration scenarios are more sensitive to information gaps than others.

2) Reservoir cyclicity - When a rule curve for the reservoirs is not present, the setting $s_{\text{cyc}} = \textit{on}$ can be used to determine an optimal cyclic storage curve for the reservoirs. Instead of an MPC setup, a single optimization is performed over the entire duration of a simulation experiment in which the reservoir storage is forced in an annual recurring pattern.

3) International flow agreements - If there are agreements about the water distribution between riparian states, these can be imposed on all riparian states with the setting $s_{\text{agree}} = \textit{on}$. With this setting it is possible to study, from a regional perspective, the lost value of such a water distribution. This term should not be used in full coordinative scenarios.

4) Self-sufficiency - Self-sufficiency refers to the situation where the national production quantity is (to a certain extent) sufficient to meet the national food and feed demand. This self-sufficiency is, in order to reduce the influence of intra-annual variability in climate forcing, not defined over a single but instead multiple growing seasons. By default, this self-sufficiency is defined per state ($s_{\text{self-suff}} = \textit{national}$). However, it is also possible to define this constraint for a region ($s_{\text{self-suff}} = \textit{regional}$). This can be used to investigate whether the region can be more self-sufficient through cooperation, and whether the associated specialization and dependence entail economic benefits.

5) Rainfed and outside agriculture - The irrigated nodes in the main catchment are always part of the optimization. Agriculture in the rainfed pixels and in the outside basins can optionally be included as data ($s_{\text{other-agri}} = \textit{off}$) or optimization variables ($s_{\text{other-agri}} = \textit{on}$). By considering production at these agricultural sites as an optimization variable, further specialization can take place. The rate at which this specialization takes place can be limited if $s_{\text{agri-change}} = \textit{on}$.

6) Dietary - The diet can be specified per product as data ($s_{\text{diet}} = \textit{product}$), but the proposed framework makes it possible to make this part of the optimization as well. If ($s_{\text{diet}} = \textit{group}$), the diet is not described per product, but per product group, which creates freedom in the composition of the relevant product group. This freedom can be limited by forcing variation in the composition of the considered group.

7) Minimum income - This setting has been added to guarantee a certain economic distribution between the riparian states. If $s_{\text{income}} = \textit{on}$, each riparian state will have to create more value than a pre-set limit. This setting guarantees that every riparian state will benefit economically in a regional coordinated scenario compared to a unilateral case. The difference in regional production value with and without this setting indicates the loss of value due to the existence of multiple sovereign states within a single river basin.

8) Population growth - The population size is known for historical simulation experiments. For experiments looking into the future, the population size is based on predictions. Because the size of the population may significantly influence the required food production and water consumption, there are three different growth settings to choose from: $s_{\text{population}} = (\textit{low, medium, high})$

3.3.1.2. Optimization variables and bounds

The optimization variables Z are subdivided into five groups: the variables related to the (1) river system (2) electricity balance, (3) food balance, (4) agricultural production, (5) reservoir cyclicity and (6) the self sufficiency in commodity production.

$$Z := \begin{bmatrix} Z_{\text{flow}} & Z_{\text{electric}} & Z_{\text{prod}} & Z_{\text{agri}} & Z_{\text{cyc}} & Z_{\text{suff}} \end{bmatrix} \tag{3.78}$$

The following pragraphs elaborate per group on the variables within the group and their respective upper and lower bounds. When some bounds are not explicitly mentioned, they are either unlimited or bounded by zero. Although the domain of some variables is indirectly limited in a hard constraint, yet most of the variables are provided with an upper bound to limit the search space. A summury of the information in these paragraphs is found in Table 3.1. To improve model performance, all variables are scaled to the domain [0,1] by substracting the lower from the upper bound and dividing the result by the original domain [Wächter, 2009]. If positively or negatively unbounded, a scaling factor should be formulated by trial and error.

Flow variables - The group of flow variables include all variables related to the water balance. All these variables are defined per time step and hence defined by:

$$Z_{\text{flow}} := \begin{bmatrix} Z_{\text{f}}^{N_{\text{st-opt}}} & \dots & Z_{\text{f}}^{N_{\text{opt-end}}} \end{bmatrix} \tag{3.79}$$

with:

$$\begin{aligned} Z_{\text{f}}^{k} := [& V_{\text{turb},j}^{k} \quad V_{\text{gate},j}^{k} \quad V_{\text{spill},j}^{k} \quad V_{\text{irr},i,c}^{k} \quad H_{\text{irr},i,c}^{k} \quad V_{\text{off},o}^{k} \quad \dots \\ & V_{\text{turb},h}^{k} \quad V_{\text{agree},s,s}^{k} \quad S_{\text{hedge},j}^{k} \quad S_{\text{fill},j}^{k} \quad \Delta S_{\text{2-fill},j}^{k} \quad S_{\text{res},j}^{k}] \end{aligned} \tag{3.80}$$

With exception of V_{agree}, S_{hedge}, S_{fill} and $\Delta S_{\text{2-fill}}$ all these variables have been discussed in the sytem dynamics in Section 3.2. The variable V_{agree} is used to describe and softly constrain the annual flow between two states. This variable has an upper bound equal to the agreed annual flow $\bar{V}_{\text{agree}}$. The hedge storage is the last bit of active storage that is in a reservoir. To prevent a reservoir from becoming too empty due to uncertainty in forcing, efforts are made not to use this buffer during the planning phase. The volume of water stored in this buffer is given as a fraction f_{hedge} of the active storage:

$$\bar{S}_{\text{hedge},j}^{k} = \underline{S}_{\text{res},j} + f_{\text{hedge}} \cdot \left(\bar{S}_{\text{res},j}^{k} - \underline{S}_{\text{res},j} \right) \tag{3.81}$$

The last two new variables are used to describe turbine flow during filling, and to work around the associated complementarity constraint. The former is limited by dead reservoir storage, and the latter, as it is a normalized constraint, by unity.

The turbine, gate, offtake flow are all limited by their respective capacity $\bar{Q}_{\text{turb}} \cdot t^k$, $\bar{Q}_{\text{gate}} \cdot t^k$, $\bar{Q}_{\text{off}} \cdot t^k$. The reservoir storage is limited to the active storage; i.e. bounded by the maximum and minimum reservoir storage $\bar{S}_{\text{res}}$ and $\underline{S}_{\text{res}}$.

Because the available water for plant uptake is limited to the potential evaporation, the irrigation supply H_{irr} is bounded by the difference between the potential evaporation and precipitation. The lower bound is for annual crops ($N_{\text{harv},c} = 1$) set to ensure a minimum water supply. This minimum requirement is defined as a fraction $c_{\text{min-ET}}$ of the potential evapotranspiration:

$$\left.\begin{array}{ll} N_{\text{harv},c} = 1 & \max\left(0, \frac{c_{\text{min-ET}} \cdot ET^k_{\text{p},i,c} - \eta_{\text{eff}} \cdot P^k_i}{\eta^k_{\text{irr},a}}\right) \\ \text{otherwise} & 0 \end{array}\right\} \leq H^k_{\text{irr},i,c} \leq \max\left(0, \frac{ET^k_{\text{p},i,c} - \eta_{\text{eff}} \cdot P^k_i}{\eta^k_{\text{irr},a}}\right) \tag{3.82}$$

If the supply is less than this requirement, the crop is said to decay. For perennial crops ($N_{\text{harv},c} > 1$) a different constraint is valid as stressed by constraint $c_{\text{l-ineq12}}$ in Equation 3.134. The maximum irrigation flow $\bar{V}_{\text{irr}}$ is defined in a similar way. The only difference is that both the upper and lower bounds are multiplied by the area A_{agri} of the agricultural site.

The run-of-the-river turbine flow is limited by the maximum electric capacity. Since the elevation level in a run-of-the-river plant is assumed to be constant, the maximum turbine flow is described by:

$$\bar{Q}^k_{\text{turb},h} \cdot t^k = \bar{P}_{\text{e},h} \cdot t^k / (\rho \cdot g \cdot \eta_{\text{hydro},h} \cdot h_{\text{net},h}) \tag{3.83}$$

Electric variables - As for the flow variables are the four electricity related variables within this group all defined per time step:

$$Z_{\text{electric}} := \left[Z^{N_{\text{st-opt}}}_{\text{e}} \quad \ldots \quad Z^{N_{\text{opt-end}}}_{\text{e}} \right] \tag{3.84}$$

with:

$$Z^k_{\text{e}} := \left[E^k_{\text{con},s} \quad W^k_{\text{fuel},v,s} \quad E^k_{\text{e},j} \quad E^k_{\text{e-exp-var},s,s} \right] \tag{3.85}$$

The national electricity consumption E_{con} is limited by electricity demand E_{dem}. The maximum fuel consumption $\bar{W}_{\text{fuel}}$ is, as described in Equation 3.87, limited by the maximum power capacity of the non-renewable power plants:

$$\bar{W}^k_{\text{fuel},v} = \bar{P}^k_{\text{e},v} \cdot t^k \cdot c_{\text{load},v} / (H_{\text{fuel},v} \cdot \eta_{\text{fuel},v}) \tag{3.86}$$

where the load constant c_{load} corrects for the daily varying energy demand, as a result of which the plant cannot always generate at full capacity.

The electricity production by each reservoir is limited by the turbine power generation capacity. As for the fuel power plants is the maximum electricty production $\bar{E}_{\mathrm{e}}$ reduced by a load factor:

$$\bar{E}^k_{\mathrm{e},j} = \bar{P}^k_{\mathrm{e},j} \cdot t^k \cdot c_{\mathrm{load},j} \tag{3.87}$$

The maximum electricity trade $\bar{E}_{\text{e-exp-var}}$ is limited by the capacity of the interconnectors. Because several countries share the same transmission lines (see Section 3.2.3.2), the maximum flow is not limited by a variable bound, but constrained by constraint $c_{\text{l-ineq17}}$. However, to set an upper bound for each trade transation from a state, the maximum trade between states is set equal to the minimum capacity of the set of required interconnectors, i.e. the maximum trading flow is equal to the smallest capacity of the transmission lines in the set L_{s_1,s_2}:

$$\bar{E}_{\substack{\text{e-exp-var} \\ l \in \mathrm{L}_{s_1,s_2}}} = c_{\mathrm{load},l} \cdot \min\left(P^k_{\mathrm{e},l} \cdot t^k\right) \tag{3.88}$$

Product variables - The six variables in this group are as well defined for each time step. The fractions for vegetative energy intake are however only considered as an optimization variable if the diet is included in the optimization objective ($s_{\mathrm{diet}} = \mathit{group}$).

$$Z_{\mathrm{prod}} := \left[Z_{\mathrm{p}}^{N_{\text{st-opt}}} \quad \ldots \quad Z_{\mathrm{p}}^{N_{\text{opt-end}}}\right] \tag{3.89}$$

with:

$$Z^k_{\mathrm{p}} := \left[f^k_{\mathrm{vegetative},p,s} \quad f^k_{\mathrm{basket},p,s} \quad F^k_{\mathrm{process},p,p,s} \quad F^k_{\mathrm{exp},p,s,s} \quad F^k_{\text{prod-basin},p,s} \quad S^k_{\mathrm{food},p,s}\right] \tag{3.90}$$

If the diet is included in the optimization, the sum of the vegetative energy intake fractions of all products within a group must be equal to the group's energy intake $f_{\text{v-group}}$ as specified by constraint $c_{\text{l-eq3}}$ in Equation 3.126. To ensure some variability within a group, the intake fraction of each product is provided with an upper bound given by:

$$\bar{f}^k_{\substack{\mathrm{vegetative},p,s \\ p \in \mathrm{P}_g}} = f^k_{\text{v-group},g,s} \cdot \left(1 - c_{\mathrm{var}}\left(1 - \frac{1}{N_{\mathrm{prod},g}}\right)\right) \tag{3.91}$$

with c_{var} a constant (defined for the range [0,1]) introduced to ensure variability in diet, and N_{prod} the number of products within a group.

As for the vegetative energy intake should all basket fractions add up to the basket product group fraction. The variability in feed basket composition is not constrained. Each variabele is therefore limited by the associated product group basket fraction $f_{\text{b-group}}$.

Because multiple raw materials can be converted into the same final product, the production of a particular product through food processing is limited in constraint $c_{\text{l-inew10}}$. The processing flux F_{process} is therefore limited by the amount required to reach the processing production capacity $\bar{F}_{\text{prod-process}}$ if only the considered raw material is used for conversion.

$$\bar{F}^k_{\mathrm{process},p,p,s} = \bar{F}^k_{\text{prod-process},p,s} / \eta_{\text{F-conv},p,p,s} \tag{3.92}$$

The product trade and food production are both positively unbounded. The food storage is defined per food group in constraint $c_{\text{l-ineq9}}$. The maximum storage of a single product is therefore set equal to the maximum storage of the associated product group $\bar{S}_{\mathrm{food},g,s}$.

Agriculture variables - The variables within this group are used to describe the occupation and harvest area. Depending on the setting for the areas outside the main basin and in the rain dependent pixels, it describes the chacteristics of all agricultural sites or just the irrigation nodes within the main basin. Both variables in this group are not defined per time step, but per growing season. However, the variables are defined such that within each new iteration it can be checked whether the surface is still optimal, and if not, the surface can be reduced.

$$Z_{\text{agri}} := \begin{bmatrix} \delta_{\text{A},a,c}^{g_{\text{y},a,c}^{N_{\text{st-opt}}}} & A_{\text{harv},a,c}^{g_{\text{y},a,c}^{N_{\text{st-opt}}}} & \dots & \delta_{\text{A},a,c}^{g_{\text{y},a,c}^{N_{\text{opt-end}}}} & A_{\text{harv},a,c}^{g_{\text{y},a,c}^{N_{\text{opt-end}}}} \end{bmatrix} \tag{3.93}$$

In the time steps before and during the start of a new growing season, the new planted area δ_{A} is unbounded (total occupation area is constraint by $c_{l-ineq14}$). However, when the first time step in the optimization horizon falls within an active growing season, the limits for annual and perennial crops differ. The new planted surface can be reduced for annual crops, to simulate that a crop that does not receive enough water will decay and be removed from the land. Since it is assumed that perennial crops are not removed from the land, once planted, δ_{A} can no longer be reduced.

$$\begin{matrix} \text{if } g_{\text{n},a,c}^k > 0,\ g_{\text{y},a,c}^k = g_{\text{y},a,c}^{N_{\text{iter}}} \\ \text{and } N_{\text{harv},c} > 1 \\ \text{otherwise} \end{matrix} \quad \begin{matrix} \delta_{\text{A},a,c}^{g_{\text{y},a,c}^{N_{\text{iter}}}} \\ \\ 0 \end{matrix} \Bigg\} \leq \delta_{\text{A},a,c}^{g_{\text{y},a,c}^k} \leq \begin{cases} \delta_{\text{A},a,c}^{g_{\text{y},a,c}^{N_{\text{iter}}}} & \text{if } g_{\text{n},a,c}^k > 0 \text{ and } g_{\text{y},a,c}^k = g_{\text{y},a,c}^{N_{\text{iter}}} \\ A_{\text{agri},a,c}^k & \text{otherwise} \end{cases} \tag{3.94}$$

The harvest area is by definition (for resasons mentioned in Section 3.2.2.1) equal or smaller than the occupation area. This is described by constraint $c_{\text{l-ineq13}}$. To prevent the harvest area for perennials from increasing during a growing season, a similar reasoning applies as above. When the first time step in the optimization horizon falls during an active growing season, the harvest area is limited by the area during the previous iteration.

$$0 \leq A_{\text{harv},a,c}^{g_{\text{y},a,c}^k} \leq \begin{cases} A_{\text{harv},a,c}^{g_{\text{y},a,c}^{N_{\text{iter}}}} & \text{if } g_{\text{n},a,c}^k > 0 \text{ and } g_{\text{y},a,c}^k = g_{\text{y},a,c}^{N_{\text{iter}}} \\ A_{\text{agri},a,c}^k & \text{otherwise} \end{cases} \tag{3.95}$$

Cyclicity variables - The variables in this group are used to find the optimal cyclic storage (rule curves) in the reservoirs. Once known and $s_{\text{cyc}} = \textit{off}$, these variables are no longer necessary and holds $Z_{\text{cyc}} = [\ ]$.

$$Z_{\text{cyc}} := \begin{bmatrix} S_{\text{cyc},j}^1 & \dots & S_{\text{cyc},j}^{N_{\text{step}}} & , & \Delta S_{\text{2-cyc},j}^{N_{\text{st-opt}}} & \dots & \Delta S_{\text{2-cyc},j}^{N_{\text{opt-end}}} \end{bmatrix} \tag{3.96}$$

The variable S_{cyc} represents the cyclic reservoir level. This variable is not defined per time step, but has one variable for all reoccuring time steps within a year. The corresponding upper and lower limits are the hedge storage $\bar{S}_{\text{hedge}}$ and the maximum reservor storage $\bar{S}_{\text{res}}$ respectively. The auxiliary variable $\Delta S_{\text{2-cyc}}$ is introduced to keep the objective linear. This variable describes the normalized squared deviation between the actual reservoir storage and the cyclic storage per time step. Since the related constraint is normalized, it is limited on the domain [0,1].

Sufficiency variables - This vector contains only one variable, namely the self sufficient production $F_{\text{con-suff}}$. This variable is required in the soft constraint describing self sufficiency. Because this constraint compares production and consumption over a future period equal to the length of the optimization horizon, the variables are only defined for the last time step within the horizon.

$$Z_{\text{suff}} := \begin{bmatrix} F_{\text{con-suff},p,s}^{N_{\text{opt-end}}} \end{bmatrix} \tag{3.97}$$

The variable represents the minimum of the production and the consumption of a considered product over the duration of the constraint. The constraint applies over a period equal to twice the duration of the optimization horizon. Half of this period looks back in the past and half looks forward into the future. With this implementation, if production proves to be less than initially planned due to the prevailing climatic conditions, additional amounts can produced at a later date. In this way, any unplanned reduction in national product storage can be supplemented at a later time. The variable $F_{\text{con-suff}}$ is bounded by the sum of the maximum national consumption for food, feed and processing as described by:

$$F_{\text{con-suff},p,s} \leq \sum_{\substack{\kappa=N_{\text{iter}} \\ -N_{\text{opt}}+1}}^{N_{\text{iter}}+N_{\text{opt}}} \bar{F}^{\kappa}_{\text{con},p,s} = \sum_{\substack{\kappa=N_{\text{iter}} \\ -N_{\text{opt}}+1}}^{N_{\text{iter}}+N_{\text{opt}}} \bar{F}^{\kappa}_{\text{food},p,s} + \bar{F}^{\kappa}_{\text{feed},p,s} + \bar{F}^{\kappa}_{\text{con-process},p,s} \tag{3.98}$$

with $\bar{F}_{\text{con}}$ the maximum national consumption and $\bar{F}_{\text{food},p,s}$, $\bar{F}_{\text{feed},p,s}$ and $\bar{F}_{\text{con-process},p,s}$ the maximum consumption for food, feed and processing respectively. The latter ones can be computed following the relations presented in Section 3.2.2 using the upper bounds for the variables $f_{\text{vegetative}}$, f_{animal} and $\bar{F}_{\text{process}}$. In case regional self-sufficiency is studied, the variable $F_{\text{con-suff}}$ is not country specific, but used to represent the minimum of the regional production and consumption. In the latter case is the variabele bounded by the regional maximum consumption as described by:

$$F_{\text{con-suff},p} \leq \sum_{\substack{\kappa=N_{\text{iter}} \\ -N_{\text{opt}}+1}}^{N_{\text{iter}}+N_{\text{opt}}} \sum_{s\in\text{S}} \bar{F}^{\kappa}_{\text{con},p,s} = \sum_{\substack{\kappa=N_{\text{iter}} \\ -N_{\text{opt}}+1}}^{N_{\text{iter}}+N_{\text{opt}}} \sum_{s\in\text{S}} \bar{F}^{\kappa}_{\text{food},p,s} + \bar{F}^{\kappa}_{\text{feed},p,s} + \bar{F}^{\kappa}_{\text{con-process},p,s} \tag{3.99}$$

3.3.1.3. Objective

The aim of the optimization is to maximize the value of the national treasury over the optimization horizon, while being constraint by eighteen linear inequality constraints, four lineair equality constraints and five non-linear equality constraints:

$$\begin{aligned} \underset{\substack{Z_{\text{flow}},Z_{\text{prod}} \\ Z_{\text{electric}},Z_{\text{suff}} \\ Z_{\text{agr}},Z_{\text{cyc}}}}{\text{maximize}} \quad & I = \sum_{\kappa=N_{\text{iter}}+1}^{N_{\text{iter}}+N_{\text{opt}}} \left(\left(\frac{1}{1+c_{\text{int}}} \right)^{(\kappa-N_{\text{iter}})} \cdot (I^{\kappa}_{\text{e-net}} + I^{\kappa}_{\text{f-net}}) \right) - I_{\text{constraint}} \\ \text{subject to} \quad & c^{k}_{\text{l-ineq1}} : c^{k}_{\text{l-ineq18}} \\ & c^{k}_{\text{l-eq1}} : c^{k}_{\text{l-eq4}} \\ & c^{k}_{\text{nl-eq1}} : c^{k}_{\text{nl-eq5}} \end{aligned} \tag{3.100}$$

with c_{int} the yearly compound rate required to include the time value of money, and $I_{\text{constraint}}$ the penalty value of the soft constraints, which are further explained in Section 3.3.1.4.

3.3.1.4. Soft constraints

Depending on the simulation experimental settings, up to six soft constraints can be included. The total penalty value $I_{\text{constraint}}$ is the sum of the individual active soft constraints. An implementation with soft constraints has been chosen over an implementation with hard constraints to increase the robustness and overcome non-smoothness difficulties with complementarity constraints [Betts, 2010]. The total penalty value $I_{\text{constraint}}$ is given by:

$$I_{\text{constraint}} = \sum_{\kappa=N_{\text{iter}}+1}^{N_{\text{iter}}+N_{\text{opt}}} \left(I^{\kappa}_{\text{cs-spill}} + I^{\kappa}_{\text{cs-flow-agree}} + I^{\kappa}_{\text{cs-hedge}} + I^{\kappa}_{\text{cs-cyc}} + I^{\kappa}_{\text{cs-fill}} \right) + I^{N_{\text{opt-end}}}_{\text{cs-suff}} \tag{3.101}$$

Table 3.1: All variables in the optimization problem with their respective lower and upper bound.

Group	Variable	Lower bound	Upper bound
Z_{flow}	$V^k_{\text{turb},j}$	0	$Q^k_{\text{turb},j} \cdot t^k$
	$V^k_{\text{gate},j}$	0	$Q^k_{\text{gate},j} \cdot t^k$
	$V^k_{\text{spill},j}$	0	∞
	$H^k_{\text{irr},i,c}$	$\begin{cases} \max\left(0, \frac{c_{\text{min-ET}} \cdot ET^k_{\text{p},i,c} - \eta_{\text{eff}} \cdot P^k_i}{\eta^k_{\text{irr},a}}\right) \\ 0 \end{cases}$	$\max\left(0, \frac{ET^k_{\text{p},i,c} - \eta_{\text{eff}} \cdot P^k_{\text{eff},i}}{\eta^k_{\text{irr},a}}\right)$
	$V^k_{\text{irr},i,c}$	$A^k_{\text{agri},i} \cdot \underline{H}^k_{\text{irr},i,c}$	$A^k_{\text{agri},i} \cdot \bar{H}^k_{\text{irr},i,c}$
	$V^k_{\text{off},o}$	0	$\bar{Q}^k_{\text{off},o} \cdot t^k$
	$V^k_{\text{turb},h}$	0	$\bar{P}_{\text{e},h} \cdot t^k / (\rho \cdot g \cdot \eta_{\text{hydro},h} \cdot h_{\text{net},h})$
	$V^k_{\text{agree},s,s}$	0	$\bar{V}_{\text{agree},s,s}$
	$S^k_{\text{hedge},j}$	$\underline{S}^k_{\text{res},j}$	$\underline{S}_{\text{res},j} + f_{\text{hedge}} \cdot \left(\bar{S}^k_{\text{res},j} - \underline{S}_{\text{res},j}\right)$
	$S^k_{\text{fill},j}$	0	$\underline{S}_{\text{res},j}$
	$\Delta S^k_{\text{2-fill},j}$	0	1
	$S^k_{\text{res},j}$	$\underline{S}_{\text{res},j}$	$\bar{S}^k_{\text{res},j}$
Z_{electric}	$E^k_{\text{con},s}$	0	$E^k_{\text{dem},s}$
	$W^k_{\text{fuel},v,s}$	0	$\bar{P}^k_{\text{e},v} \cdot t^k \cdot c_{\text{load},v} / (H_{\text{fuel},v} \cdot \eta_{\text{fuel},v})$
	$E^k_{\text{e},j}$	0	$\bar{P}^k_{\text{e},j} \cdot t^k \cdot c_{\text{load},j}$
	$E^k_{\text{e-exp-var},s,s}$	0	$c_{\text{load},l} \cdot \min\limits_{l \in \text{L},s,s} \left(P^k_{\text{e},l} \cdot t^k\right)$
Z_{prod}	$f^k_{\text{vegetative},p,s}$	0	$f^k_{\text{v-group},g,s} \left(1 - c_{\text{var}} \left(1 - \frac{1}{N_{\text{prod},g}}\right)\right)$
	$f^k_{\text{basket},p,s}$	0	$f^k_{\text{b-group},g,s}$
	$F^k_{\text{process},p,p,s}$	0	$\bar{F}^k_{\text{prod-process},p,s} / c_{\text{F-conv},p,p,s}$
	$F^k_{\text{exp},p,s,s}$	0	∞
	$F^k_{\text{prod-basin},p,s}$	0	∞
	$S^k_{\text{food},p,s}$	0	$\bar{S}_{\text{food},g,s}$
Z_{agri}	$\delta^{g^k_{\text{y},a,c}}_{\text{A},a,c}$	$\begin{cases} \delta^{N_{\text{iter}}}_{\text{A},a,c} & \text{if } g^k_{\text{n},a,c} > 0,\ N_{\text{harv},c} > 1 \\ & \text{and } g^k_{\text{y},a,c} = g^{N_{\text{iter}}}_{\text{y},a,c} \\ 0 & \text{otherwise} \end{cases}$	$\begin{cases} \delta^{N_{\text{iter}}}_{\text{A},a,c} & \text{if } g^k_{\text{n},a,c} > 0 \text{ and} \\ & g^k_{\text{y},a,c} = g^{N_{\text{iter}}}_{\text{y},a,c} \\ A^k_{\text{agri},a,c} & \text{otherwise} \end{cases}$
	$A^{g^k_{\text{y},a,c}}_{\text{harv},a,c}$	0	$\begin{cases} A^{g^{N_{\text{iter}}}_{\text{y},a,c}}_{\text{harv},a,c} & \text{if } g^k_{\text{n},a,c} > 0 \text{ and} \\ & g^k_{\text{y},a,c} = g^{N_{\text{iter}}}_{\text{y},a,c} \\ A^k_{\text{agri},a,c} & \text{otherwise} \end{cases}$
Z_{cyc}	$S^{y^k_{\text{n}}}_{\text{cyc},j}$	$\max\limits_k \left(\bar{S}^k_{\text{hedge},j}\right)$	$\max\limits_k \left(\bar{S}^k_{\text{res},j}\right)$
	$\Delta S^k_{\text{2-cyc},j}$	0	1
Z_{suff}	$F^{N_{\text{opt-end}}}_{\text{con-suff},p}$	0	$\sum\limits_{\substack{\kappa=N_{\text{iter}} \\ -N_{\text{opt}}+1}}^{N_{\text{iter}}+N_{\text{opt}}} \bar{F}^{\kappa}_{\text{con},p,s}$

with $I_{\text{cs-spill}}$ the reservoir spill penalty, $I_{\text{cs-flow-agree}}$ the penalty for violiating the international flow agreements, $I_{\text{cs-hedge}}$ the penalty value for water use from the hedge storage (storage below hedge level), $I_{\text{cs-cyc}}$ the penalty for deviation from the cyclic reservoir level (required for the production of rule curves), $I_{\text{cs-fill}}$ the penalty value for turbine flow during the reservoir filling process and $I_{\text{cs-suff}}$ the penalty value for violating the target self-sufficieny level. The individual soft constraint are elaborated in the coming paragraphs.

Reservoir spill - The reservoir spillway should only be used if the capacity of the turbine and gate is not sufficient and the reservoir is completely filled. To guarantee this, preferably the following complementarity constraint is implemented:

$$V^k_{\text{spill},j} \cdot (\bar{S}_{\text{res},j} - S_{\text{res},j}) = 0 \tag{3.102}$$

This guarantees that flow over the spillway is only possible when the reservoir level reached its maximum value. To work around this complementarity problem, the expression could be reformulated as a soft constraint, so that there is no exact solution, but an approach to the solution. One method, as proposed by Celeste and Billib [2010], to implement this is by minimizing the sum of both parts of the product mentioned in Equation 3.102. However, this has the drawback that not only the spillway flow is penalized, but also a reservoir level lower than the maximum level.

Because the latter interferes with other parts of the objective, it was decided to punish only the spillway flow (Equation 3.103). When the cost of a spill event p_{spill} is large enough, it will never be used for downstream water needs, but only if the storage constraint of the reservoir itself cannot be met.

$$I^k_{\text{cs-spill}} = p_{\text{spill}} \cdot \sum_{j \in \text{J}} V^k_{\text{spill},j} \tag{3.103}$$

International flow agreement - To prevent a problem from becoming infeasible because the international flow agreements cannot be met in a dry year, this agreement was not implemented as a hard but a soft constraint:

$$I^k_{\text{cs-flow-agree}} = p_{\text{agree}} \cdot \sum_{s \in \text{S}} \left(\sum_{\zeta \in \text{S}} 1 - \frac{V^k_{\text{agree},s,s}}{\bar{V}_{\text{agree},s,s}} \right) \tag{3.104}$$

with V_{agree} the average annual outflow over the period since the start of the simulation (see Equation 3.117 in Section 3.3.1.5), and p_{agree} the price of constraint violation. To punish each agreement to the same extent, the soft constraint is normalized by dividing the real flow by the desired flow $\bar{V}_{\text{agree}}$. Because V_{agree} has an upper bound equal to $\bar{V}_{\text{agree}}$, the soft constraint can never become negative.

Reservoir hedging - The storage in the reservoir operational zone between the minimum and the hedge level can be used, but is preferable saved for unexpected variations in climate drivers. Using a soft constraint, use of the water can be penalized, while evaporation from the storage is still possible. The penalty value related to use of water from the hedge storage is given by:

$$I^k_{\text{cs-hedge}} = p_{\text{hedge}} \cdot \sum_{j \in \text{J}} \left(1 - \frac{S^k_{\text{hedge},j}}{\bar{S}^k_{\text{hedge},j}} \right) \tag{3.105}$$

with p_{hedge} the price of constraint violation and S_{hedge} the hedge storage. To punish use of the hedge storage to the same extent for all reservoirs, the soft constraint is normalized by dividing the real hedge storage by the maximum hedge strorage $\bar{S}_{\text{hedge}}$. Since S_{hedge} has an upper bound equal to $\bar{S}_{\text{hedge}}$, the constraint cannot be negative.

Reservoir cyclicity - This soft constraint is not standard active, but only used to compute missing rule curves as these are required in constraint $c_{\text{l-ineq4}}$. It penalizes the normalized squared deviation between real reservoir storage and the optimal cyclic reservoir storage with a costs of default p_{cyc}. To reduce the non-linearities and keep the objective linear, the auxiliary variable $\Delta S_{\text{2-cyc}}$ is herefore introduced. The value of this variable is assigned by constraint $c_{\text{nl-eq2}}$ in Equation 3.115. Given this variable, the penalty value for deviation from the cyclic storage is given by:

$$I^k_{\text{cs-cyc}} = p_{\text{cyc}} \cdot \sum_{j \in \text{J}} \Delta S^k_{\text{2-cyc},j} \tag{3.106}$$

Turbine during reservoir filling - When a new reservoir becomes active, and the surface elevation is still less than the turbine intake elevation, turbine flow is physically not possible. One way to constraint premature turbine flow is with a constraint described as:

$$V^k_{\text{turb},j} \cdot (S^k_{\text{res},j} - \underline{S}_{\text{res},j}) \geq 0 \tag{3.107}$$

To circumvent this complemanatrity problem, an implementation as soft constraint has been chosen. The auxiliary variable $\Delta S_{\text{2-fill}}$, which is equal to the normalized product of the turbine flow and storage (see constraint 3.111 in Section 3.3.1.5), is penalized at a cost p_{fill}:

$$I^k_{\text{cs-fill}} = p_{\text{fill}} \cdot \sum_{j \in \text{J}} \Delta S^k_{\text{2-fill},j} \tag{3.108}$$

Self-sufficiency - When the self-sufficiency is lower than the sufficiency target for a product, the difference between both is penalized. The sufficiency target comprises for each product the same fraction c_{suff} of the total consumption. Thanks to the implementation over a longer timeframe, this condition allows to study to what extent a country could be self-sufficient without being limited by the existing storage capacity. It namely allows a country to reimport a product exported at an earlier date. Based on the sufficiency setting, the difference between the national or regional consumption and the sufficiency target is penalized at a cost p_{suff}. Therefore, if $s_{\text{self-suff}} = \textit{national}$ the penalty function in Equation 3.109 should be implemented, while the function in Equation 3.110 is used if $s_{\text{self-suff}} = \textit{regional}$. The constraints are normalised in order to equally penalize a percentual deviation for all products.

$$I^{N_{\text{opt-end}}}_{\text{cs-suff}} = p_{\text{suff}} \cdot \sum_{s \in \text{S}} \left(\sum_{p \in \text{P}} \left(\frac{\sum_{\kappa=N_{\text{iter}}-N_{\text{opt}}+1}^{N_{\text{iter}}+N_{\text{opt}}} \left(c_{\text{suff}} \cdot F^{\kappa}_{\text{con},p,s} \right) - F^{N_{opt-end}}_{\text{con-suff},p,s}}{\sum_{\kappa=N_{\text{iter}}-N_{\text{opt}}+1}^{N_{\text{iter}}+N_{\text{opt}}} c_{\text{suff}} \cdot \bar{F}^{\kappa}_{\text{con},p,s}} \right) \right) \tag{3.109}$$

$$I^{N_{\text{opt-end}}}_{\text{cs-suff}} = p_{\text{suff}} \cdot \sum_{p \in \text{P}} \left(\frac{\sum_{s \in \text{S}} \left(\sum_{\kappa=N_{\text{iter}}-N_{\text{opt}}+1}^{N_{\text{iter}}+N_{\text{opt}}} \left(c_{\text{suff}} \cdot F^{\kappa}_{\text{con},p,s} \right) \right) - F^{N_{opt-end}}_{\text{con-suff},p}}{\sum_{s \in \text{S}} \left(\sum_{\kappa=N_{\text{iter}}-N_{\text{opt}}+1}^{N_{\text{iter}}+N_{\text{opt}}} c_{\text{suff}} \cdot \bar{F}^{\kappa}_{\text{con},p,s} \right)} \right) \tag{3.110}$$

3.3.1.5. Constraints

The constraint are divided into eight groups, being: (1) reservoir filling; (2) reservoir cyclicity; (3) international flow agreements; (4) water balance; (5) product production and consumption; (6) agriculture; (7) electricity; and (8) minimum income. Five out of a total of 28 constraints are nonlinear. Those five nonlinear equality constraint all serve the same purpose. They require equality between a (specially introduced auxiliary) variable and the product of two or more other optimization variables. By reformulating the constraints with these variables, a non-condensed formulation occurs allowing the objective as well as the remainder of the constraints to remain linear, resulting in better computational performance. To further increase the performance as well as the computational time, all constraints are scaled to the same order of magnitude [Hogg and Scott, 2013].

The above groups will be elaborated in the coming paragraphs. A summary of the constraint bounds and their respective scaling is presented in Table 3.2. All constraints being presented are unless stated otherwise valid for each time step k within the range as described by Equation 3.75, or from the moment a node becomes active $(T_{\text{active},j} - T_{\text{start}} + 1) \cdot N_{step} < k \leq N_{\text{iter}} + T_{\text{opt}} \cdot N_{\text{step}}$, with T_{active} the year in which a node becomes active. Nodes become active in the first time step within the year.

Reservoir filling - The first two constraints being introduced are used to penalize premature turbine flow during the reservoir filling process as mentioned in Equation 3.108. The first nonlinear constraint $c_{\text{nl-eq1}}$ is used to define the auxiliary variable $\Delta S_{\text{2-fill}}$. This variable must be equal to the normalized product of the turbine flow and the difference between the minimum reservoir storage $\underline{S}_{\text{res}}$ and the storage during filling S_{fill}. The variable $\Delta S_{\text{2-fill}}$ has been normalized to punish equally each reservoir, regardless of size or turbine capacity $\bar{V}_{\text{turb}}$. The storage during reservoir filling should always be smaller than the real reservoir storage, as described in constraint $c_{\text{l-ineq1}}$. Because this variable has an upper bound equal to the minimum storage level, any flow through the turbine at a true reservoir storage S_{res} less than the minimum storage will result in a positive value for $\Delta S_{\text{2-fill}}$, and at a true reservoir level greater then the minimum storage will result in a zero value and hence no penalty. Both constraints are valid from the moment a reservoir becomes active, till it completed its filling phase. The filling phase is completed if the reservoir level exceeds the operational level at the end of a simulation run.

$$c^k_{\text{nl-eq1}} := \frac{\left(\underline{S}_{\text{res},j} - S^k_{\text{fill},j}\right) \cdot V^k_{\text{turb},j}}{\underline{S}_{\text{res},j} \cdot \bar{V}_{\text{turb},j}} - \Delta S^k_{\text{2-fill},j} = 0 \tag{3.111}$$

$$c^k_{\text{l-ineq1}} := S^k_{\text{res},j} - S^k_{\text{fill},j} \geq 0 \tag{3.112}$$

To guarantee an outflow during the filling stages of a new reservoir, two constraints are introduced. The constraint $c_{\text{l-ineq2}}$ requires a minimum outflow per time step $V_{\text{fill-step}}$ to ensure some outflow during a dry season, while constraint $c_{\text{l-ineq3}}$ ensures a minimal yearly outflow $V_{\text{fill-year}}$. The former constraint is just as the turbine constraints mentioned above, valid from the moment a reservoir becomes active, till it completed its filling phase. The latter is valid starting one year after the moment a reservoir becomes active $k \geq (T_{\text{active},j} - T_{\text{start}} + 2) \cdot N_{\text{step}}$ until the filling phase is completed.

$$c^k_{\text{l-ineq2}} := V^k_{\text{out},j} - V_{\text{fill-step},j} \geq 0 \tag{3.113}$$

$$c^k_{\text{l-ineq3}} := \sum_{\kappa=k-N_{\text{step}}+1}^{k} V^\kappa_{\text{out},j} - V_{\text{fill-year},j} \geq 0 \tag{3.114}$$

Reservoir cyclicity - Two constraints are being classified in this group. The first constraint is required to determine the optimal cyclic reservoir levels (i.e. create rule curves) and the second to enforce the storage in the last time step of the optimization horizon to be equal to or larger than the level prescribed by the rule curve. The first constraint assigns a value to the auxiliary variable $\Delta S_{\text{2-cyc},j}$ used in Equation 3.106. This variable should be equal to the normalised squared difference between

the real and cyclic reservoir level. Just as for the soft constraint, this constraint is not active during regular simulation experiments. It is only used to find the optimal cyclicality in the reservoir during a single optimization over the entire simulation period, in the absence of existing rule curves.

$$c^k_{\text{nl-eq2}} := \frac{\left(S^k_{\text{res},j} - S^{y^k_{\text{n}}}_{\text{cyc},j}\right)^2}{\left(\bar{S}^k_{\text{res},j} - \bar{S}^k_{\text{hedge},j}\right)^2} - \Delta S^k_{\text{2-cyc},j} = 0 \tag{3.115}$$

The second constraint $c_{\text{l-ineq4}}$ in this group is used to enforce the storage in the active reservoirs (not during the filling stage) to be equal or larger than the storage stated by the rule-curve at the given time within a year. This implicitly assumes that that the uncertainty is so significant beyond the optimization horizon, that following the rule curve gives the best approximation for operations in the period after. This constraint should prevent the reservoir from being emptied at the end of the optimization horizon.

$$c^k_{\text{l-ineq4}} := S^{(N_{\text{iter}}+T_{\text{opt}}\cdot N_{\text{step}})}_{\text{res},j} - S^{y^{(N_{\text{iter}}+T_{\text{opt}}\cdot N_{\text{step}})}_{\text{n}}}_{\text{cyc},j} \geq 0 \tag{3.116}$$

International flow agreements - Constraint $c_{\text{l-ineq5}}$ states the annual average flow between two states for use in soft constraint Equation 3.104. The inflow in a downstream state is the cumulative inflow of all nodes $n \in \text{N}_{s,s}$, with $\text{N}_{s(1),s(2)}$ the set of all nodes in downstream state s_1 that receive water from a river stetch that originates in upstream state s_2. The annual average inflow V_{agree} is computed as the average inflow in these nodes over the completed years since the beginning of the simulation experiment $(y^{k+1}_{\text{y}} - T_{\text{start}} + 1)$.

$$c^k_{\text{l-ineq5}} := \frac{1}{y^{k+1}_{\text{y}} - T_{\text{start}} + 1} \cdot \sum_{\substack{\kappa=k+1-N_{\text{step}}\cdot \\ (y^{k+1}_{\text{y}}-T_{\text{start}}+1)}}^{k} \left(\sum_{n\in \text{N}_{s,s}} V^{\kappa}_{\text{in},n} \right) - V^k_{\text{agree},s,s} \geq 0 \tag{3.117}$$

Water balance - Four constraints are classified in this group. First are the dynamics of the reservoir, as given by Equation 3.15, included in the optimization through the linear equality constraint $c_{\text{l-eq1}}$.

$$c^k_{\text{l-eq1}} := S^{k-1}_{\text{res},j} - S^k_{\text{res},j} + V^k_{\text{in},j} - V^k_{\text{turb},j} - V^k_{\text{gate},j} - V^k_{\text{back},j} - V^k_{\text{vert},j} - V^k_{\text{spill},j} = 0 \tag{3.118}$$

To implement the piecewice linear surface-elevation-storage relation, it is linearized over the active reservoir storage. The area required to compute the vertical flux is therefore a linear function of the storage with slope p_{a} and initial offset p_{b}:

$$A^k_{\text{res},j} = p_{\text{a}} \cdot S^k_{\text{res},j} + p_{\text{b}} \tag{3.119}$$

Secondly, because the outflow from an offtake or an irrigation node can never be smaller than zero, the outflow is constrained to be positive by lineair inequality constraint $c_{\text{l-ineq6}}$:

$$c^k_{\substack{\text{l-ineq6} \\ \zeta\in\{\text{I,O}\}}} := V^k_{\text{out},\zeta} \geq 0 \tag{3.120}$$

In addition, should the flow through the turbine of a run-of-the-river hydro-electric plant be smaller than the inflow in the node during the same time step as stated by lineair inequality constraint $c_{\text{l-ineq7}}$:

$$c^k_{\text{l-ineq7}} := V^k_{\text{in},h} - V^k_{\text{turb},h} \geq 0 \tag{3.121}$$

The final linear inequality constraint $c_{\text{l-ineq8}}$ within the water balance group definies the hedge reservoir level S_{hedge} for use in the soft constraint presented in Equation 3.105. The hedge reservoir level should always be smaller than the real reservoir level, but will in practice be equal to the true reservoir level or to its upper bound value $\bar{S}_{\text{hedge}}$.

$$c^k_{\text{l-ineq8}} := S^k_{\text{res},j} - S^k_{\text{hedge},j} \geq 0 \tag{3.122}$$

Product production and consumption - Within this group, seven constraints are classified that are related to the product balance, consumption and storage. The constraints related to the agricultural production are discussed in the next paragraph.

The dynamics of the food balance as described by Equation 3.24 are included through lineair equality constraint $c_{\text{l-eq2}}$. The storage capacity is thereby limited through lineair inequality constraint $c_{\text{l-ineq9}}$. The maximum storage $\bar{S}_{\text{food}}$ is prescribed per product group rather than per product. It is hereby assumed that storage facilities can be used for all products within a group, but cannot be exchanged between groups.

$$c^k_{\text{l-eq2}} := S^{k-1}_{\text{food},p,s} - S^k_{\text{food},p,s} + F^k_{\text{prod},p,s} + F^k_{\text{trade},p,s} - F^k_{\text{con},p,s} = 0 \tag{3.123}$$

$$c^k_{\text{l-ineq9}} := \bar{S}^k_{\text{food},g,s} - \sum_{p \in \text{P}_g} S^k_{\text{food},p,s} \geq 0 \tag{3.124}$$

The production from product processing is limited by a maximum production capacity $\bar{F}_{\text{prod-process}}$. This maximum processing capacity is defined on the production rather than on the consumption side, as stated by lineair inequality constraint $c_{\text{l-ineq10}}$.

$$c^k_{\text{l-ineq10}} := \bar{F}^k_{\text{prod-process},p,s} - F^k_{\text{prod-process},p,s} \geq 0 \tag{3.125}$$

The two constraints below both relate to product consumption. Linear equality constraint $c_{\text{l-eq3}}$ is stated to constrain the energy intake. If the choice is made to specify the diet as data ($s_{\text{diet}} = \textit{product}$), this constraint is always valid. If the choice is made to include the diet in the optimization, the intake ratios of specific products may vary, but the cumulative energy intake of all products within a group must remain the same and equal to $f_{\text{v-group}}$. The second linear equality constraint $c_{\text{l-eq4}}$ states, as for the energy intake, that the weight contribution of different feed products may vary as long as the the total weight intake per group $f_{\text{b-group}}$ is satisfied. Unlike the energy intake constraint $c_{\text{l-eq3}}$, this constraint is always active.

$$c^k_{\text{l-eq3}} := f^k_{\text{v-group},g,s} - \sum_{p \in \text{P}_g} f^k_{\text{vegetative},p,s} = 0 \tag{3.126}$$

$$c^k_{\text{l-eq4}} := f^k_{\text{b-group},g,s} - \sum_{p \in \text{P}_g} f^k_{\text{basket},p,s} = 0 \tag{3.127}$$

The last two constraints in this group are related to the self-sufficiency. They ensure that the self-sufficient consumption $F_{\text{con-suff}}$ is smaller than or equal to the minimum of the product production and the sufficiency target. As mentioned before, the sufficiency target is herein for all products defined as a fraction c_{suff} of the consumption. In case $s_{\text{self-suff}} = \textit{national}$ the linear non equality constraints $c_{\text{l-ineq11}}$ and $c_{\text{l-ineq12}}$ are stated as:

$$c^k_{\text{l-ineq11}} := \sum_{\kappa=N_{\text{iter}}-N_{\text{opt}}+1}^{N_{\text{iter}}+N_{\text{opt}}} F^{\kappa}_{\text{prod},p,s} - F_{\text{prod-suff},p,s} \geq 0 \tag{3.128}$$

$$c^k_{\text{l-ineq12}} := \sum_{\kappa=N_{\text{iter}}-N_{\text{opt}}+1}^{N_{\text{iter}}+N_{\text{opt}}} c_{\text{suff}} \cdot F^{\kappa}_{\text{con},p,s} - F_{\text{prod-suff},p,s} \geq 0 \tag{3.129}$$

In case $s_{\text{self-suff}} = \textit{regional}$ the variable $F_{\text{con-suff}}$ should be smaller than the minimum of the regional production or the regional sufficiency constraint, the latter being defined as a fraction of the regional consumption. In this case, the linear equality constraints $c_{\text{l-ineq11}}$ and $c_{\text{l-ineq12}}$ are given by:

$$c^k_{\text{l-ineq11}} := \sum_{\substack{\kappa=N_{\text{iter}}\\-N_{\text{opt}}+1}}^{N_{\text{iter}}+N_{\text{opt}}} \sum_{s\in \text{S}} F^{\kappa}_{\text{prod},p,s} - F_{\text{prod-suff},p} \geq 0 \tag{3.130}$$

$$c^k_{\text{l-ineq12}} := \sum_{\substack{\kappa=N_{\text{iter}}\\-N_{\text{opt}}+1}}^{N_{\text{iter}}+N_{\text{opt}}} \sum_{s\in \text{S}} c_{\text{suff}} \cdot F^{\kappa}_{\text{con},p,s} - F_{\text{prod-suff},p} \geq 0 \tag{3.131}$$

Agriculture - This group contains six constraints describing and limiting agricultural yield. First of all is the water balance on a single agricultural field, as stated in Equation 3.16, included in the problem definition by nonlinear equality constraint $c_{\text{nl-eq3}}$. H_{irr} has been specified as an optimization variable in addition to V_{iir} to prevent a nonlinear division in the yield function.

$$c^k_{\text{nl-eq3}} := V^k_{\text{irr},i,c} - H^k_{\text{irr},i,c} \cdot A^k_{\text{harv},i,c} = 0 \tag{3.132}$$

Nonlinear equality constraint $c_{\text{nl-eq4}}$ is used to the define auxiliary variable $F_{\text{prod-basin}}$. This variable equals the sum of the agricultural yields in all irrigation nodes within the basin. The constraint is not linear because the yield is a product of the harvest surface and the irrigation supplies (see Equation 3.46). By defining this variable, the food balance constraint $c_{\text{l-eq2}}$ can be implemented linearly.

$$c^k_{\substack{\text{nl-eq4}\\p\in\text{C}}} := F^k_{\text{prod-basin},p,s} - \sum_{i\in \text{I}_s} Y^k_{\text{act},i,p} = 0 \tag{3.133}$$

In contrast to the annual crops that have been implemented in such a way that a one time water shortage (specified as $ET^k_{\text{a}} < ET^k_{\text{p}}$) is already fatal, for annual crops, the minimum evaporation requirement applies over a timespan of several time steps (specified as $N_{\text{per}} \leq N_{\text{step}}$) as stated by linear inequality constraint $c_{\text{l-ineq13}}$. This implementation was chosen to enable perennial crops to grow in rain-dependent areas with multiple dry time steps. To separate the crop water balance between the growing seasons, the constraint is only valid in the last $N_{\text{step}} - N_{\text{per}} + 1$ time steps of each growing season. However, with the introduction of the logical operator, the constraint stated below is generally valid for all time steps.

$$c^k_{\text{l-ineq13}} := \mathbf{1}_{\left(g^k_{\text{n},c,a}+1\geq N_{\text{per}}\right)} \cdot \sum_{\kappa=k-N_{\text{per}}+1}^{k} \left(H^{\kappa}_{\text{avail},c,a} - H^{\kappa}_{\text{drain},c,a} - c_{\text{min-ET}} \cdot ET^{\kappa}_{\text{p},c,a}\right) \geq 0 \tag{3.134}$$

Constraint $c_{\text{l-ineq14}}$ includes the definition of the harvest area (Equation 3.29) in the optimization problem. If there is not sufficient resource to supply all crops with the required amount of water, this constraint allows the algorithm to reduce the area or to supply deficit irrigation. Because annual crops are immediately removed if the evaporation requirement is not met, the formulation below applies to

this crop group as an equality constraint. However, for perennial crops, the formulation applies as an inequality constraint. Although it is no longer possible to remove a part of the occupation area for perennial crops after seeding, the dyamics allow a reduction of the harvest area during a growing seasons. As a result can the actual harvest area be smaller than the maximum harvest area.

$$c^k_{\text{l-ineq14}} := \sum_{\tau=N_{\text{ini},c}}^{N_{\text{harv},c}} \delta^{g^k_{\text{y},a,c}-\tau+1}_{\text{A},a,c} - A^{g^k_{\text{y},a,c}}_{\text{harv},a,c} \begin{cases} = 0 & \text{if } N_{\text{harv},c} = 1 \\ \geq 0 & \text{if } N_{\text{harv},c} > 1 \end{cases} \tag{3.135}$$

The last two constraints relate to the cultivated agricultural areas. At each agricultural site, the sum of all cultivated fields should be smaller than the total available agricultural area at that site as stated by linear inequality constraint $c_{\text{l-ineq15}}$. Depending on the setting $s_{\text{other-agri}}$, this constraint is only valid for the sites within the main basin, or also for the outside basins and rainfed pixels. If $s_{\text{agri-change}} = on$ the change in occupation area between two succesive growing seasons is limited as stated by lineair equality constraint $c_{\text{l-ineq16}}$ to a fraction of the total agricultural area at the considered site.

$$c^k_{\text{l-ineq15}} := \bar{A}^k_{\text{agri},a} - \sum_{c\in\text{C}} A^k_{\text{occ},a} \geq 0 \tag{3.136}$$

$$c^k_{\text{l-ineq16}} := c_{\text{agri-ch}} \cdot \bar{A}^k_{\text{agri},a} - \left| A^{g^k_{\text{y},c,a}-1}_{\text{occ},c,a} - A^{g^k_{\text{y},c,a}}_{\text{occ},c,a} \right| \geq 0 \tag{3.137}$$

Energy balance - Three constraints with respect to the energy production and commerce are classified in this group. Firstly are the electricity dynamics, as given by Equation 3.54, included in the optimization problem through linear inequality constraint $c_{\text{l-ineq17}}$.

$$c^k_{\text{l-ineq17}} := E^k_{\text{e-con},s} - E^k_{\text{e-avail},s} \geq 0 \tag{3.138}$$

Nonlinear equality constraint $c_{\text{nl-eq5}}$ describes equality between the electricity production by a surface water reservoir and auxiliary variable $E_{\text{e},j}$. The auxiliary variable is introduced to transform formulation $c_{\text{l-ineq17}}$ into a lineair constraint. The electricity production follows the dynamics as explained in Section 3.2.3.1. The water surface elevation is hereby, as for the surface area, found by linearizing the relation over the active reservoir storage (Equation 3.140).

$$c^k_{\text{nl-eq5}} := \rho \cdot g \cdot \eta_{\text{hydro},j} \cdot V^k_{\text{turb},j} \cdot h^k_{\text{net},j} - E^k_{\text{e},j} = 0 \tag{3.139}$$

$$h^k_{\text{res},j} = q_{\text{a},j} \cdot S^k_{\text{res},j} + q_{\text{b},j} \tag{3.140}$$

The last constraint within this group limits the electricity trade. Each transmission line is characterised by a maximum power capacity $\bar{P}_{\text{e}}$. The total electric flux passing over this line should be smaller than the electric transport capacity as stated in linear inequality constraint $c_{\text{l-ineq18}}$. The electric transport capacity is herein the product of the maximum electric flow $\bar{P}^k_{\text{e},l} \cdot t^k$ and the load factor c_{load}. The latter accounts for the effects of variability in electricity demand over a period of time. Because demand is not homogeneous over a time step, the maximum capacity is used only a fraction of time.

$$c^k_{\text{l-ineq18}} := c_{\text{load},l} \cdot \bar{P}^k_{\text{e},l} \cdot t^k - \sum_{s\in\text{S}} \left(\sum_{\zeta\in\text{S}} \mathbf{1}_{(l\in\text{L}_{s,\zeta})} \cdot \left(E^k_{\text{e-exp-fxd},s,\zeta} + E^k_{\text{e-exp-var},s,\zeta} \right) \right) \geq 0 \tag{3.141}$$

Table 3.2: All hard constraint possible in the optimization problem with their respective lower and upper bound and the scaling factor. For the non negativity constraint and the run-of-the-river constraint does the scaling depend on the magnitude of the respective outflows and inflows.

Group	Constraint	Bounds	Scaling factor
Reservoir filling	$c^k_{\text{nl-eq1}}$	[0,0]	1
	$c^k_{\text{l-ineq1}}$	[0,∞]	$\bar{S}^k_{\text{res},j}$
	$c^k_{\text{l-ineq2}}$	[0,∞]	$V_{\text{fill-year},j}$
	$c^k_{\text{l-ineq3}}$	[0,∞]	$V_{\text{fill-year},j}$
Reservoir cyclicity	$c^k_{\text{nl-eq2}}$	[0,0]	1
	$c^k_{\text{l-ineq4}}$	[0,∞]	$\bar{S}^k_{\text{res},j}$
International flow	$c^k_{\text{l-ineq5}}$	[0,∞]	$\bar{V}^k_{\text{agree},s,s}$
Water balance	$c^k_{\text{l-eq1}}$	[0,0]	1
	$c^k_{\text{l-ineq6}}$	[0,∞]	-
	$c^k_{\text{l-ineq7}}$	[0,∞]	-
	$c^k_{\text{l-ineq8}}$	[0,∞]	$\bar{S}^k_{\text{res},j}$
Product production and consumption	$c^k_{\text{l-eq2}}$	[0,0]	1
	$c^k_{\text{l-eq3}}$	[0,0]	1
	$c^k_{\text{l-eq4}}$	[0,0]	1
	$c^k_{\text{l-ineq9}}$	[0,∞]	$\bar{S}^k_{\text{food},g,s}$
	$c^k_{\text{l-ineq10}}$	[0,∞]	$\bar{F}^k_{\text{prod-process},p,s}$
	$c^k_{\text{l-ineq11}}$	[0,∞]	$\sum_{\kappa=N_{\text{iter}}-N_{\text{opt}}+1}^{N_{\text{iter}}+N_{\text{opt}}} c_{\text{suff}} \cdot F^{\kappa}_{\text{con},p,s}$
	$c^k_{\text{l-ineq12}}$	[0,∞]	$\sum_{\kappa=N_{\text{iter}}-N_{\text{opt}}+1}^{N_{\text{iter}}+N_{\text{opt}}} c_{\text{suff}} \cdot F^{\kappa}_{\text{con},p,s}$
Agriculture	$c^k_{\text{nl-eq3}}$	[0,0]	1
	$c^k_{\text{nl-eq4}}$	[0,0]	1
	$c^k_{\text{l-ineq13}}$	[0,∞]	$\sum_{\kappa=k-N_{\text{per}}+1}^{k} c_{\text{min-ET}} \cdot ET^{\kappa}_{\text{p},c,a}$
	$c^k_{\text{l-ineq14}}$	$\begin{cases}[0,0] & \text{if } N_{\text{harv},c}=1\\ [0,\infty] & \text{if } N_{\text{harv},c}>1\end{cases}$	$A^k_{\text{agri},a}$
	$c^k_{\text{l-ineq15}}$	[0,∞]	$A^k_{\text{agri},a}$
	$c^k_{\text{l-ineq16}}$	[0,∞]	$c_{\text{agri-ch}} \cdot A^k_{\text{agri},a}$
Electricity balance	$c^k_{\text{nl-eq5}}$	[0,0]	1
	$c^k_{\text{l-ineq17}}$	[0,∞]	$E^k_{\text{dem},s}$
	$c^k_{\text{l-ineq18}}$	[0,∞]	$c_{\text{load},l} \cdot \bar{P}^k_{\text{e},l}$
Minimum income	$c^k_{\text{l-ineq19}}$	[0,∞]	$\sum_{\kappa=k-0.5\cdot N_{\text{inc-period}}}^{k-1+0.5\cdot N_{\text{inc-period}}} I^{\kappa}_{\text{min},s}$

Minimum income - The last and also only linear equality constraint $c_{\text{l-ineq19}}$ in this group states that the net income must be larger than a specified value. This formulation (active if $s_{\text{min-income}} = on$) is mainly required in a regional coordinative scenario (see Section 3.4) to ensure that the added value is distributed fairly among all riparian states. Because the income pattern may differ between scenarios, the constraint is, just as the international flow agreement constraint $c_{\text{l-ineq11}}$, implemented over a period that goes back in the past and looks ahead in the future. Because of this, the constraint is active for the time steps: $0.5 \cdot N_{\text{inc-period}} < k \leq N_{\text{iter}} + T_{\text{opt}} \cdot N_{\text{step}} - 0.5 \cdot N_{\text{inc-period}} + 1$.

$$c^k_{\text{l-ineq19}} := \sum_{\substack{\kappa=k-0.5\cdot \\ N_{\text{inc-period}}}}^{\substack{k-1+ \\ 0.5\cdot N_{\text{inc-period}}}} \left(I^{\kappa}_{\text{f-net},s} + I^{\kappa}_{\text{e-net},s} - I^{\kappa}_{\text{min},s}\right) \geq 0 \tag{3.142}$$

3.3.2. Simulation model formulation

The simulation follows the results of the optimization and the previously described system dynamics as far as possible. However, there are a number of circumstances where the simulation deviates from the optimization. These circumstances occur when, due to simplifications, numerical sub-optimalities or deviation in the climate forcing situations arise that do not comply with the system dynamics, or where another action is desirable. Therefore low-level controllers are assumed to be present for the three balances. For the energy and food balance, these are defined on a national level. For the river related infrastructure, these low level controllers are defined per node. The operations and principles of each low level controller are explained in subsequent sections.

3.3.2.1. Water balance

The purpose of the low level controller for the reservoir is twofold. On the one hand, it is aimed at ensuring that the outflow as determined by the optimization leaves the reservoir, and on the other, to ensure that the demanded energy production as determined by the optimization is generated. Herefore, the controller has the option to interchange part of the predicted flow between the turbine and gate conduit. Because the optimization, in contrast to the real world simulation, uses linear elevation-storage relations, the turbine flow required to fulfill the generation target could, at the same reservoir storage, deviate between both models.

There are two situations where the controller can deviate from the prescribed outflow and electricity generation. These situations occur when a difference between the predicted and actual inflow or evaporation threatens the reservoir to leave empty or overflow. When overflow threatens to occur, the flow through the gate will be increased if possible. Overflow therefore only occurs when the gate spills at full capacity. In the other situation, if the reservoir threatens to run empty, a hedge protocol will be put into action. The aim of this protocol is to preserve part of the storage for future uncertainties in climate forcing. When water is required from storage below the hedge level to meet the outflow target, the outflow will be reduced. The real outflow originating from this storage buffer follows a linear relationship with the storage in this part of the reservoir. As the predicted reservoir level prior to hedging threatens to fall deeper into the hedging buffer, an increasingly smaller percentage of the flow will be released (see Figure 3.9). The outflow after hedging is described by:

$$V^k_{\text{out},j} = \breve{V}^k_{\text{out},j} + V^k_{\text{hedge},j} \cdot \left(\left(\frac{\breve{S}^k_{\text{res},j} - \underline{S}_{\text{res},j}}{\bar{S}^k_{\text{hedge},j} - \underline{S}_{\text{res},j}} \right) + \frac{1}{2} \cdot \left(\frac{V^k_{\text{hedge},j}}{\bar{S}^k_{\text{hedge},j} - \underline{S}_{\text{res},j}} \right) - 1 \right) \tag{3.143}$$

with:

$$V^k_{\text{hedge},j} = \max\left(\min\left(\bar{S}^k_{\text{hedge},j} - \breve{S}^k_{\text{res},j}, \breve{V}^k_{\text{out},j}\right), 0\right) \tag{3.144}$$

where $\breve{S}_{\text{res}}$ represents the expected storage at the end of the time step when hedging does not occur, and $\breve{V}_{\text{out}}$ the demanded reservoir outflow before hedging.

For offtakes and irrigation nodes, a deviation from the predicted climate forcing may result in negative outflows. To prevent this, the water consumption and diversion are respectively reduced. When reducing the water consumption in an irrigation node, it is assumed that all fields receive the same fraction of the allocated volume. This reduced irrigation flow, as well as a change in evaporation and/or precipitation compared to the forecast, may result in a devation from the predicted land use. If the amount of water available for evaporation threatens to fall below the minimum evaporation requirement, the irrigation area is reduced by the minimum amount required, so that the remaining part of the cropland retains potency for harvesting at a later stage. For the annual crops this means that they are completely removed from the field, while the perennial crops go into hibernation.

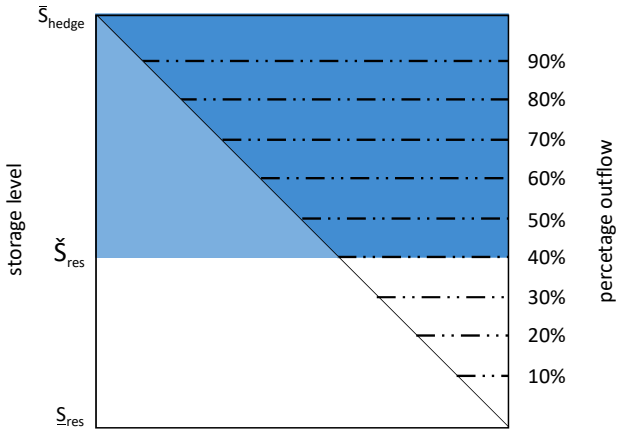

Figure 3.9: Graphical example of a situation that requires hedging. The expected reservoir level at the end of the time step $\check{S}_{res}$ is situated in the buffer zone between the minimal storage level and the hedge storage level. The blue shaded area represent the demanded outflow. However, only the dark blue shaded area is released, while the volume in the light blue shaded triangle is conserved in the reservoir storage.

3.3.2.2. Energy balance

For the energy balance, a fictional low-level controller is defined at national level. The purpose of this controller is to meet the electricity demand at minimal cost. Therefore, this controller can make a number of changes in energy generation. If a reservoir is unable to generate the required amount of energy, the production of a fuel power plant, if having spare capacity, is scaled up. Conversely, when a reservoir can generate more electricity with the prescribed outflow, the production of the fuel power plants is reduced. International electricity trading is secured in trade treaties and cannot be adjusted for this reason.

3.3.2.3. Food balance

A fictitious low-level controller also applies to the food balance. However, because the crops are already harvested in the time step before they are marketable, the uncertainty in this balance is small and the differences between the optimization and simulation model are minimal. The goal of this controller is therefore solely to overcome the suboptimalities occuring due to numerical inaccuracies in the scaled optimization problem. It might happen that the optimal solution prescribes a small flux in the opposite direction in addition to an import or export flux. The current controller solves this inaccuracy and guarantees that trading takes place in one direction only.

3.4. International cooperation scenarios

To study the economic value of cooperation, four cooperation scenarios have been implemented. Two novel cooperation scenarios have been added between the two often used extremes of unilateralism and coordination, namely: 1) flow-information and 2) trade-information. These scenarios enable us to quantify the value of information exchange about expected river flows and trade flows. By combining these four collaboration scenarios with the model/constraint options as presented in Section 3.3.1.1, a wider variety of simulation experiments can be obtained. The four scenarios are explained in the following sections in increasing order of cooperation.

3.4.1. Unilateralism

Unilateralism is a political situation where a state acts unilaterally without being dependent on cooperation with other states. In the proposed framework, there is a national planning of the water infrastructure and agriculture under this cooperative scenario. This form of planning is already more comprehensive than most worldly examples, where planning takes place at individual infrastructure level. To determine the optimal national planning, a separate optimization is carried out for each riparian state. It starts with the most upstream country, and only after all model runs for the simulation horizon are finished does the focus shift to the next country in the downstream direction.

There is no exchange of information between the riparian states, nor about the expected outflow from upstream countries, nor about electricity and product trade. This means that products can only be traded on the international market ($F_{\text{exp},s,s} \leq 0$, $F_{\text{exp},s,\text{extern}} \leq \infty$), and electricity is only traded under long term (annual) contracts ($E_{\text{e-exp-var},s,s} \leq 0$). The quantities traded under these long term contracts are specified per year before the start of the simulation experiments. For this purpose, the expected national production in each country is computed using the capacity factors of all plants. Subsequently, an one-time optimization is used to determine how countries with an expected surplus of electricity should trade in order to minimize regional shortages every year:

$$\begin{aligned} \underset{E^{g_y^k}_{\text{e-exp-fxd},s,s}}{\text{minimize}} \quad & \sum_{\kappa=1}^{\bar{N}_{\text{iter}}} \sum_{s \in \text{S}} \left(E^{\kappa}_{\text{dem},s} - E^{\kappa}_{\text{avail},s} \right) \\ \text{subject to} \quad & E^{k}_{\text{e-con},s} \leq E^{k}_{\text{e-dem},s} \\ & c^{k}_{\text{l-ineq17}} \text{ in Equation 3.141} \end{aligned} \tag{3.145}$$

Because no information is shared about the river flows, an estimate is made of the inflow for nodes located completely upstream in a downstream country. This is done by fitting a quadratic curve over the entire time horizon between the modelled inflow from the upstream country and the time-matched summed discharge over all source nodes upstream of a particular node. By using this relationship in reverse with the sum of the expected discharge over all upstream source nodes as input, the expected node inflow is estimated.

After completing the runs for all countries, the product trade is reviewed once more. If it turns out that a riparian state imports a certain product when another exports it, international trade is converted into regional trade. When several countries want to take over or offer a product, the partner is chosen at the geographically smallest distance. This is the most optimal thing to do from an optimization point of view, but does not account for the purchase power of the different countries.

3.4.2. Flow-information

The flow-information cooperation scenario largely corresponds to the unilateral scenario. Product trading is still only possible with the international market, and electricity trading is under long term contracts. The difference, however, is that information about discharge in the transboundary river is shared. This reduces the uncertainty in inflow for more downstream countries. To achieve this, optimization is still taking place per riparian state, but unlike the unilateral scenario, an optimization is carried out for each country before proceeding to the simulation. The expected outflow from an upstream country can therefore be used as forcing for the optimisation in a downstream country.

3.4.3. Trade-information

In the trade-information cooperation scenario there is still a national planning of water infrastructure and agriculture. In addition to information sharing about the expected inflow, information is also exchanged about electricity and product trade between the riparian states. More specifically, can each country share per time step how much electricity it expects to be short and which products it intends to trade on the international market. Therefore, the electricity market is driven by demand, while the product market is driven by supply. The information on food supply enables countries to purchase products, that according to the original planning should be purchased on the international

market, regionally at a lower transport rate. Because of this, it might be advantageous for a country to purchase another product (or) at any other time in the optimization horizon. Both choices will have consequences for the national agricultural planning. The information about electricity shortage enables riparian states to deviate from long-term energy contracts. Instead of a prescribed quantity, it is possible to choose per time step whether and how much electricity is exported to neighbouring countries. This freedom of choice can result in a different (competitive) use of water resources.

Because there is still an indivudual optimization for each state, this market mechanism has been implemented as an iterative process (see Figure 3.10). As a result, each riparian state goes through an optimization several times before switching to the simulation. The choice for the number of iterations is coupled with the choice for the number of time steps (with a maximum or N_{iter}) for which information is shared. In general, a larger number of time steps results in more freedom of choice and therefore requires more iterations to converge.

Each iteration contains two proceedings, both of which are preceded by an optimization. Each optimization is characterized by a unique set of limits for the trade optimization variables. In the very first iteration, as in the previous cooperation scenarios, trade is only possible with the external world ($F_{\text{exp},s,s} \leq 0,\ F_{\text{exp},s,\text{extern}} \leq \infty$). During successive proceedings, these limits are adjusted to enable regional trade. In the first proceeding, it is determined for each country which quantity of a certain product is still free to trade. This quantity of exports which is not yet allocated is defined as the total expected export from a state minus the quantities that other regional countries plan to import from this state. With this amount known, the boundary of the trade optimization variable is adjusted. The new value equals the sum of the planned import and the freely tradable quantity. In the successive optimization, it is now possible for countries to tender for this non allocated quantity. The new upper limit after completing the first proceeding is given by:

$$\begin{aligned} \bar{F}^{k}_{\underset{\alpha}{\text{exp},p,s,\alpha}} &= F^{k}_{\underset{\alpha}{\text{exp},p,s,\alpha}} + F^{k}_{\underset{s}{\text{exp},p,s,\text{extern}}} - \sum_{\omega \in \text{S}} F^{k}_{\underset{\omega}{\text{exp},p,s,\omega}} \\ &= F^{k}_{\underset{\alpha}{\text{exp},p,s,\alpha}} + F^{k}_{\text{exp-free},p,s} \end{aligned} \tag{3.146}$$

with $\bar{F}_{\text{exp},p,s,\alpha}$ the new upper bound for product trade between state s and $\alpha \in \text{S}$, $F_{\text{exp-free},p,s}$ the quantity of exports not yet allocated, and whereby the underset indicates from which national optimization problem the variable originates.

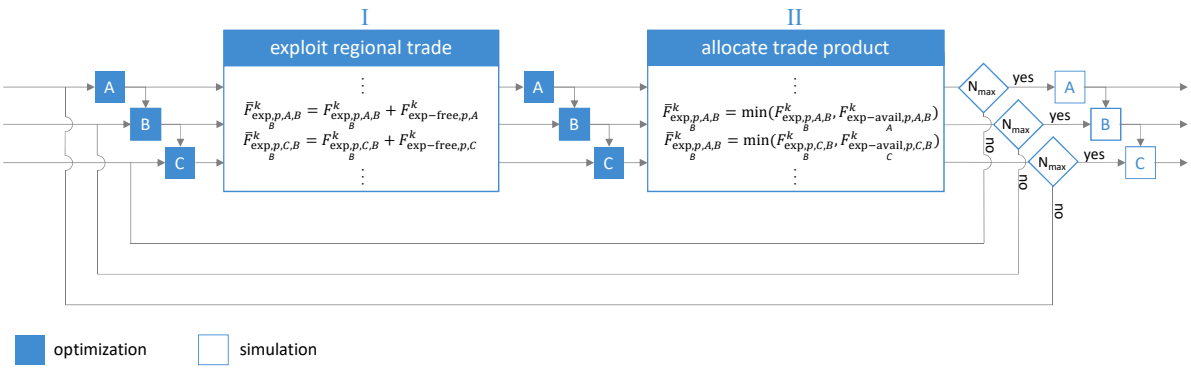

Figure 3.10: A graphical example of the iterative process in the trade-information coordination scenario. The figure shows the situation for three imaginary countries A, B and C. The process starts with an optimization for each individual country. Information about the expected river flow is shared downstream and used as forcing in the optimization. After the first optimization, the first proceeding takes place in which the freely available amounts are defined and the limits are updated. After the second round of optimization, trade quantities are allocated to a specific country after which the bounds are updated once more. Simulation only takes place when the maximum number of iterations for the trading market has been reached.

After this optimization, the second proceeding follows. In this proceeding, a certain amount of product is assigned to a trading partner. This allocation is based on geographic distance, with the nearest country provided first. As long as the combined imports of all countries are less than the exports of a considered country, each state is allocated the planned quantity. In other cases, the more distant countries may obtain less or none of the planned quantity. For the subsequent iteration, the boundary of the trade variable is set equal to the assigned amount. This optimization shows whether the countries are actually interested in importing the allocated quantity, given that other products are not available or are available to a lesser extent. The renewed upper limit is described by:

$$\begin{aligned} \bar{F}^{k}_{\substack{\text{exp},p,s,\alpha \\ \alpha}} &= \min\left(F^{k}_{\substack{\text{exp},p,s,\alpha \\ \alpha}}, F^{k}_{\substack{\text{exp},p,s,\text{extern} \\ s}} - \sum_{\omega \in \Omega_{s,\alpha}} F^{k}_{\substack{\text{exp},p,s,\omega \\ \omega}} \right) \\ &= \min\left(F^{k}_{\substack{\text{exp},p,s,\alpha \\ \alpha}}, F^{k}_{\substack{\text{exp-avail},p,s,\alpha \\ s}} \right) \end{aligned} \tag{3.147}$$

with $\Omega_{s,\alpha} = \{\omega \in \mathrm{S} \mid l_{\text{trade},s,\omega} < l_{\text{trade},s,\alpha}\}$ a locally defined set all countries where the trade distance l_{trade} to country s is shorter than the distance between states s and α.

A similar method applies to electricity trade. However, because this trade is demand oriented instead of supply, the first proceeding examines the magnitude of the national electricity shortage, given the quantities that other countries plan to export. In the second proceeding, it is determined from which country the electricity should actually be imported. If the information sharing takes place over a shorter time horizon than the optimization horizon, the long term electricity contracts will only be overruled by the short term trade contracts during this period. In the later steps in the optimization horizon, the quantities traded are still specified by the long term contracts.

3.4.4. Coordination

The coordination scenario is fundamentally different from the previous scenarios. In this scenario, planning no longer takes place at national level, but at regional level. From a mathematical point of view, this means that countries are no longer studied as individual systems, but as part of a whole. This scenario is therefore characterized by a single optimization in which all countries are included. By definition, product and electricity trade is possible with both regional and international partners ($F_{\text{exp},s,s} \leq \infty$, $F_{\text{exp},s,\text{extern}} \leq \infty$, $E_{\text{e-exp-var},s,s} \leq \infty$), and information about river discharge is shared.

Part B:

A case study in the Eastern Nile river basin.

1 Introduction

1.1. Challenges in the Eastern Nile basin

"You'd see more floods like you've seen in Mozambique in 2000, you'd see more droughts like you saw in Kenya in the late 1990s, there would be a serious threat to the water flow down the Nile on which 10 countries depend." - Nicholas Stern, 2006

Despite extraordinary amounts flowing into the Nile, the basin is practically closed and water scarcity is a major everyday complexity for the riparian states [Mohamed and Loulseged, 2008]. This contradiction between water supply and availability is primarily the result of large internal losses caused by evapotranspiration in the wetland areas, stream losses in the desert zone, and evaporation in the reservoirs [NBI, 2012]. Inefficient use of the remaining supply put the availability of water resources under pressure and complicate today's resource management. However, today's operational complexities pale when compared to challenges the future faces as a result of changes in population size, socio-economics and climate.

The Eastern Nile Basin is home to a large and rapidly growing population, living in widespread poverty without access to electricity and under difficult socio-economic conditions. Along with future population growth, changes in socio-economic conditions are expected. A predicted decline in poverty will improve the coverage of the electricity grid and alter diets and water consumption [NBI, 2012]. In order to feed its growing population, the riparian states need to boost their agricultural production [Wolters et al., 2016]. Irrigation is essential to secure future food supply under these circumstances [Swain, 2011]. The inefficiency with which this irrigation takes place, however, results in a strong increase in water demand. Since the same water resources are essential for hydropower production [NBI, 2012], fierce competition is expected. To meet the growing demand for food and energy, the Nile riparian countries have developed, and intend to further develop, their water resources. Large reservoirs, hydropower stations and irrigation areas with the ultimate goal of boosting the production of cheap hydroelectricity and increasing food security have been build, are under construction or being planned [Goor et al., 2010]. Currently, these existing reservoirs are operated independently. This not only results in under-optimized water utilization and weaker resilience to cope with seasonal and inter-annual variability, but causes spatial and temporal shifts in water availability and hence increases the already existing tension between the states [Luttikhuis, 2017].

The challenge is further exacerbated by incidence of climate variability and natural shocks such as droughts and floods. Changing rainfall patterns will mutate the sensitive Nile flows and increase the flood risks in the basin's densely populated flood plains. Furthermore, rising temperatures will raise agricultural water demand, increase irrigation requirements, lead to higher reservoir losses, increase drought risks, and accelerate land degradation [NBI, 2012]. As climate change can potentially change water supply and demand patterns in the basin, sharing of the already scarce water resources of the Nile River may become a serious security risk in the near future. With the growing multiple water demands, in combination with the high spatial and temporal variability in water availability, the necessity for cooperation and coordination among the riparian countries in the Nile basin becomes a crucial issue [Swain, 2011].

To promote this cooperation the Nile Basin countries launched the Nile Basin Initiative (NBI) in 1999 [Digna et al., 2018b; Whittington et al., 2005]. The goal of the NBI is to develop the water resources in a sustainable way and to explore opportunities for maximizing the benefits of the river waters through cooperative development and management of the basin system. If cooperative investment projects are agreed and undertaken, the riparians could move closer to achieving system-wide, economically optimal management of the shared resources of the Nile [Whittington et al., 2005]. However, as

a result of power changes in the region and the interference of global power centres, the countries have developed their plans for water resources management unilaterally in the meantime [Digna et al., 2018b; Cascão, 2009]. To reverse this unilateral trend and to promote cooperation between riparian states, a clear understanding of the potential benefits and costs for the different users to motivate engagement in coordinated operations is required. Therefore, specialized tools for analysing water resource development and addressing the related technical, environmental, social, economic and diplomatic issues are critically needed [Digna et al., 2018b].

1.2. Cooperative optimization studies: a short review

Because of the political and hydrological complexities, there is a large number of completed, ongoing and scheduled research projects which focus on water resource management in the Nile basin. Results of these studies are extensively being reported in literature. The majority of these studies applied in the Nile Basin can be divided in simulation-, optimization- and hybrid methods. Optimization methods screen a large but bounded number of configurations to find the configuration that best approaches the optimization objective, while simulation methods are used to examine system performance under limited predefined configurations (referred to as scenarios) [Digna et al., 2018b]. An optimisation method can, unlike simulation methods, be used to map the maximum attainable economic resource potential under the applicable structural conditions. This feature of optimisation algorithms have extensively been used in Nile basin model studies to address specific water resource related issues.

In these optimisation studies an assumption is made about cooperation between the riparian states. Although the spectrum of cooperation allows many possible forms, most studies assume an extreme: unilateralism or full cooperation. Unilateralism refers to the situation where each country operates his reservoirs to maximize the national interest without regard to its neighbouring riparian states. In case of full cooperation, the riparian states are expected to coordinate the reservoir operations with each other to maximize basin wide interests. All agents are assumed to allocate the water among each other such that their aggregated welfare is maximized. Both unilateral and fully cooperative systems bring disadvantages in implementation. A full coordinative system carries strong institutional assumptions. It assumes central planning and perfectly functioning of the market. Besides, it does not recognize the asymmetric accessibility of the water to users, ignores the selfishness of competing water users and assumes the best solution to the system would be accepted completely by all the participants. Although unilateralism satisfies the selfishness of each agent in maximizing its utility to achieve higher revenue, this approach yields an inefficient solution from a cooperative perspective [Ding et al., 2016].

In Whittington et al. [2005] for the first time, a deterministic hydro-economic model was developed for the entire Nile River Basin. The optimization algorithm was designed to determine the allocation pattern that maximized the sum of economic benefits from irrigated agriculture and hydropower generation. In Satti et al. [2015] a similar deterministic approach was used to study the sensitivity of Sudan's Blue Nile and main stem Nile water to changes in climate and upstream development. To account for the stochasticity of future inflows, Goor et al. [2010] introduced Stochastic Dynamic Programming (SDP) to study the impact of upstream river development on the basin wide economic benefits under steady state conditions. The same algorithm was applied by Arjoon et al. [2014] to illustrate the impact of the Grand Ethiopian Renaissance Dam (GERD), under steady state conditions, on the agricultural and energy sectors in Sudan and Egypt, including the associated risks and benefits. Where all aforementioned models assume reservoirs to be in steady state, Hassaballah et al. [2012] included the transient effects of filling a new reservoir in the Ethiopian highlands. The objective of this study is comparable with the work of Block and Strzepek [2010], who studied the downstream sensitivity to upstream developments in the Ethiopian highlands. The presented deterministic model illustrated the effects of transient and long-term periods under varying economic, construction, and climatic conditions. Notable in the latter study is the inclusion of climate change scenarios, represented either by changes in the frequency of El Niño and La Niña events or by climate projections, where aforementioned studies assumed historic discharges (or scaled versions thereof) to be representative for future scenarios.

Dinar and Nigatu [2013]; Ding et al. [2016]; Arjoon et al. [2016b] and Nigatu and Dinar [2015] move beyond the allocation optimisation and address the distributional considerations of gains. Both Dinar and Nigatu [2013] and Nigatu and Dinar [2015] propose a system where the NBI states a legal allocation and facilitates water trade among riparian countries. The optimization objective is adjusted to account for the economic benefits of water trade. Dinar and Nigatu [2013] applies thereafter approaches from game theory to study the stability of the initial legal allocation. Ding et al. [2016] proposes an agent based approach. An evolutionary algorithm is used to allocate water to maximize basin wide benefits, but to re-distribute these benefits over the countries based on the contribution to the total benefits. Finally, Arjoon et al. [2016b] proposed an pseudo-market approach where the river basin authority plays the role of water system operator and allocates the water in the most economic way. Based on the water allocation decisions and the corresponding water fluxes, users must pay the river authority for the water allocated to them. The river authority will use the collected money to compensate the agents who were not supplied.

1.3. Problem statement

The aforementioned studies each have their own purpose, and therefore cover a wide range of assumptions and applied methods. Nevertheless, it is possible to identify frequent shortcomings in the current literature that focus on optimization in the Nile basin. The majority of the studies on cooperation in the Eastern Nile use hydro-economic frameworks based on the same node-link network. This implementation has some shortcomings in the description of water productivity.

The first and maybe most important shortcoming of most optimization models is their economic description. All aforementioned models describe the economic value creation with the available water using temporally and spatially fixed economic benefits per cubic meter of water allocated to agriculture and generated kilowatt hour of hydropower. In other words, these models describe the agricultural value creation with the available water resources without an agricultural component being present in the models. Such a model implementation has two major drawbacks: only the supply is considered and the demand for a product is not accounted for, and all inhomogeneity in a river basin is lost. These shortcomings actually make the models unsuitable for studying cooperation. After all, cooperation and specialization are closely linked. The latter requires a spatially and temporally explicit description of electricity demand and crop production driven by demand, and described as part of the relevant balance.

Such a spatially defined and time-dependent model implementation is also necessary to describe the expected major social changes. The current literature does not account for the consequences of changing diets, energy consumption and land use. These changes will impact the water demand, but also the price of agricultural products and electricity. Where the models all optimize for economic value creation, these changes in economic value cannot be neglected. These changes are often not included in the current literature because of the associated uncertainty. However, this economic uncertainty, like climate uncertainty, is important for future management planning in the eastern Nile and should be included in the models. Moreover, social changes, such as population growth and consistent land-use changes, might affect water resources in the Eastern Nile more than climate variability [Koutsoyiannis et al., 2009].

Although the effects of climate change might be smaller than those related to socio-economic changes, the models should introduce the effects of climate shocks, seasonal and inter-annual variations both spatially and temporally. The importance of climate change is often neglected in models or introduced in a minimal way, while running for periods up to 100 years. There is need for a model that forms explicit functional linkages between climatic factors and many of the hydrological model components as proposed by Jeuland [2010]. In addition to the description of direct impacts of climate change, resulting in changing precipitation, evaporation, discharge, crop requirements and yield, indirect effects need to be considered. Climate change can indirectly namely change water requirements through changes in usage processes and changes in consumption patterns.

Another shortcoming is related to the deterministic character (perfect foresight) of most optimization models. This deterministic approach is useful for scholars in academics to study the potential of the region, but not for real world operational purposes. An exception in the existing literature is Goor et al. [2010], who illustrates with the introduction of the Stochastic Dynamic Programming (SDP) the usability of a stochastic approach. After all, a beneficial cooperation under perfect foresight does not yet guarantee a beneficial cooperation under imperfect foresight conditions.

Besides, all models use a modest set of cooperation scenarios. Unilateral and full coordination are two extremes when it comes to cooperation. The latter, in particular, carries as mentioned strong institutional assumptions, whereby many hurdles must be overcome prior to any form of implementation. It may be more beneficial for national governments to study the added value of easier-to-implement forms of cooperation. In addition to the points discussed above, other shortcomings in the current optimisation models are the abilities to account for (the benefits and costs of): resource degradation, sediment accumulation in the reservoirs and environmental services.

1.4. Objective and scope

Based on the challenges in the Eastern Nile basin and the shortcomings in literature, this research aims, with the formulation of a hybrid optimization-simulation strategy, to describe qualitatively and quantitatively the impacts and benefits of multiple forms of cooperation over unilateralism in the Eastern Nile basin, both under current and future climate and socio-economic circumstances.

The study focuses on water quantity and its use. Water quality parameters are just like sediment transport and the associated salinization not included. The water use is in this study limited to agricultural consumption and use for hydropower. Other forms of consumption or use like domestic and industrial are not accounted for. Environmental flows and associated economic benefits and losses are not included in this study either. To optimize the value creation, a predefined, but time variant, structural environment is considered. It is emphatically not the intention of this study to optimize the infrastructure planning itself. The whole study takes place in a deterministic framework, but leaves space to determine the value of climate foresight.

2
Study area

With a length of almost 6685 km, measured from its source close to the equator to the outflow in the Mediterranean sea, the Nile is the longest river in the Africa, and potentially the longest river in the world [Motlagh, 2018]. Today, the Nile River Basin covers eleven countries. Although the longest tributary of the Nile originates around the equator, most of the discharge comes from the Ethiopian highlands. This sub-basin of the Nile that originates in the Ethiopian highlands is referred to as the Eastern Nile. Where the basin was shared by Egypt, Sudan and Ethiopia 30 years ago, it currently covers five countries following the independence of Eritrea from Ethiopia in 1991 and the independence of South Sudan from Sudan in 2011. Because there is no river infrastructure in the Nile river basin in Eritrea, this country is not included in this case study. The remainder of this section aims to provide background on the water- energy and food systems in the riparian states. Therefore, the hydrology, climate and present river infrastructure of the Eastern Nile are introduced, followed by a description of the historic and future electricity grid and the food production and consumption patterns.

2.1. Water systems

In this section some background information is provided on the climate and hydrology in the Eastern Nile river basin. Subsequently, the expected changes in climate and hydrology due to global climate change are discussed. The section ends with a description of the river infrastructure present and planned.

2.1.1. Climate forcing

Due to its great latitudinal en altitudinal extent, the Eastern Nile basin is characterized by extreme hydroclimatic variability over space and time. The basin mainly encompasses three climate zones, namely subtropical, semiarid and arid [Shahin, 1985], each with distinctive temperature, precipitation and evapotranspiration patterns. The temperature shows a wide variation across the basin with the equatorial lakes region and the Ethiopian highlands being exposed to maximum temperatures of up to 30 °C and the main Nile, parts of the Blue Nile, Tekeze Atbara and the White Nile in Sudan being exposed to maximum temperatures of up to 45°C [Akol et al., 2016]. The former regions are also characterized by a quite uniform temperature distribution throughout the year, where the latter show a clearer variation over the seasons. The precipitation distribution in all three climate zones is unimodel. The most precipitation falls during the monsoon (March till October) in the southern subtropical region, with amounts reaching up to 2000 mm in the south west of Ethiopia [FAO, 2016b]. Less precipitation falls in the semi-arid and arid zones further north. Where in the southern parts of Sudan, just north of the Ethiopian highlands, the monsoon season still has a duration of 4 months and the precipitation an average around 400 mm, the monsoon season is reduced to 2 months in the northern part of the country with precipitation levels around 100 mm [FAO, 2015]. Going even further north, the precipitation is reduced to a minimum of nearly zero in the Egyptian desert, before starting to increase in the direction of the Mediterranean sea [FAO, 2016a]. This long term average distribution follows the latitudinal movement of the Inter Tropical Convergence Zone (ITCZ), which never reaches northermost Sudan and Egypt. In the Ethiopian Rift valley, rainfall is locally enhanced as a result of orographic lifting [Dumont, 2009]. The mean annual actual evapotranspiration grades in the same direction, while the spatial pattern of the potential evapotranspiration ET_p is opposite, with the highest values in the arid north and the lowest values in the subtropical south (see Figure 2.1) [Camberlin, 2009]. The El Nino Southern Oscillation (ENSO) is one of the main causes for this climate variability [Dumont, 2009]. Besides these contrasts in mean precipitation, temperature end evaporation, also large interannual or longer-term fluctuations are observed.

2.1.2. Hydrology

The Nile basin constitutes five major sub-basins, namely the: White Nile, Blue Nile, Tekeze-Atbara-Setite, Baro-Akobo-Sobat, downstream White Nile and main Nile. The latter five together form the Eastern Nile sub-basin. This sub-basin constitutes the major part of the Nile, both in terms of catchment area and water resources (See Figure 2.2). The river Nile has two main sources; one of them situated in the lake district in tropical Africa (the White Nile) and the other in the Ethiopian highlands (Sobat, Blue Nile and Atbara). The total contribution to the discharge and the seasonal variation of both sources shows large differences. The discharge distribution follows the spatial and temporal patterns of precipitation. The Blue Nile contributes with almost 60% most to the annual river discharge. The Atbara accounts for approximately 15% of the Nile discharge and the White Nile and the Sobat together for the remaining 24%. The arid and semiarid zone hardly contribute to the Nile discharge [Hasan et al., 2018]. However, the annual variability in flow is significant. Especially the rivers coming from the Ethiopian Highlands (Blue Nile, Baro-Akobo-Sobat and the Tekeze-Atbara) are characterised by strong seasonal and inter-annual variations, with the flow of the Blue Nile being the main contributor to the large natural variation of the Nile flow [Di Baldassarre et al., 2011]. The flow rate of the White Nile is, despite the unimodel and bimodel precipitation forcing, almost constant throughout the year [Tilmant et al., 2015; Siam and Eltahir, 2017]. The annual and interannual homogeneity in discharge originating from this tributary can be explained by the presence of large swamps in Southern Sudan. These swamps have with their storage and evaporative losses a buffering and homogenizing effect on the stream from Lake Victoria. Since almost half of the inflow is lost by evapotranspiration in the swamps [Di Baldassarre et al., 2011], the annual contribution of the White Nile to the Nile flow is limited. However, during the dry season in the Ethiopian Highlands, from November to April, the White Nile is with 70 % to 90 % the main contributor to the Nile discharge [Di Baldassarre et al., 2011].

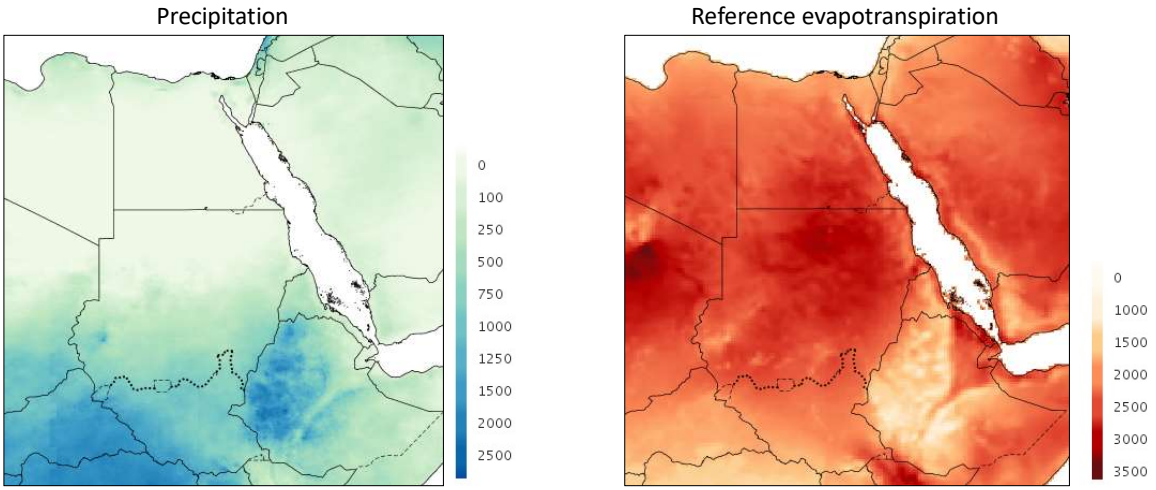

Figure 2.1: Annual precipitation and reference evapotranspiration in the Eastern Nile basin in 2018 (data originates from WaPOR [FAO, 2019]). The figures show a clear and opposite gradient in latitudinal direction for precipitation and potential evapotranspiration.

2.1.3. Climate change

The mean and standard deviation of flows and rainfall patterns of the main tributaries of the Eastern Nile (Upper Blue Nile, Sobat and Atbara) have been changing over the past 50 years. Both average and standard deviation increased with time, as indicated by 30-years moving averages. Besides this absolute increase in average and standard deviation, an increase in the 30-years moving average of the coefficient of variation indicates an increase in inter annual variability [Siam and Eltahir, 2017]. Further increases in mean and standard deviation are projected by ensemble means in the 21st century. The long term mean and standard deviation of main Nile river flow are expected to increase with almost 15% and 50% respectively in 2100 relative to the start of the 20th century. Due to the the standard deviation that grows much faster than the average, the inter-annual variability is expected to further increase in this century. The increase in flow is expected to occur mainly between 2010 and 2040, and to stabilize afterwards till the end of the century. Due to the increasing variability, the number

of normal (around average) flow events is expected to decrease, and the number of high flow events is expected to increase. The projected increase in the inter-annual variability of the flow of the Nile river is consistent with the expected frequencies of low and high flows in the river caused by increases in El Niño and La Niña events, respectively [Siam and Eltahir, 2017].

However, caution is advised regarding the results of climate models. The used approach where Global Circulation Models (GCM) are forced with a climate scenario, downscaled to regional levels and used as input for hydrological models, have several drawbacks. Firstly, have climate models a poor capacity to foresee precipitation changes. Secondly, is the variability of driving forces indicated by this approach to small to describe the natural variability of hydrological processes [Di Baldassarre et al., 2011]. Besides, one should not underestimate the uncertainties involved by the use of hydrological models, calibrated for contemporary use, for future conditions [Savenije and Hrachowitz, 2017]. Concerning climate modelling, predictions of precipitation have been shown to be highly uncertain with estimates ranging from -12% to +24%. Climate models disagree on the direction of future precipitation change, with increasing uncertainty as one goes down in scale and moves to more extreme events [Elshamy et al., 2009; Di Baldassarre et al., 2011]. In contrast, changes in temperatures predicted by climate models are usually considered more reliable. In the Nile Basin, mean annual temperature is expected to rise by between 2.0 and 4.0 degree Celsius by mid-century [Elshamy et al., 2009; Di Baldassarre et al., 2011].

2.1.4. River infrastructure

Although the water resources of the Nile have been used for human purposes for centuries, first on small scales for local irrigation and later in more organized irrigation schemes, the transformation towards the use of the Nile river water as we know it today began in the late 19th century with the construction of the Aswan Low dam in Egypt. The purpose of this dam was to enable year round irrigation of the Nile delta and to meet the industrial water demand [Dumont, 2009]. When the colonial era ended, Egypt built the Aswan dam to achieve full over-year storage and river control. In the following years, some new barrages (Assyut, Delta and Naga Hammadi [Digna et al., 2018a]) were built in the Egyptian Nile Delta and the irrigation capacity was expanded with new fields in the Toska Valley. As Egypt has currently exploited almost all of its hydropower potential, few structural changes will occur in the near future, other than expansion of existing irrigation schemes.

Also in Sudan, the development of the Nile started during the colonial era with the construction of the Sennar dam in the Blue Nile basin. The aim was to supply water to the Gezira scheme, which is one of the largest irrigation fields in the world [Awulachew et al., 2009]. The Roseries dam was later added to expand the Gezira scheme. Over the years, the White Nile and the Atbara basin have also been cultivated with the construction of the Jebel Aulia dam, the Khasm el Ghirba dam and recently the upper Atbara dam complex. All are multipurpose dams, and create in addition to the energetic potential an abundance of potential irrigation area. In order to meet the growing demand for electricity, the Merowe dam was built in the big bend just south of the Egyptian border. In future, construction of several other new dams (Shereiq, Kajbar and Dal) located between the confluence of the Atbara and Main Nile and the Aswan High Dam is being considered [Whittington et al., 2014].

Historically, Ethiopia makes little use of the Nile resources because of the difficult land accessibility and the population centers being situated in others basins [Awulachew et al., 2009]. However, because of the large natural gradients, Ethiopia has a large hydropower potential. Where initially all energy was generated with two small scale run-of-the-river plants in the Blue Nile, a turnaround in the use of Nile resources occuured with the recent completion of the Tekeze dam in the Atbara basin and the approaching completion of the Grand Ethiopian Reneaissance Dam in the Sudanese border (GERD). In the recent future, numerous projects are planned on the main stem of the Blue nile between Lake Tana and the GERD as well as in the Sobat basin [Block, 2007] to expand the hydropower potential and to enhance the regulation of the river flow. Regulating the water started with the construction of the Chara Chare weir at the outflow of Lake Tana at the beginning of the 21st century, to provide water for the small-scale irrigated agriculture around Lake Tana during dry years. Real development of the irrigation potential in the Ethiopian Nile basin started recently with the construction of the Fincha'a dam and irrigation field in the Blue Nile, followed by the Koga and Neshe dam. With the completion of the Abobo dam, the development of the Ethiopian part of the Sobat was preluded [Akol et al., 2016].

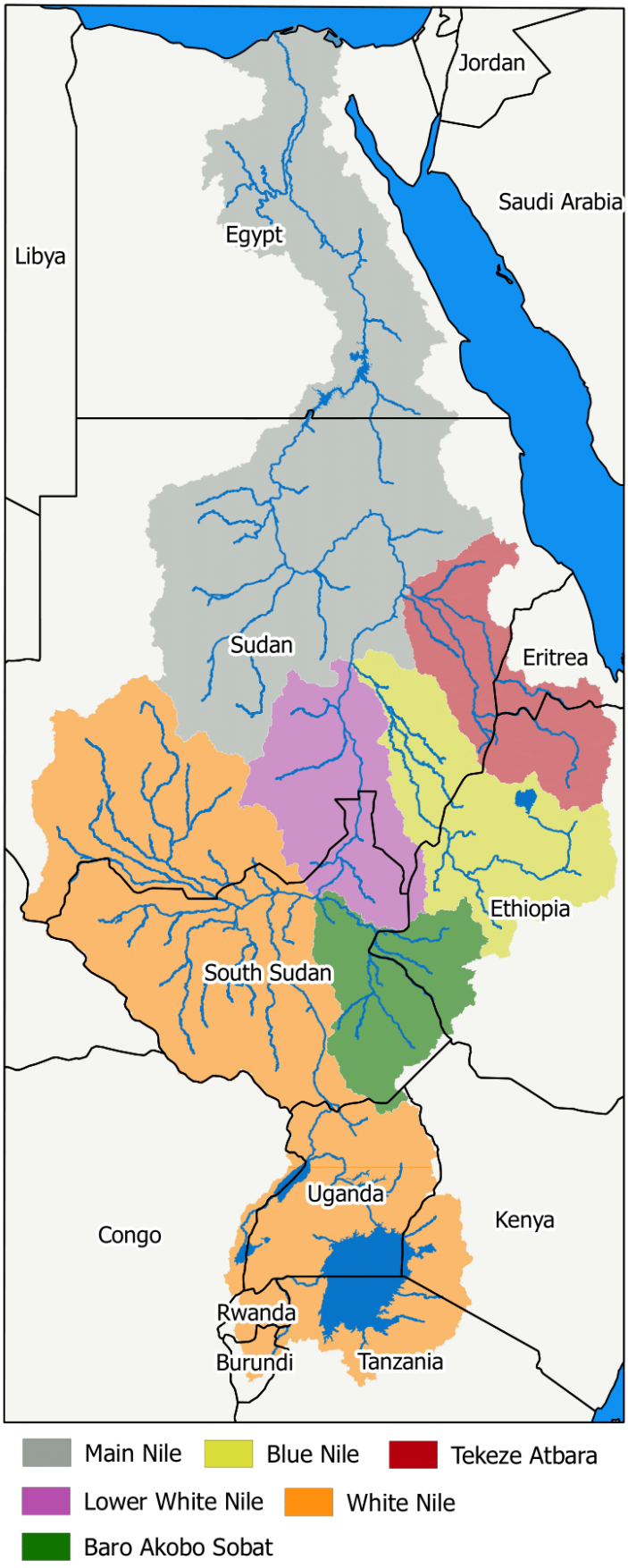

Figure 2.2: The Eastern Nile and the subdivision in five sub-basins: Blue Nile, Tekeze-Atbara-Setite, Baro-Akobo-Sobat, downstream White Nile and main Nile.

2.1.5. Electricity system

In this section some background information is provided on the electricty generation and demand. For each individual riparian state, an analyses is made of the historic generation capacities, the national electricity grid and the electricty consumption. Finally a short introduction about the Eastern Africa power pool follows.

2.1.5.1. Egypt

Due to a changing lifestyle, improved coverage and a rapidly growing population, Egypt has experienced strong growth in demand for electrical energy. With an average annual growth of 6.1%, the domestic electricity demand increased from 67 TWh in 2000 up to 173 TWh in 2016 [IEA, 2016]. Because the transmission and distribution losses decreased from 13% to 11% in the same period, the power production increased - with 5.8% annually - slightly less. Although the accessibility of the electricity network has always been high, it has increased steadily during this period until a 100% coverage was reached in 2014. In that same year, per capita power consumption amounted approximately 1700 kWh. Compared with sub-Saharan Africa countries, having an average consumption of approximately 500 kWh in 2014, Egyptian's energy consumption is high. However, under favorable economic conditions, a significant growth towards the average consumption in Arab countries (approximately 2500 kWh in 2014) is expected [WB, 2019].

The majority of the electricity in Egypt is produced via thermal power plants. In the 90s, when Egypt was still a net exporter of oil, energy production was strongly dependent on oil. However, the composition of the fuel changed radically around the year 2000. With the exploration of new gas fields and the accompanying stagnating oil production, Egypt started - in order to save more crude oil for export - to fuel a growing part of electric power plants with natural gas instead of oil [EEHC, 2017; MoPMAR, 2016; Hegazy, 2015]. In 2017, 80% of the power plants connected to the grid combusted gas [EEHC, 2017]. Hydropower is Egypt's third-largest energy source after natural gas and oil. In 2016, hydropower production accounted with a generation of 13.5 TWh for 7% of the total Egyptian production. Almost all hydroelectricity was generated by the Aswan High Dam and the Aswan Low Dam across the Nile River [EIA, 2014]. Where the percentage of hydro power energy generated increased in most other riparian states during the last decades, in Egypt the percentage is gradually decreasing since the majority of the hydropower potential has already been exploited [EIA, 2014; AFDB, 2012]. The contribution of solar and wind sources is small, but steadily increasing since the construction of the first windfarm and solar park in respectively 2010 and 2011. In 2016 these renewables accounted with an installed capacity of 887 MW and a production of 2226 GWh for respectively 2.2% of the installed capacity and 1.1% of Egyptian's total power generation.

Till 2050, an annual growth of 4.46% in energy demand is expected [Mondal et al., 2019]. To ensure power security under these circumstances, Egypt's new energy strategy aims at diversifying and increasing the efficiency of the supply portfolio, and investing in an adequate transmission capacity [EIA, 2014]. Therefore, Egypt intends to reduce the transmission and distribution losses to 8% in 2030 [MoPMAR, 2016] and increase the contribution of renewable energy technologies up to 20% in 2022 and 42% in 2035 [MoERE, 2019]. Since most of the Nile's hydroelectric potential is already exploited, and to be less vulnerable to droughts affecting the hydroelectric production, the New and Renewable Energy Authority (NREA) pursues an increase in wind and solar technologies [EIA, 2014]. Besides the renewable sources, an expansion in the thermal power capacity and the introduction of nuclear power is expected [IRENA, 2018] To ensure, given the uncertainty in the availability of fossil resources, the thermal production capacity, thermal plants capable of firing both oil and gas as well as coal stations are planned [AFDB, 2012].

Egypt's electric transmission grid is already connected to Jordan, Syria, Iraq, Turkey, and Libya, and is net delivering power to this grid. In future, an expansion of this grid is expected. By 2020 Egypt aims to be connected to both the Arab and European electricity network. Besides - as a member of the eastern African power pool - there are plans to interlink the grid with other countries within Eastern Africa, starting with a 2000 MW connection with Sudan [EEHC, 2017].

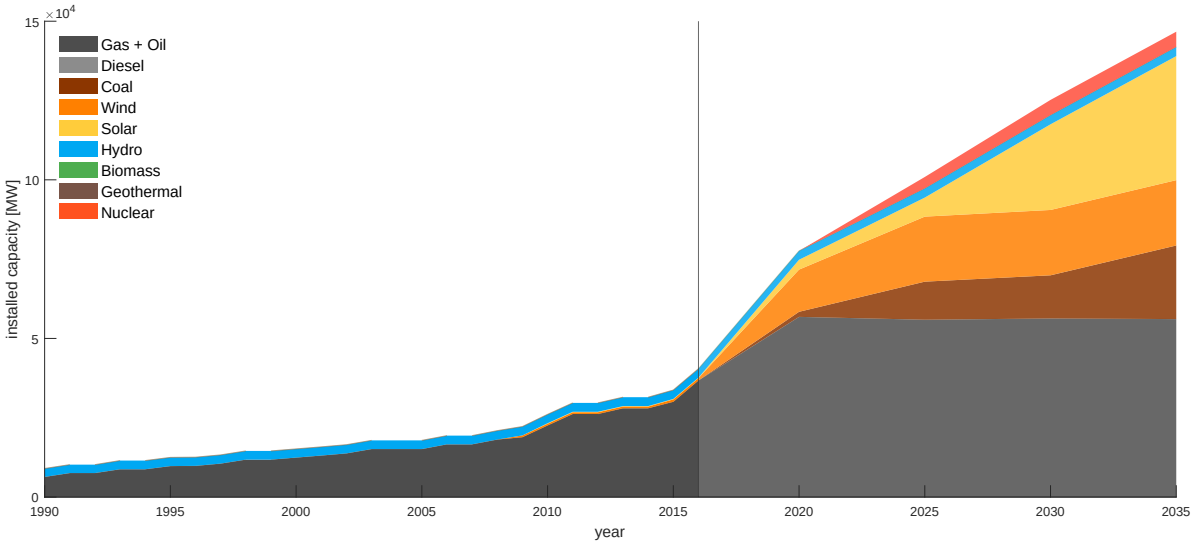

Figure 2.3: Installed electric power capacity in Egypt in the period 1990-2016 and future capacity projections. Historic capacities are based on EEHC [2017] and future projections on IRENA [2018].

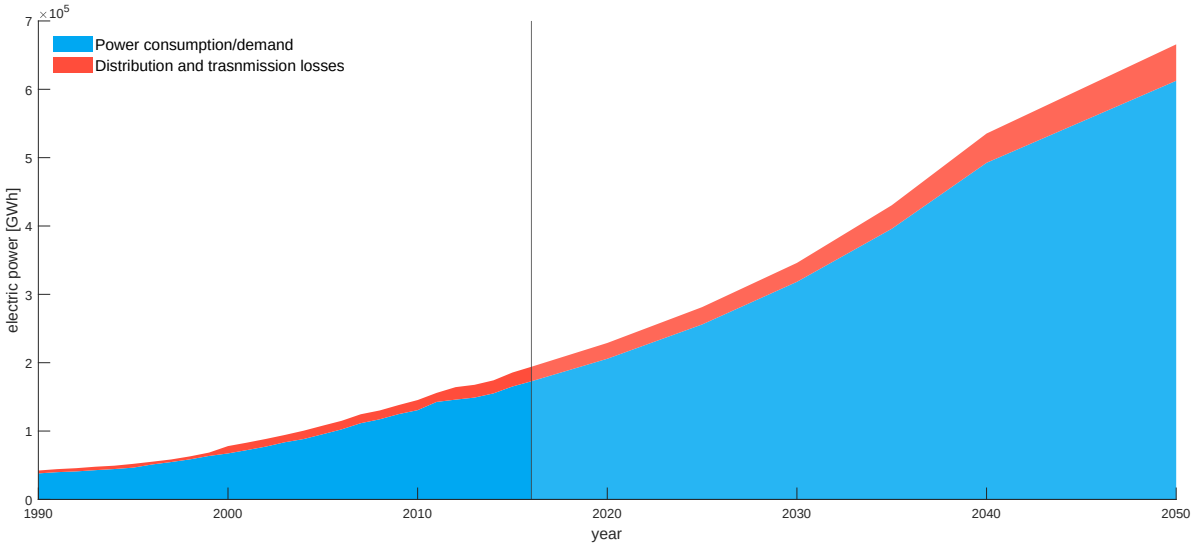

Figure 2.4: Historic energy consumption and future electric demands in Egypt supplemented with the distribution and transmission power losses. Historic consumption is based on IEA [2016], and historic losses are computed based on percentual losses as presented in WB [2019]. Demand projections are based on IRENA [2018] and losses are computed using the loss factor presented in MoPMAR [2016].

2.1.5.2. Ethiopia

With only 12% of the population having access to electricity, using on average 22.8 kWh per capita [WB, 2019] in the year 2000, the Ethiopian electricity system used to be one of the least developed of the world. The low accessibility and per capita energy consumption are the result of the low level of development in Ethiopia and the fact that only a small part of the population lives in urban centers [DoC, 2016]. However, in hand with strong economic growth, the electric sector has upgraded substantially in the last decades. In 2016, already 43% of the population had access to electricity, using on average 90 kWh per capita. As a result, energy demand has increased annually with 12% from 1.5 TWh in 2000 up to 9 TWh in 2016. To meet this growing demand for energy, the energy network - which consists of the national Inter Connected supply System (ICS) and several local Self Contained supply Systems (SCS) - experienced a rapid transition [Asress et al., 2013]. However, coupled with this growth, the transmission and distribution losses have increased up to 23% [EEPco, 2011].

In the coming decades, the growth in energy demand is expected to continue at the same pace, reaching a demand of 70 TWh by 2030 and 97 TWh by 2037 [MoWE, 2012; EEPco, 2014]. The steep increase in demand is mainly due to the expected growth of electricity intensive industries and the growing electrification of the country [MoWE, 2012]. The target is to reach 90% coverage of the country by 2020 [FDRoE, 2016]. To ensure a reliable power supply in future while keeping - as reported in the Climate Resilient Green Economy initiative (CRGE) - greenhouse gas emissions low, the government of Ethiopia is exploiting new renewable energy production technologies [FDRoE, 2011] and aiming to increase the overall efficiency [EEPco, 2014]. The planned goal is to reach an installed capacity of 17,000 MW by 2020, 25,000 MW by 2030 [MoWE, 2012], 35,000 MW by 2037 [DoC, 2016] and 45,000 MW by the year 2065 from hydropower, geothermal, solar and wind [EoS, 2016]. Ethiopia has – with a potential generating capacity of 45,000 for hydropower, 5000 MW for geothermal and 10,000 MW for wind - substantial potential to realize this using only renewable resources [Asress et al., 2013].

Despite - in addition to micro hydropower plants - small diesel generators being used in the local self-contained systems, the majority of the energy production for the national interconnected system is generated by renewable sources. Hydropower is with a share of 84% of the installed capacity the major producer of electrical energy in 2016, followed by wind energy (7%) and biothermal (6%). Although the absolute production capacity of hydropower will - with the completion of the Grand Ethiopian Renaissance dam and a few smaller hydropower stations - increase in the coming years, the government is - in order to reduce its vulnerability during droughts and to cope with the declining production potentials during the dry period - striving to reduce the relative hydropower capacity [Asress et al., 2013]. To achieve this, several large wind farms, geothermal installations and sugar-fired biomass power stations are under construction and planned, lowering the hydropower share to 80% in 2020 [FDRoE, 2016].

Besides fulfilling the domestic demand, Ethiopia sees itself as the renewable energy power house of Eastern Africa. The government is therefore investing heavily in the energy sector to enable future sales on a regional network. Nowadays, Ethiopia's energy grid is already connected to Djibouti (150 MW connector), Sudan (200 MW connector) and Kenya (1000 MW connector) [FDRoE, 2011]. Via the latter network connection they also supply power to Tanzania. In the future - under the eastern Nile trade program – will the connection to Sudan be expanded by 3200 MW, of which 2000 MW will continue to Egypt [EEPco, 2014].

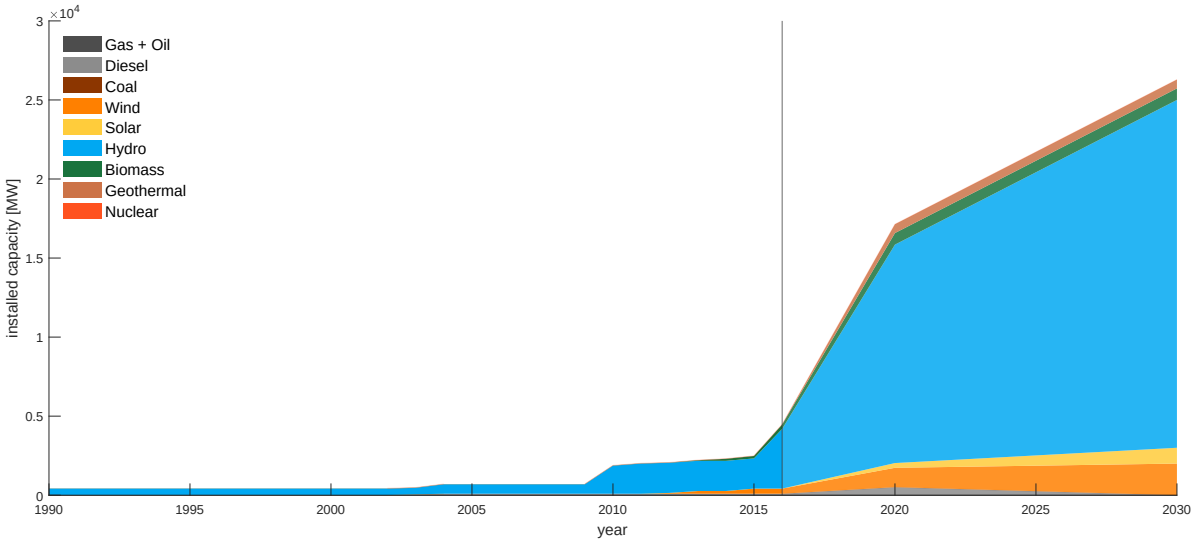

Figure 2.5: Installed electric power capacity in Ethiopia in the period 1990-2016 and future capacity projections. Historic capacities are based on EEPco [2014, 2017] and future projections on FDRoE [2016]; MoWE [2012].

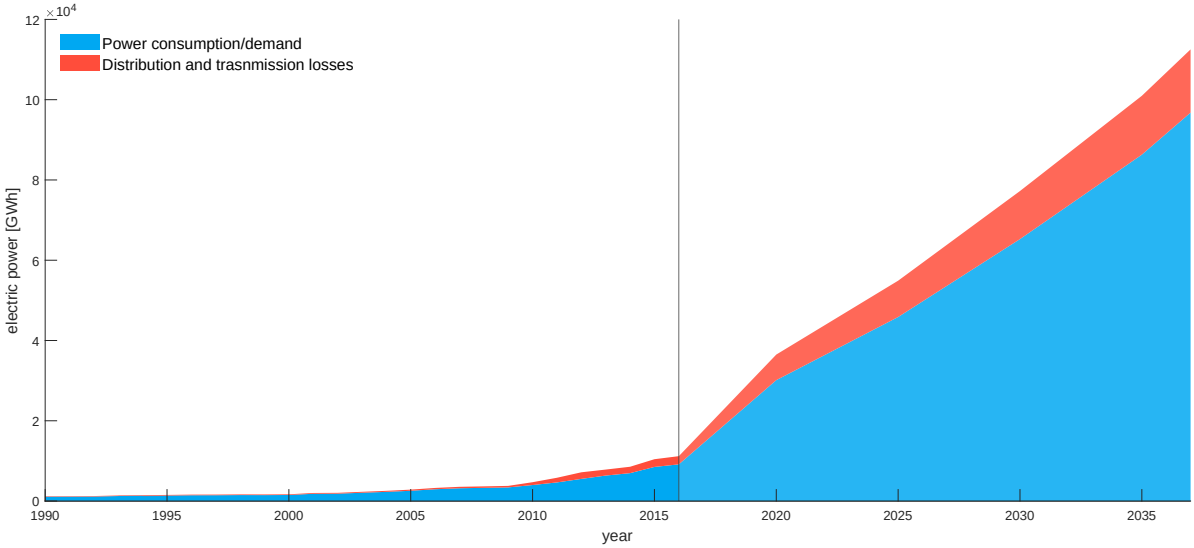

Figure 2.6: Historic energy consumption and future electric demands in Ethiopia supplemented with the distribution and transmission power losses. Historic consumption is based on IEA [2016], and historic losses are computed based on percentual losses as presented in WB [2019]. Demand projections and transmission losses are based on EEPco [2014].

2.1.5.3. Sudan

Like other African developing countries, Sudan has a shortage of electricity and a low grid accesibility. Approximately 15% of the population had access to electricity in 1990. With an expansion of the grid, this percentage had grown to 53% in 2016 [WB, 2019]. Along with this increase in accessibility, the demand for electricity grew annually with an average of 12% up to 12,570 GWh in 2016 [IEA, 2016]. This rapid expansion of the electricity network had a negative impact on transmission and distribution losses. After a sharp increase in the 90's - reaching a peak around the turn of the century - the losses in the 21st century have slowly decreased to around 15% in 2014. As a result, roughly one-fifth to one-quarter of the energy was lost during this period, which meant that up to 33% more energy had to be generated than was demanded by the users [UNDP, 2014].

The significant growth in electricity supply in recent decades is mainly possible because of the discovery - and extraction - of oil in the mid 90s. This trend has reduced the relative capacity of hydropower from 70% in 1980 to 50% in 2010 [Awad and Yossof, 2016]. However, with the succession of South Sudan in July 2011, Sudan lost 75% of its oil resources. Because the remaining oilfields are reaching maturity and new explorations in the Red Sea do not get off the ground, there is a need to become less dependent on fossil fuels [UNDP, 2014; EIA, 2018]. This development has increased the importance of a successful implementation of the renewable energy master plan.

At present - in absence of wind farms and solar plants - hydropower is the only renewable source of electricity. With the construction of the Merowe dam, the upgrade of the Roseires dam [Mulat et al., 2018] and the recent completion of the dam complex in the Upper Atbara and Setit river, the installed hydropower capacity has increased considerably in the last decade. However - despite the fact that a few dams are planned in the north of the Nile Valley - with a limited technically feasible potential or 4.920 MW for hydro-electric power generation, the bulk or future expansion will have to come from other sources. With a technical feasible potential of 5,000 MW for wind energy generation, and high solar insolation levels, Sudan has sufficient renewable sources to realize this need [UNDP, 2014]. In the renewable energy master plan, the government aims to utilize respectively 680 MW and 720 MW of this potential in 2031 with the construction of wind farms and solar plants [UNDP, 2014]. To meet the expected energy demand of 46 GWh in the same year, Sudan's government plans to install a total capacity of 14,300 MW. For this, in addition to the renewable capacity, the thermal capacity needs to expand to 9873 MW in 2031. To reduce dependence on oil, some planned installations fuel gas or coal [MoWRE, 2016].

Sudan's main electricity network consists of several interconnected regional grids on the Eastern side of the country. Besides the main network, there exist a dozen of local distributions networks fed by thermal generators [EIA, 2018]. However, most of the population lives in rural areas and does not have access to electricity (29% rural electrification) [MoWRE, 2016]. Therefore, to meet the target of 75% accessibility by 2031 - besides urban areas - large parts of remote rural areas need to be supplied. Because it is not economically feasible to connect these areas to the grid, feasibility studies are ongoing to provide electricity to these households using micro grids powered by either biogas from animal and agricultural waste or solar home systems [MoWRE, 2016].

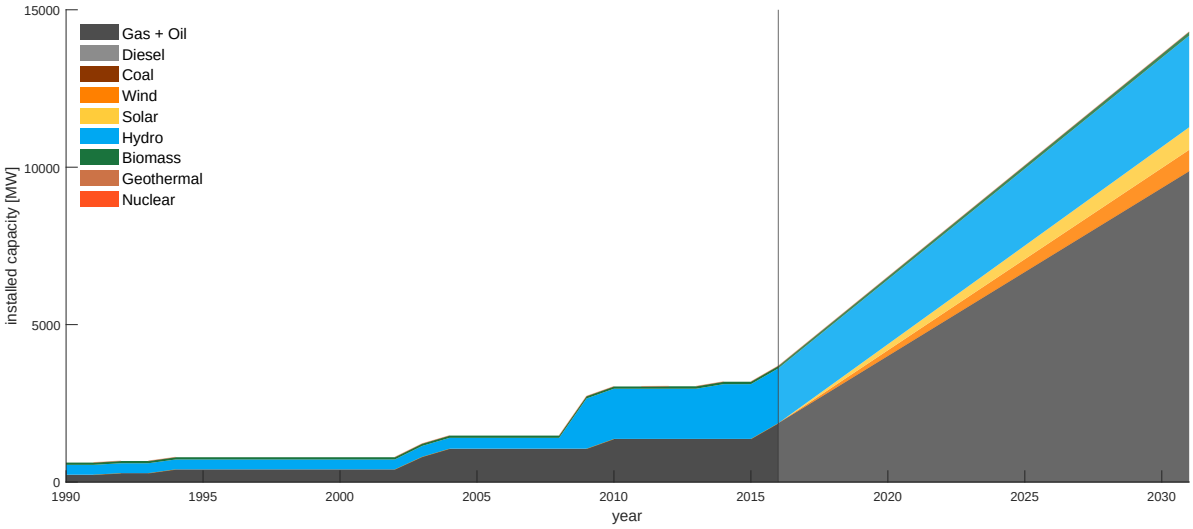

Figure 2.7: Installed electric power capacity in Sudan in the period 1990-2016 and future capacity projections. Historic capacities are based on WB [2017]; Rabah et al. [2016] and future projections on MoWRE [2016].

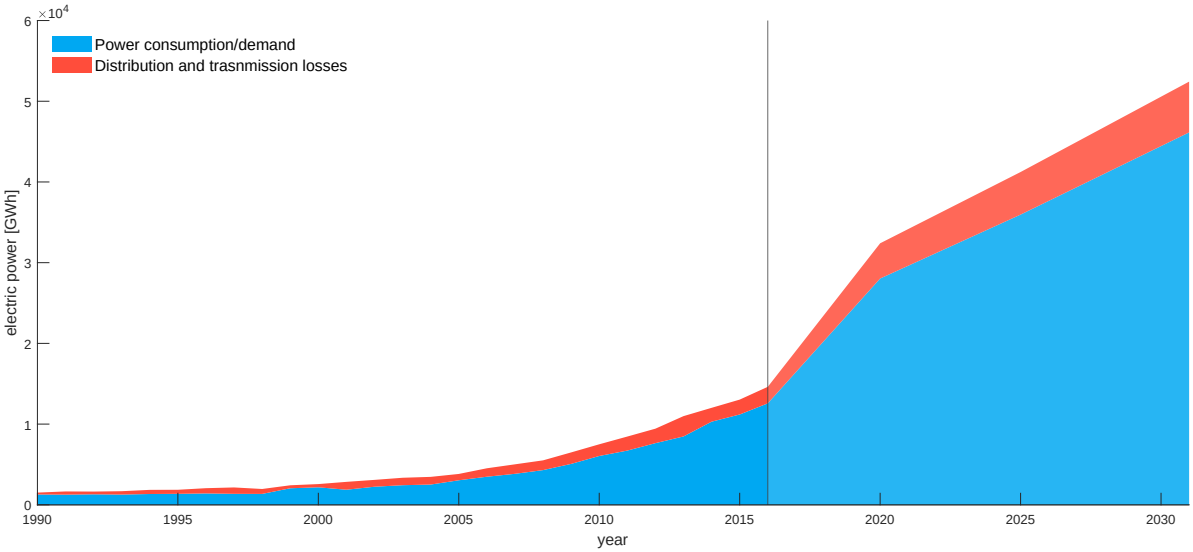

Figure 2.8: Historic energy consumption and future electric demands in Sudan supplemented with the distribution and transmission power losses. Historic consumption is based on IEA [2016], and historic losses are computed based on percentual losses as presented in WB [2019]. Demand projections and transmission losses are based on MoWRE [2016].

2.1.5.4. South Sudan

The electrical infrastructure in South Sudan is in a terrible state as a result of two civil wars in the last fifty years [AFDB, 2013]. Despite the targets set in the development plan, the power infrastructure has not changed much from the pre-independent period. At present, the grid-based electricity situation in South Sudan is characterized by a low accessibility rate, frequent blackouts and lack of efficiency [WB, 2013]. The accessibility rate of the power grid was 1.05% in 2018 and has therefore been constant for the past eleven years [SSEC, 2018]. During the same period, transmission and distribution power losses were in the order of 25 to 30% [AFDB, 2013; SSEC, 2018]. Due to these characteristics of the electric grid, many residents are dependent on diesel generators or solar installations to meet their energy needs [EIA, 2018]. However, diesel generators suffer from the demerits of high fuel costs and a short life span. As a result, South Sudan has – with a per capita electricity consumption in the range of 1-10 kWh – the lowest energy consumption rate in Africa and the highest cost of producing energy [Tiitmamer and Anai, 2018].

The electricity network consists of multiple regional grids, some of which are operated by the South Sudan Electricity Corporation (SSEC) and some by foreign companies [AFDB, 2013; Tiitmamer and Anai, 2018]. Generation sources connected to the grid consist exclusively of thermal plants firing diesel or heavy fuel oil. Supply is limited to a few towns. At the time of independence, the SSEC had an installed power capacity of 30 MW and a 32 MW interconnection with Sudan. However, due to technical problems and fuel shortage most of it was not operational [Tiitmamer and Anai, 2018]. Of the installed capacity, 22 MW was operational until 2015, and only 3 MW was exchanged with Sudan. After the Juba plant stopped operating in 2015, the available installed capacity of the SSEC dropped to 10 MW [WB, 2013; Tiitmamer and Anai, 2018].

Already today, demand in the supply areas served by the SSEC is much higher than the power company can provide. With an estimated demand growth of 8.05%, the generation capacity needs to increase. Given the local availability of fuel, there is a huge potential of establishing more hydrocarbon based thermal power plants in the country [WB, 2013]. However, although South Sudan owns the third largest oil reserves in Africa, the country lacks the capacity to refine crude oil for domestic consumption, forcing it to import almost all of its oil products for electricity generation [Tiitmamer and Anai, 2018]. This makes the country vulnerable to shortages and price fluctuations on the international market. To reduce this vulnerability in future, the government aims to diversify production using its huge potential for hydro, solar, wind and geothermal power [SSEC, 2018].

To use these renewable sources on a large scale for electricity production, an expansion and linking of regional grids is necessary. However, electricity demand is too low in the short term to justify a national grid. Moreover, political instability is currently a hurdle for potential investors. Instead of a national network, the government therefore strives to form two regional grids in the short term. A southern national grid, around Juba, will be supplied in the short term from enhanced diesel generation and the small Fula hydropower plant. A northern grid, around Malakal, will be supplied by enhanced diesel generation and interconnections with Sudan. In all other local grids, the generation capacity will be expanded with refurbished or new thermal plants [AFDB, 2013]. Given the lead time associated with commissioning of the new power plants, the risk of power supply shortage will remain for some time in the near future [AFDB, 2013]. In the longer term future will the regional networks expand, will the capacity increase with the construction of new thermal plants and large-scale hydropower installations, and will new connections be established with Ethiopia, Uganda and Kenya. The goal is to increase the grid accessibility up to 20% by 2025 and to reduce the network losses 12% [AFDB, 2013]. If the economy continues to grow in the years after 2025, the networks are expected to fully integrate around 2040 [SSEC, 2018].

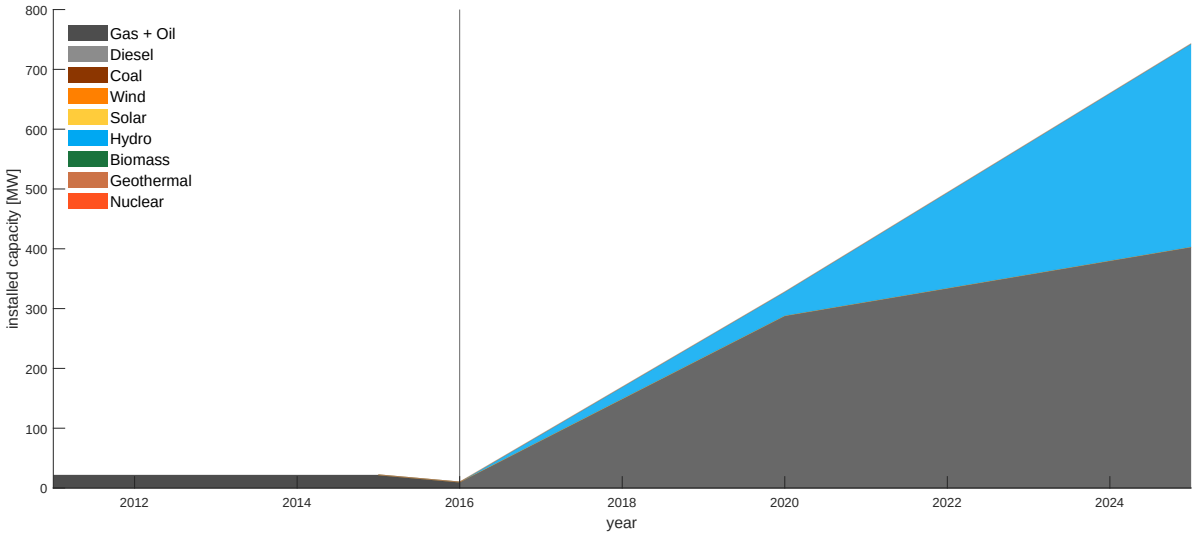

Figure 2.9: Installed electric power capacity in Sudan in the period 2011-2016 and future capacity projections. Historic capacities are based on WB [2013]; Tiitmamer and Anai [2018] and future projections on AFDB [2013].

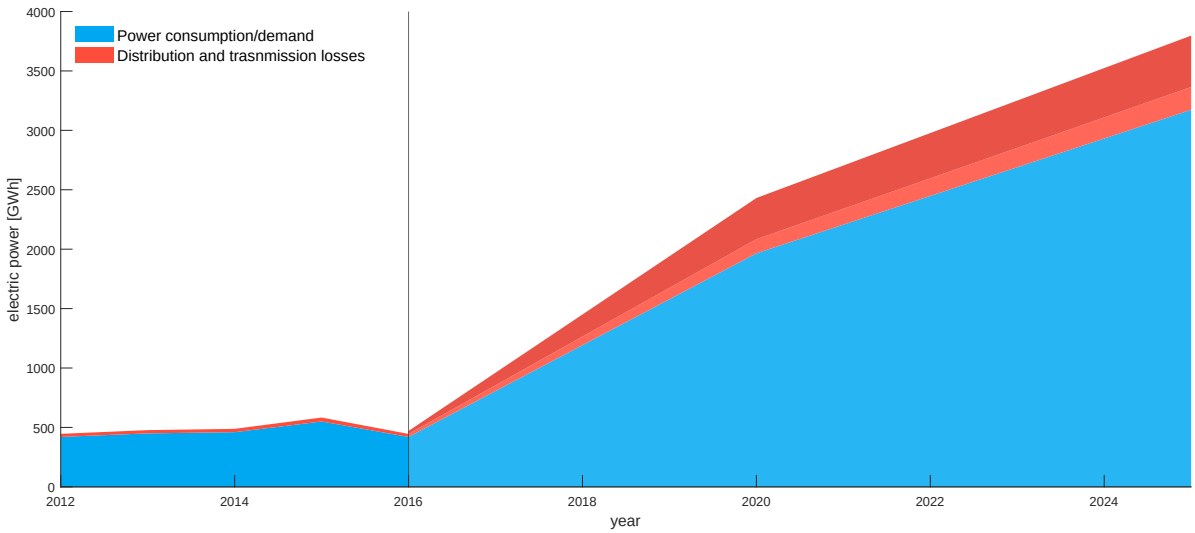

Figure 2.10: Historic energy consumption and future electric demands in Sudan supplemented with the distribution and transmission power losses. Historic consumption is based on IEA [2016], and historic losses are computed based on percentual losses as presented in WB [2019]. Demand projections are based on AFDB [2013] and [EA, 2020]. Since the transmission and distribution losses depend on the accessibility of the grid, they are presented as a range. When most electricity is generated in micro grids, the losses will remain low (around 5.7%). However, when the number of connections to regional grids increases, the losses can rise up to the expected 12% in 2025 [AFDB, 2013]

2.1.5.5. Eastern Africa power pool

Some international electricity connections on the African continent and with the Arabian Peninsula have already been discussed in the previous sections. To further promote electricity trade in Africa four power pools have been created. The Eastern Africa Power Pool (EAPP) was established in 2005 by seven countries: Burundi, Democratic Republic of Congo (DRC), Egypt, Ethiopia, Kenya, Rwanda and Sudan. In the consecutive years the pool was expanded to eleven members through the participation of Tanzania, Libya,Uganda and Djibouti [Hira et al., 2015; Jiilu, 2015].

The objective of the EAPP is to provide more residents of the member states with access to electricity resources through regional planning and coordination of energy resources. The EAPP offers a platform where a joint master plan is developed by the national ministries of electricity matters [EAPP, 2016]. Power pooling increases the size of the sales market and makes it therefore possible to invest in bigger

power plants that can exploit economies of scale. Partly because of this and because of increasing competition, the price of electricity will fall, making the resource more accessible to a larger part of the population. In addition, will the power pool, through the diversification of energy sources, make member states less vulnerable and dependent on the international fuel market and on their natural resources [Hira et al., 2015]. The latter is beneficial for the development of a green and renewable energy sector.

The first EAPP master plan was published in 2011. This master plan prescribes various international connections between the eleven member states and South Sudan. Figure 2.11 is a graphical representation of the connections between (neigbouring) countries of the Eastern Nile. Some of the proposed connections are either completed or under construction, but the majority of the connections is delayed due to a lack of concrete plans or financing.

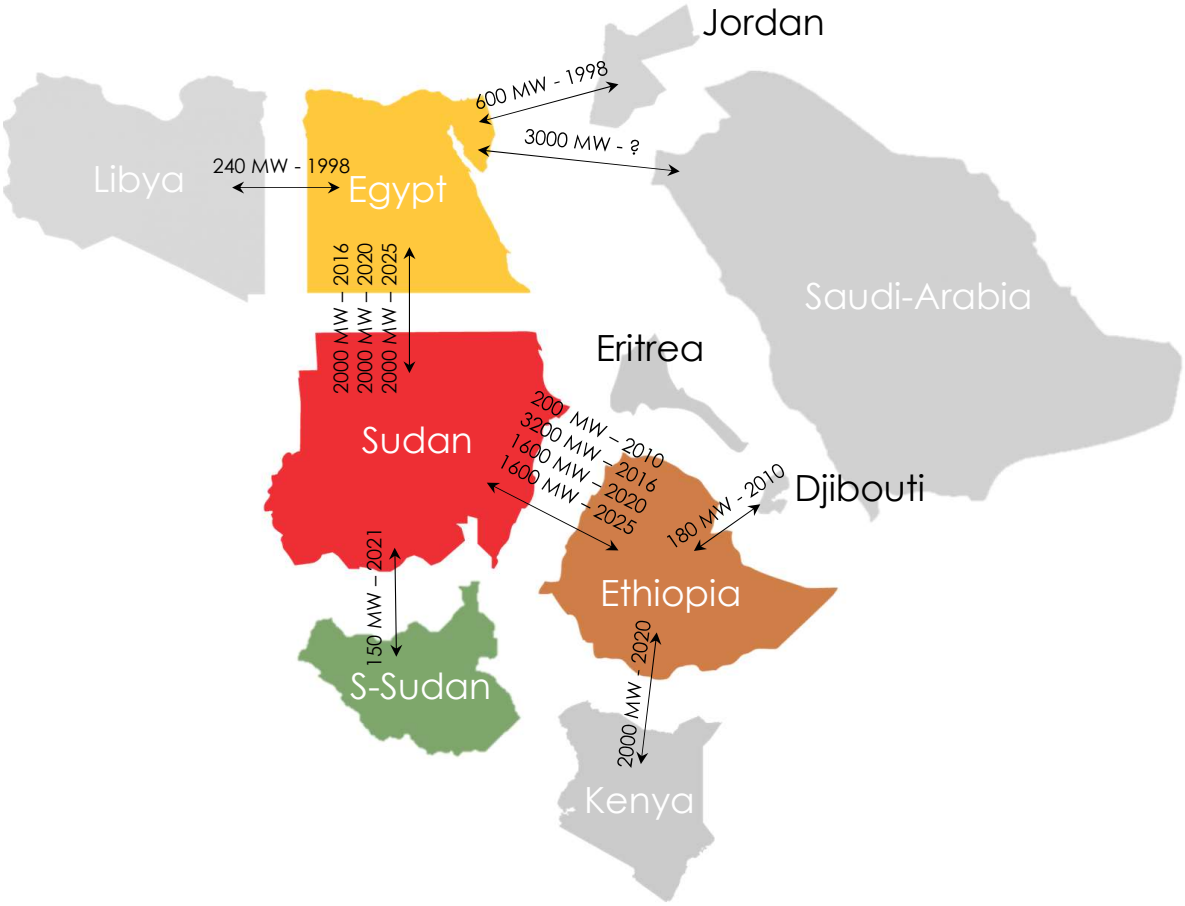

Figure 2.11: A schematic representation of the existing and planned interconnectors of the Eastern Nile riparian states. The figure is compiled with information obtained form Jiilu [2015] and ESI [2018].

2.1.6. Food system

In this section some background information is provided on the food system. For each individual riparian state a short description follows with background information on the dietary composition, the agricultural production characteristics and capacitites and the farming system.

2.1.6.1. Egypt

The Egyptian dietary energy intake gradually increased during the past decades. Where the per capita energy intake was approximately 2000 kcal in 1960 it increased to 3500 in 2008 [FAO, 2017]. This increase is mainly the result of an increase in carbohydrates and proteins but caused by an increase in food losses and waste as well. The intake of both animal fats and vegetable oils decreased. However, in 2008 the meat and vegetable oil intakes still account with 16% and 8%, respectively, for the majority of the energy intake after the carbohydrates (52%) [El Sayed, 2012; FAO, 2010]. Relatively little is consumed in terms of vegetables and fruits, and tubers and pulses.

Due to the climate, food production in Egypt takes place almost exclusively in irrigated agriculture. The agricultural areas present can be divided into the Old lands situated in the Nile Valley, Delta, and the Oases and the New lands reclaimed since the construction of the Aswan High Dam. Surface irrigation is the most widely used type of irrigation in the Old Lands. In the New Lands, sprinkler irrigation is required by law [FAO and Aquastat, 2016]. The irrigated areas have increased in recent decades and will continue to grow in future. However, as Egypt approaches its irrigation potential, this increase will be slow. An expansion of 0.25 million hectare is expected in 2050 with respect to the 3.6 million hectare present in 2010 [Multsch et al., 2017]. The soil along the Nile Delta is fertile and, in combination with the prevailing climate conditions, a large number of crops can be cultivated. The most cultivated products are cereals (rice, corn and wheat), fodder cops (berseem), vegetables (mainly tomato) and all kinds of fruit (citrus and subtropical fruits) [FAO and Aquastat, 2016; Thomas, 2003]. Cotton and sugar are the main cash crops produced for export. Yields of most of these crops have significantly increased within the past decades [FAO and Aquastat, 2016].

Because Egypt consists mainly of desert where insufficient grasses grow for natural grazing, cattle feeding almost exclusively takes place in irrigated areas. Here they consume all kinds of residues and by products, but they consume large amounts of cereals like maize barley and wheat as well. In this way they compete directly with crop production for human consumption. This competition is even further exacerbated by the enormous amounts of land used for the winter fodder crop berseem [Fitch and Soliman, 1981].

2.1.6.2. Ethiopia

The Ethiopian dietary energy supply is not sufficient to meet the population's energy requirements. Hence large part of the population is undernourished. The Ethiopian dietary patterns vary across the multiple agroecological regions, but is generally stated mainly composed of the cereals maize, sorghum and teff. The diet is supplemented with tubers, potatoes and oil seeds. Despite a large livestock population, the food supply of animal products is very limited. Only in nomadic areas is milk a major component of the diet [FAO, 2010].

The major part of the Ethiopian agriculture takes place under rainfed conditions. The major irrigated areas are located outside the Nile basin. Within the Nile basin, irrigation development started with the construction of the Fincha's scheme. Up to 2050 an expansion of 1 million hectares is expected, of which a large part will be constructed in the Blue Nile and Atbara [Multsch et al., 2017]. Cereals form the largest crop group in terms of area, and account for about three-fourths of the total area cultivated. Teff is the preferred staple food, followed by maize, sorghum, barley and wheat [Dorosh and Rashid, 2013]. The second and third most important crop groups are pulses and oilseed. These are followed by the major cash crop coffee. Vegetables, roots and fruit occupy only a small fraction of the available cropland [Dorosh and Rashid, 2013]. Compared with international standards are yields low and is the overall production, due to the large dependency on rainfed land, highly vulnerable for droughts.

Ethiopia is home to some of the largest numbers of livestock species in the world. Roughly, the farming systems can be subdivided in two groups. Mixed farming systems are found in the highlands, while pastoral systems are found in the lowlands. The Ethiopian feed basket is mainly composed of natural pasture, crop residues, cereals and to a small extent improved pastures. The exact composition differs between the agroecological regions [Bachewe et al., 2018; Tonamo, 2016].

2.1.6.3. Sudan

Nowadays, the food supply in Sudan meets with an per capita energy intake of 2500 kcal the per population energy requirements. However in the early 60's Sudan faced serious malnutrition with an approximate energy intake of 1600 kcal [FAO, 2017]. Sudan's diet is mainly based on cereals, but there are major differences between regions in the country. Sorghum and millet are the main staple crops of a major part of the rural population. Wheat is of increasing importance to the diet in urban areas and in the north. Cassava, yams and sweet potatoes are the main staples in the southern region [Awad Sahil, 2005]. The cereals and tubers are supplemented with beans, peas and cowpeas. Fresh vegetables and fruits are consumed to a limited extent. Vegetable foods are complemented with a substantial supply of milk and eggs. The meat supply, consisting mainly out of bovine, mutton and goat meat, is limited and has been fairly stable in the past decades [Awad Sahil, 2005].

Agriculture takes place in both irrigated and rainfed areas in Sudan. Spread over several irrigation sites, the irrigation area covered approximately 1.8 million ha in 2010. The Gezira scheme located in the Blue Nile is with an estimated area of approximately 0.9 million hectares the largest irrigation site. Up till 2050 an increase of 1.3 million hectares is expected [Multsch et al., 2017]. The main crops grown under irrigation are cotton, wheat, sorghum, groundnuts, pulses, green fodder, fruits, vegetables, and sugarcane and to a lesser extent roots and sunflowers [FAO and Aquastat, 2015; Awad Sahil, 2005]. The yield of most cereals is far below the potential yield. Only sugarcane yields are approaching their potential [FAO and Aquastat, 2015]. Rainfed agriculture covers by far the largest area in Sudan. The major crops cultivated in the rainfed sector include sorghum, millet, sesame, sunflower and groundnuts. The majority of the rainfed areas is situated in arid and semi-arid regions and therefore prone to serious drought risk. The area actually cultivated and total production therefore vary considerably from year to year depending on variability of rainfall [FAO and Aquastat, 2015]. In addition, large areas are degraded due to erosion, exhausting or siltation.

Sudan has next to Ethiopia the largest livestock inventories in Africa. More than 90% of the animal population is accounted for by the nomadic pastoral sector. The latter is possible because of the large areas with good natural pastures [FAO and AGAL, 2005].

2.1.6.4. South Sudan

Malnutrition is a major concern in South Sudan. Up to 60% of the population does not obtain the minimum required 2100 kcal per day and/or has a diet consisting of products from less than four food groups. Almost half the population (47%) consumes less than the minimum recommended energy intake of 1700 kcal required to live an active and healthy life [WFP, 2012]. Because of the poor infrastructure, regional differences in consumption are large. For the country as a whole, cereal consumption accounts for the major energy intake, followed by livestock products, fish, roots and oilseeds [AFDB, 2013].

The land area equipped for irrigated agriculture in South Sudan is not significant. Food production is therefore almost entirely dependent on rainfed agriculture, making it very vulnerable to climate fluctuations. However, the potential for irrigated agricultural production in South Sudan is huge. With its abundant arable land resources and untapped water resource potential, South Sudan has the potential to become a major cereal producer in Eastern Africa [WFP, 2012]. Currently is sorghum the main cultivated crop. Other cereals like millet, maize and rice are produced in small amounts. Another major cultivated crop is groundnut. It makes an important contribution to the household diet, and it is the main cash crop which contributes to farming household income at certain periods of the year. Vegetables such as onions or tomatoes are not commonly grown [AFDB, 2013].

Livestock provides the main source of livelihood for a substantial portion of the population. The majority of the livestock is raised by nomads and are entirely dependent on access to grazing land and watering points. However, the increasing number of farmers is reducing the amount of grazing land available [AFDB, 2013].

3 Methodology

This case study in the Eastern Nile applies the method presented in part A. This chapter therefore only serves as an addition to this description. First, the system boundaries used in this case study are explained. This is followed by a brief completion of the food and energy balance, and a description of the data collection and processing activities. Finally, the simulation experiments executed are presented.

3.1. System boundaries

Depending on the modeled time, three or four countries are included in the analysis. For Egypt, Sudan and South Sudan, the Nile is the only river basin within the country's administrative boundaries. In Ethiopia seven other subbasins are distinguished, being the Omo, Rift Valley, Genale Dawa, Shebele, Ogaden, the Awash and Afar. The setup for the Eastern Nile case study therefore works with seven outside basins, all of which are located in Ethiopia. The agricultural area present in these basins is clustered in the centre of gravity of the areas present in that basin. To account for the agro-climatic feasibilities within the outside basins, the maximum cultivable area varies per crop. The plant characteristics valid in the center of gravity such as the yield and duration are described as the area weighted average of the crop characteristics on the individual fields.

Rain-dependent agriculture is described in pixels with a magnitude of 1.5 degrees (approximately 28,000 km2 at the equator). In total 119 pixels are included, which are located in Ethiopia, South Sudan and the southern part of Sudan. The minimum amounts of rainfed agriculture feasible in Egypt along the Mediterranean coast are not included. The surface present within each pixel is clustered in the center point of the respective pixel. As for the agriculture in the outside basins, the crop characteristics are the area weighted average of the fields present within the pixel.

The node-link network used for the Eastern Nile is shown in Figure 3.1 and 3.2. In total, the scheme contains 216 nodes. This node-link network is based on the Eastern Nile RIBASM model [van der Krogt and Ogink, 2013]. However, some of the surface water reservoirs present in this model are not included in the presented node-link network because structural data is missing at these location. Other surface water reservoirs have been combined to reduce the number of required optimization variables. To leave the the non-linear relationship for the hydropower generation unchanged, only irrigation purpose reservoirs are merged. If a reservoir upstream an irrigation area is not included in the node-link network, the irrigation field directly downstream is also eliminated. When the upstream surface water reservoirs are combined, the downstream irrigation fields are as well. Also irrigation fields within proximity and placed in series are combined in a single node.

3.2. Filling in the balances

Defining the cultivated crops is a trade-off between the (increasing) computational demand and the (added) accuracy, limited by the availability and reliability of data sources. Subdivided into cereals, vegetables (tubers, pulses and fresh vegetables), fruit, cash crops (fiber crops, narcotics, sugar and oil) and forages, thirty-three crops are specified in this optimization study (see Appendix B.2). These thirty-three crops represent the most cultivated crops and forages in Egypt (81%), Sudan (96%), South-Sudan (96%) and Ethiopia (78%) [FAO, 2017; NBI, 2012; Abdelkader et al., 2018; Mersha et al., 2017] and embody all major crop groups. In addition to these vegetative products, the consumption of animal products has been included indirectly. Consumption of the animal meat products of beef, mutton, pig and poultry, and the dairy products milk and eggs are possible. The food production possible by product processing is classified in three groups. First of all, all oilseeds (groundnut, sesame, sunflower, soybean and rapeseed) can be converted into the related oil product. Furthermore, sugar cane and sugar beet can be converted into sugar and sorghum, millet and barley can be used for conversion into alcoholic beverages.

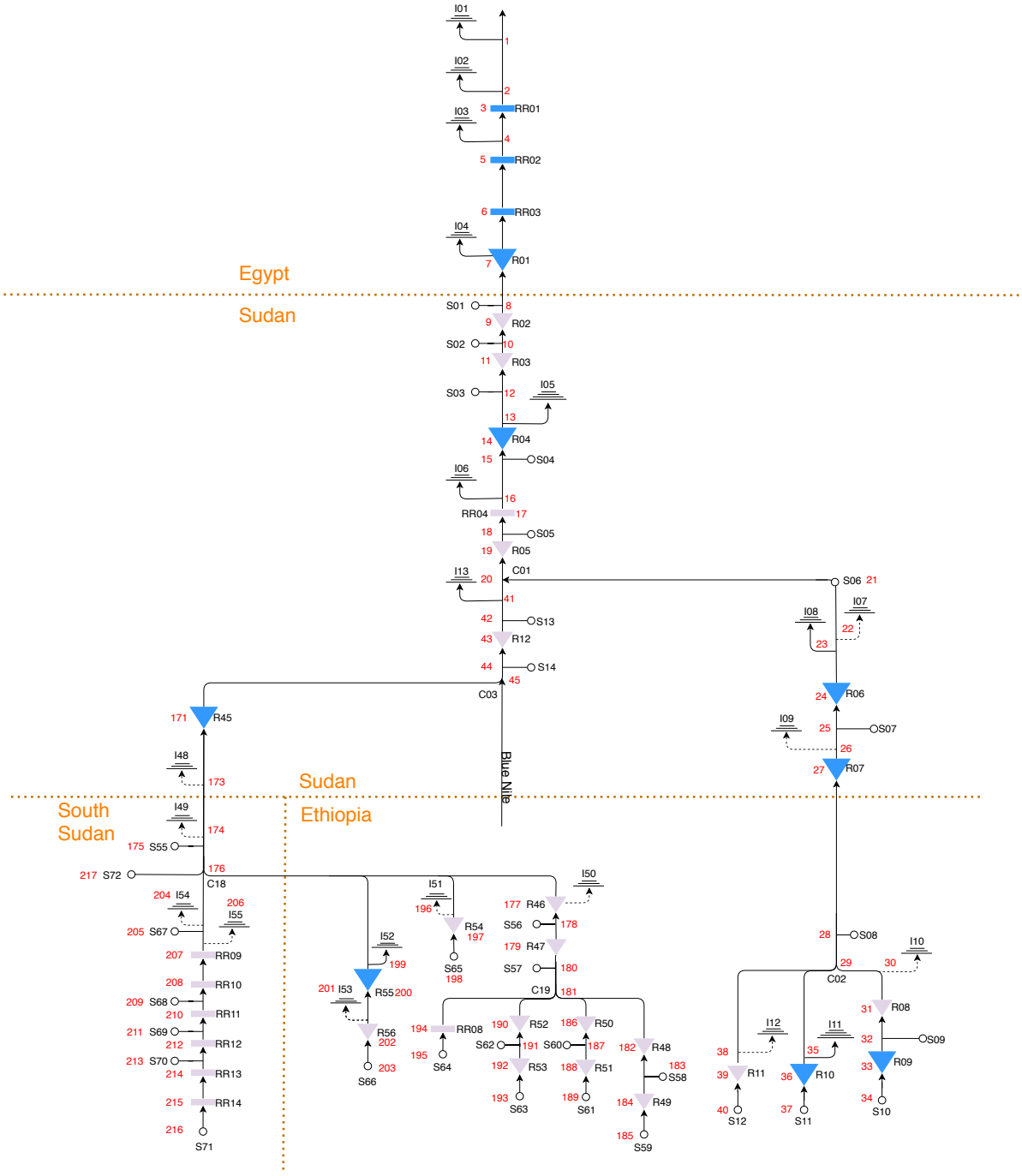

Figure 3.1: The schematization of the Eastern Nile river Basin, without the Blue Nile basin, used in this study. The figure depicts the location in the Nile streams of reservoir, irrigation, run of the river and source nodes. Reservoir nodes are depicted by triangles (blue is operational, grey is planned), irrigation nodes by a triple lines (operational if arrow is solid, planned if arrow is dashed), run of the river power generator nodes by rectangles (blue is operational, grey is planned), offtake nodes by black dots (operational if outgoing arrow is solid) and source nodes by small circles. All source, reservoir, run of river, offtake and irrigation nodes are assigned an index number given in black. All nodes, including confluence nodes, are assigned a node number in red.

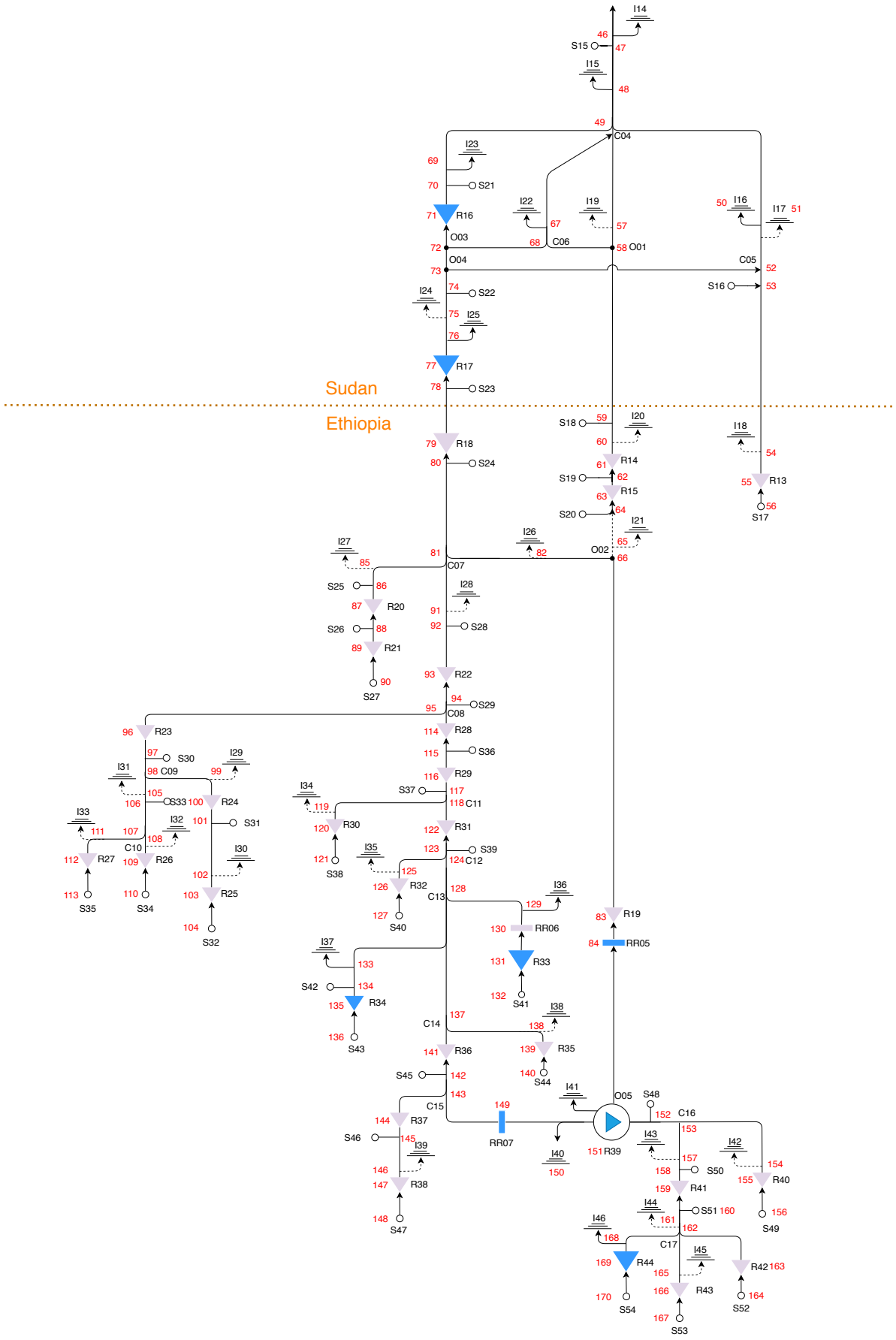

Figure 3.2: The schematization of the Blue Nile basin used in this study. The figure depicts the location in the Nile streams of reservoir, irrigation, run of the river and source nodes. Reservoir nodes are depicted by triangles (blue is operational, grey is planned), irrigation nodes by a triple lines (operational if arrow is solid, planned if arrow is dashed), run of the river power generator nodes by rectangles (blue is operational, grey is planned), offtake nodes by black dots (operational if outgoing arrow is solid) and source nodes by small circles. All source, reservoir, run of river, offtake and irrigation nodes are assigned an index number given in black. All nodes, including confluence nodes, are assigned a node number in red.

In addition to power generation through hydropower plants in the Eastern Nile, national electricity can be generated with non-renewable oil, gas, coal and nuclear plants, and the renewable wind, solar, biomass and geothermal resources. Since it is unclear whether neighbouring countries outside the region will be able to produce more electricity than they need for themselves in future, it has been assumed that imports from these countries are not possible. Since mainly Ethiopia strives to become the energy supplier of East Africa, electricity exports to these countries are feasible.

3.3. Data collection and processing

3.3.1. Climate forcing

Metreological data series are provided by the Climate Research Unit (CRU). The CRU-TS series are interpolations of ground observed data created from monthly observations around the globe. The latest CRU-TS4.1 dataset [Harris et al., 2014] provides gridded monthly mean climate data with a spatial resolution of 30' between 1901 and 2018. Besides independent climate variables (e.g. precipitation) the dataset also contains arithmetically derived variables (e.g. mean monthly maximum and minimum temperature) and secondary variables (e.g. potential evapotranspiration). The latter one is – in line with the FAO guidelines [Allen et al., 1998] – computed using a variant of the Penman-Monteith formula. Using the time-variant mean monthly maximum and minimum temperature from the CRU-TS4.1 dataset, and the time-invariant monthly values for wind speed provided by the CRU-CL1.0 terrestrial climatology dataset [New et al., 1999], the Penman -Monteith reference evapotranspiration has been converted to the Penmann open water evaporation (see Appendix A.1.1).

Basin-wide hydrologic inflow data is obtained from the Eastern Nile RIBASIM model [van der Krogt and Ogink, 2013]. This inflow data is defined per subcatchment of the Eastern Nile. This study compiled historical hydrologic data from a variety of sources with differing periods of record and filled in missing data using site-specific regression and partitioning techniques to reconstruct a dataset of 103 years (1900–2002) [Wheeler et al., 2016]. Because the historical model experiments require data for the period 1989-2013, the historical time serie has been extended. Every missing year in the period 2003-2013 has been supplemented per subcatchment with the historical discharge event from the period (1960-2002) in which timing and amounts of precipitation and evaporation show the biggest similarity (see Appendix A.1.3).

Deterministic future time series for precipitation, evapo(trans)piration and discharge are created on the basis of information obtained from the Swedish Meteorological and Hydrological Institute (SMHI). Their online database provides gridded (30') average monthly (relative) change in atmospheric forcing over a time period of 30 years between 2011-2040, 2041-2070 or 2071-2100 with respect to the reference period 1971-2000 for an ensemble of climate models, both for the moderate RCP4.5 and high RCP8.5 (Representive Concentration Pathways) emission scenarios. Besides it provides globally - for the same periods, climate models and emission scenarios – the average monthly relative change in discharge per subcatchment as computed by the open source World-Wide HYPE model [Arheimer et al., 2020].

By scaling gridded time series from the historic period (1989-2013) with their projected monthly relative change in the RCP4.5 scenario, deterministic time series for discharge and precipitation have been created for the near future (2019-2043). Future gridded monthly average daily minimum and maximum temperature series are created by adding the expected monthly average change (in °C) to historic temperature series. Time series for the open water evaporation and the potential evapotranspiration are calculated from the latter temperature series following the FAO approach [Allen et al., 1998]. For this it is assumed that both the cloud cover, wind velocity, and relative humidity remain unchanged with respect to the reference time series (see Appendix A.1.2 for more information).

3.3.2. River infrastructure

Most of the infrastructural data is obtained from van der Krogt and Ogink [2013]. However, commissioning dates are not mentioned in the dataset. commissioning dates of operational surface water reservoirs, irrigation fields, run-of-the-river plants and offtakes are obtained from literature [Whittington et al., 2014; Müller-Mahn and Gebreyes, 2019; Gebre et al., 2008; Tournier et al., 2019;

Johnston and McCartney, 2010; Ali et al.; Shiferraw and McCartney, 2008; Gupta et al., 2015] or manually determined using Landsat data in the Google Earth Engine [Lea, 2018]. With the exception of the Chara Chara weir at the outlow of Lake Tana, these commisioning dates are used for the historical experiments. The Chara Chara weir needs to been online from the start of the experiments because the description of a natural lake has not been included in the model. Because it is unclear when the majority of the infrastructures included in the node-link network in Figure 3.1 go online, based on the predicted expansion for hydropower capacity and irrigation area, as discussed in Section 2, a future structural scenario has been created (see Appendix A.2.1).

Most of the data required for the surface water reservoir is described in van der Krogt and Ogink [2013]. However, some storage-area-elevation relations, hydropower capacities and all gate capacitities are missing. The missing storage-area-elevation relations and hydropower capacitities are supplemented with data from Wheeler and Setzer [2012]. The gate capacities of operational surface water reservoirs are obtained from literture [Berga et al., 2006; DIU; Stevenson and Debebe, 2009; Abdellatif, 2004; Bashar and Mustafa, 2009; Pietrangeli et al., 2017]. For newly planned surface water reservoirs, an extreme discharge analyses is performend to estimate the gate capacities (see Appendix A.2.2). Based on a linear relationship found between the gate capacities of the existing reservoirs and the discharge during a 100 year flood event, the gate capacities of the future surface water reseroirs have been estimated.

The minimun required yearly and monthly outflow during the reservoir filling process are based on the filling approach for the GERD. Because the final reservoir filling approach is still unknown due to disputes between the Nile riparian states, the initially proposed method is used. In this method, the reservoir is filled in 6 years, which according to Wheeler et al. [2016] is achieved with an annual release of 35 BCM. According to the 103 years of discharge time series obtained from van der Krogt and Ogink [2013], this release correspond with 72% of the long term annual average inflow. This percentage is in combination with the long term annual inflow in all other reservoirs used to determine the minimum required annual outflow. The minimum required monthly outflow is set equal to the minimum flow event observed during the historic time series.

For the merged surface water reservoirs, the outflow capacity is the sum of the individual reservoirs. The elevation is not important for these combined irrigation reservoirs, but for the computation of the open water evaporation, the surface area is. To determine a new storage-area-elevation relationship, it is assumed that all merged irrigation reservoirs drain evenly i.e. that the relative storage of all reservoir is the same at all times (see Appendix A.2.3).

The A* search algorithm is used to compute the distance between succesive nodes in the flow network. The search space consists of a - manually checked and modified - flow network, delineated from a 3-arcsec SRTM digital elevation map [Lehner et al., 2006]. Source and goal node coordinates are adopted from the Eastern Nile RIBASIM model and shifted to the nearest river branch of the delineated network. In absence of specific data for each river branch, a flow velocity of 1 metre per second has been adopted. An estimate of the river losses are made using a graph presented in Whittington et al. [2005] showing the course of a cubic meter of water from Lake Tana via intermediate reservoir to the Aswan High dam. By reducing the total flow losses with the reservoir evaporation (determined in the RIBASIM model), the river losses are computed to be 5% per 1000 km (see Appendix A.2.4). This loss factor is used for all river branches, except for the links situated in the Sudanese wetlands, and are therefore not related to the prevailing climate and geological conditions in the river segments. For the links downstream of node 217 and 204, loss factors of 0.02 and 0.4, respectively, have been identified. With these loss factors, the long-term annual average flow corresponds with the discharge mentioned in FAO [2011b]. Because the flow is only delayed and reduced, and the buffering and smoothing effect of the wetland is not included in the method, the annual variability is greater than in real world observations.

3.3.3. Agriculture

Forced by the limited data availability, crop specific yield response factors, crop coefficients, relative stage lengths and dry masses are assumed uniform over the entire Eastern Nile basin. General (non location unique) yield response factors are adopted from Allen et al. [1998]. The values of the missing yield response factors are adopted from specific literature [Munoz et al., 2007; Najarchi et al., 2011; Gomes and Carr, 2003; Uçan et al., 2007; Arruda and Grande, 2003; Terink et al., 2013; Khan, 2013; Araya et al., 2011; Majnooni-Heris et al., 2014]. Crop coefficients and relative stage lengths are adopted from Allen et al. [1998] and Yihun [2015]. For the multi-cut forage crops are the relative stage lengths for all cutting cycles assumed uniform. The crop coefficient and stage lengths of fodder maize are adopted from general maize, assuming that the forage is harvested halfway through the development phase. General dry mass percentages are retrieved from FAO Feedipedia [Feedipedia, 2017] and the GAEZ model documentation [Fischer et al., 2012]. Except for sugar crops, cotton and forage crops, where the dry mass is respectively defined as the dry mass of sucrose, lint and green forage, the difference between fresh and dry mass is equal to the moisture content of the grains, roots, pulses, seeds and fruits. The resulting values are summarized in Appendix B.2.

The potential yield is retrieved from the Global Agro Ecological Zones (GAEZ) database [Fischer et al., 2000]. This dataset provides, with a 10 kilometre spatial resolution, potential yields for the majority of the cultivated crops using the period 1960 - 1990 as a baseline. The missing spatial maps for teff, lentils, sesame, berseem, Sudan-grass and fodder-maize are created by adapting the available spatial maps. The spatial distribution of the potential yield for these missing crops corresponds respectively with the distribution of wheat [Araya et al., 2011], cowpeas, groundnuts, alfalfa, sorghum and maize. These maps are scaled until their maxima correspond with values found in literature. [Hamza and El-Salam, 2015; Yadav et al., 2007; Muhammad et al., 2014; Duke, 1983; Salama, 2019].

The duration of the growth cycle is spatially described in data retrieved from the GAEZ database. The duration of those crops missing in the database, and that are not perennial nor forage crop, are obtained from FOA report 56 [Allen et al., 1998] and Araya et al. [2011]. The growth duration, and the number of cuttings for forage crops are obtained from specific literature [Suttie, 2000; Salama, 2019; Muhammad et al., 2014].

The start month of the cultivation differs between rainfed and irrigated conditions. For irrigated conditions, a crop calendar is composed with national data retrieved from the FAO [FAO, 2020] and MIRCA [Portmann et al., 2010] irrigated crop calendars. Start dates for Sudan-grass and fodder-maize are assumed to correspond with those of sorghum and maize. For rainfed conditions start months of the growth cycle are described spatially in data retrieved from the GAEZ database. These start dates are determined to optimize the crop yields under the prevailing conditions [Fischer et al., 2012]. The start data for the missing crops teff, lentil, sesame and berseem are assumed to correspond to those of respectively wheat, cowpea, sunflower and wheat. Berseem is related to wheat as both are winter crops grown in cooler regions.

The surface areas of the irrigation sites within the Nile basin are obtained from van der Krogt and Ogink [2013]. The irrigated area in Ethiopia outside the Nile is per year computed by reducing the total irrigated area as described in FAOSTAT by the area present within the Nile basin. This area was then distributed over the subbasins with the applicable ratio in 2005 (determined from AQUASTAT's 2005 global map of irrigation areas [Aquastat, 2005]. For the future simulation experiments, it is assumed that all irrigated development in Ethiopia takes place in the underdeveloped Nile basin. The surface area in the outside basins is therefore described throughout this period by the areas present in 2018. The rain-dependent surfaces are also derived from FAOSTAT data and divided over the rainfed pixels with the applicable ratios in 2000 as described in data obtained from the GAEZ database. Future rainfed areas are derived from the Asia-Pacific Integrated Model (AIM). It concerns downscaled land-use data which are aggregated from regionally aggregated information [Fujimori et al., 2018]. The data used corresponds with the SSP2 forced with RCP4.5. Because the 2040 value in Sudan is smaller than the 2018 value in the FAOSTAT data, Sudan's rainfed surface area has been kept stable throughout future simulation eperiments. The rainfed area in Ethiopia is linear interpolated between the data value in 2018 and the projection in 2040.

To describe the (initial) composition of the rainfed pixels and the irrigation sites, the data on harvested areas obtained from FAOSTAT is split into an irrigated harvest area and a rainfed harvest area. Because not all crops present in FAOSTAT are included in this case study, the surface areas have been pre-modified. The total harvested area per product group has been maintained, but within a food group, the areas of the crops included in this case study are increased proportionately with the areas of the unincorporated crops. The irrigated harvested area is described using the harvested areas metioned in the FAO irrigated crop calendars [FAO, 2020]. Because this data is only available for one specific year, the area in the remaining years is obtained through scaling with the total irrigated area. This implies that the ratio of the irrigated harvest areas between the crops within a country remains the same. The rainfed harvested area is afterwards each year computed as the difference between the total harvested area and the irrigated harvested area. The harvest areas are subsequently distributed over the available sites or pixels by means of an optimization. Given the agro-climatic fesibility and climate forcing, the aim of this optimization is to minimize the differences between the predetermined harvest areas and the modelled areas for each crop in each year (see Appendix A.3). The optimization setup used to distrbute the crops over the rainfed areas is used to determine the parameter values for the evaporation constraints as well. With the aim to describe the harvested areas of perennial crops as well as possible, while also trying to keep the minimum evaporation parameter $c_{\min}$ and the period N_{per} over which the constraint is implemented for perennial crops respectively as large and small as possible, the following parameter settings followed: $c_{\min} = 0.2$ and $N_{\text{per}} = 6$.

Management factors required to convert the climate driven potential yield into the maximum attainable yield for irrigated crops are computed using a simple yield gap analyzes on the GAEZ data. Under the assumption that water and nutrient limitations were not present, field specific management factors are computed as the ratio of the actual yield at irrigated sites in the year 2000 over the potential yield. The national management factor is then defined as the median of all field specific management factors. The median is used as an indication for the management factor in an average field without placing too much emphasis on any (false) outlier in the dataset. For crops that were not cultivated in irrigated sites in the year 2000, a similar analysis was performed on the rainfed areas. Assuming that those cells with the highest ratios did not suffer from any nutrient nor water limitations, the national management factor is defined as the 95th percentile of all field specific management factors. The 95th percentile is used to remove extreme (false) outliers from the dataset. For crops that are not included in the GAEZ database, the management factor in Egypt is determined by dividing the yield, as mentioned FAOSTAT, by the average potential harvest in the irrigation areas. In Egypt and Sudan, missing management factors have been supplemented by scaling these values in Egypt with known manegement factors within the same food groups, implictly assuming that the manegement practices for crops within the same crop group are comparable. For rainfed crops, the management factor is, after the crop allocation over the rainfed pixels, computed as the ratio between the total modeled production, and FAOSTAT-based total rainfed production. The latter is determined by subtracting the modeled irrigated production, under the assumption that water conditions were not limiting, from the total FAOSTAT crop production. Although yield gaps are expected to diminish in future, due to a lack of crop specific predictions, the historic values are used in the future simulations as well. The resulting management factors are stated in Appendix B.3.

3.3.4. Food balance

The historical diet is based on data obtained from the FAO food balance sheets [FAO, 2017]. Because not all products mentioned in the food balance are included in this case study, the data has been slightly modified. The total caloric intake per capita per day has remained unchanged, such has the contribution of the various food groups to this energy demand. However, the composition within a food group has changed. The contribution of products that are not included in this case study is divided pro rata among the products within this group that are included. Information about future dietary patterns comes from projections made by the Potsdam Institute for Climate Impact Research (PIK) [Bodirsky et al., 2015]. Projections are given for the daily caloric intake and the fraction derived from animal products for various SRES (Special Report on Emission Scenarios). The definitions used in their methodology corresponds to those of FAOSTAT. The data used belongs to the SRES B1 scenario. This dataset was used because SRES B1 matches best with RCP 4.5 [Wayne, 2013], which was used to

determine future climate forcing. The historical energy ratios between products are maintained within the vegetable and animal parts of the future diet. In the case of South Sudan, the product ratio is based on the historical diet in Sudan. A mean caloric value for each products is computed from data in the FAOSTAT food balance sheets. Missing numbers are supplemented with data from Feedipedia [2017] and US Department of Agriculture [2019]. Figures on population size, required to compute the national energy demand, are obtained from UNdata [UNdata]. Data on food losses is per food group derived from the FAOSTAT food balance sheets and supplemented with data from Gustavsson et al. [2011].

The feed basket composition for Ethiopia and Sudan is respectively obtained from ECSA [2015] and Hmdan [2015]. Renard [1997] presents the Egyptian feed basket fractions for pasture, cereals, and a combination of forage crops and by-products. The latter is split into a fraction for forage and a fraction for by-products using the annual Egyptian forage production mentioned by Muhammad et al. [2014], the animal production obtained from FAOSTAT and the feed conversion ratios for a mixed livestock system mentioned by Mekonnen and Hoekstra [2010]. Driven by the absence of specific numbers, the same composition is used in the future experiments. The compositions in Sudan and South Sudan are therefore identical. Feed conversion efficiencies are adopted from Mekonnen and Hoekstra [2010]. This study makes a distinction between livestock conversion efficiencies in North and Sub Saharian Africa. For all countries, both in the historic and future experiments, a conversion efficiency for a mixed livestock system is adopted.

Processing capacities, expressed in production quantities, are based on data from the FAOSTAT food balance sheets. The historical production data shows great inter-annual variability and missing data for some products and is not directly suitable to describe the capacity. Therefore, instead of actual production, capacity is described by the growing linear function, which at any time is greater than or equal to actual production and has the smallest RMSE relative to actual production (see Appendix A.4.1). Future processing capacities are computed by scaling the historic capacities with the population ratio halfway the experimental timelines (2000 and 2030).

The maximum storage capacities are estimated from the change in product storage mentioned in the FAOSTAT food balance. The storage capacity is defined as the maximum difference within the cumulative sum of the change in storage between the start year of the food balances (1961) and the last year of the historical experiment (2010) (see Appendix A.4.2). This is by definition an underestimate of the real capacities, but currently the best estimate possible. The disadvantage of this method, however, is that only a single storage capacity can be determined. Hence, storage capacities are not specified over time. The future storage capacities are, just like the processing capacities, computed by scaling the historic capacities with the population ratio halfway the experimental timelines.

The trade distance is defined as the geographical distance between the national centres of population. The latter mentioned locations are derived from population density maps obtained from WorldPop [Tatem, 2017]. The transport distance with the external world is set at 5000 km. Because products come from all over the world, determining a single distance for the external world is of course a simplification with extensive effect in the model. Because much of the historical import comes from South America and Russia [FAO, 2017], a distance of 5000 km has been used. This distance is actually larger than the greatest distance in the region (2500km between Egypt and Ethiopia), but smaller than the actual distance to the aforementioned regions. The latter is done to compensate for the transportation method with the external world. The product transport in the region is namely said to take place by truck with a fixed rate of $0.038 per kilometer per ton [FTA, 2014].

3.3.5. Energy system

The energy demand, the national energy losses and the installed generation capacity originate from the sources described in Section 2.1.5. When the projections do not reach till 2040, they are linear extrapolated in time. Fuel conversion efficiencies and fuel combustion heats are obtained from the US Energy Information Administration. All plants have a load factor of 0.8, corresponding with the load factors of the hydropower plants as described by van der Krogt and Ogink [2013]. Capacities factors for the renewable plants are adopted from MoWE [2012]

The optimistic planning from the master plan presented in 2011 is adopted for the desciption of the international transmission lines. The lengths of the connections lines correspond with the trade distances mentioned in the food system. For these lines, a loss factor of 0.08% per 100 kilometers is used [EPRI, 2005]. Based on the current trade between Ethiopia, Sudan en Djibouti, a load factor of 0.4 is implemented for the international transmission lines.

3.3.6. Economics

Annual product and fuel trade prices are obtained from the World Bank Commodity Price Data [WB, 2020], the IMF primary commodity database [IMF, 2020] and the Food Price Monitoring and Analyses database of the FAO [FAO and FPMA, 2015]. The prices of crops missing in these databases are computed from the FAOSTAT trade matrix. Missing years have been filled by indexing the prices of other products in the same food group. Because only the price of alfalfa is found in the forage product group, the price of other forage crops are set by scaling the aforementioned with the dry mass ratios. As a result, all forage crops are in economic terms equivalent for animal feed. Electricity trade tariffs are based on the ongoing trade between Ethiopia, Sudan and Djibouti and are set at a fixed rate of $58.3 per MWh [Addis fortune, 2018]. The same economic time series were used for the future as for the historical experiments.

Fixed costs are not relevant since the operation of the infrastructure is studied and not the construction itself. Due to a lack of data, the variable costs for fertilizer, seeds and food processing have not been added. It is assumed that these prices do not significant alter the cropping patterns and processed quantities. Labor costs are left out of the optimization because, for the vast majority of the population, there are currently no direct alternatives to agriculture, and hence no opportunity costs. The variable costs for electricity production are included. These operational and mangement costs for the electricity plants are adopted from EAPP [2014].

3.4. Simulation experiments

Simulation experiments are performed over two time periods with a duration of 20 years. The first experiment runs over the historical period between 1990 and 2010. Because South Sudan became independent in 2011, three countries are included in this experiment. The independency of Eritrea in the early 1990s is not included. The second experiment runs over the future period between 2020 and 2040. All experiments were run with an optimization horizon of 3 years and a monthly time step. The monthly time step has been used because most of the collected data is available on this time scale. The optimization horizon of 3 years is the minimum time required to ensure that the planting and harvesting of some perennial crops takes place within the same optimization. A longer period has not been chosen for now because of the non-linear paired growth in the required computational time. In addition, all experiments have a per product defined diet ($s_{\text{diet}} = \textit{product}$) and the future experiments follow projections for medium population growth ($s_{\text{population}} = \textit{medium}$).

All MPC simulation experiments require a minimal water storage at the end of the optimization horizon. Because the required rule curves are not available, there has been a single optimization both historically and for the future with a horizon of 20 years with all infrastructures characteristic for this period, and the soft constraint to compute the optimal annual reservoir cyclicality active ($s_{\text{cyc}} = \textit{on}$). In the historical scenario, the model was able to converge and thereby generate a result for the optimal cyclic reservoir levels. The reservoir levels found are not discussed in further detail, but can be found in Appendix C.4. In the future scenario, the model was unable to come to a solution in a week time, and hence the optimization was aborted. The constraint on the storage in the last time step

in therefore inactive, allowing the optimizer to completely empty the reservoir at the end of the horizon.

The same experiments were run in both time periods with a few minor exceptions. This primarily concerns the four basic cooperation scenarios: unilateral, flow-information, trade-information and regional coordination. No additional constraint and settings for international cooperation ($s_{\text{agree}} = \textit{off}$), minimum income ($s_{\text{income}} = \textit{off}$), self-suffciency ($s_{\text{self-suff}} = \textit{off}$) or climate forcing ($s_{\text{forcing}} = \textit{perfect}$) were used. In the trade-information scenario, information is only exchanged regarding the expected product exports and electricity shortages in the first time step. An increase in the trading period requires an increase in the number of iterations in the market process and therefore an increase in the (already considerable) computational time. One difference between the historical and future scenario is found in the implementation of the outside and the rainfed agriculture. In the historical scenario, the rainfed and outside agriculture area are prescribed ($s_{\text{other-agri}} = \textit{off}$), while in the future scenarios these are included in the optimization ($s_{\text{other-agri}} = \textit{on}$). This fixed historical implementation was chosen to enable some form of comparative research with the real world practices.

In addition to these four basic scenarios, a number of special scenarios have been run. First of all, the same four cooperation scenarios were run with different settings for climate forcing. Instead of the perfect predictions, the optimization in these experiments is forced with data from half a decade earlier ($s_{\text{climate}} = \textit{imperfect}$). These experiments are used to determine the value of perfect predictions. The chosen five-year time period corresponds to the average repetition time of the El Nino oscillations [van Oldenborgh, 2002], the major climate driver in the region [Camberlin, 2009]. In addition, the first three cooperation scenarios were run with an additional constraint on the annual inflow in Egypt ($s_{\text{agree}} = \textit{on}$). According to the 1959 agreement, this must be 55 BCM per year. This constraint is irrelevant for the coordination scenario as it counteracts potential cooperation. The difference in net benefits between these experiments and the four basic experiments shows the costs of this historical agreement.

The last two sets of simulation experiments are used to study agricultural self-sufficiency and the trade-offs between hydropower and agricultural water use. For both comparisons, only the two most extreme cooperation scenarios (unliteral and regional coordination) are used. For the self-sufficiency study, the unilateral scenario studies the national self-sufficiency ($s_{\text{self-suff}} = \textit{national}$) and the coordination scenario the regional self-sufficiency ($s_{\text{self-suff}} = \textit{regional}$). Both scenarios are run six times, with the target level of the soft constraint growing in equal steps from 0% to 100%. To study the trade-offs between hydropower and agricultural water consumption, the price of electricity shortage is varied in both scenarios. In addition to the standard scenario with a shortage cost of $400 per MWh, scenarios have been run with values of $60, $180, $700, $1000, $1700, $3000 and $5000 per MWh. The minimum value of $60 just exceeds the price of international electricity tradings.

3.4.1. Experimental settings

The optimization convergence settings, the costs of soft constraints and several factors used in the simulation experiments are based on exploring model runs. For the factors, it is determined which values are required to make the system feasible. Using this approach, a value of 0.1 is determined for the hedge factor f_{hedge} to ensure sufficient water in storage for unexpected climate variations. The values for the convergence settings and the penalty costs are based on the outcomes, the degree of convergence and the time required of these exploring studies. Other convergence settings are used for the historical and future simulation experiment. The constraint violation and dual infeasibility tolerance remain unchanged, but the overall tolerance is increased in the future scenario. An overview of the convergence settings and the penalty costs used can be found in Appendix B.5.

Each MPC step has been assigned a maximum number of optimization iterations and a maximum CPU time. Initially, each optimization is semi-warm started, using the results of the 2nd till 36th month of the previous optimization as the starting values for the optimization variables. If a solution cannot be found within the available time and iterations, the optimization is restarted with other initial values for the optimization variables.

4 Results

In this section, the results of the model experiments are discussed. First the observations for the historic experiments are elaborated. This will show that an unilateral approach is already benefical compared with real world practices. However, the differences in water productivity (expressed in dollars per cubic meter) between the riparian states are significant in this scenario. All following cooperation scenarios results in more economic benefits for the riparian states. The largest economic contribution, espacially in Sudan, is achieved by sharing flow information. Under regional coordination, these benefits are further expanded by a specialization in agriculture, an increase in regional trade and an enhanced resilience against droughts. This form of cooperation results in a clear redistribution of resources towards the efficient agriculture in Egypt. The discussion of the historic results are followed by an elaboration of the future simulation results. These results indicate a turnaround in economic benefits for a unilateral approach, whereby Egypt depends heavily on food imports and South Sudan and Ethiopia flourish. However, the reliability of the results of this and all subsequent scenarios will appear to be questionable.

4.1. Historic experiments

This section presents the results of the historical model experiments. First, a validation of the balance sheets is presented. Afterwards, the results of the unilateral scenario are compared with historic data. For this, the trade flows are compared with data from the FAOSTAT database, and the river discharges with data obtained from the Sudanese Ministry of Irrigation and Water Resources. The various cooperation scenarios are then compared. First at a high level, later in more detail. Finally, the outcomes of the model experiments concerning the self-sufficiency, the hydropower-agricultural water trade-off and the imperfect foresight are presented.

4.1.1. Balance validation

Closed balances are crucial for the validity of the presented WEF model. In the following sections, therefore, a graphical representation of (the balance between) the production and consumption fluxes within the water, food and energy balance is presented for the unilateral model experiment over the complete experimental runtime.

4.1.1.1. Water balance

The inflow of the national water balance consists of source flows (possibly originating from upstream countries) and additional supplies through runoff in the irrigated agriculture and precipitation on the reservoir surface. The outflow consists of evaporation losses in river and reservoirs, cross-border river flows and agricultural withdrawals. Depending on the sign, the change in storage in the river and reservoirs is considered an inflow (decrease in storage) or outflow (increase in storage). The graphs in Figure 4.1 show that the inflow equals the outflow and hence the balance is closed, for all three riparian states. Moreover, this presentation of the balances indicates that the water consumption, both through losses and for agricultural abstraction, accounts for an increasingly larger fraction of the available flow in downstream direction. In Ethiopia in particular, due to the absence of water infrastructure, consumption is small and the inflow is almost equal to the outflow. Besides the validation of the water balance, Figure 4.1 also clearly shows the significance of the evaporation in the wetlands in southern Sudan and the minimal outflow into the Mediterranean sea.

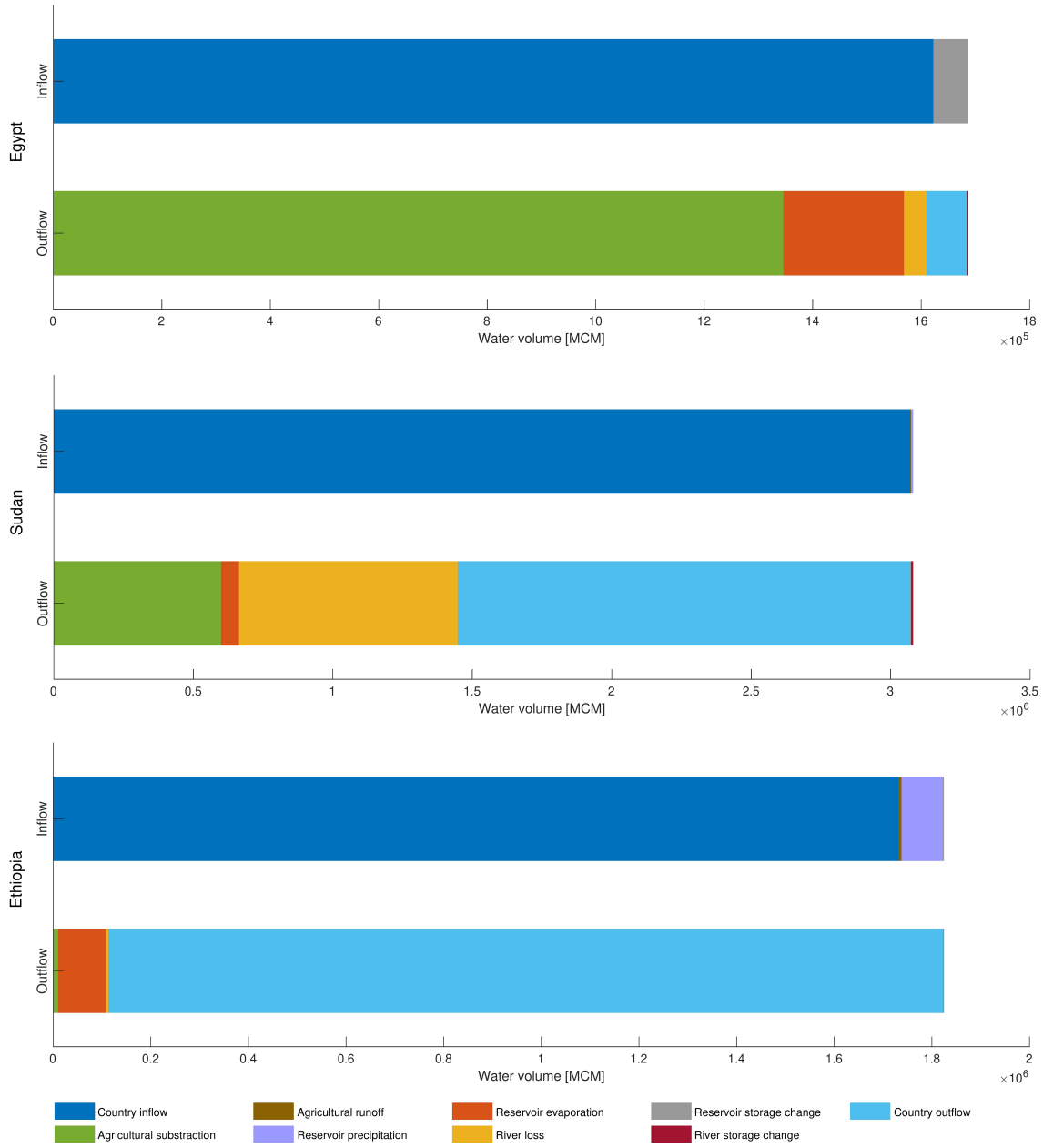

Figure 4.1: The cumulative inflowing and outflowing water fluxes over the entire experimental runtime, subdivided into source flows, agricultural runoff, reservoir precipitation and evaporation, river losses, cross border river flows, agricultural withdrawals and storage changes.

4.1.1.2. Food balance

The product balances in Figure 4.2 illustrate the cumulative production and consumption fluxes of all included products for the three riparian Eastern Nile states. The production side of the balance consists of both irrigated and rainfed agricultural production, product conversion and import. The consumption side consists of food, feed and process consumption, export and storage and transportation losses. Since the store is initially empty, any change in the final store is considered a consumption flux.

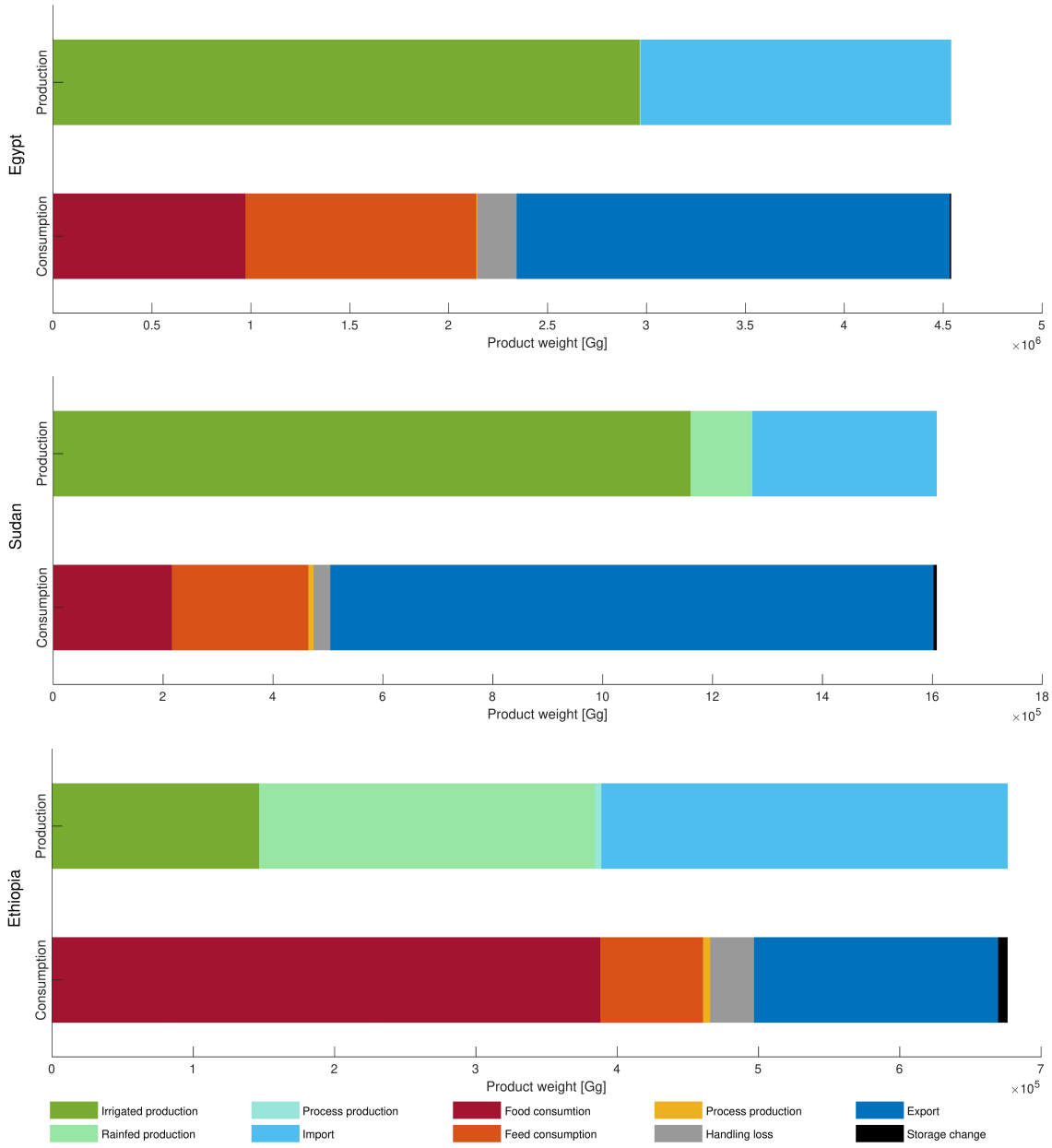

Figure 4.2: The cumulative production and consumption fluxes of all included (food)product over the complete experimental runtime, subdivided into rainfed and irrigated agricultural yield, product conversion, trade flows, losses, food and feed consumption, and storage changes.

4.1.1.3. Electricity balance

Finally, in Figure 4.3 the electricity production is plotted against the electricity consumption. Again, it is a representation of the cumulative production and consumption over the entire experimental period. The production side of the balance consists of hydropower, renewable and fuel generation and regional import. The consummption is supplemented with regional exports, national and international transmission losses and production surplus. From this figure it follows that, following the water and food balance, the electricity balance is closed as well.

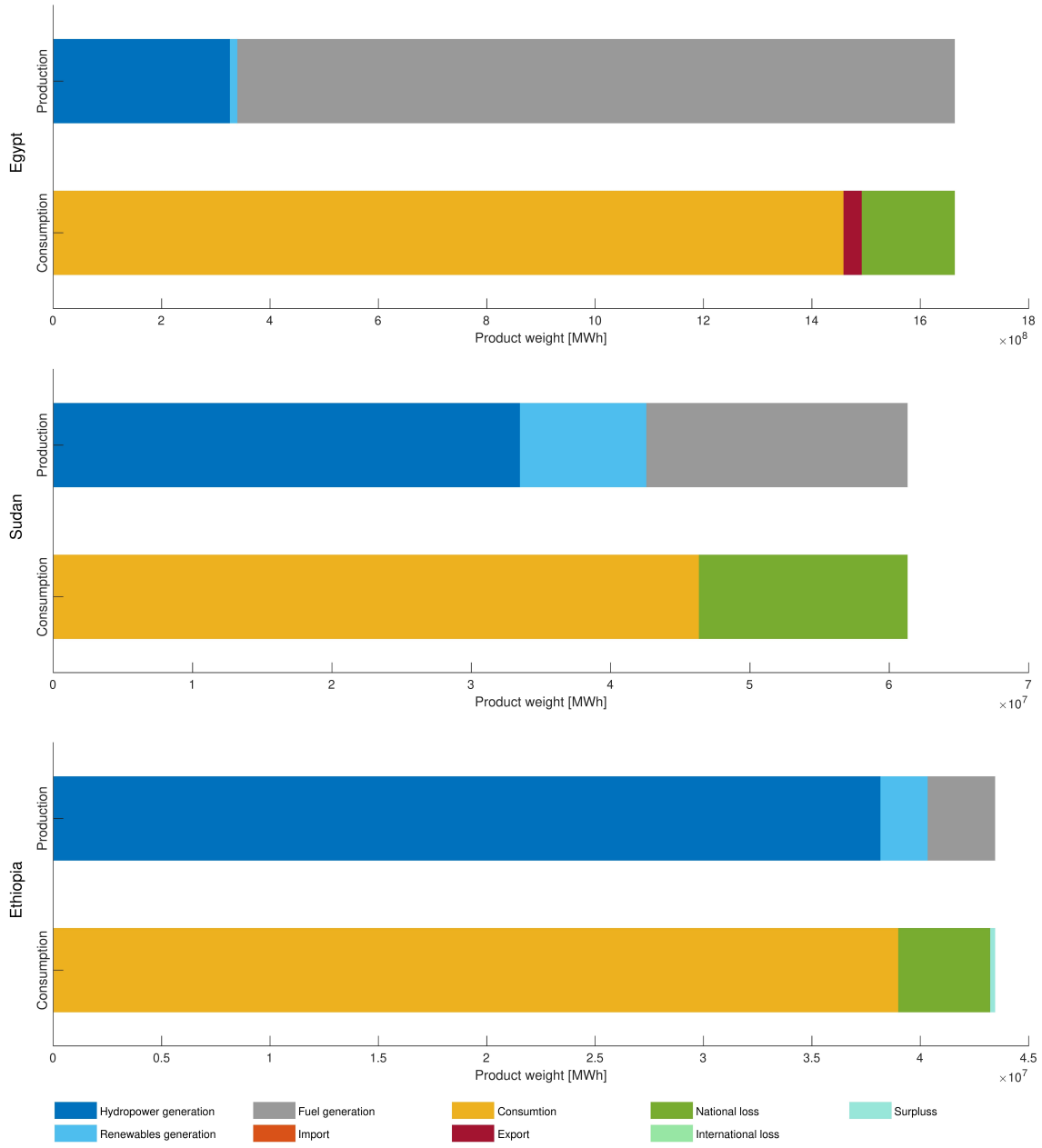

Figure 4.3: The cumulative generation and consumption electricity fluxes over the entire experimental runtime, subdivided into hydropower, renewable and fuel generation, consumption, trade flows, national and international transmission losses and production surplusses.

4.1.2. Compasrison with historic data

Before comparing the different cooperative scanarios, the unilateral scenario is first compared with the real world pratices. This comparison is not presented to validate the model, but to allow a comparison between the performance in the unilateral scenario and real world practices. After all, the results of an optimization cannot be validated against the performance of the non-optimized system. First, the modelled border flows are compared with river flows obtained from the Sudanese Ministry for Irrigation and Water Resources. Subsequently, the trade data is compared with FAOSTAT trade data.

4.1.2.1. Sudanese discharge data

In Figure 4.4 are the modelled transboundary river flows plotted against discharge data obtained from the Sudanese Ministry of Irrigation and Water Resource. Until 2002, both the monthly (which is not shown to prevent possible reproduction of data) and annual modelled hydrographs at the Ethiopian border (Diem) correspond largely to the received data. After 2002 larger deviations arise. These arise because the used discharge data of the RIBASIM model is no longer available after 2002. The discharge series from the RIBASIM model has therefore been extended with a least square method based on precipitation and evaporation (see Section 3.3), which results in incorrect discharge series. Due to the limited river infrastructure and the associated optimization choices in Ethiopia, it can be concluded that the inflow data used is valid.

For the border flow between Sudan and Egypt (Dongola), the annual data also corresponds in pattern and magnitude up to 2002. However, the deviations between both hydrographs are larger, which logically follows from the increase in possibilities for water use in agriculture, storage and evaporation in Sudan and the uncertainty in the representation of the river flow and losses. It is striking that the modeled discharge in the Eastern Nile RIBASM model, which is also shown in the figure, is almost continuously 20 BCM larger. Although the flows correspond quite well, this graph cannot be used to conclude that all river processes are properly represented in the model. After all, a false exchange can take place between agricultural withdrawals and river losses. The monthly data shows that the peak discharge is delayed a little too much. This is caused by the constant river flow velocity of 1 m/s, which is an underestimate at during peak discharge.

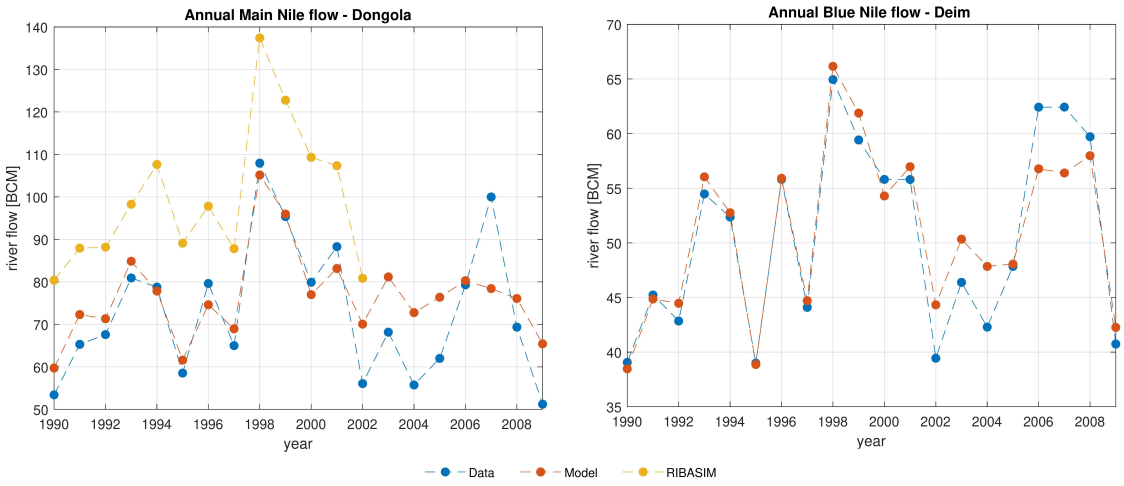

Figure 4.4: Annual cross border flow. A comparison between the modelled data in the unilateral simulation experiment and the data from the Sudanese Ministry of Irrigation and Water Resources at Diem and Dongola.

4.1.2.2. FAOSTAT trade data

For this comparison, the modelled import and export product values are compared with data obtained from the FAOSTAT database. Figure 4.5 shows the import costs and the export incomes for each riparian state during the period of the historical simulation experiment (1990-2010). For all riparian states, the import value originating from the model is over the entire duration of the experiment larger than the import value obtained from the FAOSTAT database. Although the absolute numbers do no match, the growth patterns of the import value do show a great similarity. The export values that follow from the model are as well larger than the export values in the database. However, the modeled export values show much greater variability and the patterns do not show any kind of resemblance. In addition to the values of the import and export fluxes, Figure 4.5 also illustrates the net economic result of these fluxes. It is striking that the sign of the net income in the model results and the FAOSTAT data do not match. According to the model, Egypt and Sudan can be net product exporters, while according to the data they were net importers over this historical period. For Ethiopia a reverse observation applies, where the model labels the country as an importing state, while the export dominates in the data.

The observation that Egypt and Sudan are net product exporters in the unilateral cooperation scenario, while they were net importers in the past, indicates that the available land and water resources can be used more effectively and/or more efficiently when regulated by national policies. Despite the opposite results, Ethiopia forms no exception to this observation. Ethiopia has namely been a major recipient (billions) of food aid [Trading economics, 2020]. Because this product flux is not included in the model, it results in an increase of imports, causing the income balance to become negative.

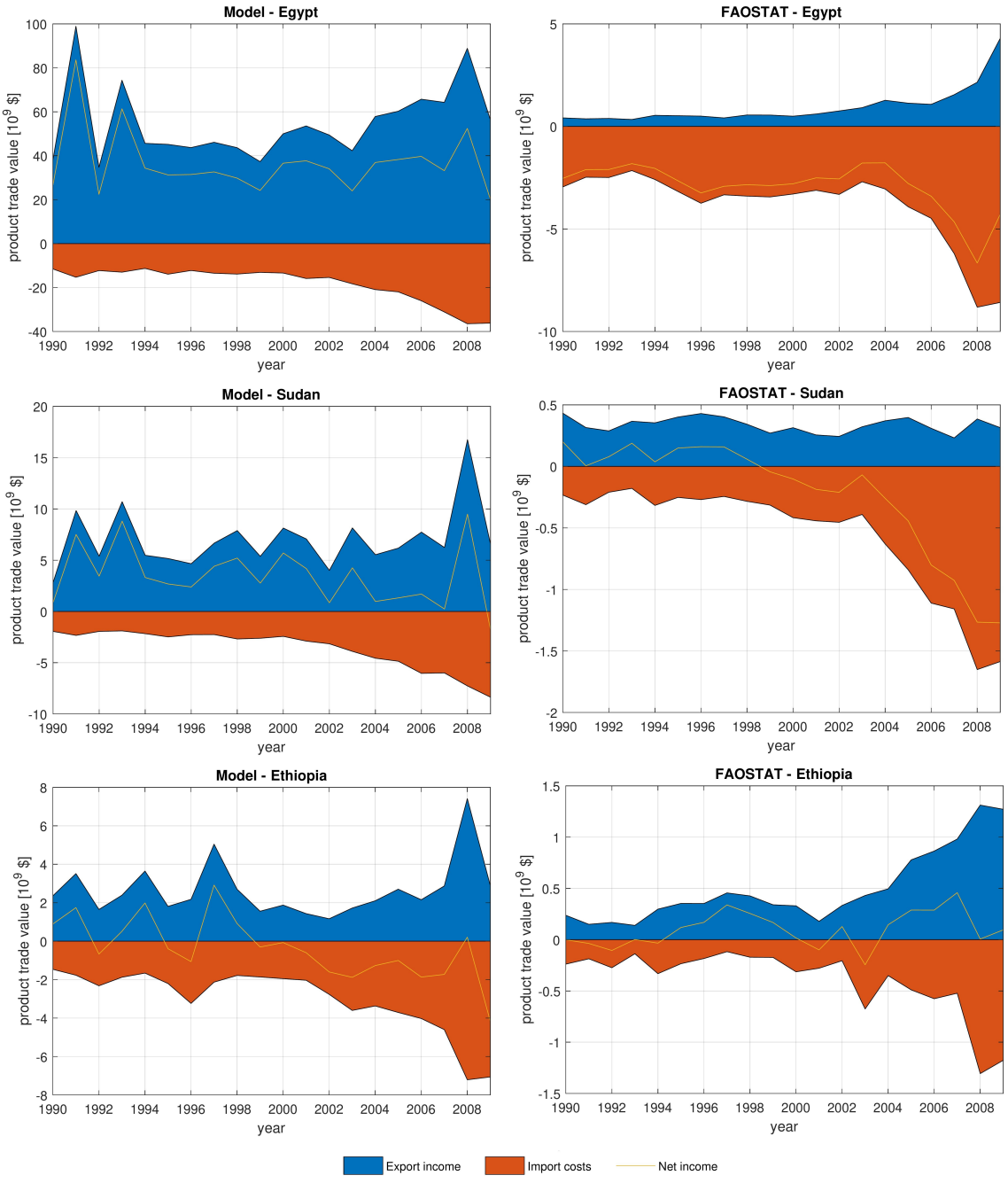

Figure 4.5: The export income and import costs for Egypt, Sudan and Ethiopia over the historical period from 1990 to 2009. The left figures show the results of the model and the right figures the data from FAOSTAT. In addition to the import and export values, the net income is indicates by the orange line.

4.1.3. Cooperation trends and observations

In this subsection, the four cooperation scenarios are compared. First of all, this is done by studying the total revenues and expenses over the model period. Afterwards, a more detailed analyses should provide some background to observed differences. To this end, the changes in the water, food and energy balance are subsequently studied.

The net income over the modeled period (1990-2009), defined as the difference between the export incomes and the import and production costs, is illustrated for the unilateral cooperation scenario in Figure 4.6. In the unilateral scenario, Sudan and Egypt are able to export more value in food and electricity than they import. Because the fixed costs and some variable costs for production have not been included, it cannot be stated with certainty whether the food and energy sector could indeed have been profitable. Ethiopa appears to be unable to use the available agricultural sites and electricity infrastructure in favor of the national treasury.

In addition to net income in the unilateral scenario, Figure 4.6 also illustrates the percentage increase in net income in the other cooperation scenarios relative to the unilateral case. The sharing of discharge information in the flow-information scenario does not affect the net income in Ethiopia, which can be explained given its upstream location. However, this scenario clearly indicates that Sudan can benefit significantly if Ethiopia shares information about the expected outflow. This information is less valuable for Egypt, possibly because of the buffering effect of Lake Nassar. If, in addition to information about the expected flow, information is also shared about the expected product exports and electricity shortages, a further increase in the incomes for Egypt and Sudan is observed. In Ethiopia, the sharing of this kind of information does not result in additional income. The coordination scenario shows that every riparian state benefits from a regional planning. Moreover, a redistribution of revenues is observed. Egypt's revenues will further increase relative to the trade-information scenario, at the expense of the additional revenues in Sudan.

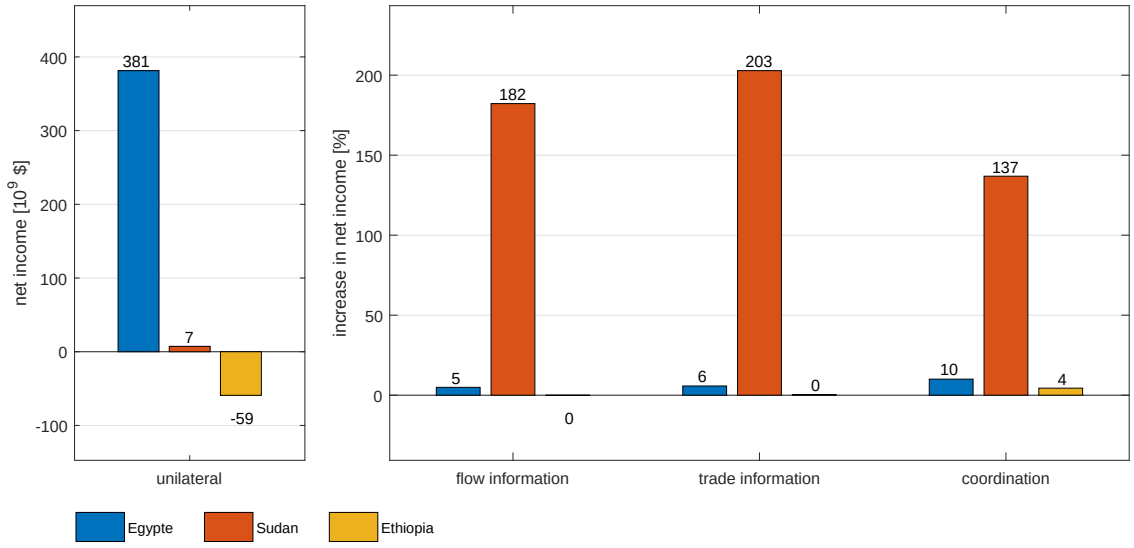

Figure 4.6: The net income over the modelled period between 1990 and 2009 for the unilateral cooperation scenario and the percentage increase in net income in the other scenarios with respect to the unilateral scenario.

In addition to the absolute changes in net income, there are changes in the composition of incomes and expenditures as well. Figure 4.7 illustrates the change in the incoming and outgoing cash flows for the flow-information, trade-information and coordination scenario compared to the unilateral scenario. For the flow-information scenario, the total change in Ethiopia, which is close to zero according to Figure 4.7, is due to an increase in transport costs. As trade in this scenario takes in principle only place with the external world, and this external trade is converted into regional trade only when another country in the region trades the same product in the opposite direction, this indicates that Sudan and/or Egypt

has a different export policy causing that a product which was initially purchased regionally now must now be bought internationally. This observation is confirmed by the changing cash flows in Sudan and Egypt in the flow-information scenario. For Sudan, revenues from exports increase and less money is spent on the import of products and the associated transport. This indicates that by sharing discharge information higher agricultural production quantities are enabled in Sudan. Since exports increase more than imports decrease, it can be said that the increased agricultural yield mainly concerns products that are not intended for the national consumption. The changes in the energy sector are negligibly small. An increase in exports is also visible in Egypt. As this increase in exports is accompanied by an increase in imports, further specialization seems to be occurring in Egypt. In addition, there is a small increase in variable costs for electricity production, which indicates a shift from hydropower to fossil generation.

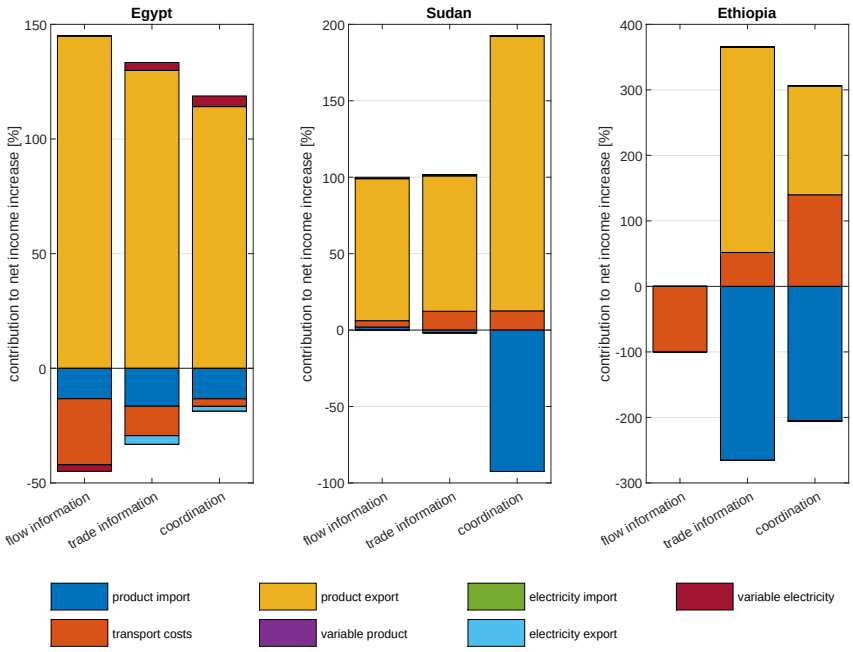

Figure 4.7: Changes in the composition of net income for flow information, trade information and coordination compared to the unilateral scenario. For the outgoing economic flows (import costs and variable costs) represent a positive change a decrease in expenses and a negative change an increase in expenses. This applies the other way around for incoming cash flows (export income), where a positive change represents an increase in income.

In the trade information scenario, according to Figure 4.6, the income in Ethiopia does not change. However, Figure 4.7 shows that there are changes in the composition of net income. Both import costs and export incomes increase, but the transport costs decrease. This contradiction in changes in import costs and transport costs can have two causes. Either more expensive products with a lower specific weight are imported, or there is an increase in regional trade. Since a similar trend is observed in the other riparian states, an increase in regional trade appears to be the most obvious explanation. Despite the fact that transport costs in Egypt are increasing compared to the unilateral scenario, the ratio of transport and import costs is decreasing compared to the flow information scenario. Besides these changes in food imports and exports, there is a decrease in electricity exports in Egypt, which is accompanied by a decrease in variable production costs. This seems to indicate that the fixed (long term contract) electricity export quantity set in advance is too optimistically.

Both this change in electricity trade and the change in transport costs seem to continue for Egypt into the coordination scenario. Although the percentage change in transport costs does not drop for Sudan, the absolute values do. After all, transport costs continue to fall compared to the unilateral scenario, despite a clear increase in imports. The increasing export, which is accompanied by this increasing import, is an indication of further specialization in the country.

4.1.3.1. Water balance

The outflow to a downstream country is a first indication of the water consumption per state. Figure 4.8 illustrates the border flow between Sudan and Egypt and Ethiopia and Sudan for the four cooperation scenarios. The horizontal black dashed line in the left figure represent the required border flow according to the historic flow agreement of 1959. It is clear that the inflow in Egypt exceeds the required 55.5 BCM per year in all scenarios.

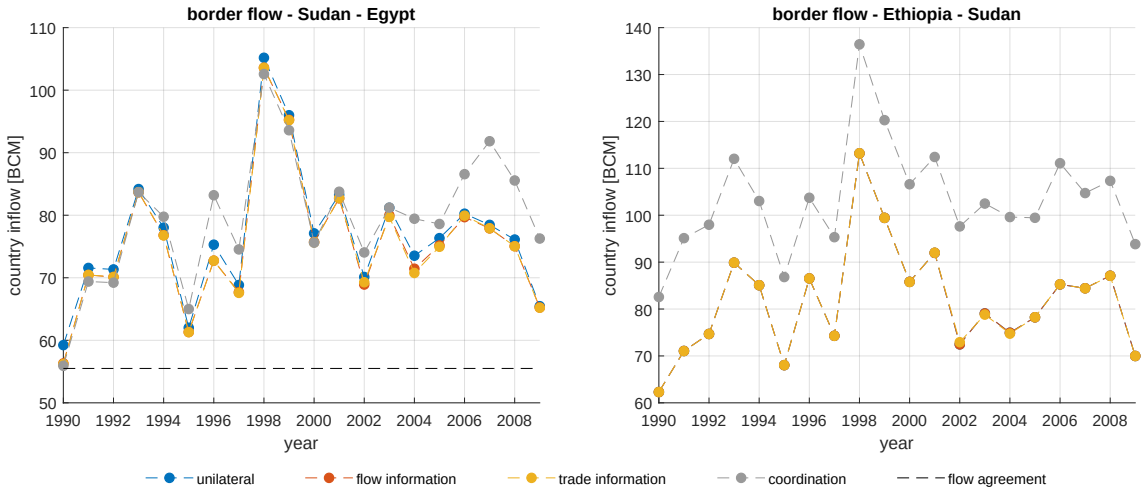

Figure 4.8: Left) the inflow into Egypt from Sudan for the four cooperative scenarios in the historic model period. The black dashed line represents the required border flow according to the 1959 histric flow agreement. Right) the flow from Ethiopia to Sudan.

The border flow between Ethiopia and Sudan shows no difference between the first three scenarios. In the cooperation scenario, on the other hand, the flow between Ethiopia and Sudan increases by about 1 to 2 BCM per year. Since evaporation in the reservoirs and Lake Tane in Ethiopia shows almost no variation between the scenarios (see Figure 4.9), this increase in border flow indicates a reduction in water consumption for agriculture in Ethiopia in a regionally coordinated system. The outflow from Sudan to Egypt does show small differences between the first three scenarios. Over the entire period, a slight decrease is visible for the flow-information and trade-information scenario compared to the unilateral scenario. Since evaporation does not seem to change substantially in Sudan either (see Figure 4.9), this reduced border flow indicates an increase in agricultural water consumption in Sudan, which is in line with the increasing exports.

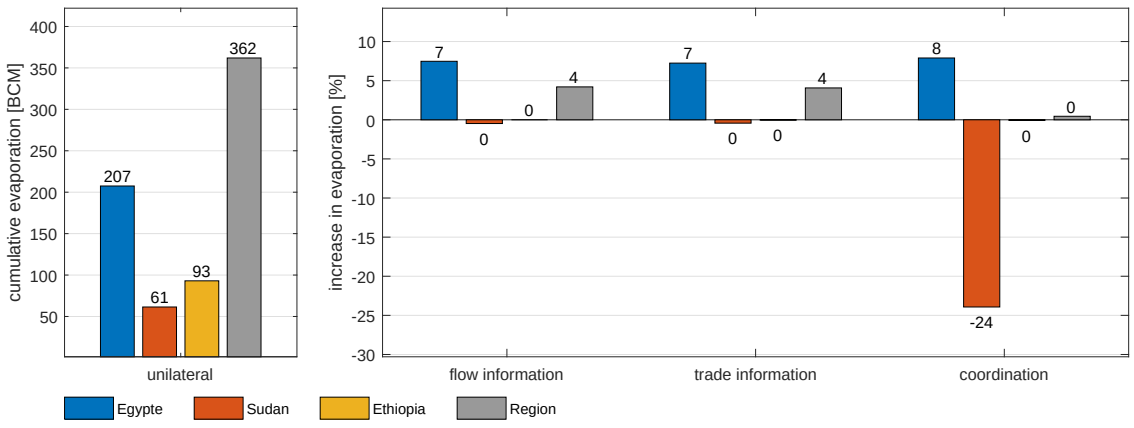

Figure 4.9: Cumulative reservoir evaporation in the unilatal scenario over the historic model timeline, and the change in the other cooperation scenarios.

In the coordination scenario, the annual border flow follows a completely different pattern. Although the inflow into Egypt is smaller during some years than in the trade-information scenario, the resulting inflow over the entire period increased. This changing flow pattern, together with the sharp decrease in evaporation in Sudan, indicates a change in water consumption patterns.

It can be deduced from the reservoir evaporation in Egypt that the storage in the lake Nasser behind the Aswan High Dam increases under all cooperation scenarios compared to the unilateral scenario. Because this increase is accompanied by a decreasing influx in the flow-information and trade-information scenario, this indicates a decrease in the downstream water demand. In the cooperation scenario, the demand for water downstream appears to be increasing. After all, the evaporation losses remain the same compared to the information sharing scenarios, while the inflow increases.

Figure 4.10 shows that the cooperation scenarios have an impact on the amounts of water stored in the surface water reservoirs. It is clearly visible that with a more extensive form of cooperation, more water is retained in the reservoirs. The influence of this collaboration is particularly noticeable in the drier years. In the wet years around the turn of the century, the differences in storage are small, while in the drier years prior to the turn of the century and around 2005, the storage in the cooperation scenario is clearly larger. Figure 4.9 shows that in the flow- and trade-information scenario this increase in storage is accompanied by an increase in regional evaporation compared to the unilateral scenario, while in a regionally coordinated system the evaporation remains the same despite the increase in storage. The latter indicates a redistribution of the water over the available reservoirs.

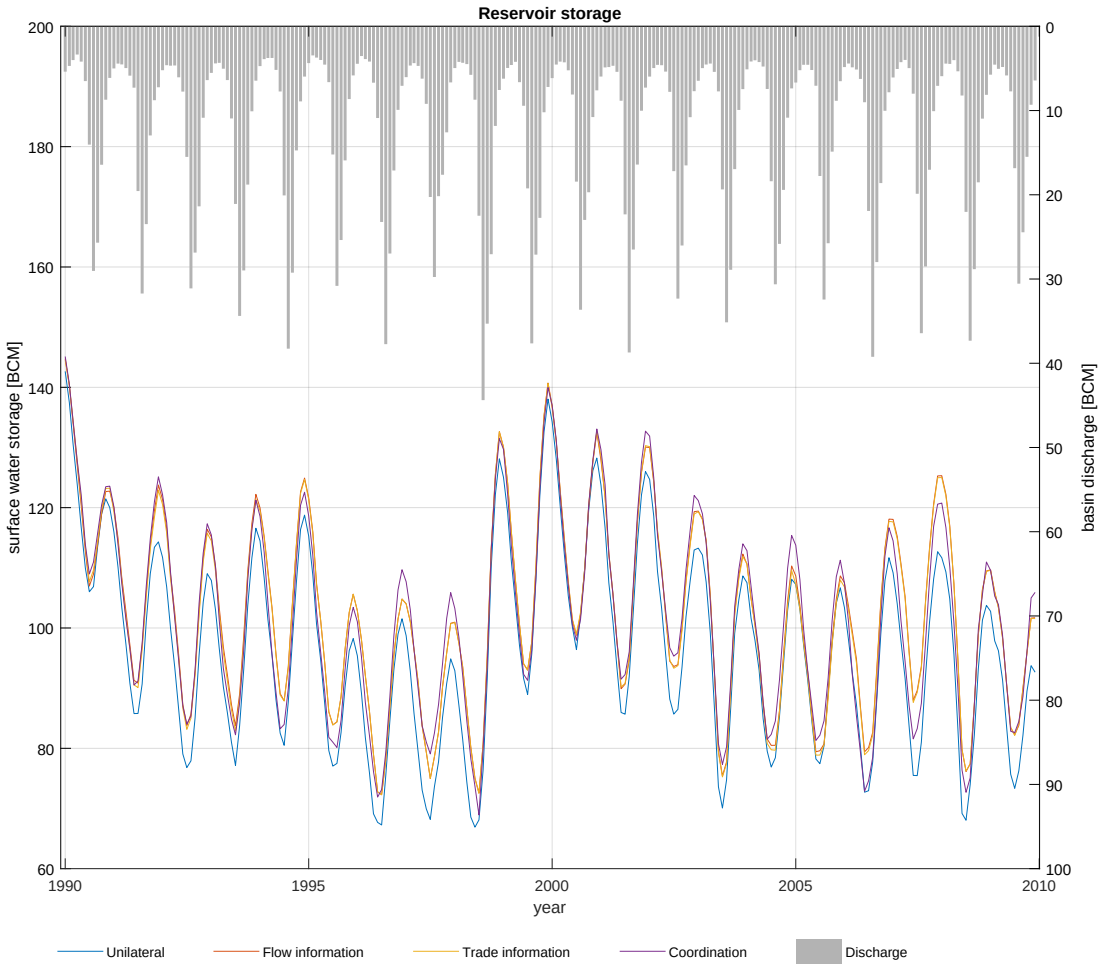

Figure 4.10: Cumulative reservoir storage in the Eastern Nile over the historic model period for all four cooperation scenarios. The bars on top illustrate the cumulative inflow in the Eastern Nile during a specific month.

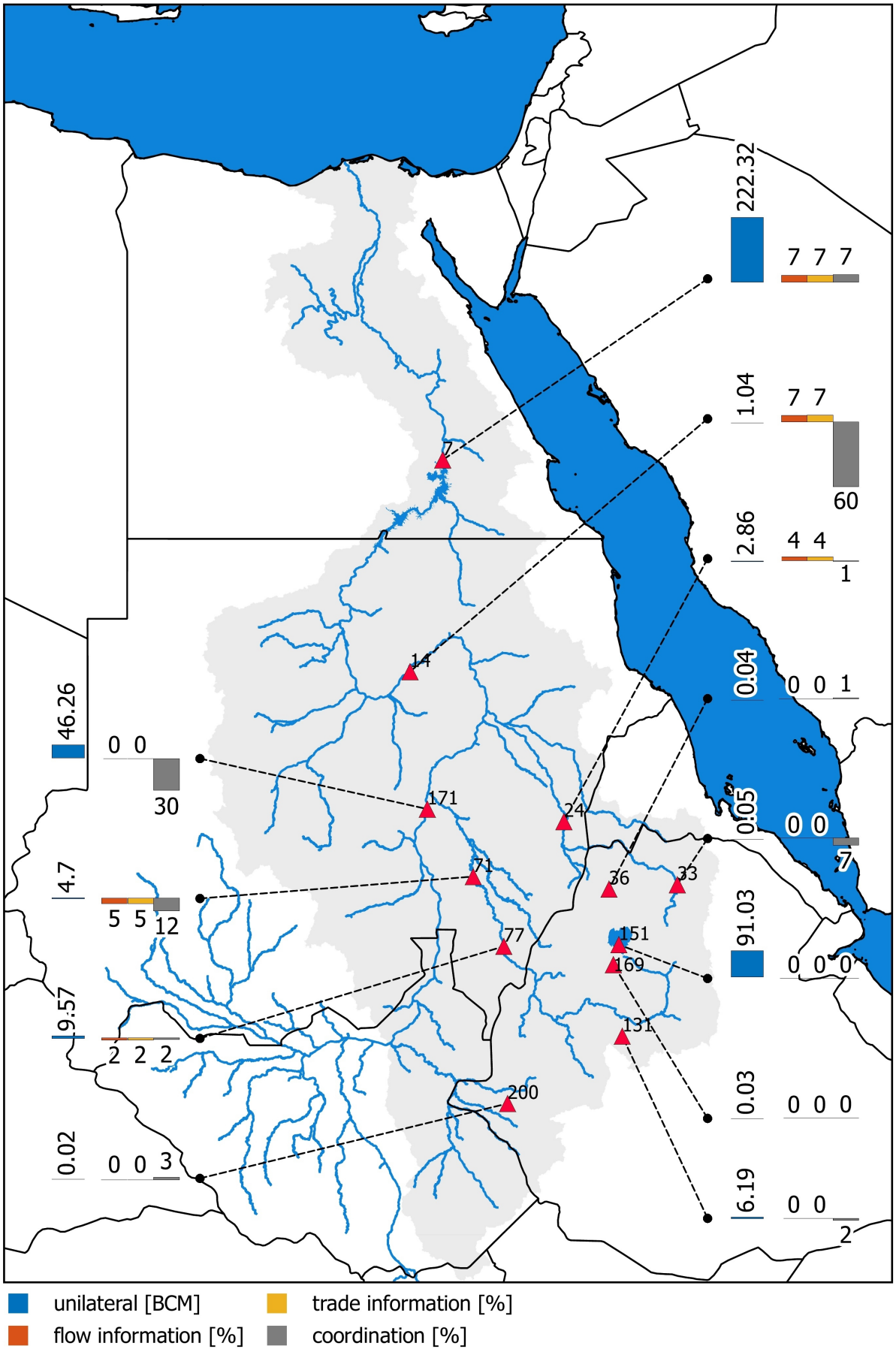

Figure 4.11: Cumulative evaporation (BCM) in all reservoirs in the Eastern Nile during the historic model period, and the percentage changes in the other cooperation scenarios with respect to the unilateral scenario.

For a better understanding of a possible redistribution in reservoir storage between the scenarios, Figure 4.11 illustrates spatially the percentage change in evaporation with respect to the unilateral scenario for each reservoir active during the historical experimental period. In Ethiopia, the differences in evaporative losses are small, indicating minimal changes in storage. Only in the cooperation scenario is slightly less water stored behind the Tekeze (node 33) and Fincha'a dam (node 131), and slightly more in the Abobo reservoir (node 200).

In Sudan, the total evaporation remains the same in the flow- and trade-infromation scenario, but there is a clear change in the location of the evaporation. The evaporation losses in the Blue Nile reservoirs Roseires (node 77) and Sennar (node 71) are decreasing, at the expense of an increase from the Khasm El Girba reservoir (node 24). However, these differences are small compared to the differences that occur in the cooperation scenario. In this scenario, there is a reduction in evaporation and thus storage in all reservoirs in Sudan. The decrease in evaporation of the Jebel Aulia (node 171) and the Merowe dam (node 14) are particularly striking. Since the Merowe dam will only come online in 2009, the contribution of this reservoir to total evaporation is small. The sharp decrease, however, indicates that it is better to fill this reservoir slower or not at all in the regional coordinated system.

4.1.3.2. Food balance

The change in agricultural water use is confirmed by Figure 4.12. It is striking that the total consumption in Ethiopia is small compared to the other riparian states. However, this is explainable given the minimal land area suitable for irrigated agriculture within the Nile basin, the significant amounts of rain and the low potential evaporations.

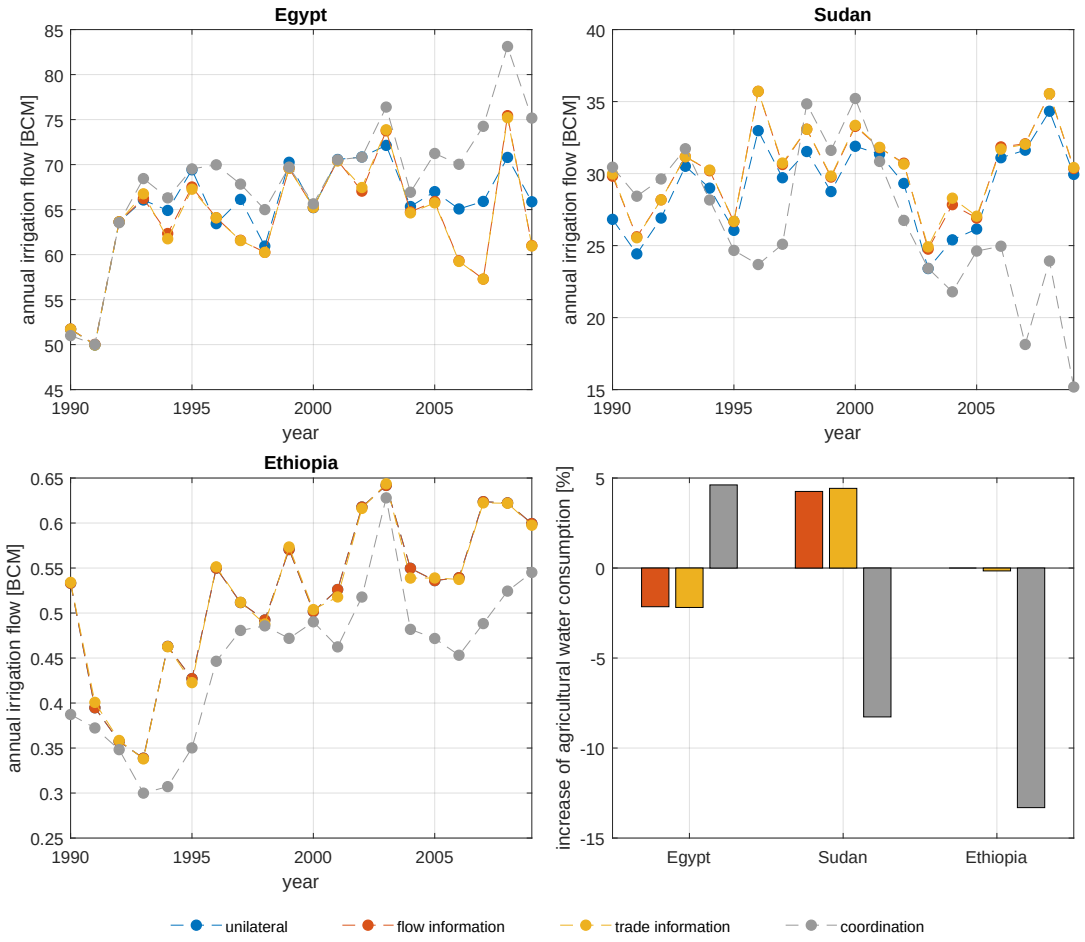

Figure 4.12: The annual agricultural water consumption per riparian state for all four cooperation scenarios, and the percentage change of the cumulative sum with respect to the unilateral scenario.

There is no change between the unilateral and flow-information scenario for Ethiopia, which can be explained given the upstream location. In the flow-information scenario in Sudan, the agricultural water consumption does indeed increase uniformly compared to the unilateral scenario. The latter is in line with the reduced outflow to Egypt and the increase in export earnings. Figure 4.13 shows that water consumption in Sudan is increasing mainly in the Blue Nile and Atbara, while the changes in the White Nile and Main Nile are small. From the fact that there is a sharp increase in water consumption all the way down in the Blue Nile, which is not at the expense of agriculture downstream in the main Nile, it can be deduced that in the unilateral scenario the planning assumes that there is not enough water to irrigate this field. That there is a specific choice not to irrigate this field is explained by the higher potential evaporation associated with its northern location. As the total amount of water entering the Sudanese Blue Nile does not change in the flow-information scenario compared to the unilateral scenario, the water is thus allocated more effectively. This is possible when less water is released from the Sennar and Rosieres dam, at times when it is not necessary for agriculture, to prevent an (incorrectly) expected overflow. In addition to the increase in allocated water in the Sudanese irrigation fields, the percentage of water allocated for deficit irrigation is decreasing, as shown in Figure 4.14. Since deficit irrigation is linked to reservoir hedging, where the actual reservoir outflow is less than the expected reservoir outflow, this indicates a decrease in (too) low reservoir levels. In Egypt, in line with the reduced influx and higher reservoir levels, water consumption for agriculture is decreasing. The deficit irrigation, which hardly occurs in the unilateral scenario, decreases by an insignificant amount in the delta.

In the trade-information scenario, minimal changes in total water consumption occur in all riparian states. The spatial distribution of the water, as well as the extent to which it is used for deficit irrigation, does not seem to change significantly. Although both the timing of water consumption and the spatial distribution hardly change in the trade-information scenario, since both import and export fluxes change (see Figure 4.7), it is used for other purposes.

Unlike between the first unilaterally directed senarios, there are significant changes in the water allocation in the coordination scenario. These changes and shifts in water consumption follow logically from the changed optimization objective. After all, certain management actions that are beneficial at a unilateral level do not need to be efficient from a regional perspective. In Egypt, despite the small percentage change, the already considerable water consumption is increasing sharply. The greatest increase occurs during the last years of the simulation experiment. In the Northern Nile Valley, this increase in water consumption in Egypt is accompanied by a 10% increase in land-use intensity (defined as the average utilization rate). Since the maximum occupation rate of this field is already 100% in both the coordination scenario and previous unilateral scenarios, this increase does not indicate a uniform increase in the unilaterally cultivated areas, but a significant change in crop composition. Since the potential yields in Egypt are large compared to other locations within the region, the growth stages are relatively short and the management losses are small, water allocation on the Egyptian irrigation fields is preferable over other locations from a regional perspective. It therefore appears to be advantageous to take the river losses for granted and, insofar as it is possible, to allow the production of water-intensive crops to take place in Egypt.

That such a redistribution of the water takes place is clear from the water consumption in Sudan. Where the allocation in Egypt has clearly increased in the last years of the experiment, it is decreasing sharply in Sudan. Figure 4.13 also shows clear greographic differences within Sudan. Although, with the exception of the Gezira irrigation scheme, water consumption decreases at all fields compared to the trade-information scenario, the strongest decreases occur in the irrigation sites along the main Nile (nodes 13, 16 and 41). These locations are not preferable for water intensive crops because of the high potential evaporation, the low management factors and the select group of crops that can grow here. The fact that the water allocation in the sites located along the White Nile, despite the relatively favorable climate conditions, is decreasing may be related to the influx required in Egypt during the dry season in the Ethiopian highlands.

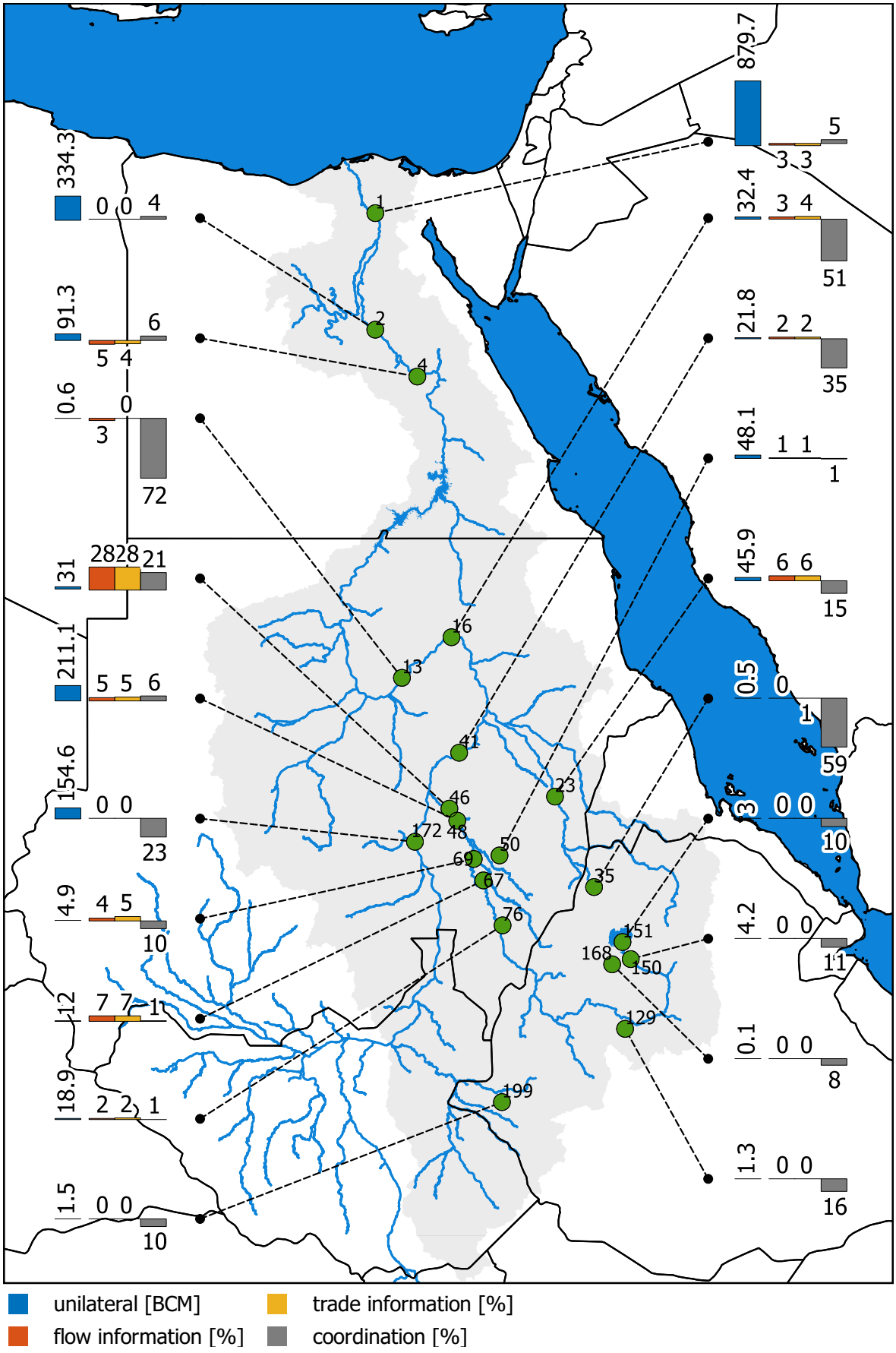

Figure 4.13: The agricultural water consumption (BCM) for all inddividual irrigation sites active during the historic simulation experiment. The orange, yellow and grey bar indictate the percentage change in the flow-inforamtion, trade-information and coordination scenario.

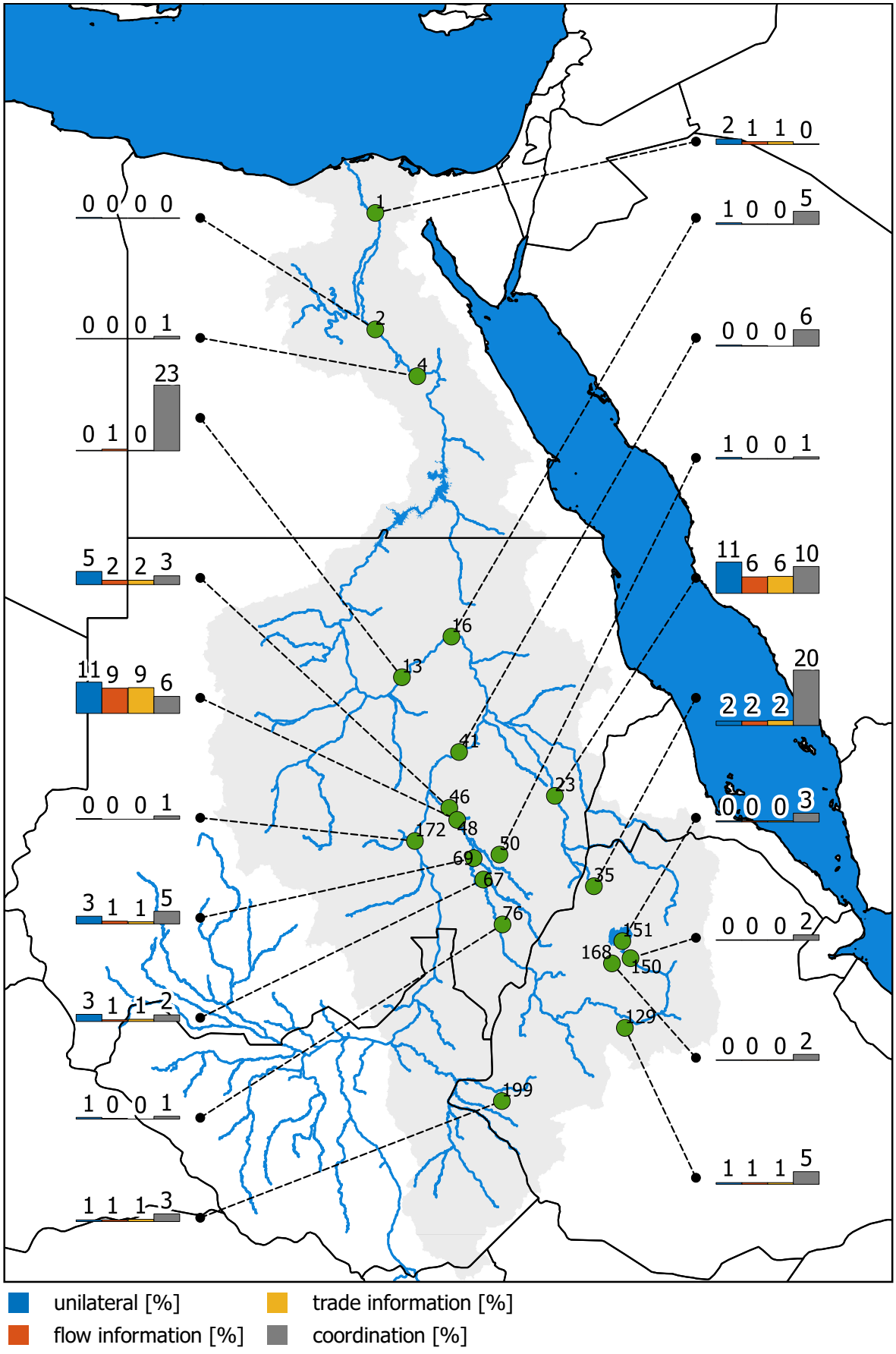

Figure 4.14: The percentage of agricultural water used for deficit irrigation at all sites active during the historic siulation experiments.

In Ethiopia there is a relatively uniform decrease of 13% in agricultural water consumption. Despite the large percentage decrease, the change is minimal when compared to the total regional consumption. It follows from Figure 4.13 that, with the exception of the small scale irrigation in Atbara, the decrease in agricultural water consumption in all sites is of the same order of magnitude. The further decrease in evaporation in the Atbara river basin can be explained by the high evaporation and low precipitation fluxes for Ethiopian standards. Since the allocated water in Ethiopia decreases relatively uniformly, and does not fluctuate strongly as in the case of Sudan, there does not seem to be any interaction depending on the available land resources in Egypt. Since the uniform decrease is accompanied by a decrease in landuse intensity, while the maximum landuse intensity remains unchanged, a changing field composition seems to underlie the change in water consumption.

It is striking that the deficit irrigation in the cooperation scenario shows the same trend as the total water consumption. With the exception of the Gezira scheme, the deficit irrigation increases in any irrigation field outside Egypt. Because the model knows exactly how much water is coming in, it appears to deliberately opt for deficit irrigation. This indicates that with the current agricultural module, yields are higher for a larger agricultural area with less water than with a smaller area with the full amount of water. This indicates that in a coordinated system where most vital agriculture takes place in Egypt, the available agricultural area is not limiting, but the available water resources. To fully utilize the available land resources in Sudan and Ethiopia, besides expansions in river infrastructure, primarily an agricultural transformation must take place.

That one location is generally preferable to another agricultural location is also evident from the agricultural water productivity. This water productivity gives the economic benefits per cubic meter of irrigated water resources. According to Figure 4.15, in the unilateral scenario, water productivity in Egypt and Ethiopia is almost equal at approximately \$0.90 per cubic meter. Agricultural water consumption in Sudan is very inefficient by comparison, with a productivity of \$ 0.20 per cubic meter. However, it should be mentioned that the agricultural production costs (both fixed and variable) have not been included in this computation, i.e. the actual values will be smaller than the numbers presented.

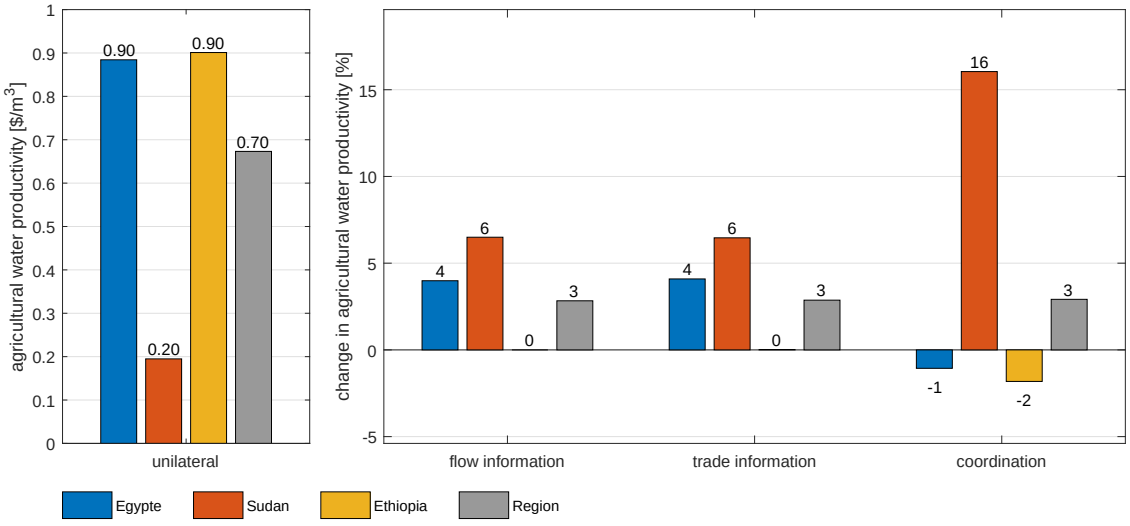

Figure 4.15: The agricultural water prouctivity, expressed in \$ per irrigated cubic metre in the unilateral scenario four all riparian states and the Eastern Nile region, together with the percentage change in the other cooperation scenarios with respect to the unilateral scenario.

The observation that the water productivity in Ethiopia is slightly higher than the productivity in Egypt is striking given the lower crop management factors. Apparently, the higher agricultural losses in Ethiopia, together with the lower potential evaporation and larger contribution of the precipitation, form a whole that is in equilibrium with the agricultural yields in Egypt under a higher potential evaporation but with lower losses. Therefore, if Ethiopia is able to reduce the agricultural management losses in future, it will most likely surpass Egypt's water productivity. The increase in agricultural water productivity in Sudan in the flow-information scenario corresponds to the decrease in the share of deficit irrigation. In Egypt, too, the increase logically follows from previous observations. After all, the net export value increases while less water is consumed. The fact that productivity in Sudan increases further in the coordination scenario despite the growing share of deficit irrigation indicates a form of regional specialization in agriculture. Although the declining water productivity values in Egypt and Ethiopia may initially seem to contradict, they support this observation of regional specialization. After all, as a result of regional specialization, each crops is grown in the place that is most suitable. However, this does not imply that all other crops have a lower yield at the given location. It solely implies that the yields of this crop are lower when grown elsewhere. Due to this changing crop composition, it is possible that a country with a high agricultural productivity such as Ethiopia consumes less water in a regionally coordinated scenario while maintaining the same land use intensity.

Such specialization can be further substantiated by the change in the production pattern. In Figure 4.16 are per group the changes in irrigated production within the Nile basin between the scenarios depicted. A list with the specific changes per crop can be found in Appendix B.4. Before moving on to the changes in the coordination scenario, first the information scenarios are studied. In Ethiopia, in accordance with expectations, there are indeed no changes in production in the flow-information scenario. In Sudan, with the exception of cereals, production of all product groups is increasing. In Egypt, a decrease in production is visible in many large product groups. In contrast, the production of water-intensive Egyptian cash crops and export products such as vegetables, fruits and fibers is increasing. Small changes occur between the flow-information and trade-information scenarios. These changes in the crop composition logically follow from the increasing regional trade.

In line with the expected specialization, the biggest changes occur in the coordination scenario. The cereal group immediately gives a clear confirmation of this supposed specialization. In Egypt, there is a clear increase in the production of cereals, while less is produced in both Sudan and Ethiopia. In addition to the absolute reduction, there is a clear shift in production in the riparian countries as well. Rice production, which probably used to be grown a lot because of the high market value, is decreasing considerably in both countries. In Sudan, this is accompanied by an increase in the production of maize and sorghum. In Ethiopia, production of all other cereals, including teff, is increasing. This growing production of teff, a product that can only be grown in Ethiopia, is a clear indication that production is no longer taking place to satisfy national demand but to satisfy regional demand. The same trend can also be observed in the production of coffee, another product that can only be grown in Ethiopia, and fruit. Because there is little demand for coffee in Ethiopia, there is little to no irrigated production in the unilateral scenarios. This is different in the cooperative scenarios where the high demand in Egypt and Sudan must be met. Since it is agro-climatic not possible to grow fruit in the irrigated fields in Sudan, this seems to be offset by an additional increase in Egypt. Sudan seems to play an important role in the cooperative scenario as a supplier of oilseed, vegetables and forage crops.

A final striking change occurs in the production of cotton. In the unilateral scenarios, this water intensive crop is grown almost exclusively in Sudan. In the coordination scenario, however, this production is almost completely canceled out with a decrease of 88%. Despite the growth in the other riparian states, the final production is only a modest fraction of the original production. Since cotton can only be used for export in the model, this is apparently a lucrative way for Sudan to make money, required to buy products they cannot grow. From a regional perspective, however, it does not appear advantageous to provide land resources for the production of this cash crop. A similar but less massive change can also be observed for the Sudanese sugarcane production.

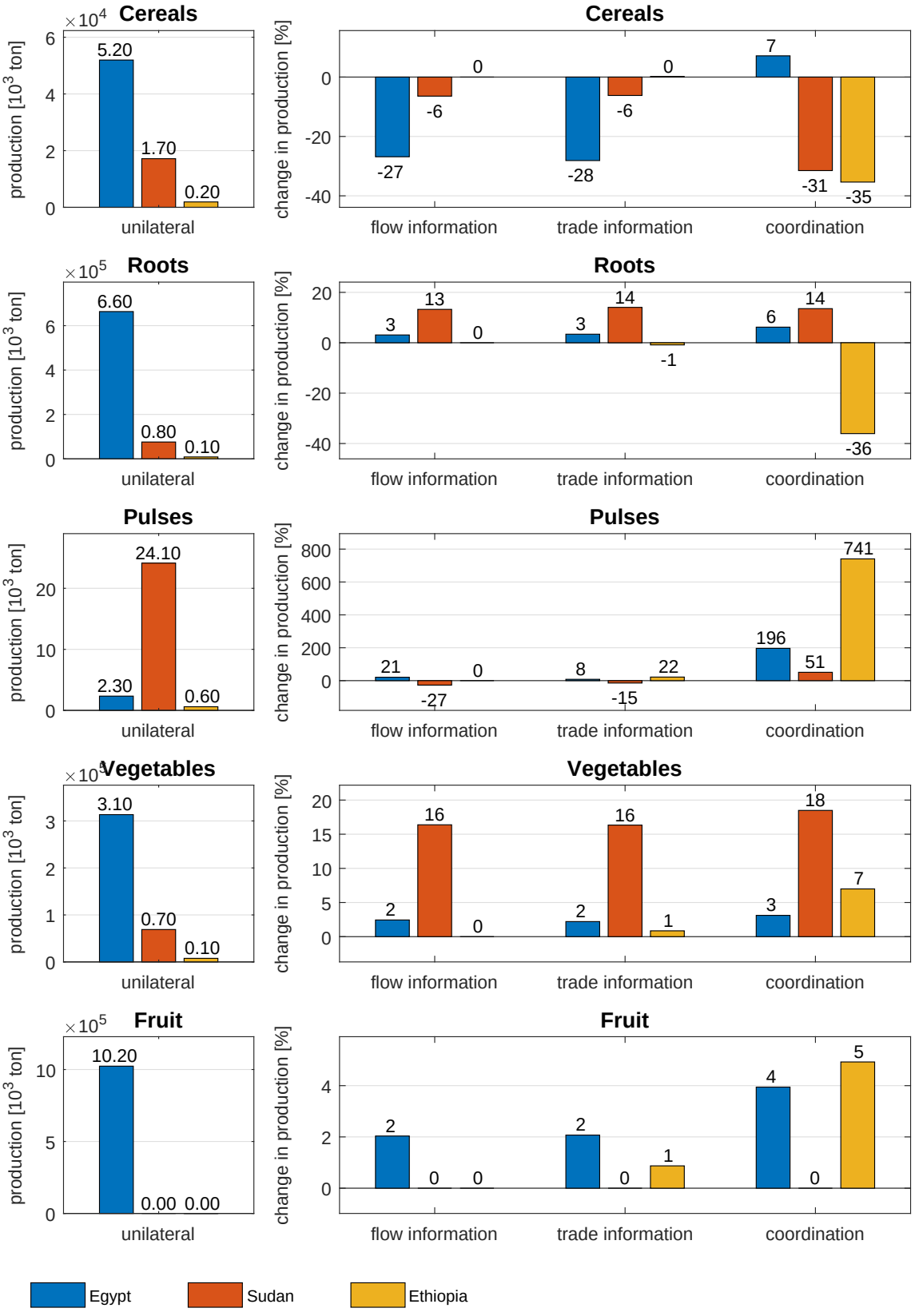
Cereals
production [10^3 ton]
×10^4
5.20
1.70
0.20
unilateral
Cereals
change in production [%]
-27
-6
0
-28
-6
0
7
-31
-35
flow information
trade information
coordination
Roots
×10^5
6.60
0.80
0.10
Roots
3
13
0
3
14
-1
6
14
-36
Pulses
24.10
2.30
0.60
Pulses
21
-27
0
8
-15
22
196
51
741
Vegetables
×10^4
3.10
0.70
0.10
Vegetables
2
16
0
2
16
1
3
18
7
Fruit
×10^5
10.20
0.00
0.00
Fruit
2
0
0
2
0
1
4
0
5
Egypt
Sudan
Ethiopia

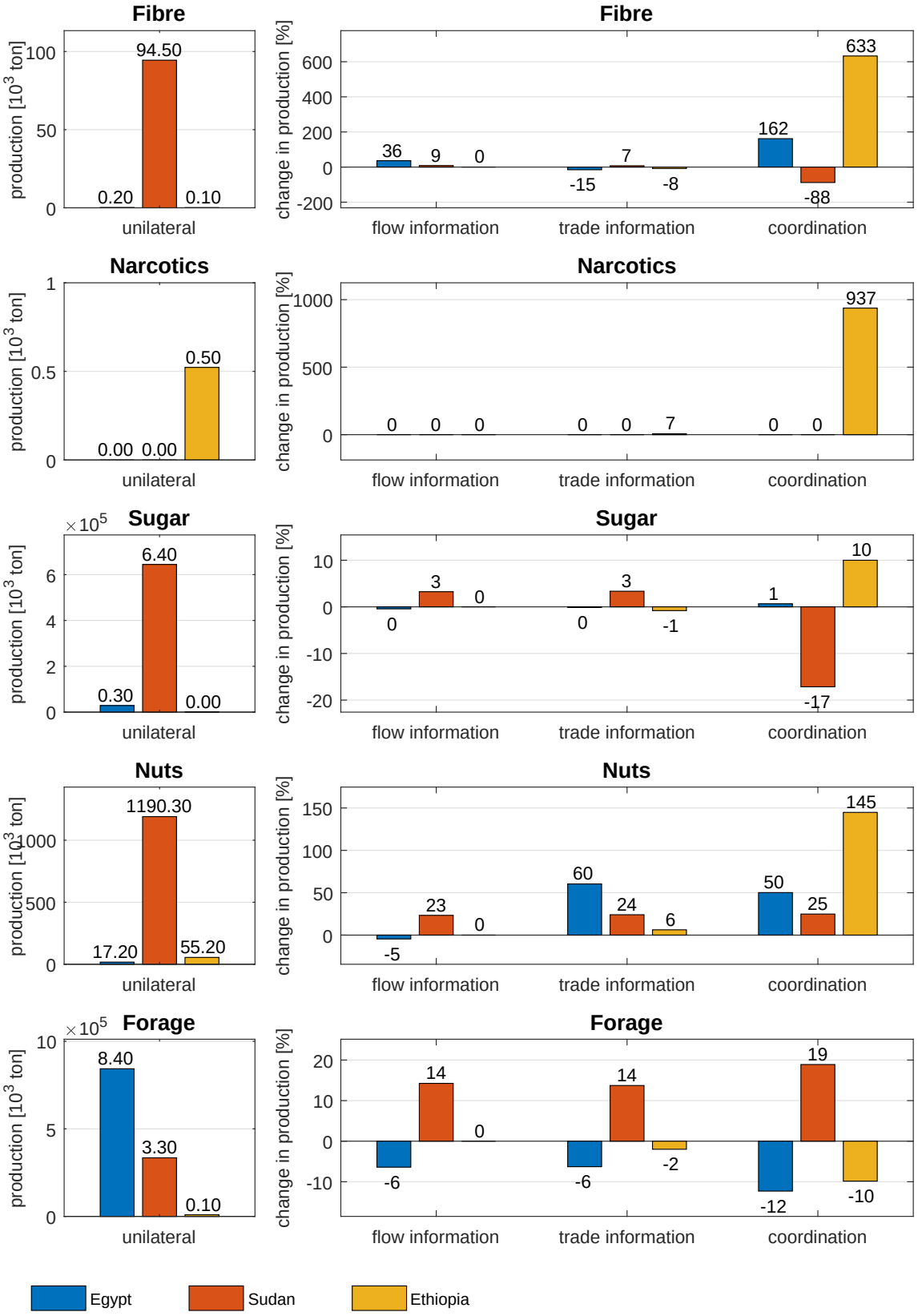

Figure 4.16: The irrigated production quantities per product group for the unilateral scenario and the changes in the other cooperation scenarios with respect to the unilateral sceanrio.

As shown in Figure 4.17, these changes in crop production lead to a change in trade flows. It is remarkable that in all scenarios both imports from and exports to the external world predominate. For Sudan, exports to the external world increase, in line with the increasing production, even further in the flow-information scenario. An inverse trend is visible in Egypt, where imports from the external world are increasing. This is also in line with previous findings, where Egypt consumes less water in total, but consumes relatively more water for the production of water intensive products for export purposes. As a result, other staple commodities must be imported. Figure 4.17 also clearly indicates that internal trade, albeit with relatively minimal quantities, is increasing in the trade-information and coordination scenario, and that this is at the expense of exports to the external world.

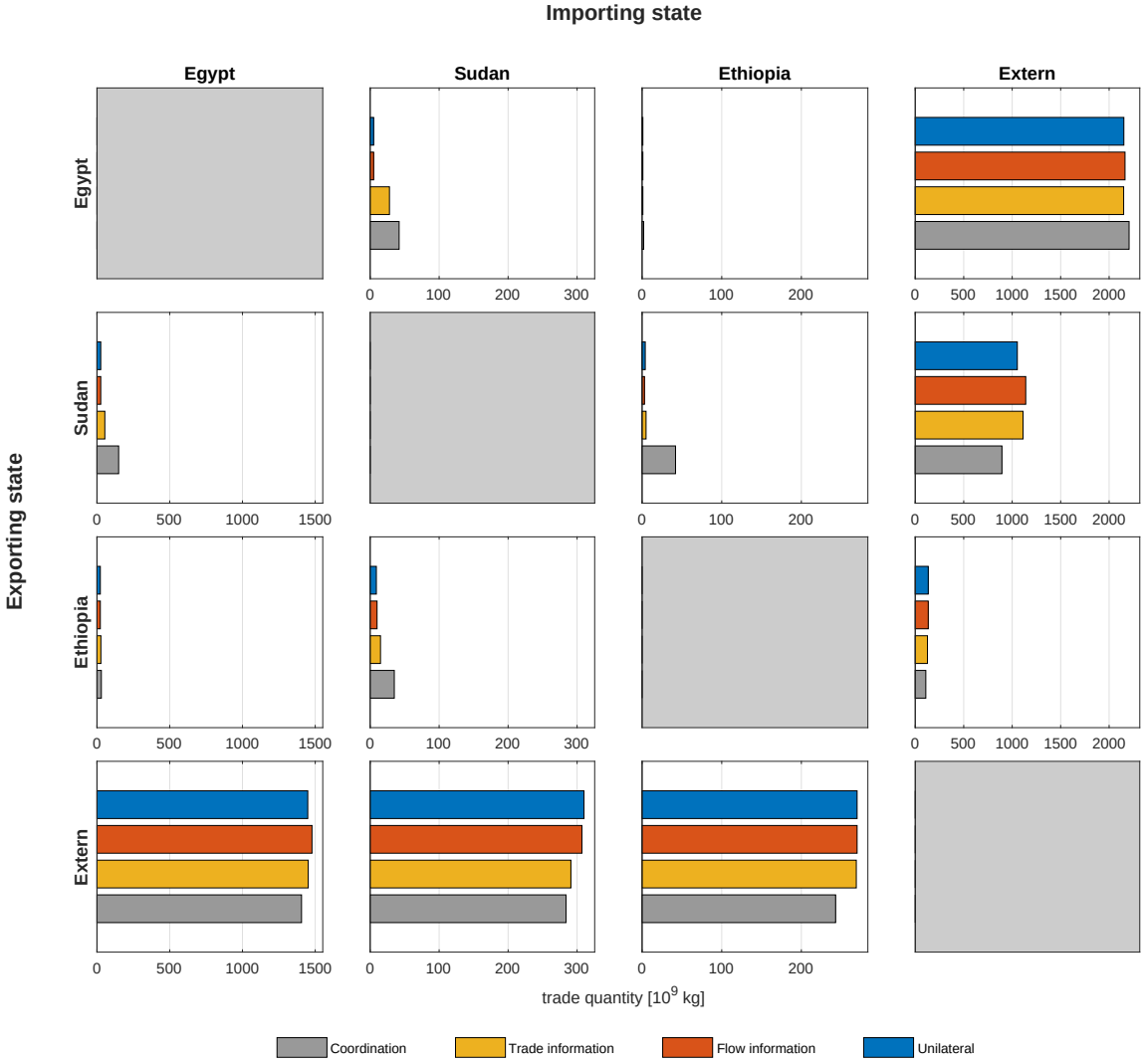

Figure 4.17: Trade quantity matrix illustrating the trade flows between the riparian states and the external world. As countries are not able to trade with themself, the diagonal of the matix is empty.

4.1.3.3. Energy balance

Since regional electricity trade is only possible between Egypt and the external world in the historical experiment, only minor changes occur between the different cooperation scenarios. The first few changes are noticeable in the electricity shortage. Figure 4.18 shows the shortage as a percentage of total demand over the entire period for each country and all scenarios. In Sudan, the model appears to be able to meet the desired demand. There are small shortages in Egypt and Ethiopia. Because historical electricity consumption data has been used as input for the electricity demand in the historical scenario, the minimal shortage in production can be seen as a validation of the energy balance in the model. The figures in Appendix C.1 show that these deficits are not uniform over the period, but mainly occur towards the end of the experimental timeline. The decrease in deficits in Egypt in the trade-information scenario is due to a decrease in trade with neighboring Arab countries (from 37 to 21 GWH). This decrease is possible because between the flow- and trade-information scenario the electricity trade changes from fixed (long term) to variable (short term). So it appears that the national generation, computed by means of capacity factors, to determine the long term trade is estimated too optimistically.

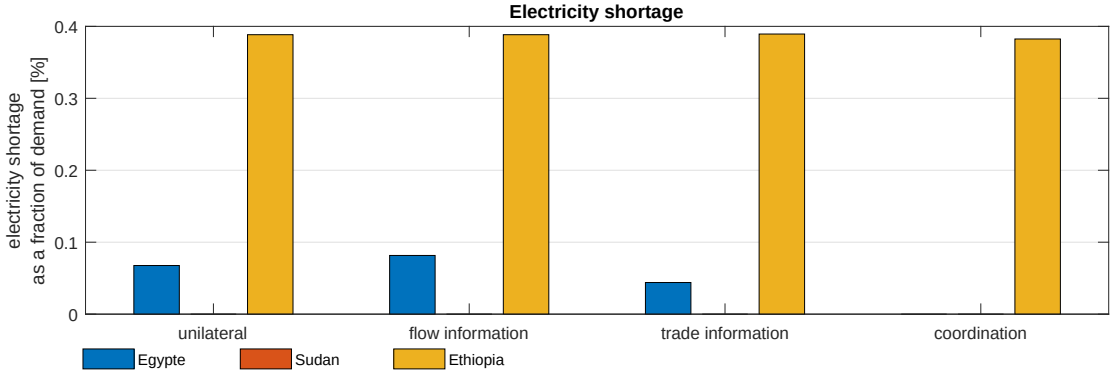

Figure 4.18: Electricity shortage per riparian state, defined as a percentage of the demand over the entire model period.

Other small changes are noticeable in electricity generation. Figure 4.19 illustrates the total production and generation mix over the entire model period. In Sudan, there is a clear increase in the hydropower generation in the flow-information scenario, which is accompanied by a decrease in the fuel generation. So besides agricultural planning, discharge information seems also relevant for the hydropower planning.

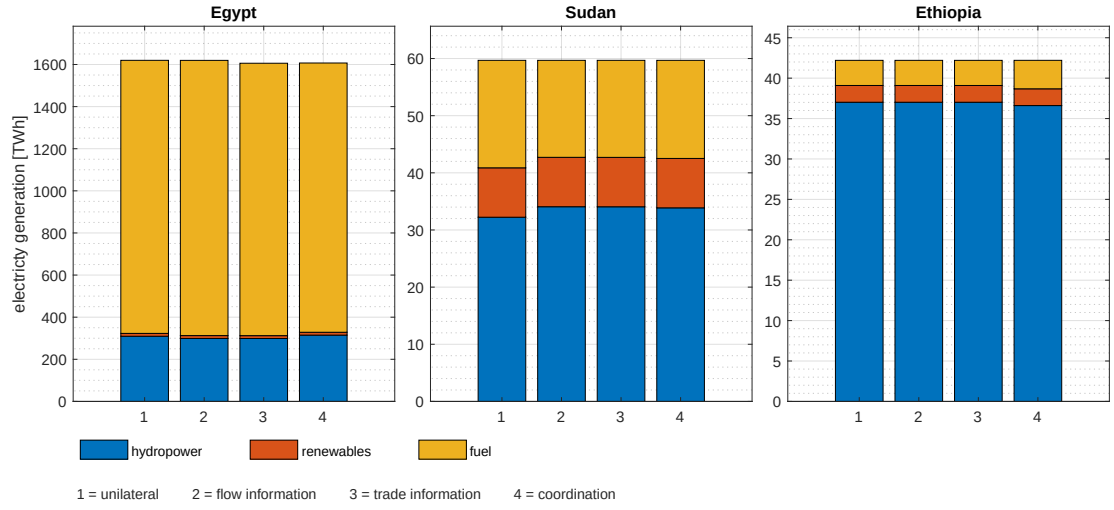

Figure 4.19: The total electricty generation and the generation mix over the entire model period dor Egypt, Sudan and Ethiopia in the four cooperative scenarios.

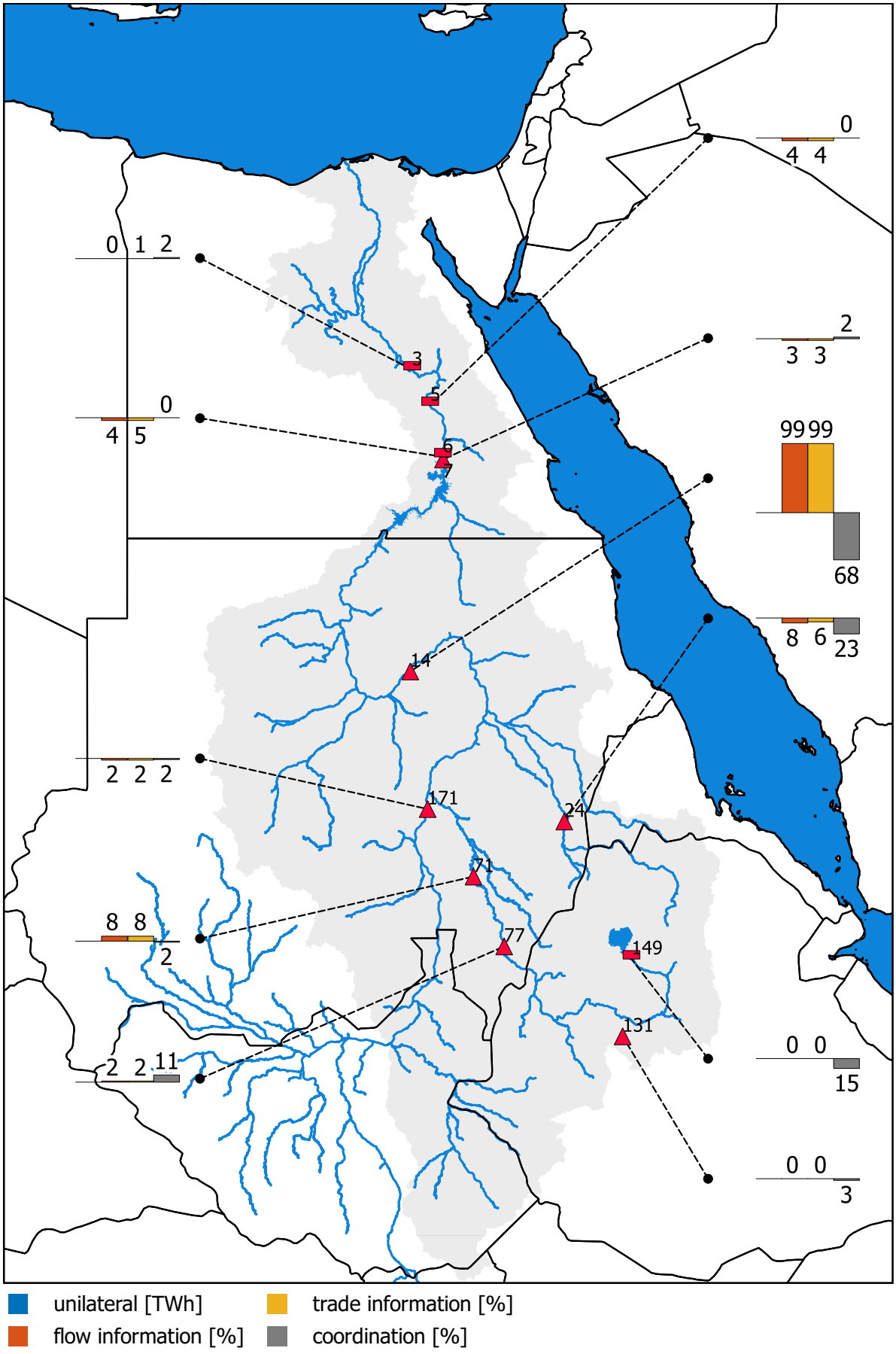

Figure 4.20: Electricity generration by all active hydropower plants (both surface water reservoirs and run-of-the-river hydro electric plants) during the entire historic mode period in the unilateral scenario, and the percentage change in the other cooperation scenarios.

Figure 4.20 illustrates that spatial shifts in hydropower generation occur in addition to the aforementioned absolute changes. Generation increases in the Sudanese Blue Nile and decreases in the White Nile and Atbara. It is striking that the generation of the Merowe dam, which only comes online in the last year of the experiment, has almost doubled. Because the border flow to Egypt is smaller in the information scenarios, the model clearly decided to fill the reservoi faster. In the coordination scenario, however, the generation decreases on this location. Because more water is going to Egypt, especially in recent years, this again indicates that the model decides to fill up the reservoir slower or not at all. The figure also indicates that hydropower production is declining at all locations in Ethiopia in the coordination scenario. The figures in Appendix C.1 illustrate that this change occurs between 2005 and 2008. Because this reduction in hydropower is compensated by fuel generation (shortages do not increase after all) the water resources seem to be more valuable elsewhere in the region.

4.1.4. Self-suffiency

In this section the results of the model experiments regarding the possible agricultural self-sufficiency are presented. As described in Section 3.2, this model study was conducted for the unilateral scenario with national self-sufficiency and for the coordination scenario with regional self-sufficiency. In both scenarios, the rain and outside agricultural areas have also been added to the optimization. The results of the unilateral self-sufficiency study are illustrated in Figure 4.21. The left figure shows that the obtained self-sufficiency grows with the increasing self-sufficiency target. For Egypt, self-sufficiency stagnates around 53%, for Sudan 40% appears to be the maximum achievable percentage, in Ethiopia the percentage continues to grow to almost 75%, and for the region as a whole a maximum self-sufficiency of 55% follows. The growth varies greatly from country to country. In Egypt and Sudan, the growth is much smaller than in Ethiopia, which indicates that from an economic perspective it is advantageous for these countries to already be self-sufficient to a certain extent. The figure on the right shows that this increase in self-sufficiency is clearly accompanied by a decrease in the agricultural production value.

The results for the regional self-suffiency are depicted in Figure 4.22. This figure illustrates that through cooperation the maximum self-suffiency grows to 58%. The decrease in agricultural production associated with this regional growth is moreover smaller than for the unilateral scenarios. In order to achieve this small growth in self-sufficiency, Sudan and especially Ethiopia, will have to sacrifice strongly on their national self-sufficiency.

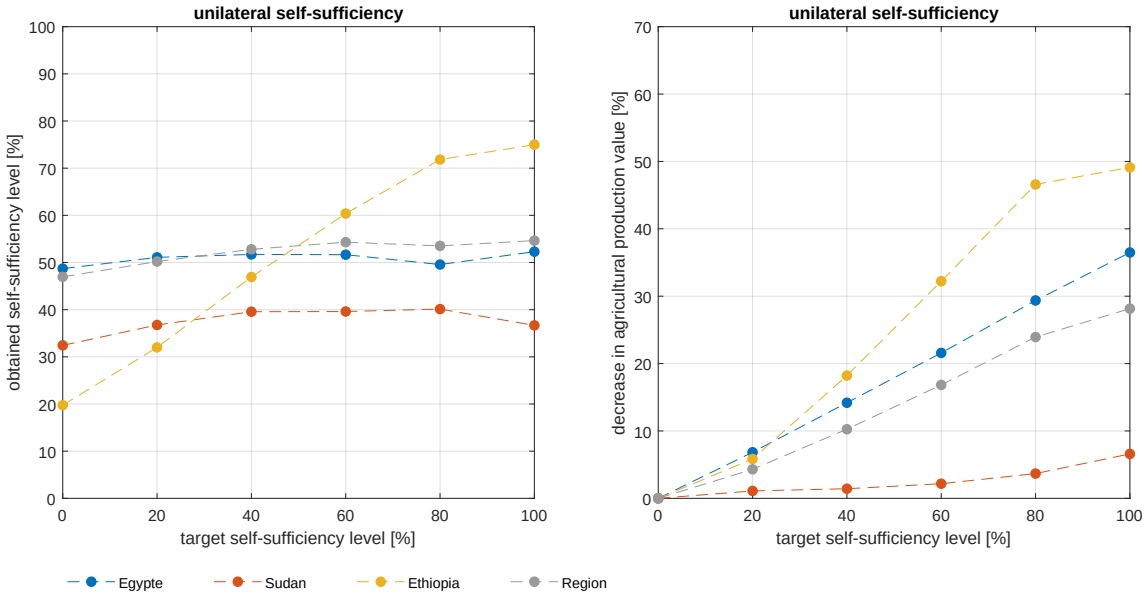

Figure 4.21: Left) the obtained self sufficiency levels for various self sufficiency targets in the unilateral scenario. Right) the decrease in agricultural production value associated with the increasing self-sufficiency. The regional self-sufficiency is not used as an objective in this scenerio, but is depicted for comparison purposes.

In addition to these general changes, there are some remarkable features. First of all, in the unilateral scenario, Sudan experiences a decline in self-sufficiency near the end, while the decline in agricultural production value continues. In addition, Egypt achieves higher self-sufficiency levels in the coordination scenario than in the unilateral scenario. The former is probably the result of the increasing complexity when the set target level cannot be reached. Because the soft constraint is directly connected to the non-linear irrigated agricultural production, this soft constraint is already very complex. However, from the moment that the stipulated condition can no longer be met, a wide variety of unrealized combinations is possible, resulting in an even more complex search space for the optimization algorithm. This in turn increases the chance of incomplete convergence or convergence to a local minimum. That the national self-suffiency for Egypt increases in the coordination scenario probably has to do with the time horizon. Because different choices are made earlier in the experimental timeline, different crop compositions may result at a later stage.

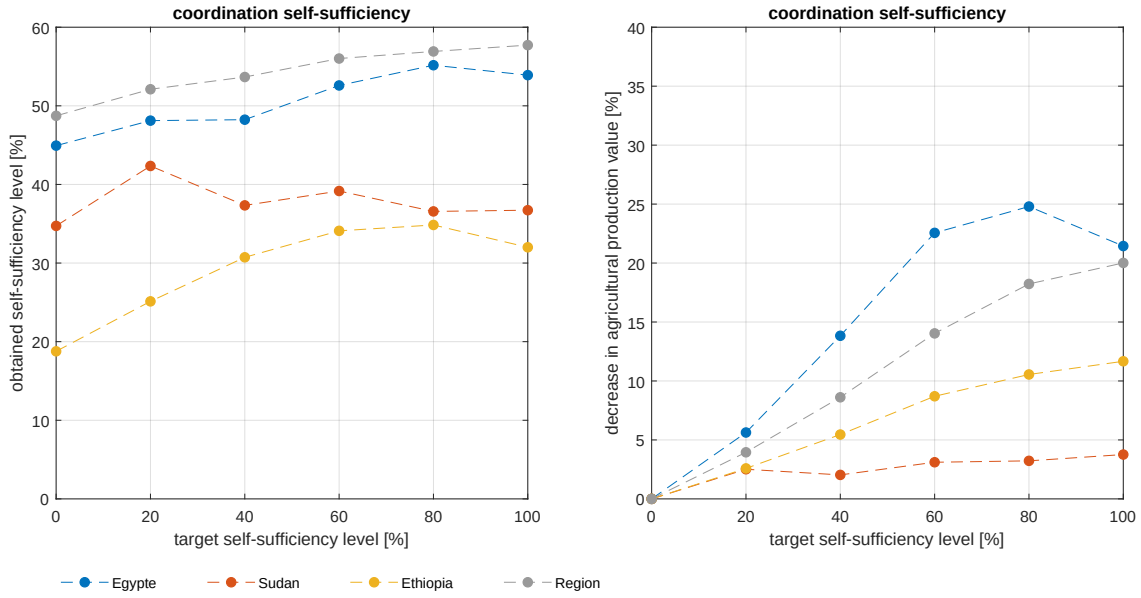

Figure 4.22: Left) the obtained self sufficiency levels for various self sufficiency targets in the coordination scenario. Right) the decrease in agricultural production value associated with the increasing self-sufficiency.

4.1.5. Agriculture-hydropower trade-off

This section discusses the results for the agricultural-hydropower water trade-off. As mentioned in Section 3.2, this model study was carried out by varying the costs of electricity shortages for the unilateral and cooperation scenario. The results for both cooperation scenarios for all three riparian states are illustrated in Figure 4.23. There are clear differences for the countries in hydropower and agricultural production value between the scenarios. In Ethiopia, for example, the production value of both hydropower and agriculture decreases in the coordination scenario. This is in line with the previously observed decline in hydropower production and agricultural water productivity. However, the differences between the experiments with varying shortage costs are minimal (represented by the numbered dots within a plot). Moreover, no trend is found with increasing shortage costs. Hence, in the historical scenarios, there is apparently no trade-off in water use between hydropower and agriculture in any riparian state. The absence of these trade-offs can be explained by the absence of electricity shortages already at a low shortage cost, and the upstream positioning of most hydropower capacity. Because these production numbers are lumped over the full 20 years of the simulation time, trade-offs may exist at specific times during this period. With an increasing demand for electricity and a shift of the major generation capacity to a downstream location with the construction of the Merowe dam and GERD, an increase in trade-offs is expected in the future.

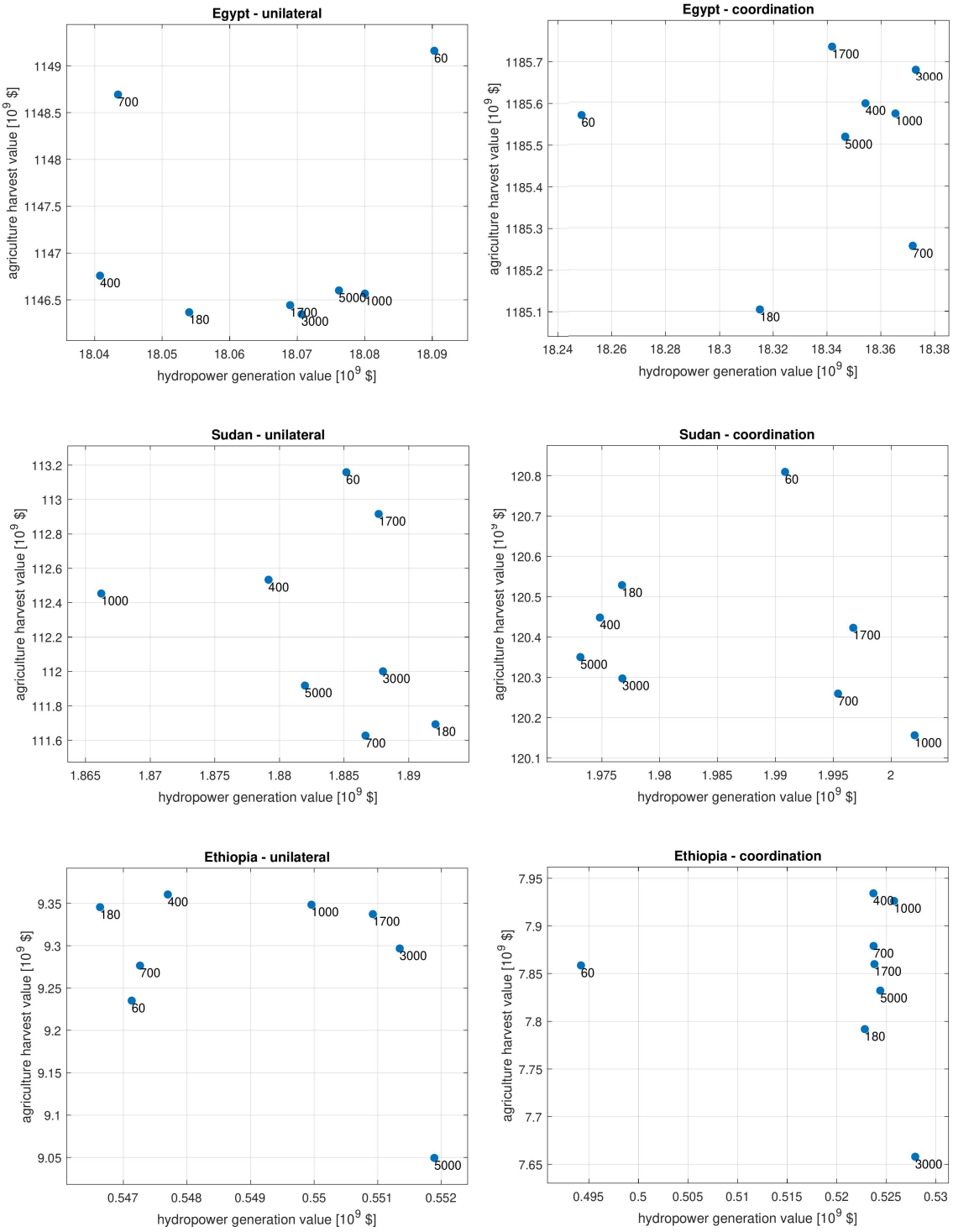

Figure 4.23: The trade-off between hydropower and agricultural water consumption. The left column illustrates the trade-off in the unilateral scenario, and the right column in the coordination scenario. The numbered dots each represent a single model realization with a different electricity shortage costs. When a trade-off in water consumption would exist, an increasing electricity shortage costs would go hand in hand with an increase in the hydropower value and a decrease in the agricultural value.

4.1.6. Impact of uncertain climate predictions

The impact if imperfect (historical) climate data on the net generated benefits are illustrated in Figure 4.24. This figure should be studied in comparison to Figure 4.6. For the unilateral scenario, the differences in revenues between the model experiments with and without perfect climate predictions are small. Net income remains the same in Ethiopia, it grows by $2 billion in Sudan, and decreases by $4 billion in Egypt. That the income in Ethiopia does not change can be explained by the large share of rain-dependent and outside agriculture, and the minimal agriculture in the Nile river basin. Moreover, Ethiopia has enough water at its disposal all year round. Changes in net benefits in the other riparian states are small because these states already experienced uncertainty in inflow under perfect climate forecasts. However small changes are present, because the predictions are different, resulting in distinctive planning choices.

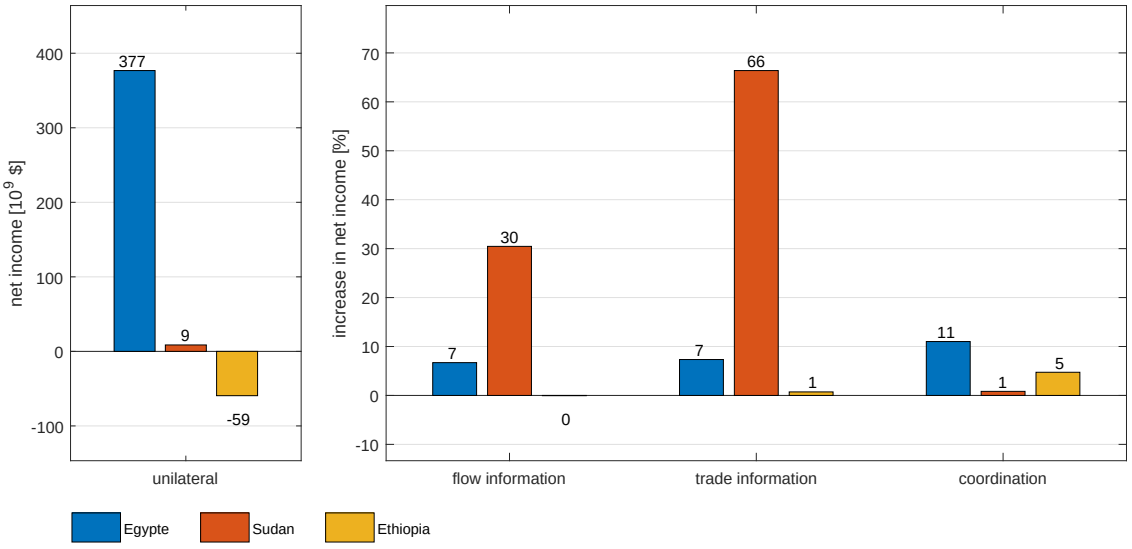

Figure 4.24: The net income over the modelled period between 1990 and 2009 for the unilateral cooperation scenario forced with historic climate data, and the percentage increase in net income in the other scenarios with respect to the unilateral scenario.

The flow information scenarios show a trend similar to that in Figure 4.6. However, the total benefits of the flow-information for Sudan are much smaller. Given the limited presence of dams on the tributaries of the Blue Nile, the uncertainty about the inflow, despite flow information from Lake Tana and the Ficha'a dam, remains considerable. Since most tributaries of the main Nile upstream of the Aswan High dam are regulated, the uncertainty about the inflow decreases sharply in Egypt. The growth in net income is therefore of the same order of magnitude as for perfect climate forecasts. In trade information, the changes are in line with those under perfect forecasts. Clear differences are observed in the coordination scenario. Despite the improvement of all riparian states, almost the entire profit of cooperation falls into the hands of Egypt.

4.2. Future experiments

The net income in the unilateral scenario and the percentage change in the other cooperation scenarios is illustrated in Figure 4.25. The unilateral scenario indicates that Egypt will become a net food importer in the future. This can be explained given the strong population growth, and the operation of the hydropower and agrocultural sector close to their potential. The strong expansion of both rainfed and irrigated agriculture will enable the other three riparian states to become net exporters. In the flow-information scenario, no changes will occur in Ethiopia and South Sudan due to their upstream location. In Sudan, which previously benefited greatly when information about the expected discharge in the Blue Nile was shared, this information does neither seem very valuable. Hence, the uncertainty about the influx is small in the unilateral scenario in the future model experiment. This change with respect to the historical experiment indicates that the presence of the GERD, with its uniform and predictable outflow, is valuable for Sudan. Despite the fact that the information does not seem very valuable to Sudan, water consumption does increase, causing a further decline in net income in Egypt. Contrary to the historical scenario, there now seems to be competitive water consumption between countries. No significant changes appear in the trade information scenario. However, these do occur in the coordination scenario. These changes suggest that every country in the region will suffer from coordination. A form of cooperation in which some participating parties benefit at the expense of others is possible, but a form of cooperation in which every country is disadvantaged is logically not feasible. Also viewed from the optimization perspective, such a solution should not be possible. Given that the unilateral solution is still feasible in the coordination scenario, there should never be a lesser outcome.

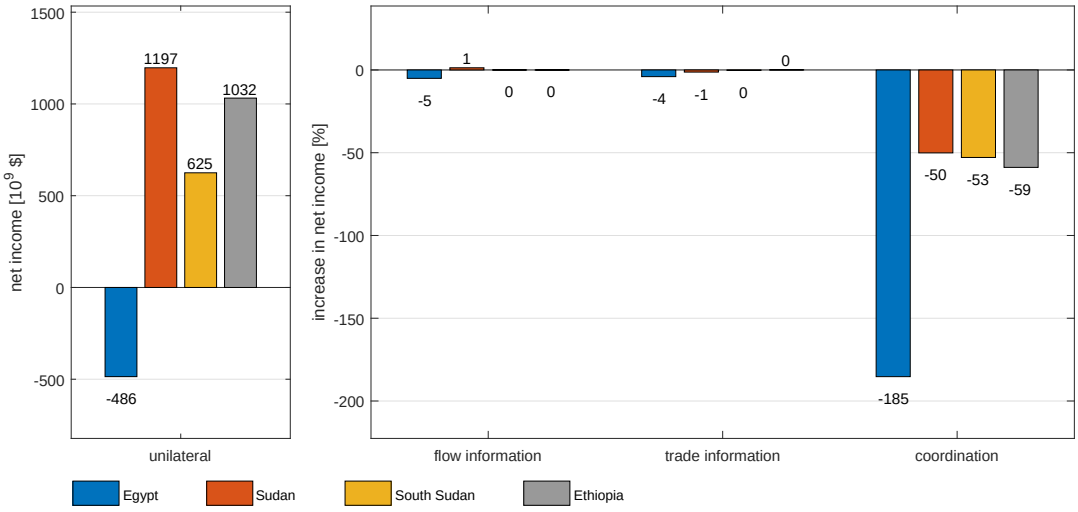

Figure 4.25: The net income over the modelled period between 2020 and 2039 for the unilateral cooperation scenario and the percentage increase in net income in the other scenarios with respect to the unilateral scenario.

That the model nevertheless comes with a lesser result can have two possible causes, both of which are related to the complexity of the problem. It may be that the optimization is interrupted prematurely before complete convergence is reached or that the model converges to a local minimum. To make the behaviour of the optimization more transparent, Figure 4.26 illustrates the income in the coordination scenario over time together with the income in the unilateral scenario. This figures shows that, especially in the first 10 years of the simulation experiment, the net income in the coordination scenario is lower than in the unilateral scenario. In the latter ten years, the incomes follow the same trend. In Egypt and Sudan is the net income during this period even slightly higher, and in the upstream countries Ethiopia and South Sudan slightly lower. This indicates that the difficulty is mainly present in the first years of experimental timeline. Because the differences are several orders of magnitude in the these years, these deviations do not seem to be due to incomplete convergence, but rather due to to convergence to local minima. To investigate this further, the same simulation experiment was restarted. In these new experiments, however, the solution from the previous MPC iteration is no longer used to warmstart the optimization, but every new optimization is performed with a random starting point.

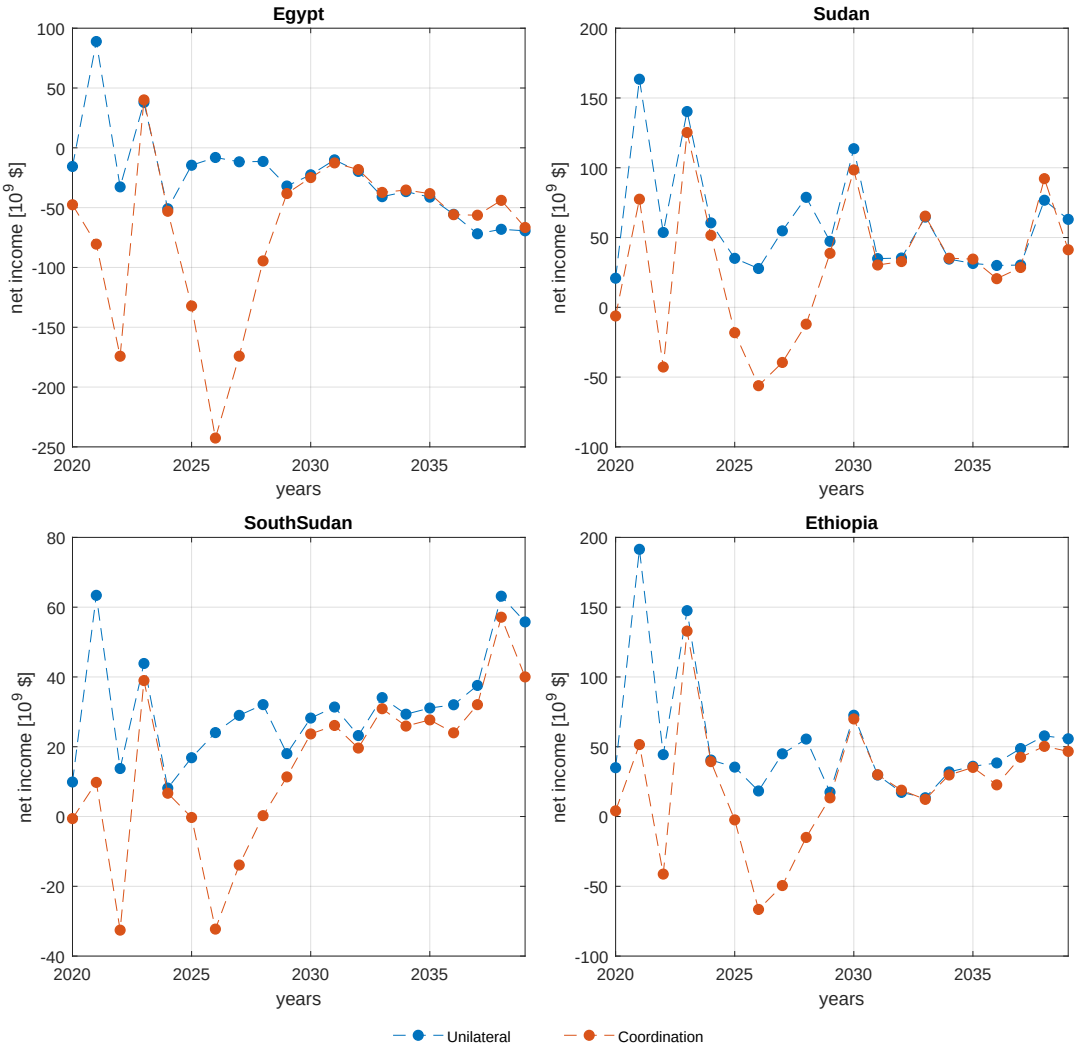

Figure 4.26: The annual net benefits of the future simulation experiment for the unilateral and coordination scenario.

The annual net income for the coordination scenario of this experiment with random starting points is together with the net income of the semi-warm start experiment plotted in Figure 4.27. The results differ across the entire experiment. However, in accordance with previous findings, the largest variations can be found in the first years of the experiment. Because the minor deviations in the later years of the experimental timeline, which are also found for the randomly started unilateral scenario (see Appendix C.3), could be caused by incomplete convergence, the model mainly seems to converge to local minima in the first years. This indicates that the complexity of the search space decreases further on in the future experimental timeline. Because with the presence of new infrastructures the number of variables and constraints is only growing over the simulation timeline, this complexity seems not to arise from the permanently present model structures. Stated otherwise, this increasing complexity of the search space is the result of temporarily present mathematical formulations. The soft constraints associated with the new surface water reservoirs is therefore an obvious candidate for this increase in complexity. This soft constraint is used to constrain the turbine flow during the reservoir filling process and circumvent the need for a very difficult to solve complementarity constraint (as explained in Section 2.4.1.1). However, the alternative formulation used (which is defined in Equation 3.108 and 3.112) appears to have a complicating effect on the search space as well. Since these large differences are not observed in the unilateral scenarios (see Appendix C.3), especially the interaction between the soft constraints for new reservoirs with an upstream-downstream connectivity appear to be problematic.

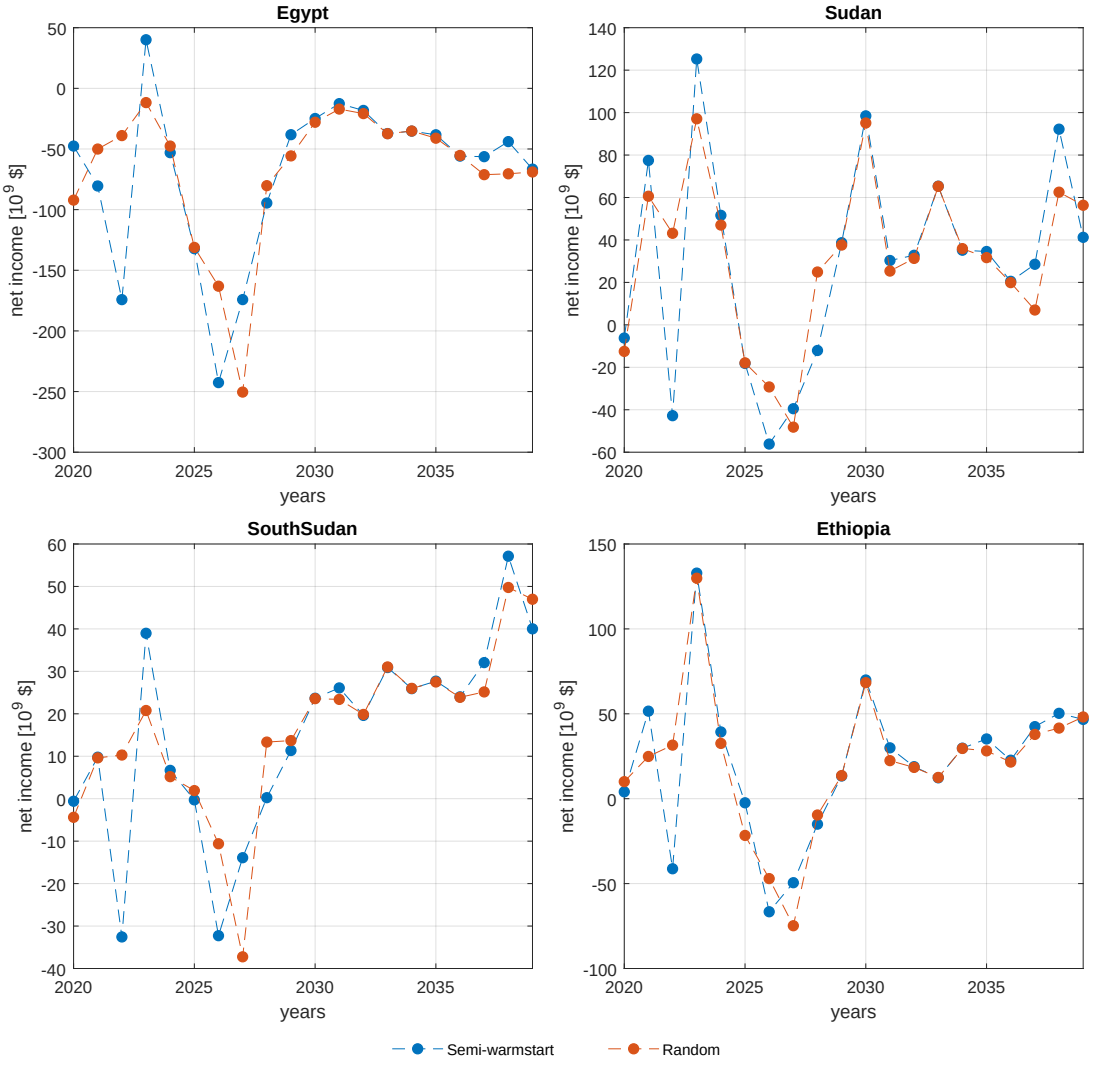

Figure 4.27: The annual net benefits of the coordination scenario in the future simulation experiment. The blue line illustrates the values using a semi-warmstart method, and the red line illustrates the values found with random starting points for each MPC iteration.

5 Discussion

The discussion presented in this section covers both the presented method in Part A and the results of the case study in Part B. The first section "Case study and results" discusses the results of the Eastern Nile case study, and the second section "Methodology" discusses the shortcomings of the methods used.

5.1. Case study and results

The discussion in this section is split into three parts. First, the reliability of the results is briefly discussed, followed by the impact of assumptions made during the data collection phase. Finally, the influence of computational settings is explained.

5.1.1. Results reliability

It is difficult to conclude whether the presented results and the model equations are reliable. The optimisation model derives new resource uses within the pysical and operational performance constraints set by the modeller. However, it is not possible to check the increase in agricultural productivity, the change in energy use or the spatial reallocation of resources found in cooperative scenarios against real world cases. For the non-cooperative cases, some comparisons can be done to study the meaningfulness of the results. But even in this case, some comparisons may not be reliable because of a lack of spatially explicit data on resource uses. For this reason, all subsystems (e.g. river losses, agricultural production, etc.) have been validated as well as possible during the data collection phase.

5.1.2. Data collection

The data used for the Eastern Nile basin case study has been compiled with the utmost care. However, to obtain a complete dataset in this data scarce environment for both historical and future experiments, a large number of assumptions is made that introduce new uncertainties. Some of the major uncertainties, and where possible their impact on the results, are explained below per balance.

The dynamics of the water balance have been influenced by assumptions regarding the data collection and the model formulation. First of all, the early introduction of the Chara Chara weir at the outflow of Lake Tana, introduced to bypass the description of a natural lake, has consequences for the entire downstream water management in the period 1990-1995. During this period, with respect to the real world case, the storage capacity in the Eastern Nile is overestimated and the flow profile is less unimodal. As a result, the region has a greater drought resilience in the early years, agricultural production in Sudan is increased in all scenarios during this period, and the value of information sharing on river discharge in Sudan is overestimated.

In addition, uncertainties in the capacity of reservoir gates and offtake canals can affect the results. As mentioned in Section 3.3.2, are the unknown gate capacities determined by us of a relationship between the extreme annual discharge and the gate capacities of existing reservoirs. However, the variation around the trend found is considerable, as a result of which the unknown gate capacities may be under- or overestimated, which in turn can lead to a misinterpretation of overflow events. However, because overflow events do not occur in any simulation experiment, not in existing ones but neither in new reservoirs, it cannot be stated with certainty whether such situations did occur.

Since the capacities of all offtakes, with the exception of the Tana Beles offtake where the capacity is determined with the characteristics of the run-of-the-river plant, are unknown, the model works with infinite capacities. Downstream in the Blue Nile in Sudan, this may have led to an excessive exchange of water resources to- and agricultural production in the irrigation fields in the adjacent river branches (see the schematics of the river network in Figure 3.2).

Many of the variables used to describe agricultural yields are assumed to be spatially uniform over the entire Eastern Nile region. However, the crop coefficient, yield response factors and stage lengths are climate dependent [Steduto et al., 2012]. Such an implementation therefore reduces variability, resulting in yield overestimations in one region and potential underestimations in another region. The same overestimation and underestimation can also occur within a country due to the national definition of the start dates for irrigated agriculture. Although the assumption of a uniform sowing date might be correct in a small country like the Netherlands, this does not account for the major agro-climatic differences present within the national border in the Nile states. Certainly in Ethiopia and Sudan, given the significant contribution of precipitation and the differences in evaporation, it may be more advantageous to start the irrigated growing season in different regions at a different times.

The nationally defined agricultural management factors, used to define the agricultural losses, have an homogenizing effect on the yields found as well. This impact is particularly major in rainfed agriculture, where the natural geology is more relevant due to a lack in access to better tillage methods and manure. In the irrigated fields will the factor used, in addition the the homogenizing effect, most likely result in an overestimation of the agricultural losses. As described in Section 3.3.3, is this factor computed by dividing the spatial description of the actual yield in the year 2000 by the potential yield found in the GAEZ database. However, although assumed, probably no perfect water supply was availabe in the year 2000, causing the harvested yield in the GAEZ database to be less than the maximum attainable yield. Because the data on actual yields presented in the database are model results as well, with associated uncertainties, it is not possible to give complete exclusion on the magnitude of the irrigated management factors.

The same applies for the magnitude of the rainfed management factors. Although these values have been carefully computed with data from the FAOSTAT database, they are the result of an accumulation of assumptions. After all, the data in the FAOSTAT database contains already many estimates. This data is then as described in Section 3.3.3, based on an irrigated crop composition occurring in a single year, divided into an irrigated and rainfed surface, to be allocated over the available rainfed land and converted into production quantities, using unproven parameters for an evaporation constraint and a yield function that does not account for the impact of water stress during individual growth stages. These rainfed management factors and the associated rainfed crop composition should therefore not be regarded as absolute truths. However, their effect on the model is considerable. Since the food balance largely determines the net benefits, a different rainfed crop composition or yield can simply mean the difference between profit and loss by a change in the composition of the irrigated land.

The parameters $c_{\min}$ and N_{per}, used to describe the minimum required ratio between the actual and potential evaporation and the duration over which this ratio is computed for perennial crops respectively, for the minimum evapotranspiration constraint in Equations 3.82 and 3.134 in part A are determined during the same process of rainfed crop allocation. Although these values may be able to reproduce historic harvests as well as possible, they are not reliable in describing real world crop wilting. Although a general value for the minimal evapotranspiration as a fraction of the potential evapotranspiration ($c_{\min}$) could not be found in the literature, a fraction of 0.2 feels intuitively too small.

In addition to these uncertainties in agricultural production, the food balance is also exposed to uncertainties in storage, commodity prices and trade distances and affected by the absence of production costs. The approach used to determine the food storage in Section 3.3.3 gives a single value for the entire model period. By definition, the computed value underestimates the actual storage capacity in the last year, but overestimates (assuming growth in capacity) the capacity in all preceding years. The result is that there is less re-import of products in the early model period, and therefore less transport costs, while near the end of the period there is most likely too much import of products that have been exported in earlier time steps.

Most of the food prices originate from reliable and consistent sources. However, there are concerns about the correctness of the products prices absent in these databases (mainly pulses, roots and vegetables), which are therefore computed from the FAOSTAT trade matrix data. All commodity prices computed from this data source show namely fluctuations in the early years of the timeline that are absent in the other databases. As a result, the model might indicate too excessive interannual variations in the production of pulses, roots and vegetables.

Agricultural production costs (e.g. seeds and fertilizer) are due to the lack of a complete and consistent description of all 33 crops in a database not included in the optimization. Therefore, agricultural water and land resources are allocated on the basis of the expected turnovers. Including these costs could (significantly) alter the cropping patterns and water allocation. Moreover, due to decreasing agricultural water productivity, it might affect the trade-off between hydropower and agricultural water use.

Besides these historic data types, data used for future simulation experiments has been prone to uncertainties. Because projections are missing for many of the required data types, it has been assumed that the historical data will remain unchanged (preservation or historic conditions) for the future interpretation of the diet, the feed basket, the agricultural management factors, the irrigation efficiency and others (see section 3.3 for a full desciption). Insofar as projections are already available, they are influenced by the assumptions and models used by the relevant institutes. Since most projections focus on one aspect, multiple independent studies have been used to obtain information about future dietary patterns, agricultural areas, electricity generation capacities, etc. Despite the fact that the collection of data focuses on uniformity in the future emission scenarios and social pathways, it cannot be guaranteed that the underlying assumptions match in all projections. In addition to the future data collection itself, post-processing also entails the necessary uncertainties. The gridded change in precipitation and discharge, as obtained from the SMHI, has been used to scale the historical data series. With the predominantly positive relative changes in precipitation and discharge the aforementioned method increases the absolute seasonal and inter-annual variation, and allows spatial changes in hydrological drivers. However, this method makes is impossible to create both drier and wetter years compared to the reference time series since a month is scaled with the same factor each year. Moreover, this scale approach cannot enable precipitation or drainage to occur in historically completely dry locations and seasons.

Because the scale of other found data projections is too general or too specific for the purpose used in this study, these projections are either converted into more specific data (downscaled) or generalized. Despite the systematic approach (see Appendix A.2.1), the downscaling of the infrastructural projections to individual commissioning years is a quite arbitrary process. These inputs should therefore not be seen as truths, but as flexible settings with which a wide variety of future pathways can be investigated. The generalization of the reservoir filling process based on the GERD gives a first impression, but does not take into account that the filling process of each unique reservoir can besides hydrological conditions also depend on up- and downstream interests.

5.1.3. (Sub)optimality of numerical solutions

The operational control strategy used and the associated optimization involve a large number of settings that can potentially influence the results found. However, the scope of this project is more on system integration than on computational optimality. The chosen optimization settings for the duration of a time step, the convergence criteria, the costs of the soft constraints and the length of the optimization horizon are therefore mainly based on the results and required runtime of exploring pilot studies. As a result, it cannot be concluded that the settings used in the case study in the Eastern Nile result in the most optimal solution or the best trade-off between computational time and accuracy.

The pilot studies also show that the model is sensitive to the applied method for scaling of the variables, constraints and objective. Although this scaling results in faster convergence, it also results in larger sub-optimisations (e.g. small import flux while exporting a product) in the linear parts of the system. A closer look at the scaling practice could potentially improve the computational cost without sacrificing accuracy.

Based on the required runtime and the results of the historical self-sufficiency and the future simulation experiments, the soft constraints used to circumvent the complementarity problems for reservoir filling and self-sufficiency seem to complicate the search space. The convergence to local minima found in the future scenario seems to be related to the soft constraint regarding reservoir filling. Whether this is indeed the case, and what the impact of local minima is on the other scenarios, further analysis must show. However, it can be stated that if soft constraints guarantee the only possible or the best implementation, more attention should be paid to the balance between the main economic objective and the soft constraints in the optimization objective on the one hand and the ratio between all soft constraint present on the other. Because the magnitude of the main economic objective can vary per country and time, it is necessary that the magnitude of the soft constraint also varies. A fixed cost for the penalty, as currently used in the methodology is not practical for this. A better scaling approach can ensure that the normalized ratio between the general objective and the penalties remains the same, resulting in a better performance.

5.2. Methodology

The discussion in this section is divided into four subsections. In these subsections, the chosen system boundaries and associated assumptions are discussed first, followed by a discussion about the the balances and linkages used and the usefulness of the results found for policy purposes. The final paragraph deals more specifically with the assumptions surrounding the implementation of the water, energy and food balance.

5.2.1. System boundaries and spatial scales

The determination of the system boundaries and the spatial scales are difficulties that always recur when setting up a nexus study [Liu et al., 2017; Zhang et al., 2018]. Nexus models are applicable at different scales ranging from an individual city to a global level. In general it holds that the smaller a spatial unit gets, the more precise the nexus can be. The aim in this study is to describe processes as much as possible at the level at which they take place, allowing the inclusion of spatial and temporal variation. Therefore, agricultural production is described at the level of an individual field and hydropower production at specific infrastructure level.

Although the agriculture planning module in the model accounts explicitly for the spatial and temporal variability in climate forcing, this heterogeneity lacks for other determining factors. Determining factors such as the management losses and the applied amounts of fertilizer are currently described at national and regional level respectively. In addition, the fertilizer applied is assumed not affect the yield in the current model setup. However, the regional differences in fertility and management, especially in rainfed agriculture, are considerable. A more detailed description on smaller spatial units can help investors and policy makers identify which areas bring the most benefits and need to be developed first. A more detailed spatial scale is as well required for electricity production and consumption. Although the hydropower production is described at individual infrastructure level, the production of the renewable and fuel plants is implemented at a national scale. This assumes the existence of a single national electricity network. However, in larger less developed countries, including countries in the case study, several regional grids coexist with the national main grid. With smaller regional units, the current defined electricity demand can be decoupled in the willingness to buy electricity from the grid and the ability to deliver this amount based on the network accessibility and the generation capacity of that specific sub network.

In addition to internal borders, setting the external borders of the system under consideration involves difficulties as well. In an ideal world, administrative regions would coincide with the boundaries of a river basin. Since this ideality has no worldly examples, and issues such as economics, policy and trade are arranged at national levels, it is unrealistic to use the boundaries of a river basin as system boundaries for optimization. However, the river basin boundaries are necessary to guarantee a balanced water system. As a result, there can be more than one transboundary river basin within a country. When a WEF-nexus model is used to study cooperation of the water resources within one transboundary river basin, this requires modelling approximations. In this case, one or more countries are classified into an administrative unit on the basis of this river basin, while they could be classified

into another administrative unit based on the other river basins. In the case study in the Eastern Nile this occurs for Ethiopia. In addition to Egypt and Sudan, the country could also be placed in an administrative unit with Kenya and Somalia on the basis of the Jubba-Shebelle basin. Despite the fact that the merging of these two regions would most likely still be technically feasible, the problem will only be solved when the scope is no longer on the Nile riparian states but the entire African continent. However, on this continental scale, the proposed methodology will no longer be technically feasible. Taking assumptions to describe the water consumption in outside basins is therefore inescapable. However, the presented assumptions (based on water stress free agriculture) are unrealistic and misplaced in scale. Ideally, the river in other river basins should also be included explicitly. Limits on consumption can be imposed to protect downstream countries. If this is not possible due to a lack of data for a river basin, the available water resources for hydropower and use in specific irrigation areas can be described on the basis of the historical availability, adjusted for the prevailing climate conditions.

Isolating a particular region from the global world also presents difficulties in describing trade. In the current methodology, all external product trade is described as if it comes from one externally located country, and external electricity import is not feasible. This assumption does not account for the global specialization and the related variation in trade distances. In the further development of the general nexus research domain, a method will have to be developed with which this global variability in food production and electricity can be used to externally force the trading system in national or regional nexus studies, such that, in addition to the geographical location, the trade routes used and transport forms (e.g. shipping and trucking) can be included.

5.2.2. Included balances and interlinkages

Because of the broad range of issues that can be studied with a nexus methodology, there are multiple variants with more or less nodes and interlinkages [Liu et al., 2017]. Growing the nexus model in terms of nodes and hard linkages (in which the factors from one balance are endogenous to other balances) makes the system more consistent, comprehensive and relevant for a wider range of administrative challenges, but inevitably increases complexity in the nexus model [Bleischwitz et al., 2018]. The presented methodology uses a three node nexus framework and includes a water, energy and food balance. Although the current setup is already suitable to study climate, socio-economic and structural pathways, and certainly to study the importance of spatial and temporal integration of conveyance infrastructure, some considerations are presented that may be relevant for the further development of the system.

Due to the inclusion of the hydro-economic approach, the three node nexus presented is strongly water centred. For a fully comprehensive approach of future policy, it is important that the system is balanced with an equal emphasis on all balances. In the current setup this can already be achieved by adding some missing linkages between the energy and food nodes. These linkages are necessary to describe the use of food resources in the energy balance (e.g. biofuels) and the use of energy resources in the food balance (e.g. agricultural machinery requirements and fertilizer production). To enable the latter, the electricity demand will no longer have to be described as static data, but as a demand depending on the industry, agriculture and population present.

Besides adding missing linkages, there are also benefits to be gained by expanding the existing balances. In line with other scholars [Obersteiner et al., 2016; Ringler et al., 2013; Bleischwitz et al., 2018], land resources are seen as a vital addition in future model representations. After all, land resources play a key role in hydrology, livelihoods, agriculture and basin development. The recognition of these processes in relation to the other balances is important for a comprehensive description. After all, the conversion from naturally occurring landuse to anthropogenic landuse entails disadvantages as well as advantages. Because the advantages are easier to describe than the disadvantages, the impact of land use changes is often ignored. In this way, not only the environment and ecological impact, expressed as a decrease of ecosystem services delivered, is overlooked, but also social and culture values associated with this landuse. A case example of the latter concerns the construction of the controversial Dal and Kajbar dam. It is feared that the construction of these reservoirs and the associated submergence and population displacement will be at the expense of the Nubian culture and give rise to new domestic conflicts [Hashim, 2014].

Recognizing the economic value of these natural, social and cultural uses is crucial for the further expansion of the models. Certainly the intended future expansion, in which the construction of new infrastructure and the accompanying change in land use will also be added as an optimization variable, cannot proceed without the implementation of social, hydrological and environmental trade-offs at different geographical locations. Without these environmental and social values, it is not possible to determine where agricultural expansion or the construction of new conveyance infrastructure would possible and desirable. This knowledge is also required to enable an improved implementation of animal husbandry. On the one hand to guarantee the continued existence of the nomadic culture, which has been pressured by the expansion of agricultural land, and on the other to prevent unrealistic expansion of livestock farming at the available grazing lands.

In general, the named linkages are difficult to describe and quantify in economic terms. With the increasing use of the nexus framework, it is therefore increasingly important that more specific research is conducted into describing these interlinkages and quantifying the economic costs and benefits of ecosystem and cultural services. Preferably, these relationships are described with hard linkages. However, in order to avoid unnecessary complexity, e.g. when describing runoff relationships with hydrological models, it will be necessary to shift to more rule-based or soft linkages.

5.2.3. Academics versus real world applications

It is important to remember that the results of this study (and nexus studies in general) are the result of optimal and efficient scenarios, which do not account for socio- and political relations (e.g. preferable trade partners). Moreover, the objective used in this study - maximizing the national benefits - ignores the specific actions of individual agents. It is a top down approach where each agent is expected to act in national interest. If model findings were not only used for identification of inefficiences and potential gains, but were directly converted into national policy, this would require the presence of a strong socialist political system. However, other model objectives imply different political systems. The results of such model studies should therefore not be seen as a detailed thread for policy implementation. It is possible that second- or third-best options are preferable over the absolute optimum found.

Moreover, despite every member state benefitting economically, not all proposed solutions are equally beneficial for the riparian states. In the trade information scenarios, for example, Ethiopia must share information without benefiting from it itself. In the coordination scenario, Sudan, on the other hand, loses income in relative terms. It is therefore uncertain whether riparian states will agree to the proposed scenarios. A game theoretical approach is required to study whether the proposed solutions are Nash equilibriums, and therefore stable for regional implementation.

Although this study is aimed at influencing national and international policy, policy-making organizations were not included in the analysis. To ensure that the results of a nexus study are actually used for policy matters, a different study approach is needed. It is vital that policy makers and stakeholders are involved at an early stage. The development of a flexible model study must take place in an interactive environment where, through communication, learning and mutual trust, expertise is exchanged and joint decisions are made on the study objectives, allowed trade-offs and simulation techniques. Only in this way can trust and information be gained with which a more detailed and more site specific study can be carried out.

5.2.4. System implementation assumptions

5.2.4.1. Water balance

Three aspects deserve more attention within the water balance. First the constrained reservoir level at the end of a single MPC horizon require more consideration. This constraint must ensure that the reservoir at the end of the horizon does not become too empty. The constraint itself is performing well, but setting the boundary is problematic. Existing rule curves, if already available, are not applicable because they have been developed for an individual infrastructure combinations (e.g. one reservoir with downstream field) and not for a cooperative system. However, the proposed method for determining the rule curves, in which the optimal annual recurring reservoir level is sought by use of a soft constraint over a longer optimization, is computationally too expensive (as the future simulation was not able to converge within a week time). It will have to be examined how the presence of this constraint influences the results, especially with changing optimization horizons. If there is a significant positive difference, it will have to be investigated whether the rule curves can be computed otherwise, or whether another method should be used to value to the remaining reservoir storage.

The river flow is in Section 3.2.1.1 described using a simple routing model that only requires three characteristics per river segment. When working with large model timesteps (order of one month), the impact of the method used is expected to be small. However, it should be investigated for which spatial and temporal river scales it is better to use other more complex routing mechanisms. Due to the linear relationship of the outflow with the inflow and storage, the limited required river specific data and the minimal number of required optimization variables, the Muskingum method is an obvious choice. Besides the routing, the river losses also require some attention. In this study, a fixed loss by seepage and evaporation was used per river segment. However, these evaporation and seepage losses depend on the specific geology, river flow and the prevailing climate conditions.

Sediment flows are not included in the scope of this project, but should be included in future studies. Especially when looking over longer periods of time, sediment management is relevant for the life time of the reservoirs. To avoid unnecessary complexity, a rule-based implementation based on actual or best performance measures is being proposed instead of an implementation using river sediment dynamics.

5.2.4.2. Food balance

The yield response factor (used to describe the sensitivity of the crop yield to water stress and introduced in Section 2.2) captures many biological, physical and chemical processes that influence the relationship between production and water use by a crop. The response factor is crop specific and varies over the growing season. In general, crops are most sensitive to water stress in the flowering and yield formation stages, and less sensitive in the vegetative and ripening stages [Steduto et al., 2012]. However, the proposed model methodology works with a fixed yield response factor for the entire growing season. In the areas where sufficient water quantities are available all year round, the impact of such an assumption is small. However, in areas where significant deficit irrigation takes place, depending on the time of the growing season, this may result in an overestimation or underestimation of the agricultural yield.

The actual evapotranspiration depends on the amount of water available in the root zone of the plant (see Section 2.2). The root zone storage or subsurface storage for plant uptake is however not included in the agricultural description. Instead, it is assumed that the plant uptake, up to an upper limit equal to the potential evapotranspiration, is equal to the water supply per time step. As a result, each crop is actually at or below the wilting point. As long as the exact amount of water required is supplied, this has no influence on agriculture. However, as soon as there is a shortage that could have been put in storage beforehand - either by irrigation or by precipitation – the evapotranspiration and hence the yield is underestimated. Besides does, for a complete water stress free irrigated crop, the current implementation imply the existence of a continuous irrigation flow; and accounts therefore not for the existing infrastructural constraints. By creating a root zone, there is an additional storage capacity where water can be stored during high flow. Such storage is especially important for rainfed perennials, or generally when working with time steps shorter than a month. With the introduction of this storage, the cumbersome multi-time solution for the evapotranspiration constraint for perennials can be replaced. Although the implementation of a root zone will increase the number of optimization

variables, and hence the model complexity, it provides a more realistic description of agriculture that is more based on reality. Therefore, excluding this storage is worth rethinking.

The livestock breeding is indirectly implemented in the methodology using feed conversion efficiencies. Thereby, the major impact of this sector on the water balance is taken into account through animal feed production. However, in the current setup it is only possible to grow meat and dairy for national demand and not for regional or international trade purposes. For countries that are real world exporters, this results in a too low modelled net income. Enabling this trade can reveal other trade-offs within a country and within a region. However, before enabling livestock trade, the breeding should be limited in a realistic way, accounting for the available land and water resources.

As a final remark within the food balance, attention is drawn to possible improvements in agricultural classification and the description of perennial crops. Currently, all available agricultural land is classified as being fully irrigated or fully rainfed. This classification should be expanded to take intermediate forms, such as small scale farmers with ponds, into account. The current methodology regarding perennial crops allows, although it can be decided not to harvest certain areas for a year, a reduction of the occupation area only to take place when the average lifespan has expired. Because the yield of perennials depends on age of the tree, a model implementation with an age-dependent yield in which the occupation area can be reduced every season is preferable. By increasing this flexibility, the optimization itself can consider whether certain agricultural areas with perennials should be maintained, or whether they should be abandoned in order to promote other types of agriculture.

5.2.4.3. Energy balance

The national energy demand is currently specified as data in the methodology. Demand has thus been decoupled from population growth, GDP and existing industry. In addition, the interactions between price, demand and supply are lost, and the accessibility to the grid not taken into account. In contrast to the global product trade, where the local changes in the Eastern Nile basin will not significantly alter global trade prices, it is advised to build in price volatility for regional electricity trade in subsequent studies. This allows the price and demand to vary per time instance and per electricity (sub)grid. With such an implementation, the type of electricity generation can be explicitly accounted for. The lower price for renewable energy can then lead to a different form of cooperation, where, in addition to specialization within a sector, specialization between sectors can occur as well.

6 Conclusion

6.1. Case study

This case study aimed to describe, qualitatively and quantitatively, the impacts and benefits of multiple forms of cooperation over unilateralism in the Eastern Nile basin, both under current and future climate and socio-economic circumstances. However, due to the numerical unreliable results in the future regionally coordinated scenario, in which all countries are disadvantaged by regional cooperation, this conclusion focuses mainly on the historical results.

The results indicate that a unilateral cooperative scenario with a top-down approach already would have been advantageous over the real world practices, and would have enabled Sudan and Egypt to generate incomes with the available resources. With increasing levels of cooperation, the basin wide benefits would have increased monotonically. Moreover, despite the significant differences in relative benefits, there are no scenarios with significant deterioration in net benefits in specific riparian states. Over the twenty-year period, the flow-information, trade-information and regional coordination scenarios could have resulted in savings of approximately $32 billion, $37 billion and $50 billion respectively in the region.

Historically, the added value obtained by sharing flow information would have been by far the greatest. Sharing flow information would have allowed Sudan to use the available water resources more effectively. Total consumption would have increased and deficit irrigation decreased. Because Egypt would have been able to create more value with its agricultural land resources despite the decrease in total allocated water, sharing of flow information also appears to have been beneficial for Egypt. Sudan could have benefited relatively most from this form of cooperation, but it is Egypt that would have created with $19 billion most additional value. Moreover, for Sudan this income would have been strongly related to the availability of perfect climate forecasts in Ethiopia.

Sharing information about expected exports and required energy imports would have resulted in changes in both product and electricity trade flows, resulting in a decrease in transport costs and minor changes in crop composition and fuel mix. However, the additional benefits of $5 billion that would have been generated by sharing this type of information in the first following time step are small compared to the benefits of sharing flow information.

Under further cooperation, a clear redistribution of water resources within and across the states would have been accompanied by an emerging specialization in crop production. The result would have been a regional increase in water productivity and a decrease in product transport costs. Every country could have benefited quantitatively from this far-reaching form of cooperation, but the extent varies significantly across the states. In addition to these quantitative benefits, regional coordination would also have resulted in more qualitative benefits. The redistribution of water resources over the surface water reservoirs would have resulted in a larger regional storage without growth in accompanying evaporation, increasing the resilience of the regional system against long lasting droughts. Moreover, when the riparian states did cooperate, the countries could have achieved the same degree of self-sufficiency with a smaller decrease in agricultural production value, i.e. the countries could have increased their resilience for price fluctuations in the external market at low costs by regional coordination of their resources. Trade-offs between the water consumption of agricultural and hydropower plants remained absent and unchanged in all scenarios.

Adverse effects do not occur historically with increasing levels of cooperation. However, caused by the decline in benefits in Sudan under regional resource coordination, there is not one scenario that is most beneficial for all states. In future experiments, where in the flow-information scenario an increase in water consumption in Sudan is at the expense of consumption in Egypt, conflicting interstate water use does occur.

6.2. Methodology

This study has overall aimed to address the shortcomings of both the current generation of WEF-nexus models and hydro-economic models in studying regional resource management by investigating the possibilities for, the relevance of and the challenges and difficulties associated with the explicit integration of both the spatial and temporal heterogeneity in resource availability, agro-climatic constraints, and socio-economic characteristics and the river and electric conveyance infrastructure in regional WEF-nexus models.

The historical case study in the Eastern Nile basin illustrates the possibility to formulate large nonlinear optimization problems with spatial and temporal variation in resource availability, climate drivers, agricultural feasibility, product demands and explicit integration of conveyance infrastructure and related constraints. The case showed that the proposed framework can account for spatial and temporal multisectoral trade-offs while finding non-trivial solutions for multiple forms of national and regional cooperative resource management. Moreover, despite the simplifications in the growth phases, the agricultural dynamics implemented shows actual agronomic behavior with a preference for irrigation shortage over the reduction of agricultural areas. In addition to a single optimization, the selected control approach proved to enable users to study optimal management practices not only in isolation, but in coherence with real world events.

The relevance and needs for the inclusion of these spatial and temporal variations is apparent from the historical case study. The operational choices that introduce shifts in food production (specialization), changes in (deficit) water allocation for hydropower and agriculture and modified operations of new river infrastructure indicate, as well as the diversity in water productivity, that inadequate inclusion of this variability results in incomplete and potentially incorrect conclusions.

However, the implementation of this spatial and temporal variability comes with some challenges. The collection of a coherent set of data and the decisions required for the associated assumptions and simplifications remain the major difficulty when buidling these models. Related to this is the problem of choosing appropriate scales and dilineating system boundaries. Due to gaps in the available data, not all processes (e.g. national electricity transmission, flow in outside basins and crop management) can be described at sufficient detail, causing spatial variability to be lost. Apart from deciding on the included processes and collection of reliable data, the formulation of the proposed nexus based reservoir optimisation problems are highly nontrivial, resulting in large and numerically difficult to solve non-convex optimisation problems.

Non-trivialities arise when describing processes on different time scales (e.g. crop seasons and the difference between annuals and perennial crops), when keeping the problem feasible in case predictions deviate from real events (e.g. the hedging zone and possible reduction of crop area) and when implementing non smooth complementarity problems. Complementary problems arise when describing the flow over the spillway and when limiting the turbine flow during the reservoir filling process. The former can be successfully circumvented by describing it as a soft constraint where all spill flow is penalized with a value greater than the downstream production value. The non-linear soft constraint used to circumvent the latter compementarity constraint shows good performance in the historical and future unilateral scenarios, but the interaction between these constraints when multiple upstream-downstream connected reservoirs are filled complicates the search space resulting in convergence to local minima.

7
Future research

Based on found limitations in the results and the shortcomings mentioned in the discussion, some recommendations are presented for future research. The recommendations for future research presented in this section gradually transition from adjustments to additions to the proposed methodology.

A first step in future research is to investigate the model behaviour in the future simulation experiments. By implementing new surface water reservoirs pre-filled into the model, the soft constraints (used to work around the complementarity problem) for filling the reservoir can be avoided. Although the water balance is no longer closed with such an implementation, this can provide insight into the model behaviour. If this confirms the conclusion that the local minima are caused by the implementation of complimentary constraints as soft constraints, one could opt to solve this problem with a more sophisticated scaling of the objective function, or reconsider the soft constraints and opt for a hierarchical and multi stage optimisation approach. If this is not the problem, the model complexity will need to be reduced while preserving sufficient dynamics for optimisation purposes. This requires a new trade-off between completeness and complexity. If necessary, a potential first step could be to reduce the number of products per food group and the associated agricultural areas and trade fluxes.

At the same time, further research into the robustness of the system can be performed on the historic models. It is advised to perform a systematic sensitivity analyses on the settings for the optimization horizon, the end-of-horizon storage and convergence criteria, and to use multi-start methods to further investigate the effects of local minima. It should also be studied whether information sharing over multiple timesteps in the trade-information scenario results in a movement towards the regional coordination scenario, and thereby yields an increase in the modest additional benefits of this scenario.

After completing the sensitivity study into the settings for the optimization, future research should focus on the assumptions and methods used in the simulation part of the model predictive control approach. The scope of this research is twofold. First of all, it will have to focus on improving the representation of real world practices in the simulation model when the occurring conditions deviate from the predictions used in the optimization, e.g. what happens when less water is available for irrigation, which crops will still receive water, and which crops not? In addition, it is recommended to study imperfect scenarios in addition to the perfect and efficient scenarios. Forcing simulations in future projections with unexpected events with a significant impact (shocks like the ongoing locust plague) can provide new insights into the robustness of the system and model [Taleb, 2007].

The first adjustments proposed to the system dynamics relate to the food balance. Firstly, it is recommended to collect data regarding the costs of seedlings and fertilizer. In addition, it is recommended to adjust the system dynamics in such a way that other forms of agriculture are possible (e.g. rainfed with ponds), the actual yields also depend on the amount of fertilizer applied, an early reduction of the by perennials occupied land is possible and water storage in the root zone becomes feasible. In addition to these changes in agriculture, the methodology can also benefit from a more realistic description of livestock farming. Explicit recording of the livestock numbers present, broken down between production forms (nomadic and mixed-systems) and use (meat and dairy), is a first step required to enable trade in animal products.

Secondly, adjustments should resolve the discussed problems with regard to the spatial scale. First, for a more realistic and small-scale description of agricultural management losses and electricity consumption, should the spatial scale be refined. A second change concerns the product trade. Ideally, a method would be developed to externally force the trading system in national or regional nexus studies that accounts for the length of the trade routes and the used transport forms (e.g. shipping and

trucking). A simpler alternative is to determine, based on historical trade information, which products originate where and what the associated transport costs were. With this knowledge an average transport price can be computed per product. A possible implementation of both the refinement and the external trade depend on the availability of consistent data.

When the electricity can be described on a finer spatial scale, it is proposed to change the implementation. In this new approach, the demand should no longer be described as data, but as a willingness to buy a certain amount of electricity for a given price. With such an implementation, where the demand curves vary between the existing sectors (e.g. domestic, industrial and agricultural) and the supply curve depends on the existing generation mix, further national and regional trade-offs, both within the electricity balance and between the resources balances, can be studied. This approach also recognizes existing power relations and overcomes shortcomings related to only geographic-based trading relationships. Moreover, this implementation is required to add infrastructure decisions in the optimization at a later stage.

By explicitly defining the electricity demand for agriculture, a second hurdle in the system dynamics has already been identified. A further extension of the method requires a more overarching approach, that not only focusses on interactions from the water balance, but also on interactions from and between other balances. When the missing linkages are included, a further extension of the balances used is advised. The addition of the land resources balance is initially necessary for a better description of nomadic livestock farming, which in turn is a necessity for allowing trade in animal products. Besides are the recognition of social and ecological values and the description of the feasible land uses a precondition for inclusion of infrastructural decisions in the optimization.

If this condition is met and the price volatility in the electricity market can be described, infrastructural decisions can be added in the optimization. Besides describing the impacts of new infrastructures on existing land uses (e.g. submersion) and the trade-offs with changing land uses, the lifespan of infrastructure must also be included in the methodology. For surface water reservoirs, this requires a (rule-based) description of the over-time remaining storage capacity. To enable the implementation of these infrastructural decisions, the non linear problem solver will have to be replaced by a mixed integer non linear problem solver.

As final extensions to the presented methodology, it is proposed to switch to a stochastic method and to include game theory. Inclusion of uncertainties in both climate and economic drivers may provide a more realistic and complete support tool for policy makers to devise robust plans. Inclusion of game theory may help to understand the behaviour of states in the cooperative game and to study the stability of the solutions found.

References

Abdelkader, A., A. Elshorbagy, M. Tuninetti, F. Laio, L. Ridolfi, H. Fahmy, and A. Hoekstra
2018. National water, food, and trade modeling framework: The case of egypt. *Science of the total environment*, 639:485–496.

Abdellatif, M.
2004. *Operation of Roseires and Sennar Dams Using Artificial Neural Network*. PhD thesis, Thesis.

Addis fortune
2018. electricity-export-generates-81-6m. *Addis fortune*. Accessed: 2020-06-10.

Adeloye, A. J. and Q. V. Dau
2019. Hedging as an adaptive measure for climate change induced water shortage at the pong reservoir in the indus basin beas river, india. *Science of the total environment*, 687:554–566.

AFDB
2012. Clean energy development in egypt. Technical report, The African Development Bank.

AFDB
2013. South sudan: An infrastructure action plan. Technical report, The African Development Bank.

Akol, P., R. Galla, S. Wanyonyi, D. Bosuben, and J. Rutandura
2016. Nile basin water resources atlas. Technical report, NBI.

Alessio, A. and A. Bemporad
2009. A survey on explicit model predictive control. In *Nonlinear model predictive control*, Pp. 345–369. Springer.

Ali, Y. S., A. E. E. Hayaty, and Y. A. Mohamed
. Modifying the operation rules of jebel aulia reservoir for higher reservoir levels.

Allen, R. G., L. S. Pereira, D. Raes, M. Smith, et al.
1998. Crop evapotranspiration-guidelines for computing crop water requirements-fao irrigation and drainage paper 56. *Fao, Rome*, 300(9):D05109.

Altamirano, M., A. van Bodegom, N. van der Linden, H. de Rijke, A. Verhagen, T. Bucx, A. Boccalon, and B. van der Zwaan
2018. Operationalizing the wef nexus: quantifying the trade-offs and synergies between the water, energy and food sectors: Dutch climate solutions research programme. Technical report, ECN.

Aquastat, F.
2005. A global information system on water and agriculture.

Araya, A., L. Stroosnijder, G. Girmay, and S. Keesstra
2011. Crop coefficient, yield response to water stress and water productivity of teff (eragrostis tef (zucc.). *Agricultural water management*, 98(5):775–783.

Arheimer, B., R. Pimentel, K. Isberg, L. Crochemore, J. Andersson, A. Hasan, and L. Pineda
2020. Global catchment modelling usingworld-wide hype (wwh), open data, and stepwise parameter estimation. *Hydrology and Earth System Sciences*, 24(2):535–559.

Arjoon, D., Y. Mohamed, Q. Goor, and A. Tilmant
2014. Hydro-economic risk assessment in the eastern nile river basin. *Water Resources and Economics*, 8:16–31.

Arjoon, D., A. Tilmant, and M. Herrmann
2016a. Sharing water and benefits in transboundary river basins. *Hydrology & Earth System Sciences*, 20(6).

Arjoon, D., A. Tilmant, and M. Herrmann
2016b. Sharing water and benefits in transboundary river basins. *Hydrology and Earth System Sciences*, 20(6):2135–2150.

Arruda, F. B. and M. A. Grande
2003. Fator de resposta da produção do cafeeiro ao déficit hídrico em campinas. *Bragantia*, 62(1):139–145.

Asress, M. B., A. Simonovic, D. Komarov, and S. Stupar
2013. Wind energy resource development in ethiopia as an alternative energy future beyond the dominant hydropower. *Renewable and Sustainable Energy Reviews*, 23:366–378.

Awad, A. and I. Yossof
2016. Electricity production, economic growth and employment nexus in sudan: A cointegration approach. *International Journal of Energy Economics and Policy*, 6(1):6–13.

Awad Sahil, O.
2005. Nutrition country profile: Republic of sudan. Technical report, Food and Agricultural Organization of the United Nations.

Awulachew, S. B., M. McCartney, T. S. Steenhuis, and A. A. Ahmed
2009. *A review of hydrology, sediment and water resource use in the Blue Nile Basin*, volume 131. IWMI.

Bachewe, F. N., B. Minten, F. Tadesse, and A. S. Taffesse
2018. *The evolving livestock sector in Ethiopia: Growth by heads, not by productivity*, volume 122. Intl Food Policy Res Inst.

Bashar, K. E. and M. O. Mustafa
2009. Water balance assessment of the roseires reservoir. *Improved Water and Land Management in the Ethiopian Highlands: Its Impact on Downstream Stakeholders Dependent on the Blue Nile*, P. 38.

Bauer, N., K. Calvin, J. Emmerling, O. Fricko, S. Fujimori, J. Hilaire, J. Eom, V. Krey, E. Kriegler, I. Mouratiadou, et al.
2017. Shared socio-economic pathways of the energy sector–quantifying the narratives. *Global Environmental Change*, 42:316–330.

Bazilian, M., H. Rogner, M. Howells, S. Hermann, D. Arent, D. Gielen, P. Steduto, A. Mueller, P. Komor, R. S. Tol, et al.
2011. Considering the energy, water and food nexus: Towards an integrated modelling approach. *Energy policy*, 39(12):7896–7906.

Bekchanov, M., A. Sood, and M. Jeuland
2015. *Review of hydro-economic models to address river basin management problems: structure, applications and research gaps*, volume 167. International Water Management Institute (IWMI).

Berga, L., J. Buil, E. Bofill, J. De Cea, J. G. Perez, G. Mañueco, J. Polimon, A. Soriano, and J. Yagüe
2006. *Dams and Reservoirs, Societies and Environment in the 21st Century, Two Volume Set: Proceedings of the International Symposium on Dams in the Societies of the 21st Century, 22nd International Congress on Large Dams (ICOLD), Barcelona, Spain, 18 June 2006*. CRC Press.

Betts, J. T.
2010. *Practical methods for optimal control and estimation using nonlinear programming*, volume 19. Siam.

Bleischwitz, R., C. Spataru, S. D. VanDeveer, M. Obersteiner, E. van der Voet, C. Johnson, P. Andrews-Speed, T. Boersma, H. Hoff, and D. P. Van Vuuren
2018. Resource nexus perspectives towards the united nations sustainable development goals. *Nature Sustainability*, 1(12):737–743.

Block, P. and K. Strzepek
2010. Economic analysis of large-scale upstream river basin development on the blue nile in ethiopia considering transient conditions, climate variability, and climate change. *Journal of Water Resources Planning and Management*, 136(2):156–166.

Block, P. J.
2007. Integrated management of the blue nile basin in ethiopia: hydropower and irrigation modeling. Technical report.

Bodirsky, B. L., S. Rolinski, A. Biewald, I. Weindl, A. Popp, and H. Lotze-Campen
2015. Global food demand scenarios for the 21st century. *PloS one*, 10(11).

Bouwer, H.
1987. Effect of irrigated agriculture on groundwater. *Journal of Irrigation and Drainage Engineering*, 113(1):4–15.

Bradley, S. P., A. C. Hax, and T. L. Magnanti
1977. Applied mathematical programming.

Brouwer, C., A. Goffeau, and M. Heibloem
1985. Irrigation water management: Training manual no. 1-introduction to irrigation. *Food and Agriculture Organization of the United Nations, Rome, Italy*, Pp. 102–103.

Brouwer, R. and M. Hofkes

2008. Integrated hydro-economic modelling: Approaches, key issues and future research directions. *Ecological Economics*, 66(1):16–22.

Camacho, E. F. and C. B. Alba
2013. *Model predictive control*. Springer Science & Business Media.

Camberlin, P.
2009. Nile basin climates. In *The Nile*, Pp. 307–333. Springer.

Cascão, A. E.
2009. Changing power relations in the nile river basin: Unilateralism vs. cooperation? *Water Alternatives*, 2(2).

Celeste, A. B. and M. Billib
2010. The role of spill and evaporation in reservoir optimization models. *Water resources management*, 24(4):617–628.

Chang, F.-J., L. Chen, and L.-C. Chang
2005. Optimizing the reservoir operating rule curves by genetic algorithms. *Hydrological Processes: An International Journal*, 19(11):2277–2289.

Chinneck, J.
2015. Chapter 16: Introduction to nonlinear programming. *Practical Optimization: a Gentle Introduction*, Pp. 1–13.

Currie, J. and D. I. Wilson
2012. OPTI: Lowering the Barrier Between Open Source Optimizers and the Industrial MATLAB User. In *Foundations of Computer-Aided Process Operations*, N. Sahinidis and J. Pinto, eds., Savannah, Georgia, USA.

Daher, B. T. and R. H. Mohtar
2015. Water–energy–food (wef) nexus tool 2.0: guiding integrative resource planning and decision-making. *Water International*, 40(5-6):748–771.

de Condappa, D., A. Chaponnière, and J. Lemoalle
2009. A decision-support tool for water allocation in the volta basin. *Water International*, 34(1):71–87.

Di Baldassarre, G., M. Elshamy, A. van Griensven, E. Soliman, M. Kigobe, P. Ndomba, J. Mutemi, F. Mutua, S. Moges, Y. Xuan, et al.
2011. Future hydrology and climate in the river nile basin: a review. *Hydrological Sciences Journal–Journal des Sciences Hydrologiques*, 56(2):199–211.

Digna, R., M. Castro-Gama, P. van der Zaag, Y. Mohamed, G. Corzo, and S. Uhlenbrook
2018a. Optimal operation of the eastern nile system using genetic algorithm, and benefits distribution of water resources development. *Water*, 10(7):921.

Digna, R. F., Y. A. Mohamed, P. van der Zaag, S. Uhlenbrook, W. van der Krogt, and G. Corzo
2018b. Impact of water resources development on water availability for hydropower production and irrigated agriculture of the eastern nile basin. *Journal of Water Resources Planning and Management*, 144(5):05018007.

Dinar, A. and G. S. Nigatu
2013. Distributional considerations of international water resources under externality: The case of ethiopia, sudan and egypt on the blue nile. *Water Resources and Economics*, 2:1–16.

Ding, N., R. Erfani, H. Mokhtar, and T. Erfani
2016. Agent based modelling for water resource allocation in the transboundary nile river. *Water*, 8(4):139.

DIU
. Dams implementation unit: Merowe dam project. `http://www.merowedam.gov.sd/en/structure.html`. Accessed: 2020-06-08.

DoC
2016. Ethiopia: Power sector market. Technical report, U.S. depertment of commerce: commercial service.

Doorenbos, J.
1975. Guidelines for predicting crop water requirements. *Fao, Rome*, 24.

Doorenbos, J. and A. Kassam
1979. Yield response to water. *Irrigation and drainage paper*, 33:257.

Dorosh, P. and S. Rashid
2013. *Food and agriculture in Ethiopia: Progress and policy challenges*. University of Pennsylvania Press.

Duke, J. A.
1983. Handbook of energy crops. newcrops web site, purdue university.

Dumont, H. J.
2009. *The Nile: origin, environments, limnology and human use*, volume 89. Springer Science & Business Media.

EA
2020. Development of the ethiopian electricity sector – in a regional perspective. Technical report, Energy Analyses, Copenhagen.

EAPP
2014. Eapp regional power system master plan volume ii: Data report. Technical report, EAPP, EA energy analyses, Energinet.dk.

EAPP
2016. The easter africa power pool. `https://www.http://eappool.org/`. Accessed: 2020-02-02.

Earthscan and FAO
2011. *The state of the world's land and water resources for food and agriculture: Managing systems at risk*. Routledge.

ECSA
2015. Agricultural sample survey 2014-2015. Technical report, The Federal Democratic Republic of Ethiopia: Central Statistical Agency.

EEHC
2017. Annual report 2016/2017. Technical report, Arab Republic of Egypt Ministry of Electricity and Renewable Energy: Egyptian electricty holding company.

EEPco
2011. Ethiopian electric power corporation now and in de folliwing years. Technical report, Ethiopian Electric Power Corporation.

EEPco
2014. Power sector development: powering africa. Technical report, Ethiopian Electric Power Corporation.

EEPco
2017. Ethiopian electric power - facts in brief. Technical report, Ethiopian Electric Power Corporation.

EIA
2014. Country analysis brief: Egypt. Technical report, U.S. Energy Information Administration.

EIA
2018. Country analysis brief: Sudan and south sudan. Technical report, U.S. Energy Information Administration.

El Sayed, N.
2012. Egypt nutrition landscape analyses report. Technical report, Ministry for Primary HealtCare, Preventive Medicine and Family planning.

Elshamy, M., I. A. Seierstad, and A. Sorteberg
2009. Impacts of climate change on blue nile flows using bias-corrected gcm scenarios.

Endo, A., K. Burnett, P. M. Orencio, T. Kumazawa, C. A. Wada, A. Ishii, I. Tsurita, and M. Taniguchi
2015. Methods of the water-energy-food nexus. *Water*, 7(10):5806–5830.

EoS
2016. Energy report - ethiopia. Technical report, Embassy of Sweden, Addis Abeba.

EPRI, A.
2005. Transmission line reference book–200 kv and above. *Electric Power Research Institute*.

Erleben, K.
2013. Numerical methods for linear complementarity problems in physics-based animation. Technical report, University of Copenhagen.

ESI
2018. Regional motivation to develop south sudan's hydro power capacity. *ESI-africa*, (5).

FAO
2010. Nutrition country profiles. Technical report, Food and Agricultural Organization of the United Nations.
FAO
2011a. *" Energy-smart" food for people and climate: issue paper*. Food and Agriculture Organization of the United Nations.
FAO
2011b. Information products for nile basin water resources management. Technical report, Food and Agricultural Organization of the United Nations.
FAO
2014. The water-energy-food nexus: a new approach in support of food security and sustainable agriculture.
FAO
2015. Country profile – sudan. Technical report, Food and Agriculture Organization of the United Nations (FAO). Rome, Italy.
FAO
2016a. Country profile – egypt. Technical report, Food and Agriculture Organization of the United Nations (FAO). Rome, Italy.
FAO
2016b. Country profile – ethiopia. Technical report, Food and Agriculture Organization of the United Nations (FAO). Rome, Italy.
FAO
2017. Food balances (old methodology and population). http://www.fao.org/faostat/en/data/FBSH. Accessed: 21-04-2020.
FAO
2019. Wapor - the fao portal to monitor water productivity through open access of remotely sensed derived data. `https://wapor.apps.fao.org/home/1`. Accessed: 28-06-2019.
FAO
2020. Quastat - irrigated crop calendars. `http://www.fao.org/aquastat/en/databases/crop-calendar`. Accessed: 2020-09-06.
FAO and AGAL
2005. Livestock sector brief: Sudan. Technical report, Food and Agricultural Organization of the United Nations, Livestock Information Sector Analysis and POlicy Branch.
FAO and Aquastat
2015. Country profile - sudan. Technical report, Food and Agricultural Organization of the United Nations.
FAO and Aquastat
2016. Country profile - egypt. Technical report, Food and Agricultural Organization of the United Nations.
FAO and FPMA
2015. Food price monitoring and analysis, october 2015.
FAO, IDF, and IFCN
2014. World mapping of animal feeding systems in the dairy sector. *Food and Agriculture Organisation of the United Nations, the International Dairy Federation, the IFCN Dairy Research Network, Rome*.
FDRoE
2011. Ethiopia's climate-resilient green economy: Green economy strategy. Technical report, Federal Democratic Republic of Ethiopia.
FDRoE
2016. Growth and transformation plan ii. Technical report, Federal Democratic Republic of Ethiopia.
Feedipedia
2017. Animal feed resources information system.
Fischer, G., F. O. Nachtergaele, S. Prieler, E. Teixeira, G. Tóth, H. Van Velthuizen, L. Verelst, and D. Wiberg
2012. Global agro-ecological zones (gaez v3. 0)-model documentation.
Fischer, G., H. T. van Velthuizen, and F. O. Nachtergaele
2000. Global agro-ecological zones assessment: methodology and results.

Fitch, J. and I. Soliman
1981. The livestock economy in egypt: an appraisal of the current situation. Technical report.
Flammini, A., M. Puri, L. Pluschke, and O. Dubois
2014. *Walking the nexus talk: assessing the water-energy-food nexus in the context of the sustainable energy for all initiative*. FAO.
FTA
2014. Manager's guide to distribution costs. Technical report, Freight Transport Association.
Fujimori, S., T. Hasegawa, A. Ito, K. Takahashi, and T. Masui
2018. Gridded emissions and land-use data for 2005–2100 under diverse socioeconomic and climate mitigation scenarios. *Scientific data*, 5(1):1–13.
Gebre, A., D. Getachew, and M. McCartney
2008. Stakeholder analysis of the chara chara weir, lake tana. Technical report.
Gilbert, J.
2017. *General Equilibrium Analysis Part I: Introduction to CGE*. Utah State University.
Gomes, F. and M. Carr
2003. Effects of water availability and vine harvesting frequency on the productivity of sweet potato in southern mozambique. ii. crop water use. *Experimental Agriculture*, 39(1):39–54.
Goor, Q., C. Halleux, Y. Mohamed, and A. Tilmant
2010. Optimal operation of a multipurpose multireservoir system in the eastern nile river basin. *Hydrology and Earth System Sciences*, 14(10):1895–1908.
Gorinevsky
2005. *Model Predictive Control Part 1: The Concept*. Stanford University.
Gupta, R., H. Shankar, et al.
2015. Global energy observatory.
Gustavsson, J., C. Cederberg, U. Sonesson, R. Van Otterdijk, and A. Meybeck
2011. Global food losses and food waste.
Hamza, M. and R. A. El-Salam
2015. Optimum planting date for three sesame cultivars growing under sandy soil conditions in egypt. *American-Eurasian Journal Agricultural & Environment Sciences*, 15(5):868–77.
Hanks, R. J., R. W. Hill, et al.
1980. *Modeling crop responses to irrigation in relation to soils, climate and salinity.*, number 6. International Irrigation Information Center.
Harou, J. J., M. Pulido-Velazquez, D. E. Rosenberg, J. Medellín-Azuara, J. R. Lund, and R. E. Howitt
2009. Hydro-economic models: Concepts, design, applications, and future prospects. *Journal of Hydrology*, 375(3-4):627–643.
Harris, I., P. D. Jones, T. J. Osborn, and D. H. Lister
2014. Updated high-resolution grids of monthly climatic observations–the cru ts3. 10 dataset. *International journal of climatology*, 34(3):623–642.
Hasan, E., A. Tarhule, P.-E. Kirstetter, R. Clark III, and Y. Hong
2018. Runoff sensitivity to climate change in the nile river basin. *Journal of Hydrology*, 561:312–321.
Hashim, M. J.
2014. The political impact of damming the nile: the case of sudan, ethiopia and egypt. *Resources, Peace and Conflict in the Horn of Africa*, P. 229.
Hassaballah, K., A. Jonoski, I. Popescu, and D. Solomatine
2012. Model-based optimization of downstream impact during filling of a new reservoir: case study of mandaya/roseires reservoirs on the blue nile river. *Water resources management*, 26(2):273–293.
Hatch and Artelia
2015. Hydropower expansion plan and regional integration plan of south sudan into regional electricity grid – final report. Technical report.
Haugh, J. S., J. Thompson, J. Price, J. Brynda, and B. Holtham
2014. Federal guidelines for dam safety: Glossary of terms. Technical report, FEMA.
Hegazy, K.
2015. Egypt's energy sector: Regional cooperation outlook and prospects of furthering engagement with the energy charter. Technical report, Energy Charter Secretariat Knowledge Centre.
Herzog, R. and J. Keller
2011. Advanced control: An overview on robust control. Technical report, MSE.

Hill, R. W., R. J. Hanks, and J. L. Wright
1987. Crop yield models adapted to irrigation scheduling programs. In *Irrigation Systems for the 21st Century*, Pp. 699–706. ASCE.

Hira, N., F. Omondi, and D. Kakembo
2015. The roadmap to a fully integrated and operational east african power pool. Technical report, Deloitte.

Hmdan, M. I.
2015. Livestock feed resources and feed system in sudan. Technical report, Ministry of Livestock - Republic of Sudan.

Hoff, H.
2011. Understanding the nexus: Background paper for the bonn2011 nexus conference.

Hoff, H., C. Bonzi, B. Joyce, and K. Tielbörger
2011. A water resources planning tool for the jordan river basin. *Water*, 3(3):718–736.

Hogg, J. D. and J. A. Scott
2013. On the effects of scaling on the performance of ipopt. *arXiv preprint arXiv:1301.7283*.

IEA
2016. statistics data browser. https://www.iea.org/statistics. Accessed: 27-08-2019.

IMF
2020. Imf primary commodity prices. `https://www.imf.org/en/Research/commodity-prices`. Accessed: 2020-06-10.

IRENA
2018. Renewable energy outlook egypt. Technical report, International Renewable Energy Agency.

Jeuland, M.
2010. Economic implications of climate change for infrastructure planning in transboundary water systems: An example from the blue nile. *Climate change and Water Infrastructure*, 46.

Jiilu, J.
2015. Building collaboration between east african nations via transmissio interconnectors. Technical report, KETRACO.

John, E. and E. A. Yıldırım
2008. Implementation of warm-start strategies in interior-point methods for linear programming in fixed dimension. *Computational Optimization and Applications*, 41(2):151–183.

Johnson, N., P. Burek, E. Byers, G. Falchetta, M. Flörke, S. Fujimori, P. Havlik, M. Hejazi, J. Hunt, V. Krey, et al.
2019. Integrated solutions for the water-energy-land nexus: Are global models rising to the challenge? *Water*, 11(11):2223.

Johnston, R. M. and M. McCartney
2010. *Inventory of water storage types in the Blue Nile and Volta river basins*, volume 140. IWMI.

Kahsay, T. N., D. Arjoon, O. Kuik, R. Brouwer, A. Tilmant, and P. van der Zaag
2019. A hybrid partial and general equilibrium modeling approach to assess the hydro-economic impacts of large dams–the case of the grand ethiopian renaissance dam in the eastern nile river basin. *Environmental Modelling & Software*, 117:76–88.

Khan, M. I.
2013. Optimal water allocation for rice production under climate change. *School of Economics, La Trobe University: Thesis for Doctor Philosophy*.

Koussis, A. D.
2009. Assessment and review of the hydraulics of storage flood routing 70 years after the presentation of the muskingum method. *Hydrological sciences journal*, 54(1):43–61.

Koutsoyiannis, D., A. Montanari, H. F. Lins, and T. A. Cohn
2009. Climate, hydrology and freshwater: towards an interactive incorporation of hydrological experience into climate research. *Hydrological Sciences Journal*.

Krogt, V. d.
2008. Ribasim version 7.00. *Technical reference manual. Delft: WNM Deltares*.

Lanzer, E. A. and Q. Paris
1981. A new analytical framework for the fertilization problem. *American Journal of Agricultural Economics*, 63(1):93–103.

Lea, J. M.
2018. The google earth engine digitisation tool (geedit) and the margin change quantification tool (maqit)-simple tools for the rapid mapping and quantification of changing earth surface margins. *Earth Surface Dynamics*, 6(3):551–561.

Lehner, B., K. Verdin, and A. Jarvis
2006. Hydrosheds technical documentation, version 1.0. *World Wildlife Fund US, Washington, DC*, Pp. 1–27.

Lipinski, B., C. Hanson, J. Lomax, L. Kitinoja, R. Waite, and T. Searchinger
2013. Reducing food loss and waste. *World Resources Institute Working Paper*, Pp. 1–40.

Liu, J., H. Yang, C. Cudennec, A. K. Gain, H. Hoff, R. Lawford, J. Qi, L. d. Strasser, P. Yillia, and C. Zheng
2017. Challenges in operationalizing the water–energy–food nexus. *Hydrological Sciences Journal*, 62(11):1714–1720.

Liu, P., S. Guo, X. Xu, and J. Chen
2011. Derivation of aggregation-based joint operating rule curves for cascade hydropower reservoirs. *Water resources management*, 25(13):3177–3200.

Lugt, D.
2018. Operating sittaung's reservoirs: A two-stage model predictive control method for managing a multi-reservoir system for hydropower, irrigation and flood mitigation.

Luttikhuis, P.
2017. Van wie is het water van de nijl? *NRC*.

Luxemburg, W. and A. Coenders
2017. *Hydrological Processes and Measurements*. TU Delft.

Majnooni-Heris, A., A. H. Nazemi, A. A. Sadraddini, et al.
2014. Effects of deficit irrigation on the yield, yield components, water and irrigation water use efficiency of spring canola. *J Biol Environ Sci*, 5:44–53.

McKinney, D. C.
1999. *Modeling water resources management at the basin level: Review and future directions*, volume 6. Iwmi.

Mekonnen, M. M. and A. Y. Hoekstra
2010. *The green, blue and grey water footprint of farm animals and animal products*, volume 1. UNESCO-IHE Institute for water Education Delft.

Men, B., Z. Wu, H. Liu, Y. Li, and Y. Zhao
2019. Research on hedging rules based on water supply priority and benefit loss of water shortage—a case study of tianjin, china. *Water*, 11(4):778.

Mersha, A., W. Fekade, and A. James
2017. Eastern nile multi- sector investment opportunity analysis. Technical report, Eastern Nile Technical Regional Office.

MoERE
2019. Renewable energy targets. http://nrea.gov.eg/test/en/About/Strategy. Accessed: 27-08-2019.

Mohamed, Y. and M. Loulseged
2008. *The Nile Basin water resources: overview of key research questions pertinent to the Nile Basin initiative*, volume 127. IWMI.

Mondal, M. A. H., C. Ringler, P. Al-Riffai, H. Eldidi, C. Breisinger, and M. Wiebelt
2019. Long-term optimization of egypt's power sector: Policy implications. *Energy*, 166:1063–1073.

MoPMAR
2016. Sustainable development strategy: Egypt's vision 2030. Technical report, Arab Republic of Egypt Ministry of Planning, Monitoring and Administrative Reform.

Motlagh, M.
2018. *Prospects of Cooperation in the Eastern Nile Basin*. PhD thesis, Universitäts-und Landesbibliothek Bonn.

MoWE
2012. Scaling up renewable energy program ethiopia: Investment plan. Technical report, Federal Democratic Republic of Ethiopia: Ministry of Water and Energy.

MoWRE
2016. Sudan potentials , opportunities and challenges in energy field. Technical report, Republic of Sudan: Ministry of Water Resources and Electricity.

Muhammad, D., B. Misri, M. EL-Nahrawy, S. Khan, and A. Serkan
2014. Egyptian clover (trifolium alexandrinum) king of forage crops. *FAO, Regional Office for the Near East and North Africa, Cairo, Egypt*.

Mulat, A. G., S. A. Moges, and M. A. Moges
2018. Evaluation of multi-storage hydropower development in the upper blue nile river (ethiopia): regional perspective. *Journal of Hydrology: Regional Studies*, 16:1–14.

Müller-Mahn, D. and M. Gebreyes
2019. Controversial connections: The water-energy-food nexus in the blue nile basin of ethiopia. *Land*, 8(9):135.

Multsch, S., M. Elshamy, S. Batarseh, A. Seid, H.-G. Frede, and L. Breuer
2017. Improving irrigation efficiency will be insufficient to meet future water demand in the nile basin. *Journal of Hydrology: Regional Studies*, 12:315–330.

Munoz, G., F. Maraux, and R. Wahaj
2007. *Actual crop water use in project countries a synthesis at the regional level*. The World Bank.

Najarchi, M., F. Kaveh, H. Babazadeh, M. Manshouri, et al.
2011. Determination of the yield response factor for field crop deficit irrigation. *African Journal of Agricultural Research*, 6(16):3700–3705.

NBI
2012. State of the river nile basin. Technical report, Nile Basin Initiative.

New, M., M. Hulme, and P. Jones
1999. Representing twentieth-century space–time climate variability. part i: Development of a 1961–90 mean monthly terrestrial climatology. *Journal of climate*, 12(3):829–856.

Nigatu, G. and A. Dinar
2015. Environment and development economics. *Hydrology and Earth System Sciences*, 21:532–555.

Obersteiner, M., B. Walsh, S. Frank, P. Havlík, M. Cantele, J. Liu, A. Palazzo, M. Herrero, Y. Lu, A. Mosnier, et al.
2016. Assessing the land resource–food price nexus of the sustainable development goals. *Science Advances*, 2(9):e1501499.

Oudin, L., F. Hervieu, C. Michel, C. Perrin, V. Andréassian, F. Anctil, and C. Loumagne
2005. Which potential evapotranspiration input for a lumped rainfall–runoff model?: Part 2—towards a simple and efficient potential evapotranspiration model for rainfall–runoff modelling. *Journal of hydrology*, 303(1-4):290–306.

Pietrangeli, G., A. Bezzi, C. Rossini, A. Masciotta, and D. D'Alberti
2017. Design of grand ethiopian renaissance rcc main dam (h= 175m). *Hydropower & Dams*.

Portmann, F. T., S. Siebert, and P. Döll
2010. Mirca2000—global monthly irrigated and rainfed crop areas around the year 2000: A new high-resolution data set for agricultural and hydrological modeling. *Global biogeochemical cycles*, 24(1).

Rabah, A. A., H. B. Nimer, K. R. Doud, and Q. A. Ahmed
2016. Modelling of sudan's energy supply, transformation, and demand. *Journal of Energy*, 2016.

Rahbeh, M., D. Chanasyk, and J. Miller
2013. Modelling the effect of irrigation on the hydrological output from a small prairie watershed. *Canadian Water Resources Journal*, 38(4):280–295.

Ramanan, R. R.
2018. *Introduction to sustainability analytics*. CRC Press.

Rao, N., P. Sarma, and S. Chander
1988. A simple dated water-production function for use in irrigated agriculture. *Agricultural Water Management*, 13(1):25–32.

Rasul, G.
2014. Food, water, and energy security in south asia: A nexus perspective from the hindu kush himalayan region. *Environmental Science & Policy*, 39:35–48.

Rawlings, J. B.
2000. Tutorial overview of model predictive control. *IEEE control systems magazine*, 20(3):38–52.

Renard, C.
1997. *Crop residues in sustainable mixed crop/livestock farming systems*. International Crops Research Institute for the Semi-Arid Tropics.

Ringler, C., A. Bhaduri, and R. Lawford
2013. The nexus across water, energy, land and food (welf): potential for improved resource use efficiency? *Current Opinion in Environmental Sustainability*, 5(6):617–624.

Ringler, C., J. von Braun, and M. W. Rosegrant
2004. Water policy analysis for the mekong river basin. *Water International*, 29(1):30–42.

Salama, H. S. A.
2019. Yield and nutritive value of maize (zea mays l.) forage as affected by plant density, sowing date and age at harvest. *Italian Journal of Agronomy*, 14(2):1383.

Satti, S., B. Zaitchik, and S. Siddiqui
2015. The question of sudan: a hydro-economic optimization model for the sudanese blue nile. *Hydrology and Earth System Sciences*, 19(5):2275–2293.

Savenije, H.
2014. *Hydrologie 1 dictaat CTB2420*. TU Delft.

Savenije, H. H. and M. Hrachowitz
2017. Hess opinions catchments as meta-organisms–a new blueprint for hydrological modelling. *Hydrology and Earth System Sciences*, 21(2):1107–1116.

Shahin, M. M.
1985. *Hydrology of the Nile basin*, volume 21. Elsevier.

Sharad, K. J.
2020. *Introduction to reservoir operation*. NIH, Roorkee.

Shiferraw, A. and M. McCartney
2008. Investigating environmental flow requirements at the source of the blue nile river. Technical report.

Siam, M. S. and E. A. Eltahir
2017. Climate change enhances interannual variability of the nile river flow. *Nature Climate Change*, 7(5):350.

Solvers, F.
2016. Optimization and simulation user guide. *Frontline Systems Inc., Incline Village, Nevada*.

Spalding-Fecher, R., B. Joyce, and H. Winkler
2017. Climate change and hydropower in the southern african power pool and zambezi river basin: System-wide impacts and policy implications. *Energy Policy*, 103:84–97.

SSEC
2018. South sudan oil and power 2018: South sudan electric power development. Technical report, South Sudan electricity corporation.

Steduto, P., T. C. Hsiao, E. Fereres, and D. Raes
2012. *Crop yield response to water*, volume 1028. fao Rome.

Stevenson, J. and A. Debebe
2009. Hydro power in ethiopia - the staged construction of tekeze arch dam.

Stewart, J. I. and R. M. Hagan
1973. Functions to predict effects of crop water deficits. *Journal of the irrigation and drainage division*, 99(4):421–439.

Suttie, J. M.
2000. *Hay and straw conservation: for small-scale farming and pastoral conditions*, number 29. Food & Agriculture Org.

Swain, A.
2011. Challenges for water sharing in the nile basin: changing geo-politics and changing climate. *Hydrological Sciences Journal*, 56(4):687–702.

Taleb, N. N.
2007. *The black swan: The impact of the highly improbable*, volume 2. Random house.

Tatem, A. J.
2017. Worldpop, open data for spatial demography. *Scientific data*, 4(1):1–4.

Terink, W., P. Droogers, J. Van Dam, G. Simons, M. Voogt, and A. Ines
2013. Satellite based data mining to support egypt's agriculture. In *Industrial Conference on Data Mining-Workshops*, Pp. 171–180.

Thomas, H.
2003. Wto agreement on agriculture. the implementation experience. developing country case studies.

Tiitmamer, N. and J. G. Anai
2018. Transitioning to renewable energy: An analysis of energy situation in juba, south sudan.

Tilmant, A., G. Marques, and Y. Mohamed
2015. A dynamic water accounting framework based on marginal resource opportunity cost. *Hydrology and Earth System Sciences*, 19(3):1457–1467.

Tonamo, A.
2016. A review on cattle husbandry practices in ethiopia. *International Journal of Livestock Production*, 7(2):5–11.

Tournier, J.-P., T. Bennett, and J. Bibeau
2019. *Sustainable and Safe Dams Around the World/Un monde de barrages durables et sécuritaires: Proceedings of the ICOLD 2019 Symposium,(ICOLD 2019), June 9-14, 2019, Ottawa, Canada/Publications du symposium CIGB 2019, juin 9-14, 2019, Ottawa, Canada*. CRC Press.

Trading economics
2020. Ethiopia - gross oda aid disbursement for developmental food aid/food security assistance. `https://tradingeconomics.com/ethiopia/gross-oda-aid-\ \disbursement-for-developmental-food-aid-food-security-assistance\ \-dac-donors-total-current-us-wb-data.html`. Accessed: 2020-19-06.

Uçan, K., F. Kılı, C. Gençoğlan, and H. Merdun
2007. Effect of irrigation frequency and amount on water use efficiency and yield of sesame (sesamum indicum l.) under field conditions. *Field Crops Research*, 101(3):249–258.

UN Water
2008. Transboundary waters: sharing benefits, sharing responsibilities. *Thematic paper*, 20.

UNdata
. A world of information. `http://data.un.org/Default.aspx`. Accessed: 2020-06-08.

UNDP
2014. Promoting utility scale power generation from wind energy. Technical report, United Nations Development Programme.

US Department of Agriculture, A. R. S.
2019. Fooddata central.

Valin, H., R. D. Sands, D. Van der Mensbrugghe, G. C. Nelson, H. Ahammad, E. Blanc, B. Bodirsky, S. Fujimori, T. Hasegawa, P. Havlik, et al.
2014. The future of food demand: understanding differences in global economic models. *Agricultural Economics*, 45(1):51–67.

van den Boom, T. J. and T. Backx
2010. Model predictive control. *DISC Course, Lecture Notes*, 16.

van der Krogt, W. and H. Ogink
2013. Development of the eastern nile water simulation model. *Main Report*.

Van Ittersum, M. K., K. G. Cassman, P. Grassini, J. Wolf, P. Tittonell, and Z. Hochman
2013. Yield gap analysis with local to global relevance—a review. *Field Crops Research*, 143:4–17.

van Oldenborgh, G.
2002. Komt el niño er weer aan? *Meteorologica*.

Van Overloop, P.-J.
2006. *Model predictive control on open water systems*. IOS Press.

Verstraeten, W., F. Veroustraete, and J. Feyen
2008. Assessment of evapotranspiration and soil moisture content across different scales of observation. *Sensors*, 8(1):70–117.

Wächter, A.
2009. Short tutorial: getting started with ipopt in 90 minutes. In *Dagstuhl Seminar Proceedings*. Schloss Dagstuhl-Leibniz-Zentrum für Informatik.

Wachter, A. and L. Biegler
2006. On the implementation of a primal—dual interior point filter line search algorithm for large-scale nonlinear programming, mathematical programming. *Math. Program*, 106(1).
Wada, Y., M. Flörke, N. Hanasaki, S. Eisner, G. Fischer, S. Tramberend, Y. Satoh, M. Van Vliet, P. Yillia, C. Ringler, et al.
2016. Modeling global water use for the 21st century: Water futures and solutions (wfas) initiative and its approaches. *Geoscientific Model Development*, 9:175–222.
Ward, R. C. and M. Robinson
1967. Principles of hydrology. Technical report, McGraw-Hill New York.
Wayne, G.
2013. The beginner's guide to representative concentration pathways. skeptical science, version 1.0.
WB
2013. Republic of south sudan: Electricity sector strategy note for south sudan. Technical report, the World Bank.
WB
2017. Sudan power plants. https://datacatalog.worldbank.org/dataset/sudan-power-plants. Accessed: 28-08-2019.
WB
2019. World development indicators. https://datacatalog.worldbank.org/dataset/world-development-indicators. Accessed: 27-08-2019.
WB
2020. World bank commodity price data (the pink sheet). Technical report, the World Bank.
WFP
2012. Report on food security and nutrition in south sudan: How a new country can feed its people. Technical report, World Food Program.
Wheeler, K. and S. Setzer
2012. Eastern nile riverware planning model – final report. Technical report, Nile Basin Initiative.
Wheeler, K. G., M. Basheer, Z. T. Mekonnen, S. O. Eltoum, A. Mersha, G. M. Abdo, E. A. Zagona, J. W. Hall, and S. J. Dadson
2016. Cooperative filling approaches for the grand ethiopian renaissance dam. *Water International*, 41(4):611–634.
Whittington, D., J. Waterbury, and M. Jeuland
2014. The grand renaissance dam and prospects for cooperation on the eastern nile. *Water Policy*, 16(4):595–608.
Whittington, D., X. Wu, and C. Sadoff
2005. Water resources management in the nile basin: the economic value of cooperation. *Water policy*, 7(3):227–252.
Wolters, W., R. Smit, M. Nour El-Din, E. Sayed Ahmed, J. Froebrich, and H. Ritzema
2016. Issues and challenges in spatial and temporal water allocation in the nile delta. *Sustainability*, 8(4):383.
Yadav, S. S., D. McNeil, and P. C. Stevenson
2007. *Lentil: An ancient crop for modern times*. Springer.
Yihun, Y. M.
2015. *Agricultural water productivity optimization for irrigated Teff (Eragrostic Tef) in water scarce semi-arid region of EthiopiaAgricultural water productivity optimization for irrigated Teff (Eragrostic Tef) in water scarce semi-arid region of Ethiopia*. CRC Press/Balkema.
Zarfl, C., A. E. Lumsdon, J. Berlekamp, L. Tydecks, and K. Tockner
2015. A global boom in hydropower dam construction. *Aquatic Sciences*, 77(1):161–170.
Zhang, C., X. Chen, Y. Li, W. Ding, and G. Fu
2018. Water-energy-food nexus: Concepts, questions and methodologies. *Journal of Cleaner Production*, 195:625–639.

A

Data collection and processing

A.1. Climate forcing

A.1.1. Open water evaporation

The Penman-Monteith formula for reference evapotranspiration ET_p (Equation A.1) is derived from the Penman equation for open water evaporation E_0 (Equation A.2) by introducing a crop resistance factor in the denominator of the formula [Luxemburg and Coenders, 2017]:

$$ET_{\mathrm{p}} = \frac{\frac{\Delta \cdot R_{\mathrm{n}}}{\rho \cdot \lambda} + \frac{c_{\mathrm{p}} \cdot \rho_{\mathrm{a}}}{\rho \cdot \lambda} \frac{e_{\mathrm{s}} - e_{\mathrm{a}}}{r_{\mathrm{a}}}}{\Delta + \gamma \left(1 + \frac{r_{\mathrm{c}}}{r_{\mathrm{a}}}\right)} \tag{A.1}$$

$$E_0 = \frac{\frac{\Delta \cdot R_n}{\rho \cdot \lambda} + \frac{c_p \cdot \rho_a}{\rho \cdot \lambda} \frac{e_s - e_a}{r_a}}{\Delta + \gamma} \tag{A.2}$$

with Δ [kPa/°C] the slope of the saturation vapour pressure curve, R_n [J/s/m^2] the net radiation, ρ [kg/m^3] the density of water, λ [J/kg] the latent heat of vaporization, c_p [J/kg/°C] the specific heat of air at constant pressure, ρ_a [kg/m^3] the density of air, e_s [kPa] the saturation vapour pressure, e_a [kPa] the actual vapour pressure, γ [kPa/°C] the psychrometer constant, r_a [s/m] the aerodynamic resistance and r_c [s/m] the crop resistance [Allen et al., 1998]. Hence, the open water evaporation can be computed from the reference evapotranspiration using:

$$E_0 = ET_{\mathrm{p}} \frac{\Delta + \gamma \left(1 + \frac{r_{\mathrm{c}}}{r_{\mathrm{a}}}\right)}{\Delta + \gamma} \tag{A.3}$$

With the crop resistance for the grass reference surface being constant (70 s/m) in this formula, a spatial value is required for citep the slope of the saturation vapor pressure and the aerodyanmic resistance. On a monthly time scale, the slope of the vapour pressure is a function of the mean monthly temperature T_{month} [°C] computed as the mean of the monthly average daily minimum temperature T_{min} and the monthly average daily maximum temperature T_{max} [Allen et al., 1998]. The slope of the saturation vapour pressure curve is defined as:

$$\Delta = \frac{4098 \cdot \left(0.6108 \cdot \exp\left(\frac{17.27 \cdot T_{\mathrm{month}}}{237.3 + T_{\mathrm{month}}}\right)\right)}{(237.3 + T_{\mathrm{month}})^2} \tag{A.4}$$

The aerodynamic resistance is a function of the wind velocity at 2 m height U_2 [m/s]. Because the measurements of wind velocity in the CRU-CL1.0 dataset [New et al., 1999] are assumed to be at 10 m elevation, a conversion coefficient (computed as 0.7471) was used [Harris et al., 2014]. Assuming a constant crop height of 0.12 m [Allen et al., 1998], the aerodynamic resistance for the grass reference surface becomes:

$$r_{\mathrm{a}} = \frac{208}{0.7471 \cdot U_{10}} \tag{A.5}$$

A.1.2. Future evaporation

Future time series for the open water evaporation and the potential evapotranspiration are computed using temperature data obtained from Arheimer et al. [2020] following the FAO approach [Allen et al., 1998]. The changes in temperature are given for the monthly mean daily minimum and maximum temperature. Following the framework of the FAO, the new monthly minimum, maximum and mean temperature are all in °C given by:

$$T_{\text{max}} = T_{\text{max-old}} + T_{\text{max-change}} \tag{A.6}$$

$$T_{\text{min}} = T_{\text{min-old}} + T_{\text{min-change}} \tag{A.7}$$

$$T_{\text{month}} = \frac{1}{2} \cdot (T_{\text{max}} + T_{\text{min}}) \tag{A.8}$$

with $T_{\text{max-old}}$ the monthly mean daily maximum temperature in the reference month, and $T_{\text{max-old}}$ the monthly mean daily maximum temperature in the future month.

With changing maximum and minimum temperatures, the radiation fluxes and saturation vapor pressures change. Because monthly time steps are used, the new saturation vapor pressure can be computed with:

$$e_s = \frac{1}{2} \cdot (e_s(T_{\text{max}}) + e_s(T_{\text{min}}) \tag{A.9}$$

where:

$$e_s(T) = 0.6108 \exp\left(\frac{17.27 \cdot T}{T + 237.7}\right) \tag{A.10}$$

To compute the actual vapout pressure, it is assmued that the relative humidity (RH) remains unchaned with respect to the reference period. Hence, the actual vapout pressure is given by:

$$e_a = RH \cdot e_s \tag{A.11}$$

The net radiation is the difference between the net incoming short wave radiation R_{ns} and the outgoing long wave radiation R_{nl}:

$$R_{\text{n}} = R_{\text{ns}} - R_{\text{nl}} \tag{A.12}$$

The net short wave radiation depends on the reflectance (albedo) of the surface area α, the extraterrestial incoming short wave radiation R_{a} and the relative sunshine hours $\frac{n}{N}$ (or its opposite the cloud cover ratio CLD). The net shortwave radiation is given by:

$$R_{\text{ns}} = (1 - \alpha) \cdot R_{\text{s}} \tag{A.13}$$

with

$$R_{\text{s}} = (a_{\text{s}} + b_{\text{s}} \cdot \frac{n}{N}) \cdot R_{\text{a}} = (a_{\text{s}} + b_{\text{s}} \cdot (1 - CLD)) \cdot R_{\text{a}} \tag{A.14}$$

Because local calibration with real solar radiation was not possible, the recommended parameter values for $a_s = 0.25$ and $b_s = 0.5$ are used. The abedo $\alpha = 0.23$ for the reference surface area is used and the for the cloud cover is, just as for the relative humidity, assumed that this one remaind unchanged.

The longwave energy emission is proportional to the absolute temperature of the surface raised to the fourth power. This relation is expressed quantitatively by the Stefan-Boltzmann law. However, the net energy flux leaving the earth's surface is due to absorption and sky refectance less than given by the Stefan-Boltzmann law. As humidity and cloudiness play an important role, the Stefan-Boltzmann law is corrected by these two factors:

$$R_{nl} = \sigma \left(\frac{(T_{max} + 273.16)^4 + (T_{min} + 273.16)^4}{2} \right) \cdot (0.34 - 0.14\sqrt{(e_a)}) \cdot \left(1.35 \frac{R_s}{R_{so}} - 0.35 \right) \tag{A.15}$$

where:

$$R_{so} = (a_s + b_s) \cdot R_s \tag{A.16}$$

with σ the Stefan-Boltzmann constant and R_{so} the clear-sky solar radiation. The parameters values for the latter computation are the same as for the short wave radiation.

With the vapour pressures and net radiation known, the reference evapotranspiration and open water evaporation are computed with Equations A.1 and A.2. The required slope of the saturation vapour pressure and the aerodynamic resistance follow from Equations A.4 and A.5. For the latter it is assumed that the wind velocity remains unchanged compared with the reference period.

A.1.3. Discharge time series expansion

The historical discharge time series has been extended by supplementing for each year in the period 2003-2013, per subcatchment, the historical discharge event from the period (1960-2002) in which timing and amounts of precipitation and evaporation show the biggest similarity. The RMSE has been used as a measure of the similarity between the monthly precipitation and evaporation between a considered year and all historic years in the period 1960-2002. The year in which the summed RMSE of the precipitation and evaporation is the smallest is used to complete the time series for a specific inflow node. To minimize the influence of the hydrological memory, this operation was performed per hydrological year. The first month of a hydrological year has been determined per node as the month in which the annual discharge minimum occurs most frequently in the time series between 1990-2002. The mathemathical expression used to elongate the time series is, using of local variables and indices, given by:

$$Q_{s,j,t} = Q_{s,x,t} \qquad \text{where} \qquad RMSE_{s,x,j} = \min_i (RMSE_{s,i,j}) \tag{A.17}$$

where:

$$RMSE_{s,i,j} = \sqrt{\frac{1}{12} \sum_{t=1}^{12} \left(P_{r,s,i,t} - P_{f,s,j,t} \right)^2} + \sqrt{\frac{1}{12} \sum_{t=1}^{12} \left(ET_{r,s,i,t} - ET_{f,s,j,t} \right)^2} \tag{A.18}$$

with t the month index within a hydrological year, j the index for the hydrological year in the missing time series, i the index for the hydrological year in the reference time series, P_r and ET_r the monthly precipitation and evapotranspiration in the reference year and P_f and ET_f the monthly precipitation and evapotranspiration in the missing year.

A.2. River infrastructure

A.2.1. Future structural scenario

Because it is unclear when irrigated areas, run-of-the-river plants and surface water reservoir will come online in the future, a structural scenario has been created. This scenario is based on projections for expansion in hydropower capacity and irrigated land use, and is therefore an optimistic approach. A complete list with historic and future commissioning dates of the structures used in the node-link network this study is given in Appendix B.1.

With the exception of South Sudan, the projection presented in Section 2.1.5 is followed for the hydropwer plants. If the last years of the projection are missing, it is linearly extrapolated from the last part of the known projection, assuming that the hydropower fraction remains the same. This approach does not apply to South Sudan because for this specific country a timeline is presented in Hatch and Artelia [2015] with the development of the run-of-the-river plants on the White Nile. In the specific case of Ethiopia, where hydropower can also be generated outside the Nile basin, except for the reservoir currently under construction, all developments are taking place in the Nile basin. Despite the fact that the proposed scenario is largely arbitrary, it is attempted to use a systematic approach. Firstly, the reservoir and run-of-the-river plants that are currently under construction have been added, followed by the structures that are labeled as committed by EAPP [2014], followed by the reservoirs that are designated as candidates. In addition, it has been ensured that the development on a river branch is phased, so that the filling processes of surface water reservoirs do not overlap. Figure A.1 illustrates the hydropower capacities for the future experiments together with the projections for all riparian states.

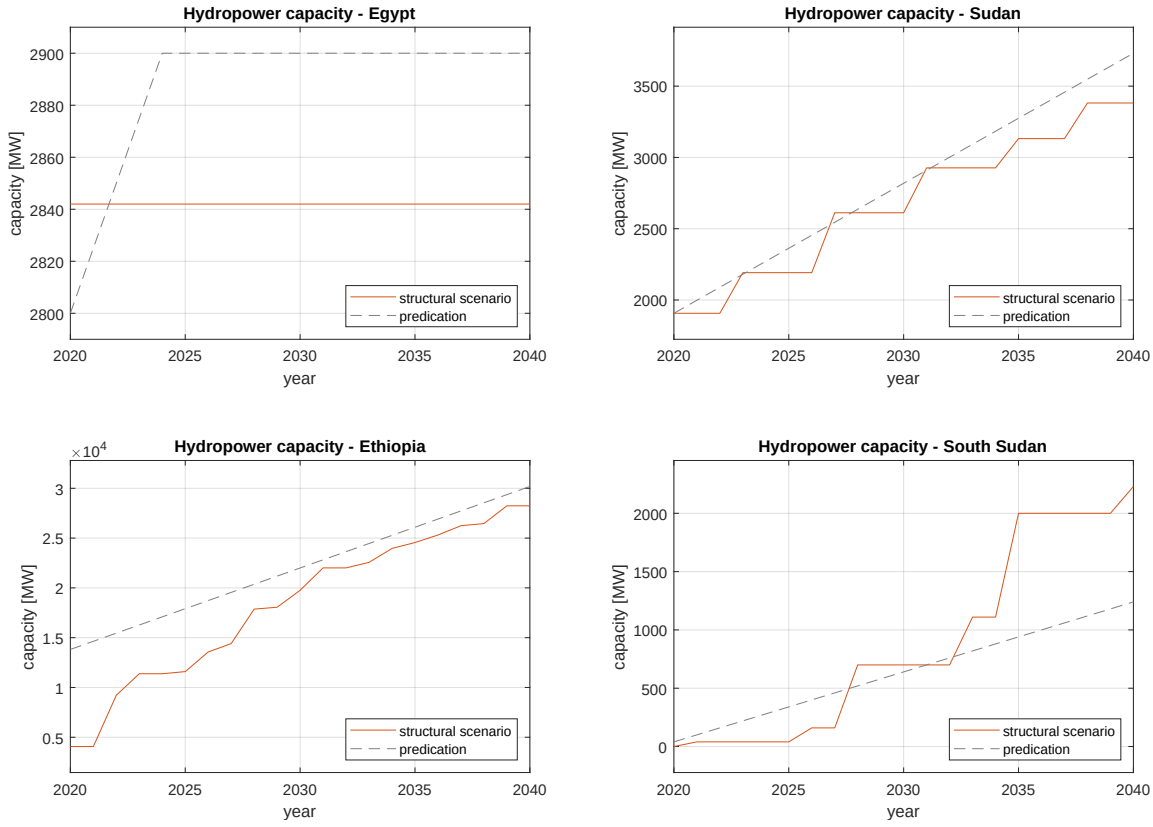

Figure A.1: The projection for the installed hydropower capacity as given in Section 2.1.5 together with the real installed capacities in the future simulation experiments for all riparian states.

The used projections for the irrigated area are obtained from Multsch et al. [2017]. Because this study expresses current and future quantities in harvested area, enable double counting, the areas are divided by the current cropping intensities. These are computed by dividing the current harvest areas by the

available irrigated area as mentioned in the FAOSTAT. To simulate the gradual occupation of new irrigation areas, it has been assumed that the surface area cultivated will linear increase in five years to full capacity. The moments an irrigation area comes online is linked to the moments the reservoirs come online. When a hydropwer plant comes online, the downstream irrigation area immediately follows. Conversely, when irrigation area comes online, the upstream surface water reservoir follows. In Figure A.2 the irrigation capacity is illustrated over the future years together with the projections for all riparian states.

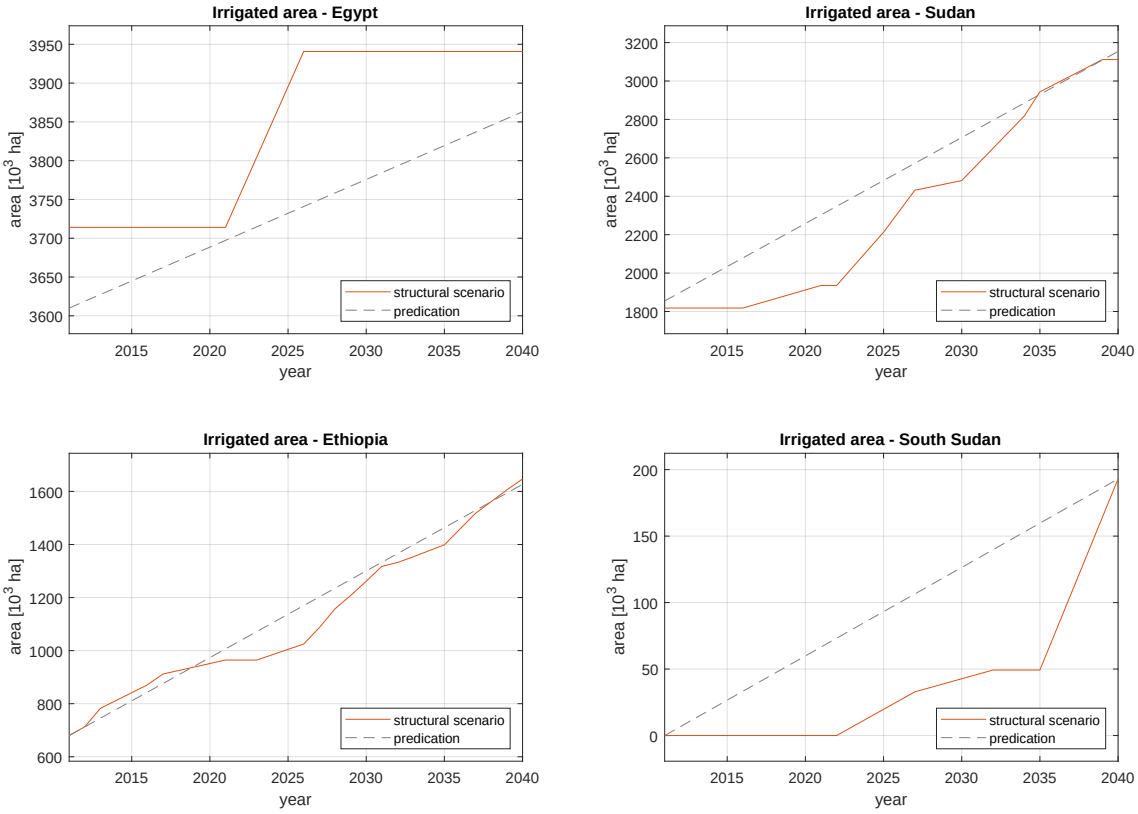

Figure A.2: The irrigation capacity for the riparian states in the future simulation experiments, together with the projections based on Multsch et al. [2017].

A.2.2. Gate capacities

Because the gate capacities are missing in the structural data obtained from van der Krogt and Ogink [2013], an estimate is made for the reservoirs whose capacity cannot be found in the literature. Using a Gumbel dsitribution, the return period of certain flood events was determined for 8 reservoirs with known gate capacities, based on the 103-year time series obtained from van der Krogt and Ogink [2013] (see Figure A.3).

The flood event with a 100 years return period is subsequently plotted against the gate capcities (see Figure A.4). The figure shows that reservoirs with a higher discharge during a 100 years flood event have a larger gate capacity. That the capacities do not correspond to a 100 year flood event can have various causes. Some obvious reasons are that the reservoirs may have been designed for a different design flood, the flood events have been determined at a shorter time interval than one month, and other data sets have been used. However, because most reservoirs have a larger gate capacity than follows from the 100 years of design flood, it is not the design flood itself, but the least square error fit between the known capacities and the discharge used to determine the capacities for the other reservoirs.

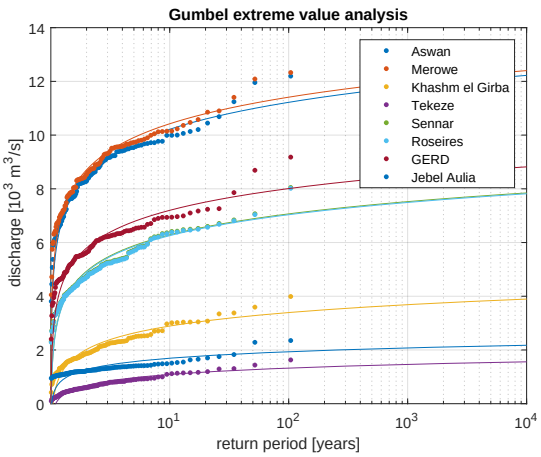

Figure A.3: The results of a Gumbel extremene analysis for eight reservoirs with gate capacities obtained from literature. The extreme analyses is performed on the maximum monthly flow occuring during a year. Data is obtained from van der Krogt and Ogink [2013].

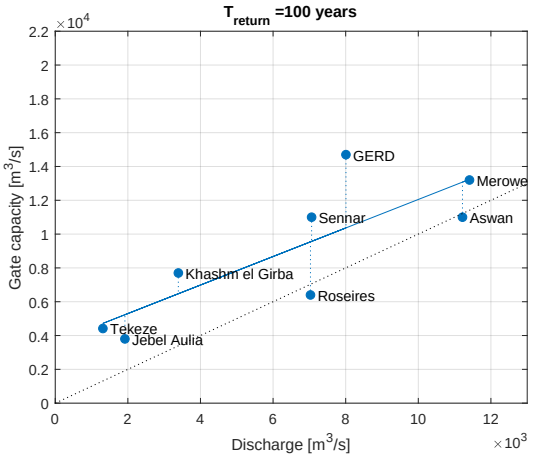

Figure A.4: The gate capacities voor eight reservoir plotted against the discharge during a 100 years flood event. The gate capacities show a clear increasing trend with increasing gate capacities, but most are larger than required based on this analysis.

A.2.3. Reservoir merging

When reservoirs are combined into a single node, a new storage-area-elevation relation is required. Because only irrigation reservoirs (without turbine) are merged, the elevation is nof no importance. For the relation between storage and surface area multiple forms are possible. The grey dots in Figure **??** indicate all possible surface areas for a specific storage caapcity in three individual reservoirs. If the assumption is made that all combined reservoirs empty at the same, the blue relation describes the new storage-area realtion.

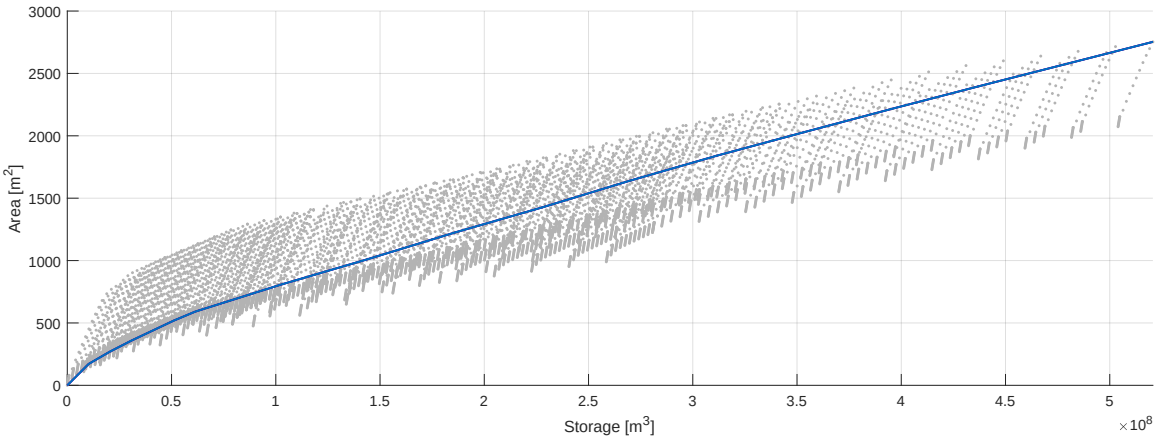

Figure A.5: The figure illustrates all possivle storage area combinations of three individual reservoirs. Based on the assumption that all combined reservoir empty at the same pace, the blue line illustrates the newly obtained surface-area relation.

A.2.4. River losses

The river evaporation and seepage losses for the majority of the river branches are computed using data from Whittington et al. [2005]. This study gives an indication of the fractions lost due to seepage and evaporation between the outflow from Lake Tana and the inflow into the Aswan High Dam (Figure A.6). Using the Eastern Nile RIBASIM model, for the same route is computed which fractions remain when only reservoir evaporation takes place. The difference between the two is defined as the river losses. When describing the difference at the Aswan High Dam with a homogeneous loss factor over the entire river length, a loss factor of 5% per 1000 km is found.

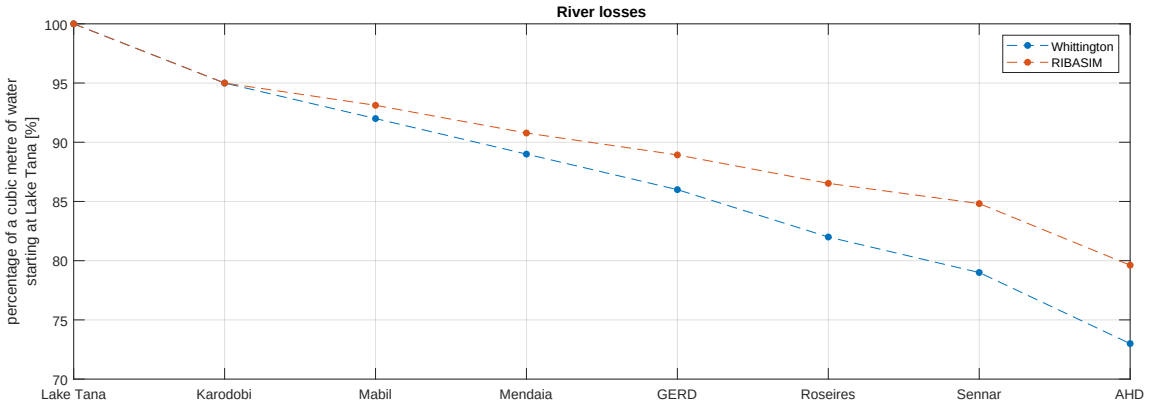

Figure A.6: The percentage of a cubic metre of water leaving Lake Tana at various stages during its downstream travel. The blue points correspond with the data obtained from Whittington et al. [2005] and account for seepage and evaporation losses. The orange points are computed with the RIBASIM model and only account for the evaporation losses.

A.3. Agriculture

A.3.1. Crop distribution

To describe the (initial) composition of the irrigated and rainfed agricultural sites, the crops are distributed in such a way that the modelled harvest area corresponds with data obtained from the FAOSTAT database. The distribution is done through an optimization process. Goal of this optimzization is to find at each agricultural site the annual sowing/planting areas δ_{A} that result in the smallest difference between the modelled harvest area and the data. The optimization process is constraint by the maximum area of a irrigation site, and the crop specific feasible area at a particulair site. The latter is introduced for agricultural sites outside the main basin, where the maximum crop area can, due to the clustering of individual sites with varying agro-climatric feasibilities, be smaller than the available area. For the irrigated sites, it is assumed that there is always sufficient water available, so that the prevailing climate conditions are not relevant. The optimization problem for these irrigated agriculture areas are mathematically expressed as:

$$\begin{aligned} \underset{\delta_{\mathrm{A},c,i}}{\text{minimize}} \quad & \sum_{g_{\mathrm{y},c,i}=T_{\mathrm{start}}}^{T_{\mathrm{end}}} \sum_{c\in\mathrm{C}} \left(A_{\mathrm{harv},c,i}^{g_{\mathrm{y},c,i}} - A_{\mathrm{data},c,i}^{g_{\mathrm{y},c,i}} \right)^2 \\ \text{subject to} \quad & \sum_{c\in\mathrm{C}} A_{\mathrm{harv},c,i}^{g_{\mathrm{y},c,i}^{k}} \leq A_{\mathrm{agri},i}^{g_{\mathrm{y},c,i}^{k}} \\ & A_{\mathrm{harv},c,i}^{g_{\mathrm{y},c,i}} \leq c_{\mathrm{feas},c,i} \cdot A_{\mathrm{harv},c,i}^{g_{\mathrm{y},c,i}} \end{aligned} \tag{A.19}$$

with i being used as a local index for both the irrigated sites within and outside the Nile basin, c_{feas} the fraction of the available agricultural area feasible to cultivate a specific crop and A_{data} the target harvest area obtained from the FAOSTAT database.

A similair optimization methodology applies to rainfed crops. However, in contrast to the optimization for irrigated agriculture, climate conditions are also accounted for. Only when the evaporation constraint is met a crop can be harvested in a specific rainfed pixel. For the annual crops, this means that the actual evapotranspiration must be greater than a fraction c_{min} of the potential evapotranspiration every month. For perennial crops, this requirement applies over a period of N_{per} months.

$$\begin{aligned} \underset{\delta_{\text{A},c,r}}{\text{minimize}} \quad & \sum_{g_{\text{y},c,r}=T_{\text{start}}}^{T_{\text{end}}} \sum_{c\in\text{C}} \left(A_{\text{harv},c,r}^{g_{\text{y},c,r}} - A_{\text{data},c,r}^{g_{\text{y},c,r}} \right)^2 \\ \text{subject to} \quad & \sum_{c\in\text{C}} A_{\text{harv},c,r}^{g_{\text{y},c,r}^{k}} \leq A_{\text{agri},r}^{g_{\text{y},c,r}^{k}} \\ & A_{\text{harv},c,r}^{g_{\text{y},c,r}} \leq A_{\text{feas},c,r}^{g_{\text{y},c,r}} \end{aligned} \tag{A.20}$$

where:

$$A_{\text{feas},c,r}^{g_{\text{y},c,r}} = \begin{cases} c_{\text{feas},c,r} \cdot A_{\text{harv},c,r}^{g_{\text{y},c,r}} & \text{if} \begin{cases} ET_{\text{a},c,r}^{g_{\text{n},c,r}} \geq c_{\text{min}} \cdot ET_{\text{p},c,r}^{g_{\text{n},c,r}} \;\forall\; g_{\text{n},c,r} = 1 : N_{\text{grw}} & \text{if } T_{\text{harv},c} = 1 \\ \sum_{\kappa=0}^{N_{\text{per}}-1} ET_{\text{a},c,r}^{g_{\text{n},c,r}-\kappa} \geq c_{\text{min}} \cdot \sum_{\kappa=0}^{N_{\text{per}}-1} ET_{\text{p},c,r}^{g_{\text{n},c,r}-\kappa} \;\forall\; g_{\text{n},c,r} = N_{\text{per}} : 12 \end{cases} \\ 0 & \text{otherwise} \end{cases} \tag{A.21}$$

A.4. Food balance

A.4.1. Food processing capacity

To determine a capacity from the actual food production, which shows large inter-annual differences and contains missing data points, a linear line is fitted. This line must be above all measured points, have a positive slope and have a minimal deviation from the measuring points. The slope and the initial offset of the line followe from the following minimization problem:

$$\begin{aligned} \underset{a,b}{\text{minimize}} \quad & \sqrt{\frac{1}{N}\sum_{k=1}^{N} \left(f(k) - d(k)\right)^2} \\ \text{subject to} \quad & f(k) \geq d(k) \\ & f(k) = a \cdot k + b \\ & a \geq 0 \end{aligned} \tag{A.22}$$

with d the avaialble production data, f the linear function with slope a and offset b and N the number of years in the time series. Two results of this analyses are depcitedin Figure A.7.

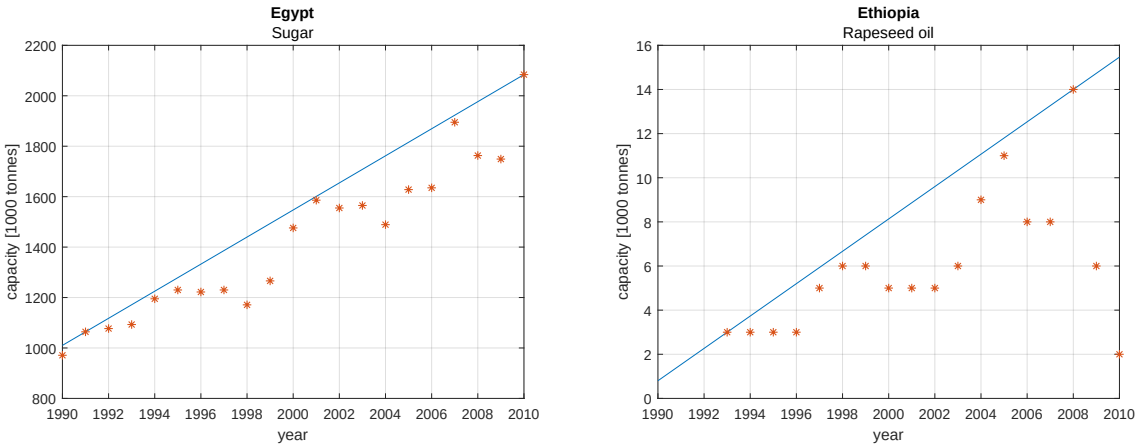

Figure A.7: The results of the lineair analyses for sugar processing in Egypt and rapeseed pressing in Ethiopia. The orange starts illustrate the data points obtained from the FAOSTAT food balace sheets, the blue line the linear function with the mean RMSE.

A.4.2. Product storage capacity

The product storage capacity is per prodct group derived from FAOSTAT data. It is defined as the difference between the maximum and minumum value in the cumulative sum of the storage changes between 1961 and 2010 as illustrated in Figure A.8

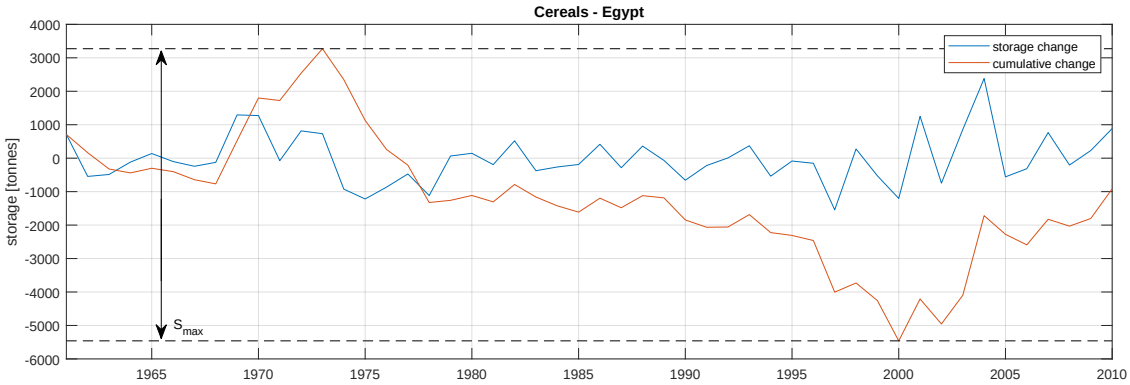

Figure A.8: Illustration of the methodology to determine the food storage capacity with an example for cereals in Egypt. The storage is defined as the difference between the maximum and the minimum of the cumulative sum over the stoarge changes as defined in the FAOSTAT food balance.

B Tables

B.1. Infrastructure commissioning dates

Table B.1: Commissioning dates for the river infrastructure used in this study. The numbers match with the node-link network illustrated in Figure 3.1. The nodes for sources and confluences are missing in this table. The years indicate when a specific feature of the structure comes online. The four features included are irrigation (I), surface water reservoir (R), run-of-the-river plants (RR) and an offtake (O).

Nr	I	R	O	RR	Country	Name
1	<1990				Egypt	Delta
2	<1990				Egypt	Assyut
3				2008	Egypt	Naga Hammadi
4	<1990				Egypt	Naga Hammadi
5				1993	Egypt	Esna Dam
6				1902	Egypt	Low Aswan Dam
7	2022	1970			Egypt	High Aswan Dam
9		2027			Sudan	Dal Dam
11		2038			Sudan	Kajbar Dam
13	2009				Sudan	Merowe
14		2009			Sudan	Merowe Dam
16	<1990				Sudan	Main Nile Pump Schemes
17				2023	Sudan	Dagash
19		2031			Sudan	Shereiq Dam
22	2023				Sudan	Upper Atbara
23	<1990				Sudan	New Halfa
24		1964			Sudan	Khashm El Girba Dam
26	2017				Sudan	Rumela
27		2017			Sudan	Upper Atbara dam complex
30	2028				Ethiopia	Humera
31		2028			Ethiopia	Humera Dam
33		2009			Ethiopia	Tekeze Dam (TK5)
35	<1990				Ethiopia	Small Scale
36		<1990			Ethiopia	Small Scale Dams
38	2100				Ethiopia	Metema
39					Ethiopia	Metema Dam
41	<1990				Sudan	Main Nile Khartoum Atbara
43		2035			Sudan	Sabaloka Dam

Nr	I	R	O	RR	Country	Name
46	<1990				Sudan	Blue Nile Pump Schemes
48	<1990				Sudan	Guneid Sugar + Gezira Managil
50	<1990				Sudan	Rahad
51	2035				Sudan	Rahad 2
54	2024				Ethiopia	Rahad III + Galegu
55		2024			Ethiopia	Galegu Dam + Rahad Dam
57	2026				Sudan	South Dinder
58			<1990		Sudan	
60	2033				Ethiopia	Lower Dinder
61		2100			Ethiopia	Lower Dinder Dam
63		2033			Ethiopia	Upper Dinder Dam
65					Ethiopia	Upper Dinder
66			2033		Ethiopia	
67	<1990				Sudan	E lSuki
69	<1990				Sudan	Sennar Sugar Scheme
71		1925			Sudan	Sennar Dam
72			<1990		Sudan	
73			<1990		Sudan	
75	2031				Sudan	Kenana
76	<1990				Sudan	Abu Naama Seleit Blue Nile PumpScheme
77		1966[1]			Sudan	Roseires Dam
79		2022			Ethiopia	Grand Renaissance Dam
82	2013				Ethiopia	Lower Beles + Upper Beles
83		2027			Ethiopia	Upper Beles Dam
84				2010	Ethiopia	Tana Beles
85	2027				Ethiopia	Dabus + Dale Bilutsu
87		2027			Ethiopia	Lower Dabus Dam
89		2035			Ethiopia	Upper Dabus Dam
91	2028				Ethiopia	Lower Dura Pump
93		2028			Ethiopia	Mendaia Down Dam
96		2031			Ethiopia	Lower Didessa Dam
99	2033				Ethiopia	Nekemte
100		2033			Ethiopia	Nekemte Dam
102	2035				Ethiopia	Dale + Anger
103		2035			Ethiopia	Aleltu Dam + Anger Dam
105					Ethiopia	Dimtu
108	2024				Ethiopia	Arjo Didessa + Hida + Wama + other
109		2023			Ethiopia	Negeso Dam + Upper Didessa Dam
111	2033				Ethiopia	Upper Dabana + Dabana
112		2033			Ethiopia	Upper Dabana Dam
114		2031			Ethiopia	Mendaia Up Dam
116		2034			Ethiopia	Mabil Dam
119					Ethiopia	Fettam
120					Ethiopia	Fettam Dam

Nr	I	R	O	RR	Country	Name
122		2037			Ethiopia	Beko Abo Dam
125	2039				Ethiopia	Middle B
126		2039			Ethiopia	Upper Birr Dam
129	<1990				Ethiopia	Fincha
130				2027	Ethiopia	Chemoga Yeda
131		1973			Ethiopia	Fincha'a Dam
133	2012				Ethiopia	Neshe + Nedi Amarti
135		2012			Ethiopia	Neshe Dam
138	2039				Ethiopia	Chemoga Kola
139		2039			Ethiopia	Chemoga Dam
141		2039			Ethiopia	Karadobi Dam
144					Ethiopia	Lower Guder Dam
146					Ethiopia	Upper Guder
147					Ethiopia	Upper Guder Dam
149				1964[2]	Ethiopia	Tis Abbay
150	1990				Ethiopia	Wonda + Yemosht + Seba + other
151	<1990	<1990	2010		Ethiopia	Lake Tana
154	2017				Ethiopia	Hod + Jigna + Beks + Mene + other
155		2017			Ethiopia	Gumera + Ribb + Megech Dam
157	2030				Ethiopia	Amri Plain + Gug And Insewi + other
159		2030			Ethiopia	Gigel Abai B. Dam
161					Ethiopia	Ambo Plain
163					Ethiopia	Gigel Abai A. Dam
165	2034				Ethiopia	Jemma
166		2034			Ethiopia	Jemma Dam
168	2008				Ethiopia	Koga
169		2008			Ethiopia	Koga Dam
171		1937[3]			Sudan	Gebal Aulia Dam
172	1990				Sudan	Hagar Asalaya + Sondos + other
173					Sudan	Kenana IV
174	2023				South Sudan	Malakal Rice
177	2025	2025			Ethiopia	Itang Dam + Gambela Dam
179		2030			Ethiopia	Tams dam
182		2025			Ethiopia	Geba R. Dam
184		2028			Ethiopia	Geba A. Dam
186		2033			Ethiopia	Birbir R.Dam
188		2036			Ethiopia	Birbis A.Dam
190		2026			Ethiopia	Baro II Dam
192		2039			Ethiopia	Baro I Dam
194				2038	Ethiopia	Genji
196	2036				Ethiopia	Gilo
197		2036			Ethiopia	Gilo III Dam

Nr	I	R	O	RR	Country	Name
199	1995				Ethiopia	Left Bank From Abobo
200		1995			Ethiopia	Abobo Dam
201	2031				Ethiopia	Alwero + Mey + Dumbong Dams
202		2031			Ethiopia	Dumbong Dam + Chiru Dam
204	2028				South Sudan	Fengco Jonglei
206	2036				South Sudan	Mangala
207				2028	South Sudan	Bedden
208				2026	South Sudan	Juba barrage
210				2033	South Sudan	Laki
212				2040	South Sudan	Shukole
214				2035	South Sudan	Grand Fula
215				2021	South Sudan	Fula rapid

[1] The Roseires dam is elevated with 10 meter in 2013
[2] The capacity of the Tis Abay run-of-the-river plant is expanded with 73 MW in 2001
[3] Hydropower turbines were installed in 2005 in the Jebal Aulia dam.

B.2. Crop characteristics

Table B.2: Crops and crop characteristics used in the case study in the Eastern Nile. The table contains the values for the yield factor K_y, the crop coefficients K_{cc}, the relative stage duration L and the dry mass percentage DM.

	K_y	$K_{cc,ini}$	$K_{cc,mid}$	$K_{cc,lat}$	L_{ini}	L_{dev}	L_{mid}	L_{lat}	DM [%]
Wheat	1,0	0,7	1,2	0,3	0,1	0,2	0,4	0,3	87,5
Maize	1,3	0,3	1,2	0,6	0,2	0,3	0,3	0,2	87,0
Rice	1,1	1,1	1,2	0,9	0,2	0,2	0,4	0,2	87,5
Sorghum	0,9	0,3	1,1	0,6	0,2	0,3	0,3	0,2	88,0
Millet	1,2	0,3	1,0	0,3	0,2	0,2	0,4	0,3	90,0
Barley	1,0	0,3	1,2	0,3	0,1	0,2	0,4	0,3	87,1
Teff	1,0	0,6	1,1	0,8	0,2	0,2	0,4	0,2	88,3
Cassava	1,1	0,3	1,1	0,5	0,4	0,1	0,3	0,2	35,0
Potato	1,1	0,5	1,2	0,8	0,2	0,2	0,3	0,2	25,0
Yams	1,1	0,5	1,1	1,0	0,3	0,3	0,3	0,1	35,0
Sweetpotato	1,1	0,5	1,2	0,7	0,1	0,2	0,4	0,2	30,0
Chickpea	1,2	0,4	1,1	0,5	0,2	0,3	0,3	0,2	100,0
Cowpea	1,2	0,4	1,0	0,4	0,2	0,3	0,4	0,2	100,0
Lentil	1,2	0,4	1,1	0,3	0,1	0,2	0,4	0,2	100,0
Bean	1,2	0,5	1,1	0,9	0,2	0,3	0,3	0,1	100,0
Tomato	1,1	0,6	1,2	0,8	0,2	0,3	0,4	0,2	12,5
Onion	1,1	0,7	1,1	0,8	0,1	0,2	0,5	0,3	12,5
Cabbage	1,0	0,7	1,1	1,0	0,2	0,4	0,3	0,1	12,5
Banana	1,3	0,7	0,7	0,7	0,2	0,3	0,3	0,3	21,9
Citrus	1,0	1,0	1,2	1,1	0,3	0,2	0,5	0,0	15,8
Cotton	0,9	0,4	1,2	0,7	0,2	0,3	0,3	0,3	100,0
Coffee	1,0	0,9	1,0	1,0	0,2	0,3	0,3	0,3	35,0
Sugarbeet	1,0	0,4	1,2	0,7	0,2	0,3	0,5	0,1	14,0
Sugarcane	1,2	0,4	1,3	0,8	0,1	0,2	0,6	0,2	10,0
Groundnut	0,7	0,4	1,2	0,6	0,3	0,3	0,3	0,2	67,0
Sesame	0,7	0,4	1,1	0,3	0,2	0,3	0,4	0,2	92,8
Sunflower	1,0	0,4	1,1	0,3	0,2	0,3	0,4	0,2	90,0
Soybean	0,9	0,4	1,2	0,5	0,1	0,3	0,4	0,2	90,0
Rapeseed	0,9	0,4	1,1	0,4	0,2	0,3	0,4	0,2	90,0
Alfalfa	1,1	0,4	1,2	1,2	0,2	0,3	0,3	0,2	19,9
Berseem	1,1	0,4	1,2	1,1	0,2	0,3	0,3	0,2	12,5
Sudangrass	0,9	0,5	1,2	1,1	0,3	0,3	0,2	0,1	20,8
Maizeforage	1,3	0,3	0,8	0,0	0,5	0,5	0,0	0,0	23,3

B.3. Crop management factor

Table B.3: National management factors for irrigated and rainfed agriculture.

	Irrigated			Rainfed	
	Egypt	Sudan	Ethiopia	Sudan	Ethiopia
Wheat	0,80	0,60	0,40		0,16
Maize	0,40	0,10	0,20	0,05	0,14
Rice	0,80	0,30	0,30		
Sorghum	0,50	0,20	0,30	0,04	0,15
Millet		0,20	0,10	0,06	0,27
Barley	0,30	0,30	0,40		0,16
Teff			0,50		0,30
Cassava	0,70	0,10	0,40	0,04	0,12
Potato	0,60		0,40	0,07	0,04
Yams	0,70	0,10	0,40	0,10	0,24
Sweetpotat	0,60	0,70	0,40	0,70	0,24
Chickpea	0,70	0,70	0,60		0,42
Cowpea	0,70	0,10	0,10	0,49	0,42
Lentil	0,90	0,90	0,80	0,63	0,64
Bean	0,60	0,80	0,30	0,64	0,27
Tomato	0,50	0,40	0,30	0,40	0,30
Onion	0,30	0,20	0,20	0,20	0,20
Cabbage	0,50		0,30		0,30
Banana	0,90	1,00	0,20	1,00	0,20
Citrus	0,40		0,20	0,30	0,20
Cotton	0,60	0,40	0,30	0,40	0,30
Coffee			0,20		0,20
Sugarbeet	0,90				
Sugarcane	0,80	0,80	0,90	0,80	0,90
Groundnut	0,50	0,30	0,20	0,15	0,18
Sesame	0,70	0,30	0,50	0,09	0,30
Sunflower	0,70	0,40	0,20	0,24	0,18
Soybean	0,40	0,60	0,60	0,12	0,24
Rapeseed	0,70		0,20		0,16
Alfalfa	0,60	0,20	0,40	0,08	0,24
Berseem	0,50	0,20	0,30		0,18
Sudangrass	0,70	0,30	0,40	0,06	0,20
Maizeforage	0,50	0,10	0,30	0,05	0,21

B.4. Crop specialisation

Table B.4: Irrigated crop production in the unilateral scenario in Egypt and percentage change in the other cooperation scenarios.

	Unilateral [10^3 ton]	Flow information [%]	Trade information [%]	Coordination [%]
Wheat	1443,3	29,8	0,0	15,3
Maize	1,6	105,4	10,3	137,5
Rice	8540,4	-17,3	-17,2	11,5
Sorghum	1,5	91,6	-3,0	143,6
Millet	0,0	0,0	0,0	0,0
Barley	41971,6	-30,7	-31,3	6,0
Teff	0,0	0,0	0,0	0,0
Cassava	541222,7	2,5	2,8	-1,0
Potatoes	18903,1	9,1	10,3	98,5
Yams	0,7	2,9	56,9	552,9
Sweet potatoes	103296,1	5,3	5,2	26,8
Chickpea	0,4	47,3	12,0	263,4
Cowpea	0,7	29,8	23,0	228,7
Lentil	0,3	28,1	-19,5	172,7
Bean	0,9	0,3	2,3	148,9
Tomato	247524,4	2,7	2,5	3,3
Onion	1848,0	17,7	14,4	229,8
Cabbage	64075,1	0,9	0,8	-4,0
Banana	937500,2	1,6	1,6	3,6
Citrus	85897,7	7,1	7,0	7,6
Cotton	0,2	36,3	-15,3	161,8
Coffee	0,0	0,0	0,0	0,0
Sugar beet	4,6	60,3	10,4	260,4
Sugar cane	28484,3	-0,4	-0,1	0,6
Sugar	0,0	0,0	0,0	0,0
Groundnut	14,6	-12,8	68,1	17,3
Sesame	0,7	29,8	12,1	147,9
Sunflower	0,8	38,8	27,3	245,4
Soybean	0,5	52,0	14,7	276,9
Rapeseed	0,7	48,1	15,4	272,7
Peanut oil	0,0	0,0	0,0	0,0
Sesame oil	0,0	0,0	0,0	0,0
Sunflower oil	0,0	0,0	0,0	0,0
Soybean oil	0,0	0,0	0,0	0,0
Rapeseed oil	0,0	0,0	0,0	0,0
Beer	0,0	0,0	0,0	0,0
Alfalfa	117967,5	-4,9	-4,9	26,8
Berseem	493670,9	-7,8	-7,2	-11,0
Sudangrass	226333,5	-5,8	-6,4	-34,1
Maizeforage	4996,5	66,7	54,5	-72,0

Table B.5: Irrigated crop production in the unilateral scenario in Sudan and percentage change in the other cooperation scenarios.

	Unilateral [10^3 ton]	Flow information [%]	Trade information [%]	Coordination [%]
Wheat	0,6	-52,3	-58,5	128,8
Maize	12,5	-75,9	-58,2	268,5
Rice	14279,9	11,9	12,1	-22,8
Sorghum	53,3	-72,5	-70,9	302,4
Millet	2811,4	-97,8	-97,6	-83,2
Barley	0,5	-55,0	-59,2	111,3
Teff	0,0	0,0	0,0	0,0
Cassava	7279,2	8,2	13,2	53,8
Potatoes	0,0	0,0	0,0	0,0
Yams	0,1	-53,4	-73,6	716,8
Sweet_potatoes	68649,1	13,8	14,1	9,3
Chickpea	0,4	-54,4	-58,9	169,8
Cowpea	2,4	-26,1	-11,2	52,2
Lentil	1,1	-59,6	-68,9	584,6
Bean	20,3	-25,2	-11,2	19,0
Tomato	68610,1	16,1	16,2	18,0
Onion	330,0	77,7	53,9	117,8
Cabbage	0,0	0,0	0,0	0,0
Banana	0,0	0,0	0,0	0,0
Citrus	0,0	0,0	0,0	0,0
Cotton	94,5	8,7	7,4	-88,1
Coffee	0,0	0,0	0,0	0,0
Sugar beet	0,0	0,0	0,0	0,0
Sugar cane	644330,4	3,3	3,4	-17,2
Sugar	0,0	0,0	0,0	0,0
Groundnut	1162,2	24,7	25,2	18,3
Sesame	7,5	-58,3	-62,1	1048,1
Sunflower	0,1	27,8	-24,4	1832,7
Soybean	20,4	-26,3	-10,7	16,6
Rapeseed	0,0	0,0	0,0	0,0
Peanut oil	0,0	0,0	0,0	0,0
Sesame oil	0,0	0,0	0,0	0,0
Sunflower oil	0,0	0,0	0,0	0,0
Soybean oil	0,0	0,0	0,0	0,0
Rapeseed oil	0,0	0,0	0,0	0,0
Beer	0,0	0,0	0,0	0,0
Alfalfa	0,0	0,0	0,0	0,0
Berseem	0,0	0,0	0,0	0,0
Sudangrass	334501,4	14,3	13,7	18,8
Maizeforage	27,1	-57,4	-52,3	1269,8

Table B.6: Irrigated crop production in the unilateral scenario in Ethiopia and percentage change in the other cooperation scenarios.

	Unilateral [10^3 ton]	Flow information [%]	Trade information [%]	Coordination [%]
Wheat	0,3	0,0	19,8	806,1
Maize	2,9	0,0	-7,3	335,8
Rice	1897,4	0,0	0,1	-37,1
Sorghum	4,3	0,0	20,4	326,8
Millet	0,1	0,0	4,0	934,8
Barley	0,2	0,0	18,5	767,5
Teff	0,2	0,0	18,3	822,1
Cassava	3931,7	0,0	-0,5	-34,7
Potatoes	2697,1	0,0	0,8	-28,3
Yams	9,7	0,0	6,7	286,5
Sweet_potatoes	2061,2	0,0	-3,7	-50,3
Chickpea	0,2	0,0	24,6	886,7
Cowpea	0,0	0,0	15,6	670,3
Lentil	0,2	0,0	18,4	672,9
Bean	0,2	0,0	23,6	686,1
Tomato	6113,6	0,0	0,2	6,9
Onion	290,1	0,0	20,4	74,2
Cabbage	1189,5	0,0	-0,5	-9,0
Banana	29,3	0,0	7,2	199,1
Citrus	153,2	0,0	-0,3	-32,2
Cotton	0,1	0,0	-8,1	632,9
Coffee	0,5	0,0	6,6	937,4
Sugar beet	0,0	0,0	0,0	0,0
Sugar cane	1090,9	0,0	-0,8	10,0
Sugar	0,0	0,0	0,0	0,0
Groundnut	0,2	0,0	30,5	824,9
Sesame	54,3	0,0	5,9	134,9
Sunflower	0,0	0,0	41,3	1007,7
Soybean	0,6	0,0	25,4	750,5
Rapeseed	0,0	0,0	41,8	1017,5
Peanut oil	0,0	0,0	0,0	0,0
Sesame oil	0,0	0,0	0,0	0,0
Sunflower oil	0,0	0,0	0,0	0,0
Soybean oil	0,0	0,0	0,0	0,0
Rapeseed oil	0,0	0,0	0,0	0,0
Beer	0,0	0,0	0,0	0,0
Alfalfa	6,0	0,0	46,0	14937,5
Berseem	6,1	0,0	44,2	2837,7
Sudangrass	9180,4	0,0	-2,1	-26,8
Maizeforage	17,7	0,0	20,7	2746,6

B.5. Optimisation settings

Table B.7: IPOPT convergence tolerances for the historic and future simulation experiments.

	historic [1990-2010]	future [1990-2010]
tolerance	1e-6	1e-4
constraint violation tolerance	1e-6	1e-6
complementary infeasibility tolerance	1e-3	1e-3
acceptable tolerance	1e-1	1e-0
acceptable constraint violation tolerance	1e-3	1e-3
acceptable complementary infeasibility tolerance	1e-6	1e-6
acceptable objective change tolerance	1e-6	1e-6
acceptable iterations	10	10

C Figures

C.1. Electricty consumption

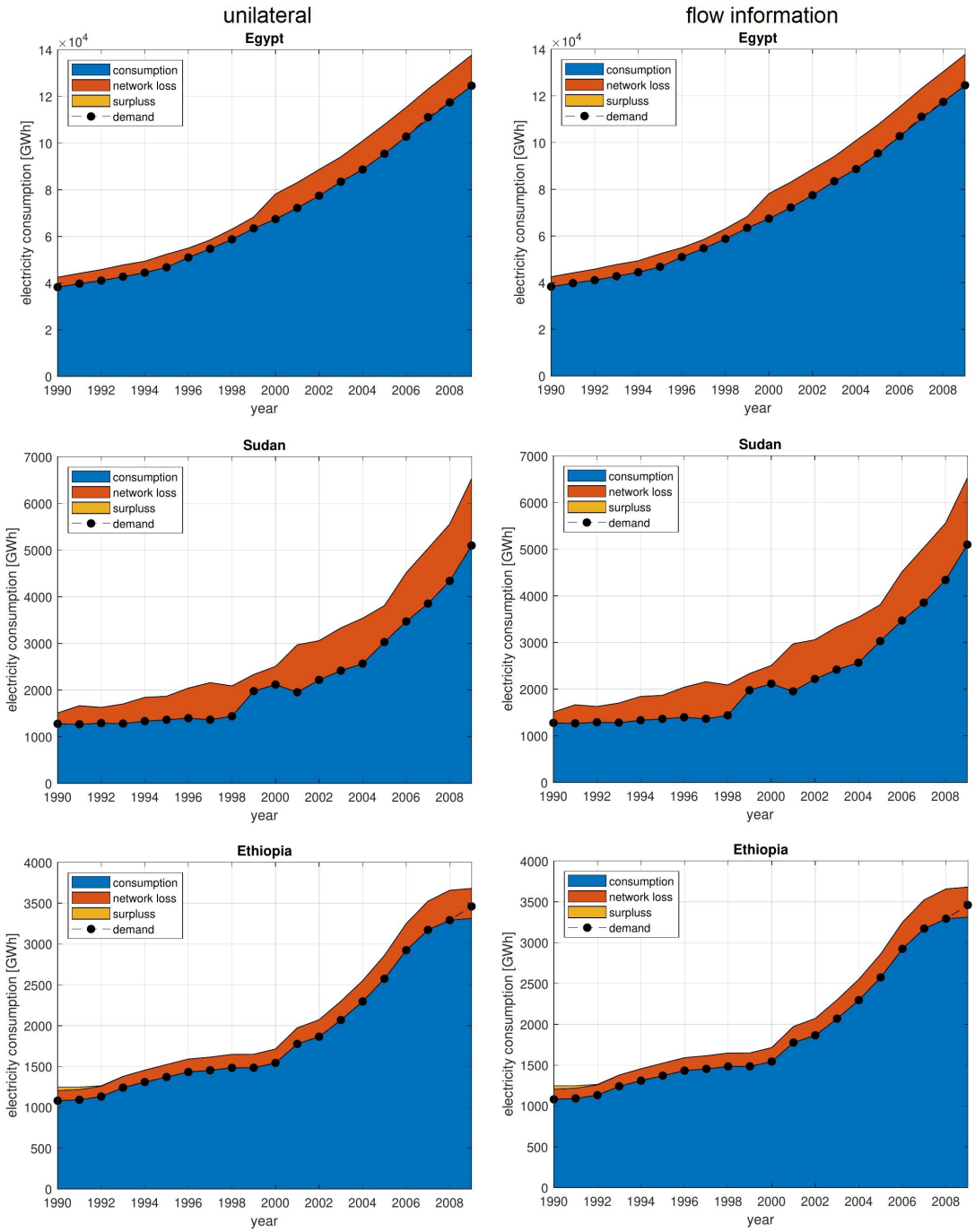

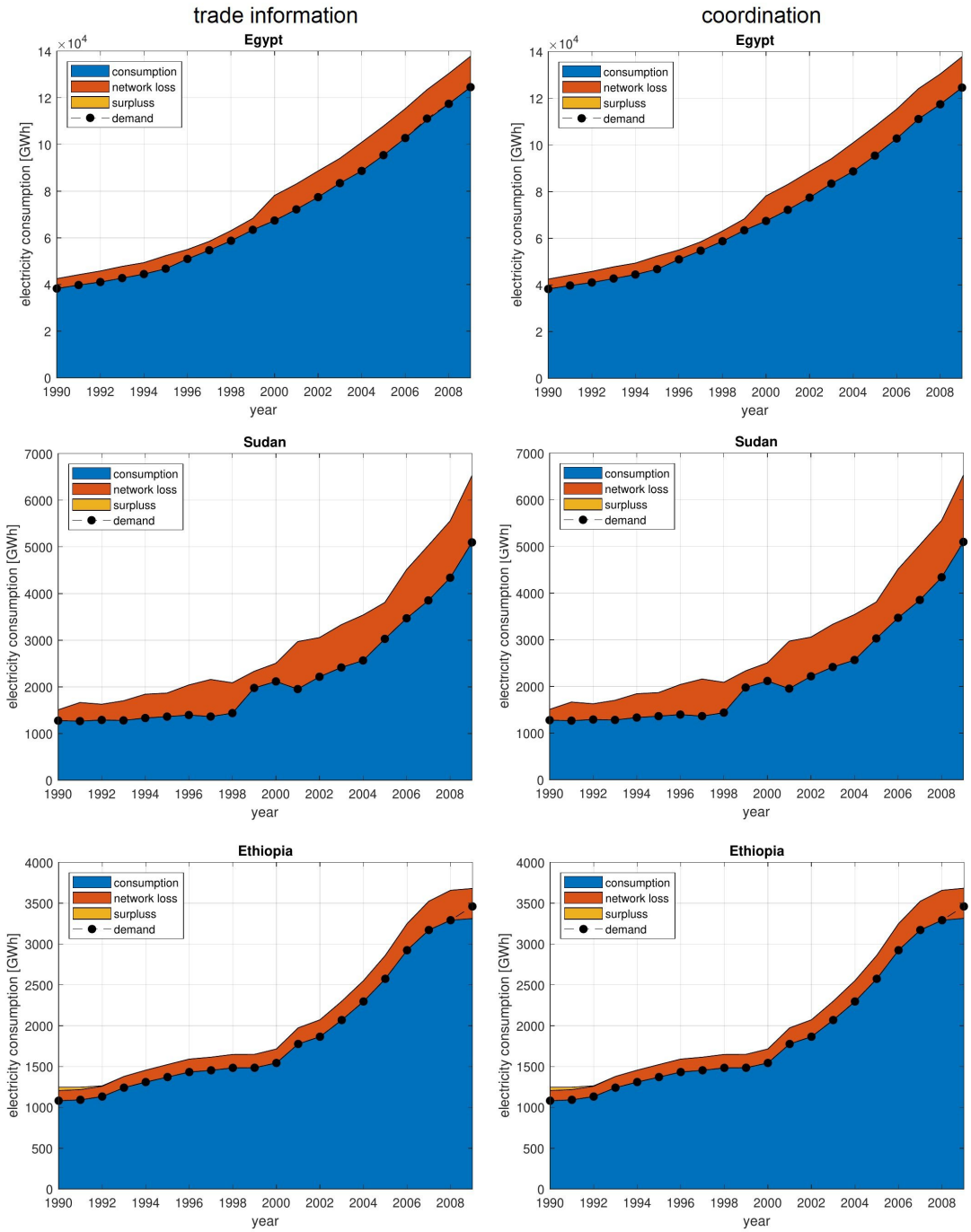

Figure C.1: Electricity consumption, network losses and demand for the cooperation scenarios

C.2. Electricty generation

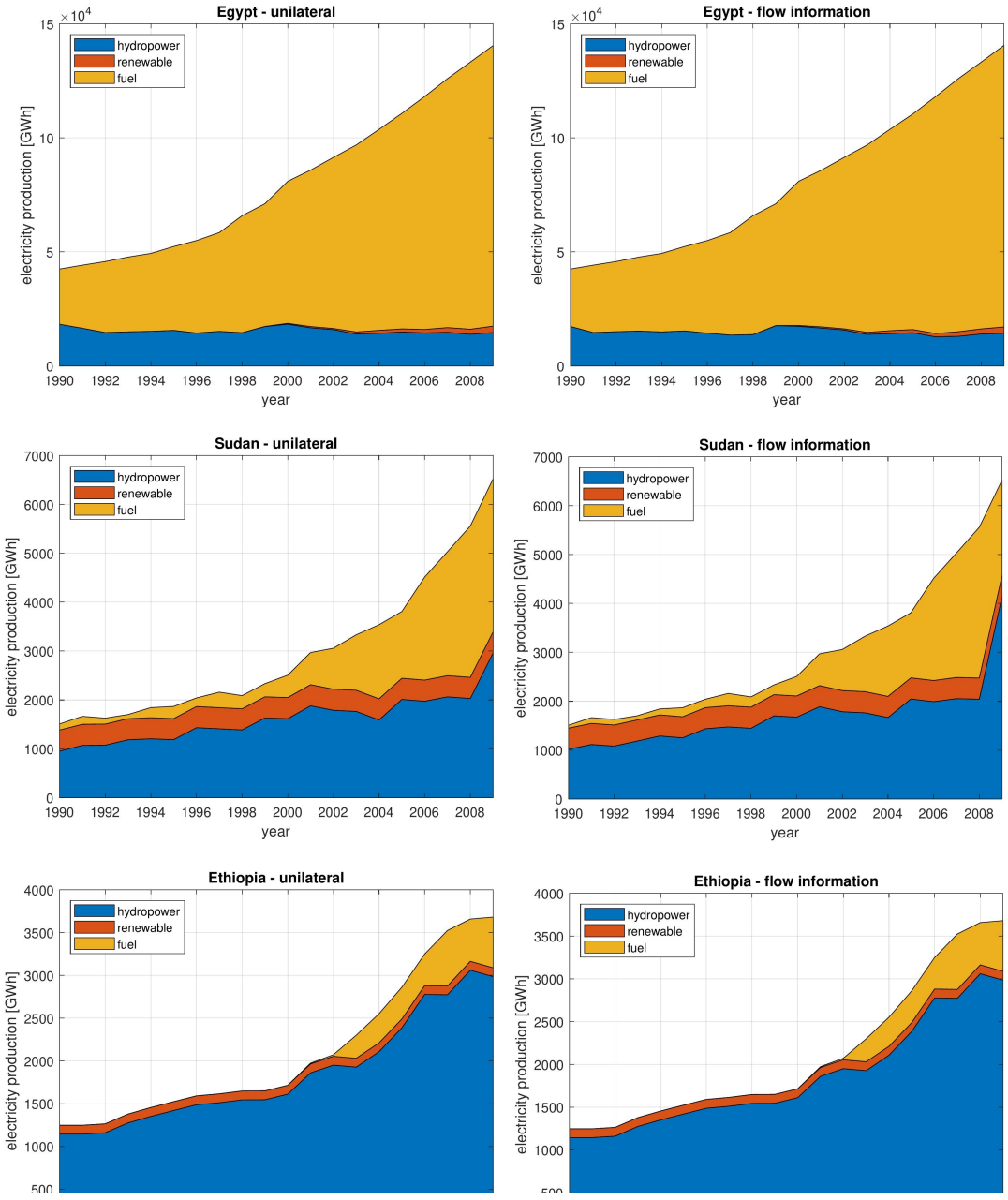

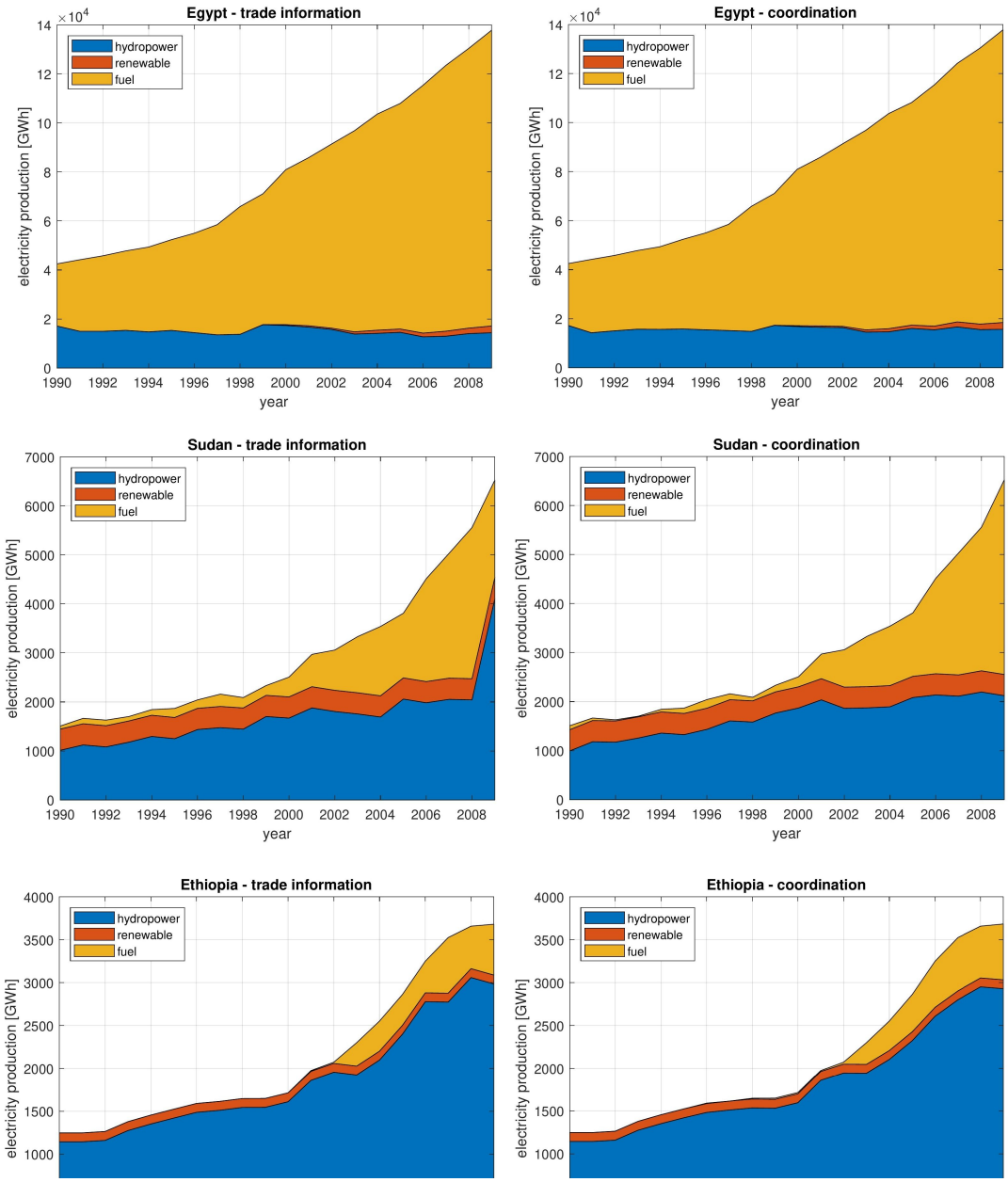

Figure C.2: Electricity generation distinguished by the production source for the cooperation scenarios.

C.3. Random starting point

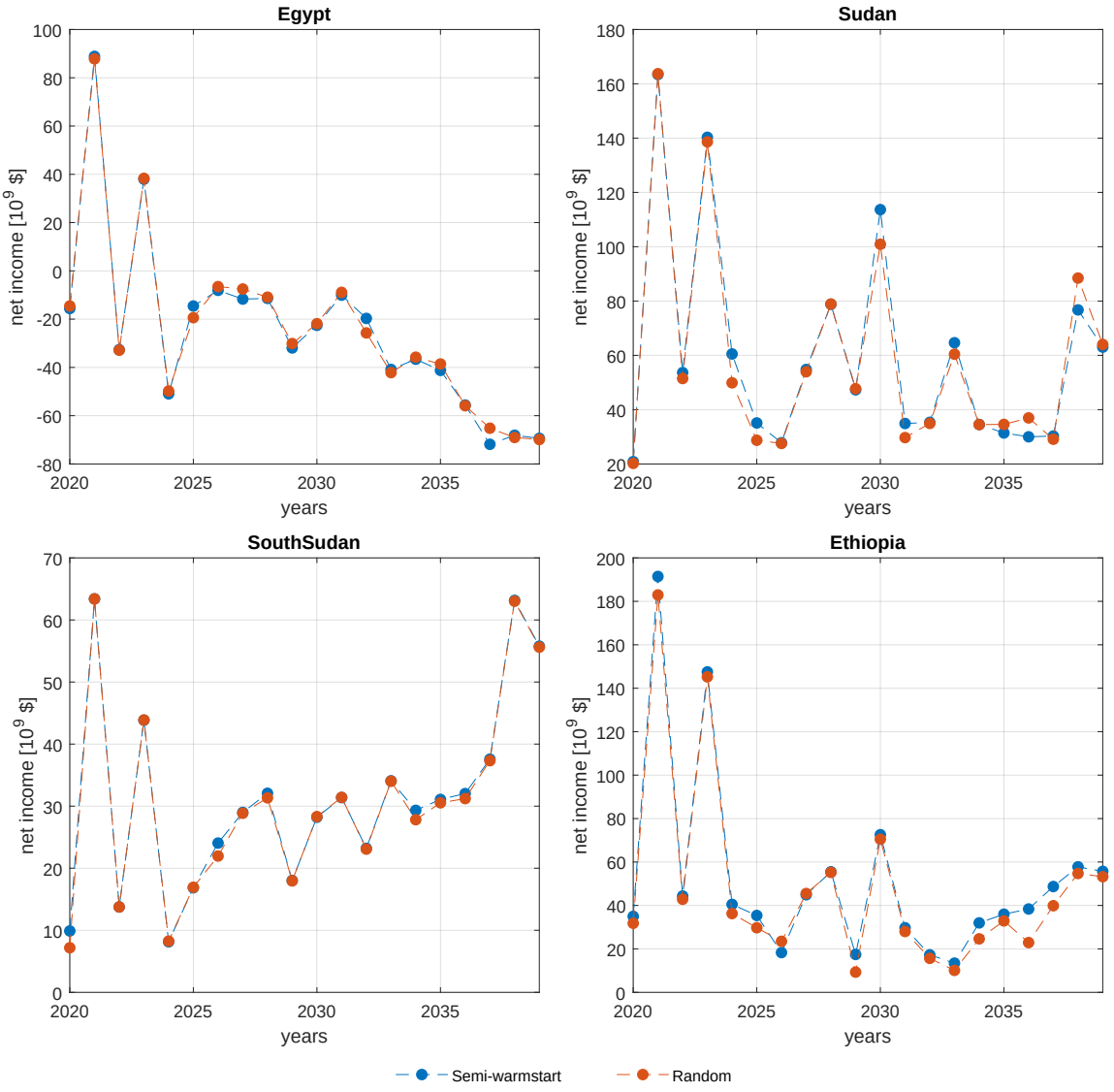

Figure C.3: The annual net benefits of the unilateral scenario in the future simulation experiment. The blue line illustrates the values using a semi-warmstart method, and the red line illustrates the values found with random starting points for each MPC iteration.

C.4. Reservoir rule curves

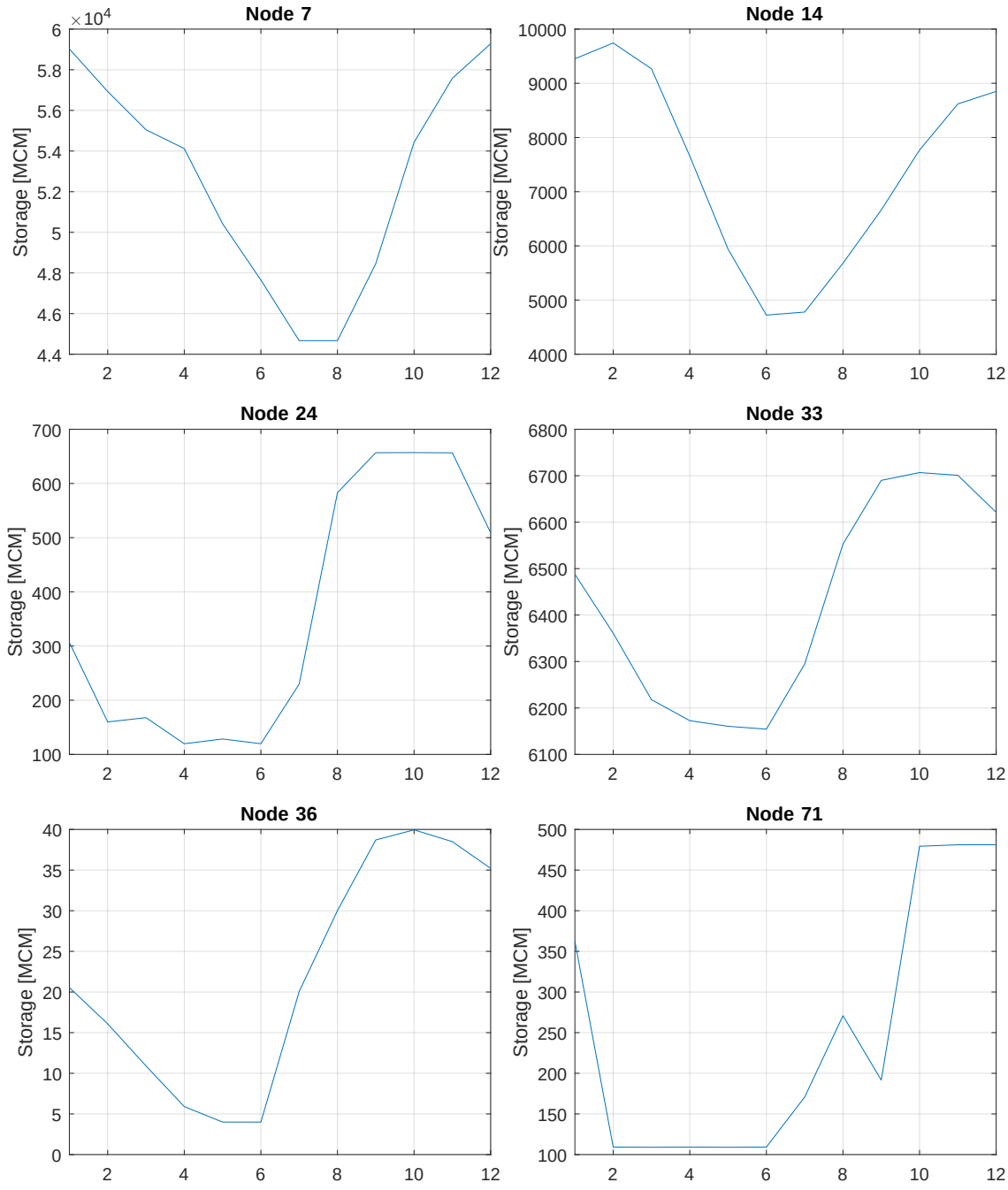

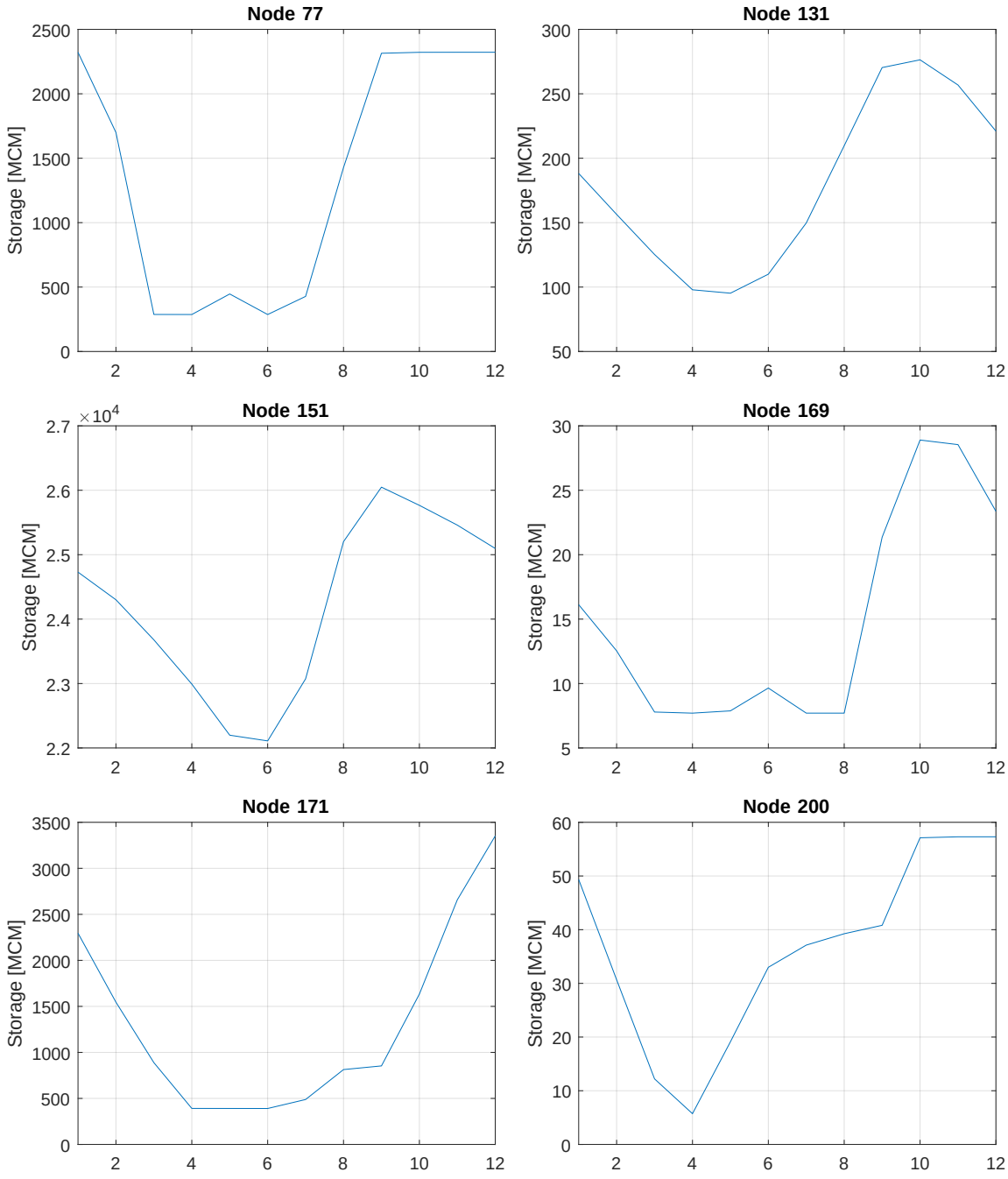

Figure C.4: Surface water reservoir rule curves for the reservoir active during the historic simulation experiments.